BENZIMIDAZOLE DERIVATIVES AS POTENTIAL DUAL INHIBITORS FOR POLY (ADP-RIBOSE) POLYMERASE-1 AND DIHYDROOROTATE DEHYDROGENASE

ISKANDAR BIN ABDULLAH

FACULTY OF SCIENCE
UNIVERSITY OF MALAYA
KUALA LUMPUR

2015

BENZIMIDAZOLE DERIVATIVES AS POTENTIAL DUAL INHIBITORS FOR POLY (ADP-RIBOSE) POLYMERASE-1 AND DIHYDROOROTATE DEHYDROGENASE

ISKANDAR BIN ABDULLAH

THESIS SUBMITTED IN FULFILMENT OF THE REQUIREMENTS FOR THE DEGREE OF

DOCTOR OF PHILOSOPHY

DEPARTMENT OF CHEMISTRY
FACULTY OF SCIENCE
UNIVERSITY OF MALAYA
KUALA LUMPUR

2015

UNIVERSITY OF MALAYA

ORIGINAL LITERARY WORK DECLARATION

Name of Candidate: **ISKANDAR BIN ABDULLAH**

Registration/Matric No: **SHC 100027**

Name of Degree: **Doctor of Philosophy**

Title of Project Paper/Research Report/Dissertation/Thesis ("this Work"):

Benzimidazole Derivatives as Potential Dual Inhibitors for Poly (ADP-Ribose) Polymerase-1 and Dihydroorotate Dehydrogenase

Field of Study: **Organic Synthesis / Molecular Modeling**

I do solemnly and sincerely declare that:

(1) I am the sole author/writer of this Work;
(2) This Work is original;
(3) Any use of any work in which copyright exists was done by way of fair dealing and for permitted purposes and any excerpt or extract from, or reference to or reproduction of any copyright work has been disclosed expressly and sufficiently and the title of the Work and its authorship have been acknowledged in this Work;
(4) I do not have any actual knowledge nor do I ought reasonably to know that the making of this work constitutes an infringement of any copyright work;
(5) I hereby assign all and every rights in the copyright to this Work to the University of Malaya ("UM"), who henceforth shall be owner of the copyright in this Work and that any reproduction or use in any form or by any means whatsoever is prohibited without the written consent of UM having been first had and obtained;
(6) I am fully aware that if in the course of making this Work I have infringed any copyright whether intentionally or otherwise, I may be subject to legal action or any other action as may be determined by UM.

Candidate's Signature Date:

Subscribed and solemnly declared before,

Witness's Signature Date:

Name:

Designation:

ABSTRACT

Poly (ADP-ribose) polymerases (PARPs) play diverse roles in various cellular processes that involve DNA repair and programmed cell death. Amongst these polymerases is PARP-1, which is the key DNA damage-sensing enzyme that acts as an initiator for the DNA repair mechanism. Dihydroorotate dehydrogenase (DHODH) is an enzyme in the pyrimidine biosynthetic pathway and has been an important target for anti-hyperproliferative and anti-inflammatory drug design. Since these enzymes share a common objective in the DNA replication and repair mechanisms, it may be beneficial to target both PARP-1 and DHODH in our attempt to design new anti-cancer agents.

Benzimidazole derivatives have shown a wide variety of pharmacological activities including PARP-1 and DHODH inhibition. Thus, molecular modeling, synthesis and bioactivity evaluation of a series of benzimidazole derivatives using PARP-1 colorimetric assay and DHODH enzymatic assay were carried out in the search of dual inhibitors for both PARP-1 and DHODH enzymes.

Independently, compounds **9h**, **10b**, **10c**, **10f**, **10h** and **11e** displayed good activities in PARP-1 enzyme while compounds **7b**, **7e**, **7f** and **7g** exhibited good activities in DHODH enzyme. Nevertheless, dual inhibition activities for both of PARP-1 and DHODH enzymes were demonstrated by compounds **7e**, **9h**, **10h** and **11e** albeit low activity was observed.

ABSTRAK

Enzim-enzim Poly (ADP-ribose) polymerase (PARP) menunjukkan kepelbagai peranannya di dalam pemprosesan sel di mana ia melibatkan pemulihan DNA dan juga kematian sel yang diprogramkan. Di antara enzim-enzim polymerase tersebut adalah enzim PARP-1 yang merupakan kunci penting di dalam mengenalpasti DNA yang telah mengalami kerosakan dan juga menjadi pemangkin kepada proses mekanisma pemulihan DNA. Enzim Dihydroorotate dehydrogenase (DHODH) adalah merupakan enzim yang terlibat di dalam laluan biosintesis penghasilan pirimidina. Dari segi penghasilan ubat-ubatan, enzim ini juga merupakan enzim yang penting dan dikaji untuk merencatkan pertumbuhan sel dan pembengkakkan. Disebabkan kedua-dua enzim yang dinyatakan ini mempunyai beberapa persamaan di dalam mekanisma pemulihan dan pembelahan DNA, penghasilan agen anti-kanser di mana secara khususnya untuk PARP-1 dan DHODH adalah amat berguna.

Benzimidazole dan juga terbitannya telah menunjukkan kesan farmakologi yang meluas termasuk juga perencatan proses-proses PARP-1 dan DHODH. Justeru itu, permodelan molekul, sintesis dan penilaian biologi bagi satu siri terbitan benzimidazole menggunakan PARP-1 kolometrik asai dan asai enzim DHODH telah dijalankan dalam usaha mencari agen dwi-perencatan enzim-enzim PARP-1 dan juga DHODH.

Secara berasingan, sebatian-sebatian **9h**, **10b**, **10c**, **10f**, **10h** and **11e** menunjukkan perencatan yang baik kepada enzim PARP-1 manakala sebatian-sebatian **7b**, **7e**, **7f** and **7g** pula menunjukkan perencatan yang baik kepada enzim DHODH. Walaubagaimanapun, dwi-perencatan telah ditunjukkan oleh sebatian-sebatian **7e**, **9h**, **10h** and **11e** walaupun kesannya adalah rendah.

ACKNOWLEDGEMENTS

Without the help, support and guidance from the kind people surrounding me, this doctoral thesis would not be a success. But above all, I am grateful and thankful to the Almighty God for His blessings and guidance for the life I have.

My special gratitude goes out to my wonderful supervisor Prof. Dr. Noorsaadah Abd. Rahman for all her help, guidance and motivation. Thank you for believing in me, learned a lot from the comments she gave that inspired me giving all of my best and her patience reading all the drafts over and over again. Thank you for spending so much time in our questions and never fail to correct where it went wrong. May she always have a good life and blessed by God.

I would sincerely like to thank both of my parents and my family for their love, their unstoppable encouragement, helps and support for this thesis to be possible. I am who I am because of them.

I am also very grateful to Aurigene Discovery Technologies Ltd. (India and Malaysia) especially K Satish Reddy, Dr. Siva Sanjeeva Rao Thunuguntla, and group members in their effort throughout this project. Also to my labmates Dr. Lee Yean Kee, Dr. Chee Chin Fei for their great assistance and other members of DDDRG (Drug Design and Development Research Group) for their help, support and a pleasurable working environment throughout the years.

Last but not least, thank you very much to the Department of Chemistry staffs for their aid in NMR, LCMS and X-ray crystallography analysis.

TABLE OF CONTENTS

LIST OF FIGURES

LIST OF SCHEMES

LIST OF TABLES

LIST OF SYMBOLS AND ABBREVIATIONS

%	Percent
^{13}C	Carbon-13
^{1}H	Proton
2D	2-Dimensional
3D	3-Dimensional
Å	Angstrom
ABT-888	Veliparib
AcCl	Acetyl chloride
AcOH	Acetic acid
ADMET	Adsorption, distribution, metabolism, excretion and toxicity
Ala	Alanine
Arg	Arginine
Asn	Asparagine
Asp	Aspartic acid
BER	Base excision repair
BRCA	Breast cancer associated genes
BRCA-1	Breast cancer gene 1
BRCA-2	Breast cancer gene 2
BRCT	BRCA1 C-Terminus
C	Carbon
CaH_2	Calcium hydride
CD_3OD	Methanol-d_3
$CDCl_3$	Chloroform-d
CDI	1,1'-Carbonyldiimidazole

CH_2CL_2	Dichloromethane
CoQ	Ubiquinone
CS_2CO_3	Cesium Carbonate
d	Doublet
DCC	Dicyclohexylcarbodiimide
DCIP	2,6-Dichloroindophenol
DCM	Dichloromethane
dd	Doublet of a doublet
DHODH	Dihydroorotate dehydrogenase
DIC	*N*,*N*'-Diisopropylcarbodiimide
DiPEA	*N*,*N*-Diisopropylethylamine
DMA	*N*,*N*-dimethylacetamide
DMAP	4-Dimethylaminopyridine
DMF	Dimethylformamide
DMP	Dess-Martin Periodinane
DMSO	Dimethylsulfoxide
DMSO-d_6	Dimethylsulfoxide-d6
DNA	Deoxyribonucleic acid
DSBs	Double-strand breaks
DUQ	Decylclubiquinone
EDCI.HCl	1-Ethyl-3-(3-dimethylaminopropyl)carbodiimide
ESI	Electrospray ionisation
EtOAc	Ethyl Acetate
F	Fluorine
FMN	Flavin mononucleotide
g	gram

Gln	Glutamine
Glu	Glutamic acid
Gly	Glycine
H	Hydrogen
H-O-H	Water
H_2O	Water
HATU	1-[Bis(dimethylamino)methylene]-1H-1,2,3-triazolo[4,5-b] pyridinium 3-oxid hexafluorophosphate
HBC	Hereditary breast cancer
HCl	Hydrochloric acid
Hex	Hexane
HGSC	High grade serous cancer
His	Histidine
HOBt	1-Hydroxybenzotriazole
HPLC	High performance liquid chromatography
HR	Homologous recombination
HRMS	High resolution mass spectrometer
*Hs*DHODH	Human DHODH
IC_{50}	Half maximal inhibitory concentration
Ile	Isoleucine
J	J coupling
K_2CO_3	Potassium carbonate
Ki	Inhibitory constant
KOAc	Potassium acetate
L	Liter
Leu	Leucine

Lig III	DNA ligase III
LiOH	Lithium hydroxide
Lys	Lysine
m	meta
m	Multiplet
MeOH	Methanol
Met	Methionine
$MgSO_4$	Magnesium sulphate anhydrous
MHz	Megahertz
mL	Milliliter
mM	Millimolar
mmol	Millimole
MS	Mass spectrometer
MsCl	Methanesulfonyl chloride
N	Nitrogen
N.A	Not active
N_2	Nitrogen gas
$Na(OAc)_3BH$	Sodium triacetoxyborohydride
NAD	Nicotinamide adenine dinucleotide
$NaHCO_3$	Sodium bicarbonate
$NaHSO_3$	Sodium hydrogen sulfite
ng	Nanogram
NH_4Cl	Ammonium chloride
NHEJ	Non-homologous end joining
nM	Nanomolar
nm	Nanometer

NMP	N-Methyl-2-pyrrolidone
NMR	Nuclear magnetic resonance
°	Degrees
o	ortho
O	Oxygen
°C	Degrees Celcius
p	para
PARP	Poly (adenosine diphosphate-ribose) polymerase
PARP-1	NAD^+ ADP-ribosyltransferase 1
$Pd(dppf)Cl_2$	[1,1'-Bis(diphenylphosphino)ferrocene]dichloropalladium
$Pd(PPh_3)_2Cl_2$	Bis(triphenylphosphine)palladium(II) dichloride
Pd/C	Palladium-on-carbon
pdb	Protein Databank
Phe	Phenylalanine
pKa	Acid dissociation constant
PKs	Pharmacokinetic
pol β	DNA polymerase beta
Pro	Proline
PyBOP	3-Pipecolinic acid
q	Quartet
RA	Rheumatoid arthritis
RNA	Ribonucleic acid
S	Sulphur
s	Singlet
Ser	Serine
$SOCl_2$	Thionyl chloride

SSBs	Single-strand breaks
t	Triplet
T-cell	Thymus cell
TEA	Triethylamine
THF	Tetrahydrofuran
Thr	Threonine
TLC	Thin layer chromatography
Trp	Tryptophan
Tyr	Tyrosine
v/v	Volume to volume
Val	Valine
XP	Extra precision
XRCC1	X-Ray cross complementing gene 1
μ	Micro
μM	Micromolar
π	Pi

CHAPTER 1: INTRODUCTION

1.1 BRCA Mutation Associated Cancers

BRCA-1 (breast cancer gene 1) and BRCA-2 (breast cancer gene 2), found in human genes, are responsible in producing tumor suppressor proteins. These normal genes play important role in repairing DNA double-strand breaks via homologous recombination (HR), a mechanism that perfectly repairs any damaged DNA. The cytogenic locations of BRCA-1 (Figure 1.1) and BRCA-2 (Figure 1.2) are at 17q21 (Hall *et al*., 1990; Miki *et al*., 1994) and 13q12.3, respectively (Wooster *et al*., 1994, 1995). Mutations and alterations in the genes may result in genetic modifications that lead to increased risk of cancer development, such as breast cancer, ovarian cancer, prostate cancer and other cancers (Sloots, Ausems, & de Haan, 2002). Mutations in these genes have been logged for 30-50% of hereditary breast cancer (HBC) (Passaperuma *et al*., 2010), about 5-10% of other breast cancers (Campeau, Foulkes, & Tischkowitz, 2008), most hereditary ovarian cancers especially the high grade serous cancer (HGSC) type, and in 15% of prostate cancer in men (Fraser *et al*., 2014).

Hereditary cancer is a cancer that develops from mutated genes of a biological parent to offspring inheritance. Gene mutation is heritable either from a mother or a father that is passed on to their sons or daughters, termed as *germline mutations*. Thus there is a 50% chance for a child to inherit a mutated gene also makes them susceptible to develop colon cancer and pancreatic cancer (Judson & Van Le, 1998). As reported by the University of Cambridge in 2002, British women with BRCA-1 mutations aged above 70 have 36% and 28% are at risk in developing breast cancer and ovarian cancer. Similarly, a 69% chance of breast cancer development and a 17% chance for ovarian

cancer were reported for those who had BRCA-2 mutations. This figure is notably higher when compared with women of the same age group without BRCA mutation, with who are at 5% risk of developing breast cancer. This shows that individuals who are carriers of BRCA-1 and BRCA-2 mutations have a higher risk of developing breast and ovarian cancers relative to the general population (Antoniou *et al*., 2002).

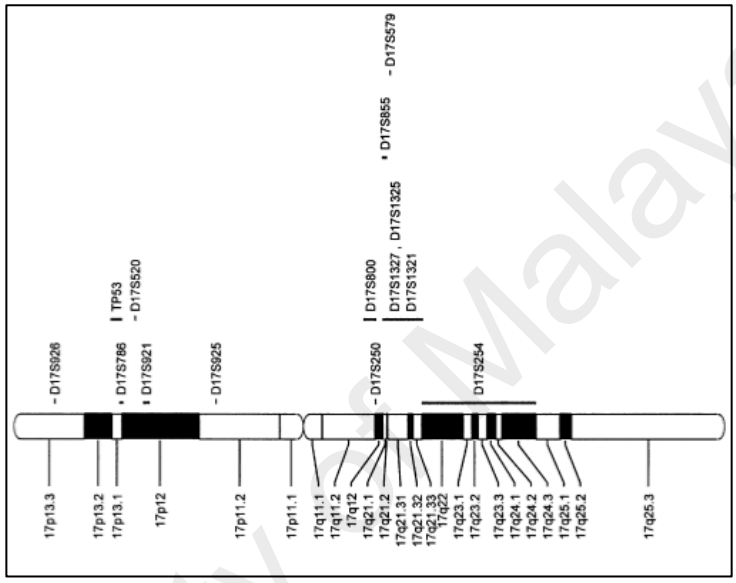

Figure 1.1. Cytogenic location of BRCA-1 (Försti *et al*., 2001).

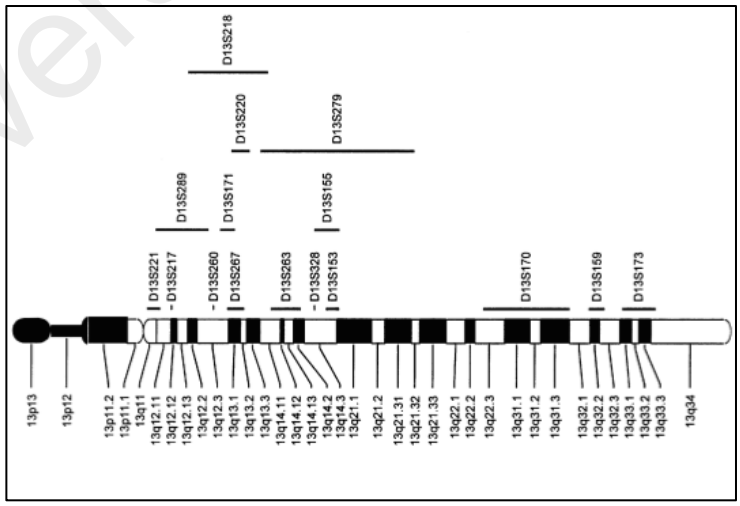

Figure 1.2. Cytogenic location of BRCA-2 (Försti *et al*., 2001).

In men, carriers of the BRCA-2 mutations are more likely to have a higher risk for prostate cancer compared to carriers of BRCA-1 mutations. In addition, environmental

elements, non-genetic and genetic modifiers can also affect and promote this occurrence (Chung, 1996; Levy-Lahad & Friedman, 2007). In normal cells, homologous recombination (HR) pathway remains the primary mechanism for DNA repair. However, in tumor cells that contain dysfunctional BRCA, the PARP expression related to base excision repair (BER) mechanism is enhanced in response to DNA damage (Wesierska-Gadek *et al*., 2012). Evidently, it was shown that mutagenic cells were more sensitive towards PARP-1 inhibitors, compared to normal cells (Gandhi *et al*., 2010; Giannini *et al*., 2014). Judging from the mechanism and findings, synthetic lethality tactic would be a novel approach in cancer therapy. This is because single-strand breaks (SSBs), induced by accumulation of PARP inhibitors, increase double-strand breaks (DSBs) that would subsequently lead to cell death in tumor cells (Glendenning & Tutt, 2011).

1.2 Poly (Adenosine Diphosphate-ribose) Polymerase

Poly (adenosine diphosphate-ribose) polymerase, PARP, discovered by Chambon and co-workers (Chambon, Weill, & Mandel, 1963), is a family of proteins involved in a number of cellular processes, including modulation of chromatin structure, transcription, replication, recombination and DNA repair. It comprises 18 putative members that have potential PARP activity (Figure 1.3). Per unit polymer, PARP proteins are made of 2 phosphates and 2 ribose moieties, where PARP-1 is the best understood protein (Weil & Chen, 2011). The main roles of PARP are in the DNA repair mechanism and regulation of transcription. Notably, PARP activity increases when DNA is damaged cause due to induced-radiation and DNA damaging agents (Morales *et al*., 2014). Normal cells use PARP to repair itself to maintain normal life

cycle. Unfortunately, cancer cells also act in a similar manner as normal healthy cells in using PARP to repair the damaged DNA. However, unlike normal cells, this makes the growth in cancer cells become uncontrollable. The NAD^+ ADP-ribosyltransferase 1 (PARP-1) and PARP-2 (Figure 1.4) are the only PARP family members that contain DNA-binding domains with PARP-1 as the main family member (Ame, Spenlehauer, & de Murcia, 2004). This would clinically be useful for the treatment of several cancers, especially breast, ovarian and prostate cancer (Gagne, Rouleau, & Poirier, 2012).

There are three structural domains that control the activity of PARP: DNA binding domain of N-terminal, which contains two zinc fingers that bind to the damaged DNA; an auto-modification domain containing BRCT protein-protein interaction and the C-terminal catalytic region that contains the active site (Sodhi, Singh, & Jaggi, 2010). PARP-1 is an enzyme that is mainly involved in sensing, it assisting in repairing single-strand breaks (SSBs) and is found to be active in the homodimer form. When DNA damage occurs, especially during single-strand breaks, the enzyme recognizes it and binds to the site of damage. Binding to the damaged site stimulates PARP-1 to catalyze the synthesis of polymers of the ADP-ribose (linear and branched) by using nicotinamide adenine dinucleotide (NAD^+) as the substrate with the release of nicotinamide. The synthesized polymers are then transferred to acceptor proteins, which can be found in the PARP-1 itself or on other proteins mainly involved in the DNA repair (White *et al*., 2000).

Through the base excision repair pathway (BER), PARP-1 signals and recruits other DNA repair proteins, such as the X-Ray cross complementing gene 1 (XRCC1), DNA ligase III (Lig III), DNA polymerase beta (pol β), and kinase to participate in the single-strand break repair machinery (El-Khamisy *et al*., 2003; Ame, Spenlehauer, & de

Murcia, 2004; Penning *et al*., 2010). In normal and healthy cells, homologous recombination (HR) overpowers the DNA reparation, whereby this mechanism is potentially an error-free repair mechanism in conjunction with BRCA genes (BRCA1 and BRCA2) (Rehman, Lord, & Ashworth, 2010).

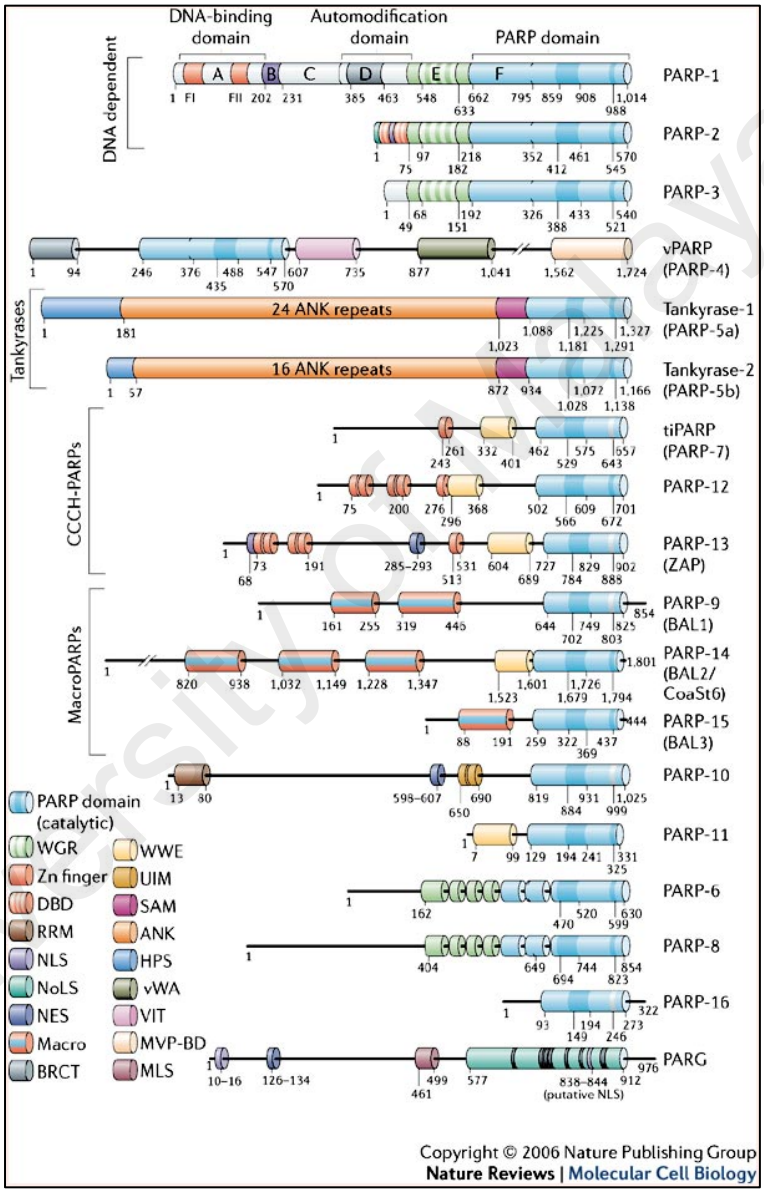

Figure 1.3. Structure of PARP (Source: Schreiber *et al*., 2006).

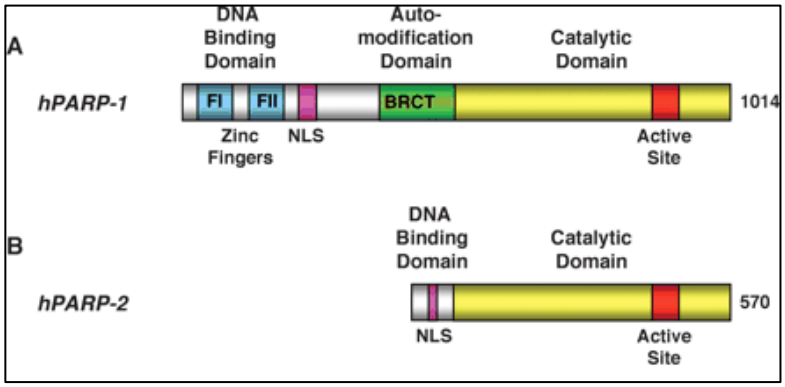

Figure 1.4. Structure of human PARP-1 and PARP-2 (Source: Kim, Zhang, & Kraus, 2005).

1.3 Dihydroorotate Dehydrogenase

Dihydroorotate dehydrogenase (DHODH), is a mitochondrial enzyme that plays a crucial part in the *de novo* biosynthesis of pyrimidine bases (Fritzson *et al*., 2010). Through redox process, the enzyme catalyzes the oxidation conversion of dihydroorotate to orotate with the aid of the prosthetic group, flavin mononucleotide (FMN), and ubiquinone (CoQ) as co-factors (Evans & Guy, 2004; McLean *et al*., 2010) (Figure 1.5).

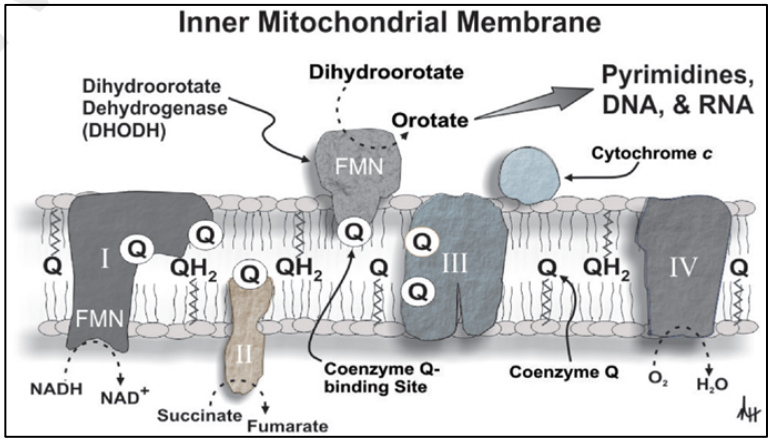

Figure 1.5. Role of DHODH in the inner mitochondrial membrane. Reprinted with permission (Velez *et al*., 2013).

In the DNA and RNA syntheses, rapid proliferation of human T cells require the *de novo* biosynthesis of pyrimidines in strand-break repair, biosynthesis of membrane-lipid as well as in protein glycosylation (Liu *et al*., 2000). DHODH consists of two families, a cytosolic enzyme encoded in family 1, and an enzyme associated within the inner membrane of the mitochondrial, encoded as family 2. Family 1 DHODHs use fumarate and NAD as electron acceptors. In contrast, the family 2 DHODHs consist of the human DHODH (*Hs*DHODH), and *P. falciparum* DHODH (*Pf*DHODH) that rely on the respiratory chain function, and ubiquinone as the direct electron acceptor (Zameitat *et al*., 2007). Mutations in this gene cause Miller Syndrome, but it is unclear how the signs and symptoms lead to this phenomenon (Ng *et al*., 2010).

1.4 PARP inhibitors

PARP inhibitors are drugs that were designed to prevent the reparation of DNA damaged cancer cells by PARP proteins (Ame, Spenlehauer, & de Murcia, 2004). Evidently, PARP inhibitors showed both *in vitro* and *in vivo* anticancer effects in cells deficient of breast cancer associated genes (BRCA-1 and BRCA-2) at high sensitivity (Liu, Konstantinopoulos, & Matulonis, 2014; Powell *et al*., 2010). Furthermore, anticancer activities were also observed in prostate cancer (Castro *et al*., 2013; Levy-Lahad & Friedman, 2007) and ovarian high-grade serous cancer (Liu, Konstantinopoulos, & Matulonis, 2014). In addition, therapeutic benefits of PARP inhibitors were also reported for many other diseases, such as in ischemic kidney disease, ischemic liver disease, ischemic-reperfusion disorder, myocardial infarction, hemorrhagic shock, inflammatory lung disease, stroke, spinal cord trauma, and colitis (Graziani & Szabo, 2005; Lord *et al*., 2009).

By inhibiting base excision repair with PARP inhibitors, reparation of single strand breaks, caused by cytotoxic chemotherapy and ionizing radiation is halted. Therefore, formation of double strand breaks occurs, as DNA replication at the forks of single strand breaks is stalled. Subsequent repair of the accumulative double strand breaks is also stunted due to faulty homologous recombination (HR) pathway in the mutated BRCA cells leads to cell death, creating synthetic lethality effect (Scarpelli *et al*., 2010; Weil & Chen, 2011; Liu, Konstantinopoulos, & Matulonis, 2014).

An alternative DNA repair pathway that exerts anticancer mechanism is called non-homologous end joining (NHEJ), an error prone repair mechanism. Homologous recombination (HR) cell death is increased by phosphorylation of catalytic subunit enzyme known as DNA-dependent protein kinase (Park *et al*., 2009; Peng *et al*., 2014). Trapping PARP-1 and PARP-2 in the PARP enzyme with PARP inhibitors producing DNA-PARP complexes showed potential DNA replication disturbance (Murai *et al*., 2012). The use of PARP inhibitors as competitive inhibitors is through blocking the NAD^+ in the active site of the PARP enzyme to obtain 90% inhibition, is ideal for DNA reparation obstruction (Scarpelli *et al*., 2010; Weil & Chen, 2011; Giannini *et al*., 2014).

It is discovered that PARP inhibitors can be used as a single agent, or in combination therapies (Giannini *et al*., 2014). As a result of its potential therapeutic effect, these small molecule inhibitors sparked interest in various organisations to fight cancer at the DNA level (Tong *et al*., 2009). Classical PARP inhibitors, such as nicotinamide (Clark, Ferris, & Pinder, 1971) and 3-aminobenzamide (Cosi, 2002) were tested and reported to be low in potency, limited cellular resistance time and cell uptake, and showed non-specific effects. Thus, newer versions of PARP inhibitors, consists of benzimidazole

core, primary amide and lactam components, were disclosed by Alex W. White and co-workers (White *et al*., 2000) with relatively small scaffold and high intrinsic potency (Peninng *et al*., 2008). This was mainly due to the network of hydrogen bond interactions and π–stacking that structurally mimics the binding mode of nicotinamide inside the binding site of PARP-1 (Tong *et al*., 2009). These inhibitors showed improvement in inhibition in terms of potency and specificity. One example is veliparib (ABT-888), which has a carboxamide attached to a benzimidazole (Sodhi *et al*., 2010), that will be described in the following section.

1.5 DHODH inhibitors

DHODH inhibitors are a class of drugs that exhibit immunosuppressant (Lolli *et al*., 2012) and anti-proliferative effects on rapidly dividing cells for the treatment of cancer, rheumatoid arthritis and multiple sclerosis (Sutton & Clardy, 2006; Erra *et al*., 2009; McLean *et al*., 2010) as well as for the prevention of transplant rejection (Breedveld & Dayer, 2000). The effects of these inhibitors were shown to be the most pronounced during thymus cell (T-cell) proliferation, (Leban *et al*., 2004; Baumgarnet *et al*., 2009; Davies *et al*., 2009). DHODH inhibitors were designed and developed responsibly to block the pyrimidine biosynthesis that converts dihydroorotate to orotic acid through oxidation process, resulting in the depletion of pyrimidine nucleotides. This would lead to the inhibition of DNA and RNA syntheses, as well as arresting cell proliferation (Herrmann, Schleyerbach, & Kirschbaum, 2000). During proliferation, approximately 8 folds of pyrimidine pool in activated lymphocytes are expanded, while an increase for purine pools is only 2 folds. The demand for both *de novo* and salvage pathways increases as the requirement for nucleotides increases, subsequently suppressing the

immune system (Breedveld & Dayer, 2000). There are several DHODH inhibitors that reached clinical development such as Brequinar, Leflunomide and its active metabolite Teriflunomide, but failed in clinical trials due to its inadequate therapeutic evidence (Lolli *et al*., 2012).

1.6 Veliparib

Veliparib (ABT-888) is one of the well known PARP inhibitors that inhibits PARP-1 and PARP-2 at Ki = 5.2 nM and 2.9 nM, respectively. It was discovered and developed by Abbot Laboratories (Scheme 1.1) and has a decent oral bioavailability where the efficacy and potency of the drug were shown both *in vivo* and *in vitro* (Zhu *et al*., 2006).

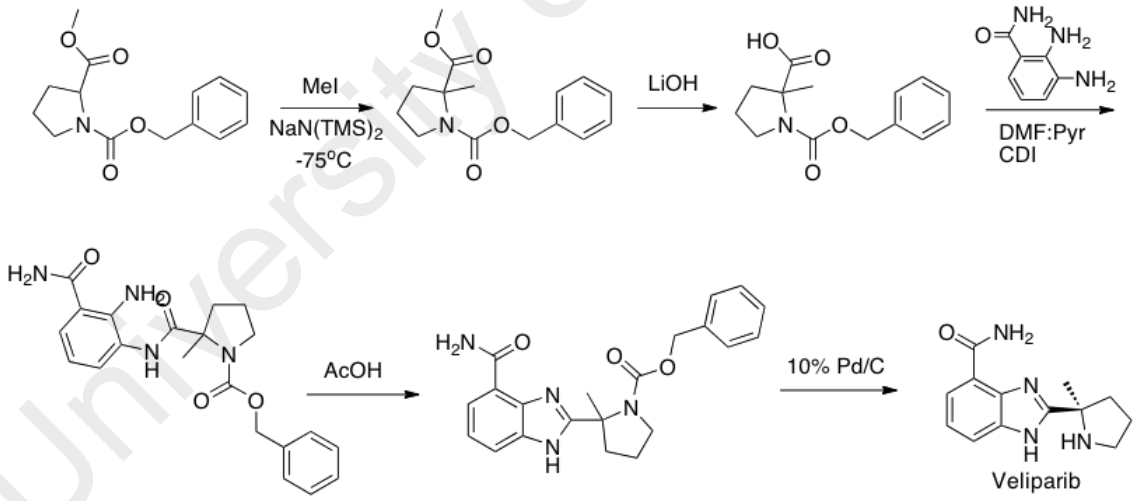

Scheme 1.1. Synthesis of Veliparib.

Furthermore, this compound penetrated the blood-brain barrier in rat under pharmacokinetic (PKs) studies (Weil & Chen, 2011). In syngeneic and xenograft tumor models, veliparib potentiates a number of DNA damaging agents such as termozolomide, chemotherapy and radiation. On top of these, veliparib has interestingly

been reported to potentially act as a single-agent activity inhibitor. With these wide ranging therapeutic potentials, veliparib has entered Phase I and II clinical trials for various malignant solid tumors (Donawho *et al*., 2007; Palma *et al*., 2008; Weil & Chen, 2011).

1.7 Brequinar

Brequinar was first synthesized by DuPont Merck Pharmaceuticals by using 5-flouroindoline-2,3-dione and 1-(2'-fluoro-[1,1'-biphenyl]-4-yl)propan-1-one as the starting materials, using Pfitzinger condensation method (Scheme 1.2) (Batt *et al*., 1995).

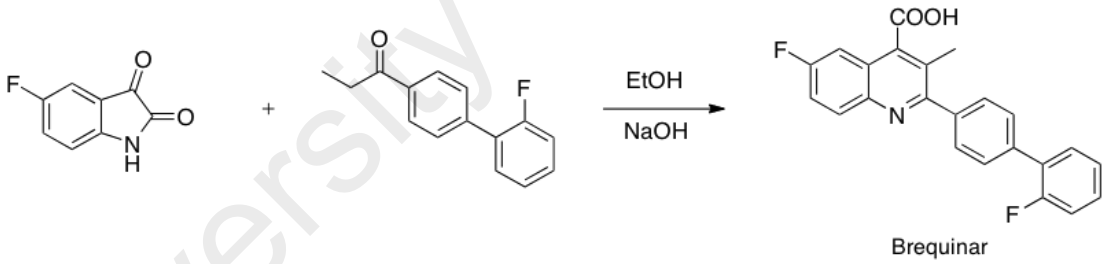

Scheme 1.2. Synthesis of Brequinar.

It is a small molecular weight inhibitor for DHODH, which has gone through clinical development with an IC_{50} of 12 nM (Erra *et al*., 2011). Reports showed that brequinar has two major contributions in the binding of the family-2 DHODH at the highly variable tunnel of N-terminus site, which is polar and hydrophobic (Hurt *et al*., 2006). Originally, organ transplant rejection therapy was the main cause of the drug development, but directions towards cancer therapy were then pursued as brequinar showed potential immunosuppressive and antiproliferative activities by inhibiting

DHODH (Allison, 2000). Other potential applications exhibited by brequinar are for the treatment of rheumatoid arthritis (RA) and psoriasis (Batt *et al*., 1998). Unfortunately, this compound failed in clinical trials due to its narrow therapeutic window, where oral administration leads to toxic effects (Baumgartner *et al*., 2006).

1.8 Benzimidazole

Generally, benzimidazole (Figure 1.6) is an organic bicyclic hetero compound that is made up from the fusion of a benzene connected to 4th and 5th position of an imidazole ring (Tonelli *et al*., 2010). It is classified as amphoteric substance with its acid dissociation constant (pKa) value at 12.8 for benzimidazole and 5.6 for conjugate acid. It is also known as 1,3-benzodiazole that has both basic and acidic characteristics, whereby the presence of free NH group serves as both a strong acid and a weak base. Another feature of this benzimidazole is its capability of forming salt formation (Wright, 1951).

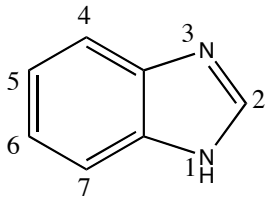

Figure 1.6. Structure of benzimidazole.

The first benzimidazole synthesis was discovered by Hobrecker in 1872 (Hobrecker, 1872) where he obtained tautomers of 2,5- and 2,6-dimethylbenzimidazole, **b**, by reducing 2-nitro-4-methylacetanilide, **a** (Scheme 1.3), and found this scaffold to be a pre-eminent structure (Gaba, Singh, & Mohan, 2014).

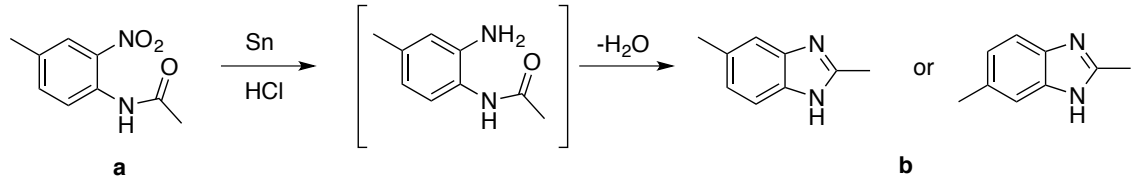

Scheme 1.3. Synthesis of benzimidazole by Hobrecker in 1872.

The hydrogen that is attached to the nitrogen at the first position is readily tautomerised as shown in Figure 1.7, where certain derivatives may appear, as isomers but are actually tautomers in reality. Isomeric form exists when larger groups compared to hydrogen are present, attached to the first position of the nitrogen. In addition, the hydrogen at the first position seems to be acidic enough to give N-metal benzimidazole compound which was first reported by Bamberger and Lorenzen and later by various other organizations with various metals (Wright, 1951).

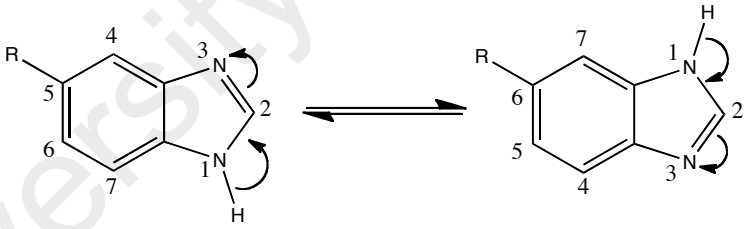

Figure 1.7. Tautomerisation of benzimidazole.

In nature, *N*-ribosyl-dimethylbenzimidazole exists as the most prominent compound that serves as an axial ligand for cobalt in vitamin B_{12} (Ramanpreet *et al*., 2011). A general method for obtaining benzimidazole compounds is by reacting 1,2-diaminobenzenes with carbonyl-containing compounds, such as aldehyde, carboxylic acid and others under strong acidic condition such as polyphosphoric acid, hydrochloric acid, *p*-toluenesulfonic acid or boric acid (Scheme 1.4). The use of Lewis acids, mineral

acids, or even inorganic clays in this reaction improved yield, as well as purity (Ingle & Magar, 2011).

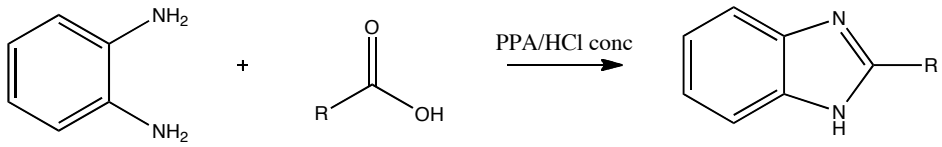

Scheme 1.4. General reaction of benzimidazole.

The emergence of benzimidazole and its derivatives in medicinal chemistry may be accounted by their significantly privileged structures due to the diversity of the compounds in various therapeutic applications (Gong *et al*., 2014), such as antitumor (Wang *et al*., 2014), antiviral, anticancer, antimicrobial (Seenaiah *et al*., 2014), antihypertensive (Yang *et al*., 2014), anxiolytic (Chen *et al*., 2014), antihistaminic agents (Tonelli *et al*., 2010) and others.

1.9 *In-silico* Design for PARP-1 and DHODH Enzymes Inhibitors

Various organizations have independently reported extensive *in-silico* design for both PARP-1 and DHODH enzyme inhibitors. Back in the 1980's, 3-aminobenzamide (IC_{50} = 30 μM), synthesized by Purnell and Whish, along with nicotinamide (IC_{50} = 210 μM) as basic competitive inhibitor gave insights into the modern pharmacophore improvisation techniques for designing more potent PARP-1 inhibitors (Purnell & Whish, 1980). More refined work was further done by others, demonstrating that potency of PARP-1 inhibition would be beneficial by restricting the degree of freedom of amide moiety (Banasik & Ueda, 1994). Later on, imidazole and benzoxazole carboxamide were introduced by Griffin and Golding where intramolecular hydrogen

bond formed between the primary amide and the nitrogen of the imidazole, created a 'pseudo-ring' (Griffin *et al*., 1995) benzimidazole carboxamide core, exhibiting improved potency (IC_{50} = 95 nM) (White *et al*., 2000). Langlier and Pascal reported on the role of PARP-1 to a damaged DNA by utilising the zinc fingers as detectors, based on crystal structure (Langelier & Pascal, 2013). X-ray co-crystal structure of PARP-1 with known PARP inhibitors, such as nicotinamide, 3-aminobenzamide and veliparib (ABT-888), showed similar H-bond networks as the substrate of NAD^+ in the nicotinamide binding pocket, as shown in Figure 1.8 (Zhu *et al*., 2013).

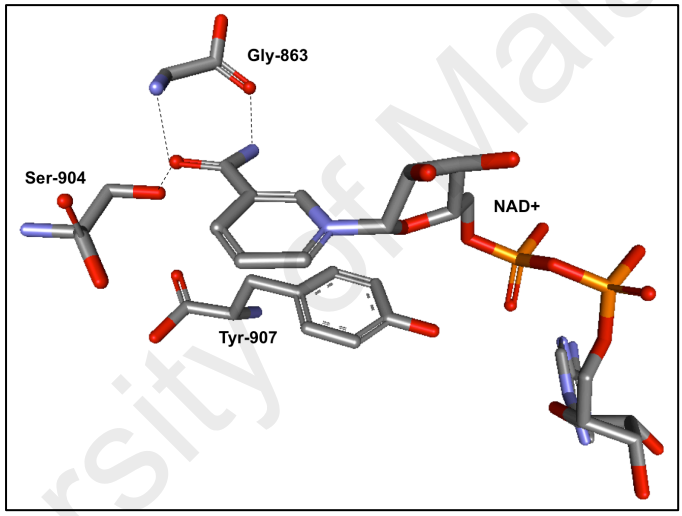

Figure 1.8. Interactions of NAD^+ in the active site of PARP-1 enzyme. Hydrogen bonds are shown in dashed lines.

The key interaction is the three hydrogen bonds donors-acceptors, formed between the carboxamide group of the inhibitor core and two amino acids designated Ser-904 and Gly-863, in the catalytic domain of PARP-1 (Ferraris e*t al*., 2003). In addition, π- π stacking interaction with Tyr-907 was also involved (Penning e*t al*., 2008). In some cases, conserved water molecule may or may not act as a H-bond mediator between Glu-988 and inhibitor (White e*t al*., 2000; 2004). Increment of the inhibitor potency was due to a certain location of the heteroatom in the benzimidazole scaffold, creating network with the residue (Ferraris e*t al*., 2010)**.** Another interesting feature of the NAD^+

binding pocket is the advantageous adenine-ribose binding site. It is a large hydrophobic pocket that is adjacent to the nicotinamide binding site where improvement in solubility, potency and other pharmacology properties can be further exploited for improvement (Kinoshita e*t al*., 2004).

In the case of DHODH, particularly for human DHODH (*Hs*DHODH), brequinar, leflunomide and teriflunomide (A771726) exhibited immunosuppressive and antiproliferative activities (Kim, Na, & Löffler, 2003; Cowen e*t al*., 2010). Later on, these compounds were further developed for use as cancer therapy. However, they failed in clinical trials due to limited therapeutic potentials (Davies e*t al*., 2009). Nonetheless, leflunomide has been marketed for more than 10 years for the treatment of rheumatoid arthritis treatment (Munier-Lehmann e*t al*., 2013). Brequinar, however is a known non-competitive inhibitor for DHODH (Breedveld & Dayer, 2000).

The first co-crystallization of *Hs*DHODH complexed with brequinar analogue inhibitor, was reported in August 2000 (Liu e*t al*., 2000). The *Hs*DHODH consist of two domains, a small N-terminal and a C-terminal that are connected by an extended loop. The location of brequinar and its analogue in the *Hs*DHODH were located in the ubiquinone binding site where polar and hydrophobic predominant promotes to the binding (Fritzson e*t al*., 2010). The head-group structure of brequinar, 6-flouro-3-methyl-4-quinoline carboxylic acid binds deep in the polar region and the aromatic rings, the tail-end extends out in the hydrophobic region of the binding site (Liu e*t al*., 2000). The key interaction between the inhibitor and the enzyme is the carboxylate group of the quinoline, creating well oriented H-bonds to Arg-136 residue. In addition, hydrogen bond between Gln-47 and the carboxylate were also found. Hydrophobic

contacts between nine residues and the biphenyl ring of the inhibitor were also observed in Figure 1.9 (Baumgartner e*t al*., 2006).

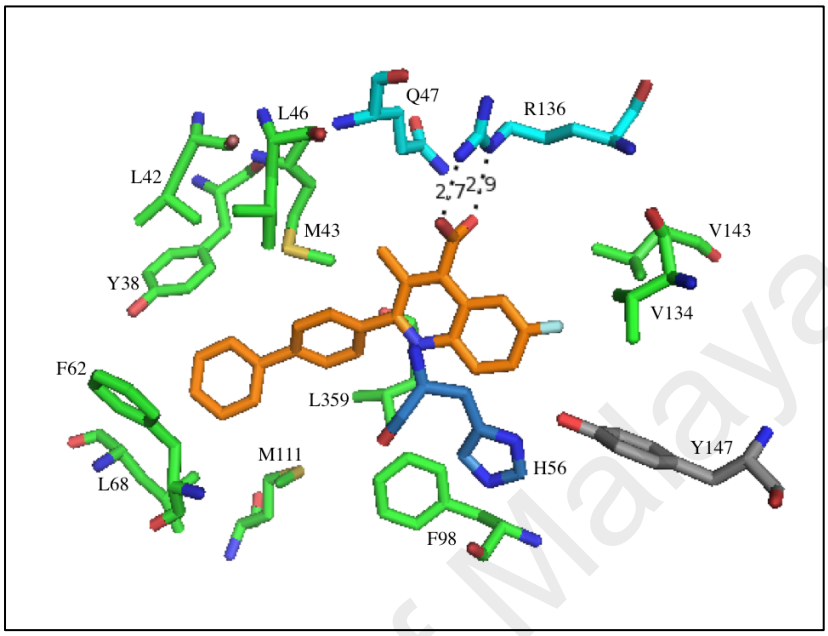

Figure 1.9. Brequinar analogue binding mode in human DHODH showing the contributing residues in the binding site. Cyan residues show electrostatic interaction, Green stick residues represent hydrophobic interactions and light blue indicates aromatic stacking.

The inhibitor binding site shows amphipathic features. Entrance of the cavity mostly consists of hydrophobic amino acids and polar surroundings at the inner end of the cavity with Val-143 and Val-134 forming small hydrophobic pocket (Baumgartner e*t al*., 2006; Hurt e*t al*., 2006). The natural substrate, ubiquinone, also binds in the same region that the head group very well overlays each other, thus showing a similar binding mode (Liu e*t al*., 2000).

In this work, *in-silico* design has been proposed and carried out by Aurigene Discovery Technologies Limited, Bangalore, India. Using veliparib and brequinar as reference for PARP-1 and DHODH inhibitors, respectively, Aurigene has developed a series of compounds that retains the benzimidazole as basic scaffold, and generated new

pharmacophore features at the second, fourth and sixth position of the scaffold, essential for inhibition improvement. Starting from 2-([1,1'-biphenyl]-4-yl)-1H-benzoimidazole-4-carboxamide, **I1** (Thunuguntla e*t al*., 2010), the compound was docked with the binding mode resemblance to brequinar (Figure 1.10) and an IC_{50} value of 0.75 µM.

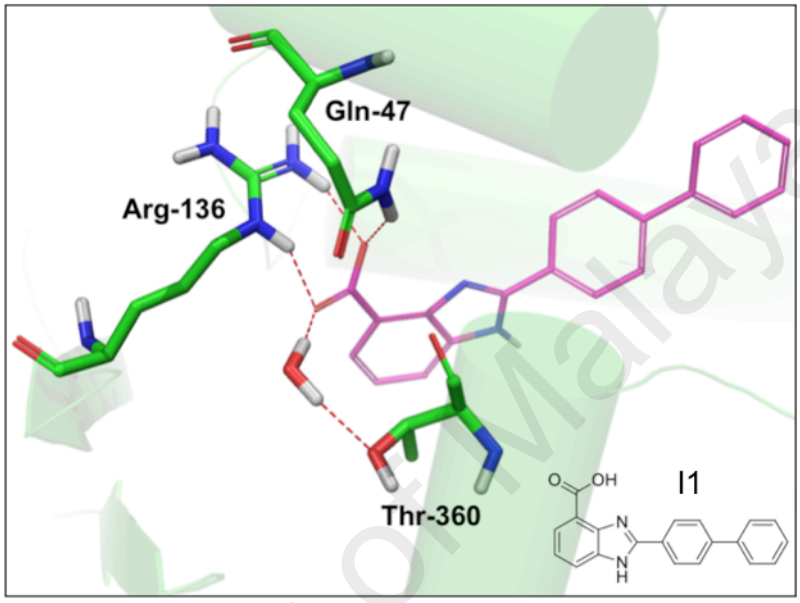

Figure 1.10. Binding mode of compound **I1** in DHODH (pdb ID: 41GH) showing interactions with Arg-136 and Gln-47. Also a water mediated interaction with Thr-360 is observed.

This result postulates the consistency of what other organizations have proposed and reported. The latter (compound **I1**) were then optimized for better potency and drug properties for both PARP-1 and DHODH.

1.10 Scope and objective of this thesis

Due to its vast prominent features in medical treatment in various diseases, benzimidazole based compounds have been the object of many studies for more than three decades. Amongst the activities shown by these compounds are included

anticancer, antihypertensive and immunosuppressive effects. Nonetheless, other scaffolds also showed potential therapeutic benefits towards the same goal. Known compounds have reached clinical trials but failed due to limited therapeutic window, and there are no natural products, which are reported as potent inhibitors for PARP and DHODH enzymes. The aim and objectives of this study are as follow:

I. Design and synthesis would be an alternative way to explore new compounds to generate hits-to-lead since treatment at the level of DNA would notably be worth investigating.
II. No reports up to now showed dual inhibition of these two enzymes. Thus, the aim is to develop compounds with better potency to enhance the drug properties.
III. The objective of present study is to design and synthesise a series of benzimidazole compounds as dual inhibitors of PARP-1 and DHODH enzymes and to investigate their therapeutic activities.

CHAPTER 2: SYNTHESIS OF BENZIMIDAZOLE

2.1 Introduction to Benzimidazole Synthesis

As described in the earlier chapter, benzimidazole shows a wide range of therapeutic effects in other applications, such as fungicide-pesticide (Ma, Yoshimura, & Michailides, 2003; Boubaker, 2008; Malandrakis, Markoglou, & Ziogas, 2011), and as anthelmintic (Baliharová e*t al*., 2003; Ancheta e*t al*., 2004). Hence, there are many works that have been carried out by various organisations to develop more potent and diversified benzimidazole derivatives.

The first benzimidazole compound was synthesised by Hobrecker (Hobrecker, 1872). Currently, there are several methods that are commonly used to produce benzimidazole; condensation reaction between 1,2-diaminobenzene as starting material with a carboxylic acid or an aldehyde, Schiff bases, pseudo bases and others (Wright, 1951).

Unfortunately, condensation reaction between 1,2-diaminobenzene as starting material with either a carboxylic acid or an aldehyde had their disadvantages. For the coupling of 1,2-diaminobenzene with a carboxylic acid, strong acidic condition and high temperature are required. While condensation of 1,2-diaminobenzene with aldehyde involves dehydration, requires stoichiometric amount of oxidising agent. Often, regioisomers and disubstituted side products are obtained from this reaction (Kim e*t al*., 2011). Over the years, the synthesis of benzimidazole have evolved and expanded with little modification to produce higher product yield, shorter reaction time and better selectivity of the scaffold.

Scheme 2.1 shows a reported one-pot synthesis of 2H-benzimidazole derivatives, using heterocyclic 2-nitroamines as substrate, and iron as the reductant (Hanan e*t al*., 2010).

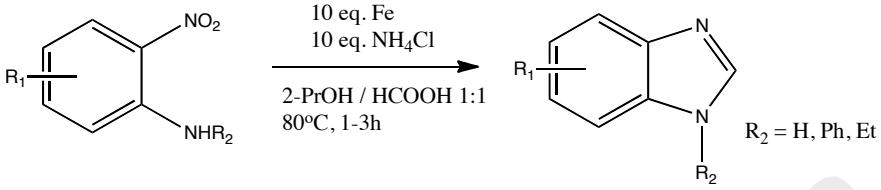

Scheme 2.1. General method for a one-pot synthesis of aromatic and heteroaromatic 2-nitroamines to bicyclic 2H-imidazoles (Hanan e*t al*., 2010).

In this method, formic acid, in combination with isopropanol was used as the solvent and the formic acid acts also as the source of methylene for Phillips cyclisation to occur. Optimum condition were established using 10 equivalents of iron and 10 equivalents of ammonium chloride, as additive to reduce the nitro group, to produce more than 95% pure product, following an aqueous workup with no further purification (Hanan e*t al*., 2010).

Nannapaneni and co-workers reported the synthesis of benzimidazole using ammonium chloride, an inexpensive and commercially available compound as catalyst, in the condensation of 1,2-diaminobenzene and an aldehyde to give excellent yield under ambient temperature as shown in Scheme 2.2 (Nannapaneni e*t al*., 2010).

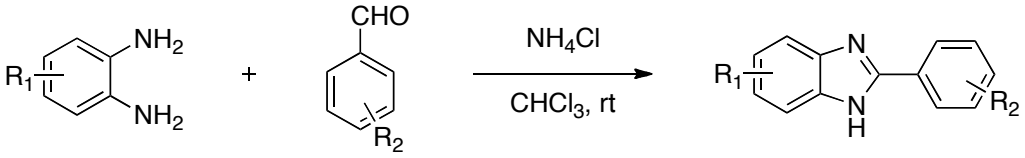

Scheme 2.2. Synthesis of 2-arylbenzimidazole catalyzed by ammonium chloride.

Solvent and catalyst-free redox reaction between aliphatic amine and *ortho*-amine/mercaptan/hydroxyl anilines were developed by Nguyen Thanh Binh and co-workers in their effort to develop a "green" condition to produce benzazoles. Here, elemental sulfur was used as traceless oxidising agent under moderate temperature (Scheme 2.3**)** (Nguyen e*t al*., 2012).

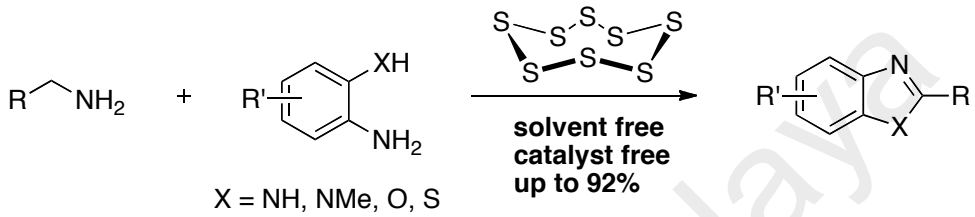

Scheme 2.3. Benzazole general reaction with elemental sulfur as traceless oxidising agent.

Sulfur was chosen as the oxidising agent in place of oxygen due to its low reactivity at ground state, as well as for being non-toxic, readily available, and stable under normal conditions with low explosion rate. In addition, chemoselectivity was observed in the reaction although no metal catalyst was involved. This oxidative coupling reaction to form benzimidazole provided moderate to excellent yield (70-92% isolated yield) which is advantageous for large scale synthesis, presumably with lower environmental pollution (Nguyen e*t al*., 2012).

Jinsong Peng and co-workers (Peng e*t al*., 2011) developed an intramolecular N-arylation reaction to construct the benzimidazole scaffold through a C-N cross coupling reaction catalysed by copper instead of the more expensive palladium, or the highly toxic nickel as the catalyst. Five mol percent of catalyst loading in combination with 1,2-bis(methylamino)ethane (DMEDA), and 2 equivalents potassium carbonate in water at 100^{o}C was found to be optimum to produce the benzimidazole in relatively good yield (Scheme 2.4).

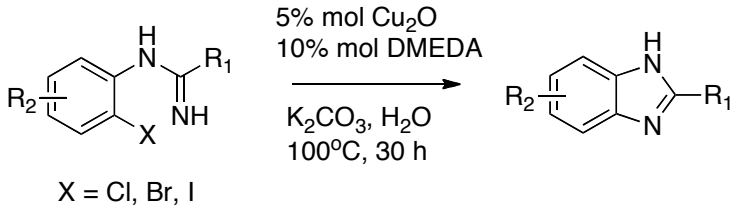

Scheme 2.4. Copper catalyzed benzimidazole formation in base-aqueous condition.

The use of water in this reaction, along with the cheap copper catalyst provides environmental and economical advantages for the production of large number of benzimidazole libraries (Peng e*t al*., 2011).

Another convenient method to produce benzimidazole was reported by Penning and co-workers, Tong and co-workers and Xue and co-workers through a peptide coupling reaction. Reaction of the 2,3-diaminobenzamide with carboxylic acid and 1,1'-carbonyldiimidazole (CDI) as the coupling reagent, followed by acid-promoted cyclisation under reflux (Scheme 2.5), gave good to excellent yield of the benzimidazole product (Penning e*t al*., 2008, 2009, 2010; Tong e*t al*., 2009; Xue e*t al*., 2011).

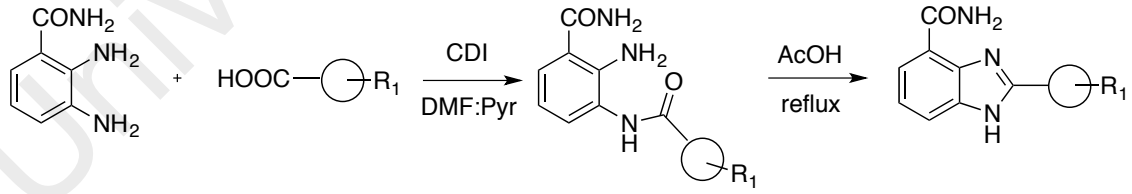

Scheme 2.5. Benzimidazole synthesis from peptide coupling.

In a similar approach, benzimidazole was synthesised by Jufang H. Barkalow and co-workers (Scheme 2.6), by reacting 1,1'-carbonyldiimidazole (CDI) with 1-methyl-2-pyrrolidone (NMP) and piperidine acid to produce acylimidazole, which was subsequently combined with 2,3-diaminobenzamide under moderate heat to give the

hydrochloride salt amide intermediate with excellent yield and high purity. The salt then underwent cyclisation under water-acetic acid condition to give the succinate salt of benzimidazole which was then crystallized with isopropyl acetate-methanol (Barkalow e*t al*., 2007).

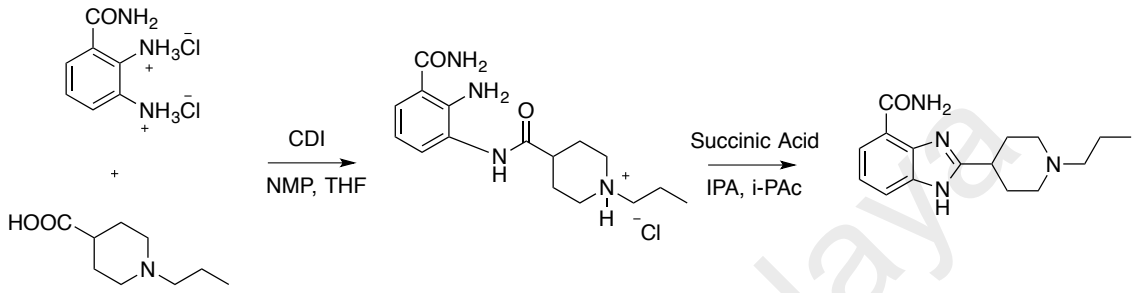

Scheme 2.6. Synthesis of 2-(1-Propyl-4-piperidinyl)-1H-benzimidazole-4-carboxamide Succinate Salt via the acylimidazole route (Barkalow e*t al*., 2007).

In another approach, acylation of methyl 2,3-diaminobenzoate with an acid chloride in the presence of tertiary amine and 4-dimethylaminopyridine (DMAP) as the catalyst provides the intermediate **A,** which subsequently underwent cyclisation under acidic condition with acetic acid to give the desired benzimidazole **B** (Scheme 2.7) (White e*t al*., 2000). However, this method was found to be inefficient and not applicable as a general route.

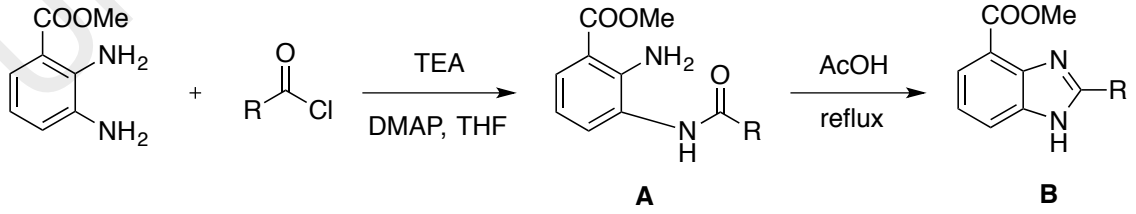

Scheme 2.7. Acylation reaction towards benzimidazole synthesis.

It was later modified by Weidenhagen using either 2,3-diaminobenzoic acid or 2,3-diaminobenzamide with an aryl aldehyde as starting material and copper (II) acetate as

catalyst to give the benzimidazole product, as illustrated in route I in Scheme 2.8 (White e*t al*., 2000).

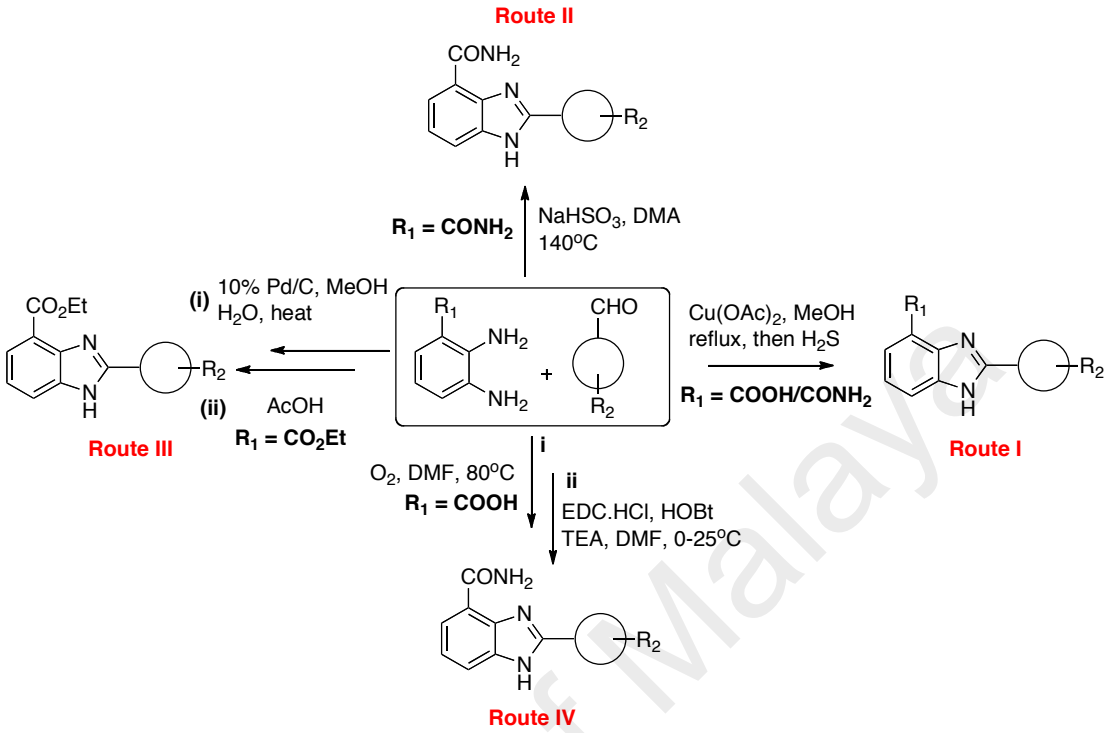

Scheme 2.8. General strategy for the syntheses of benzimidazole scaffold.

As outlined in route II of Scheme 2.8, White and co-workers discovered that heating 2,3-diaminobenzamide with the aryl halide in *N,N*-dimethylacetamide (DMA) and sodium hydrogen sulfite ($NaHSO_3$) also produced the desired benzimidazole derivatives (White e*t al*., 2004). Route III (Scheme 2.8) illustrates the synthesis of benzimidazole compounds from 2,3-diaminobenzamide and pyridine-containing aryl aldehyde catalyzed by palladium-on-carbon (Pd/C) catalyst (Penning e*t al*., 2010), while in route IV (Scheme 2.8), 2,3-diaminobenzoic acid was heated in dimethylformamide (DMF) with the aldehyde to furnish the benzimidazole intermediate in which the carboxylic acid head group was converted into the carboxamide with EDCI.HCl / HOBt as the desired product (Xue e*t al*., 2011).

Apart from the main skeleton of benzimidazole, various substituents at the second position of the benzimidazole ring also play critical role in determining the bioactivity of the benzimidazole compounds. Benzimidazole side-chain preparation have been abundantly reported, some of which will be described in the next section.

2.2 Boronic acid and Miyaura Borylation

Borylation reaction is a reaction that converts an activated carbon-hydrogen bond, both aliphatic and aromatic, to a carbon-boron bond, usually catalysed by transition metal catalyst (Hartwig, 2011). Boronic acids (Figure 2.1) (Wu, Neumann, & Beller, 2010) and boronate esters, mainly bis(pinacolato)diboron (Figure 2.2), are common compounds extensively used as the source of boron in Suzuki coupling reactions. These boronic compounds are used mainly due to the ease of transmetalation particularly with organopalladium compounds (Miyaura & Suzuki, 1995).

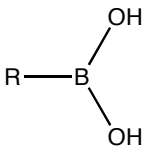

Figure 2.1. General structure of boronic acid.

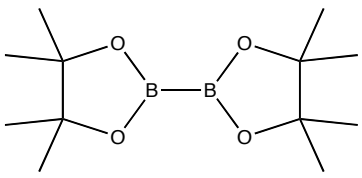

Figure 2.2. Structure of bis(pinacolato)diboron.

2.3 Miyaura-Suzuki Coupling

Miyaura-Suzuki Coupling is considered to be one of the recognized reactions in chemistry, which provides carbon-carbon bond formation, that serves as key steps in building many complex molecules (Suzuki, 1992, 2002). As illustrated in Scheme 2.9, this reaction can be performed either by using (4-(methoxycarbonyl)phenyl)boronic acid with tert-butyl 2-chloro-1H-pyrrole-1-carboxylate, or methyl 4-bromo-2-fluorobenzoate with (1-(tert-butoxycarbonyl)-1H-pyrrol-2-yl)boronic acid in the presence of palladium as catalyst and base (Ishida e*t al*., 2006; Penning e*t al*., 2010).

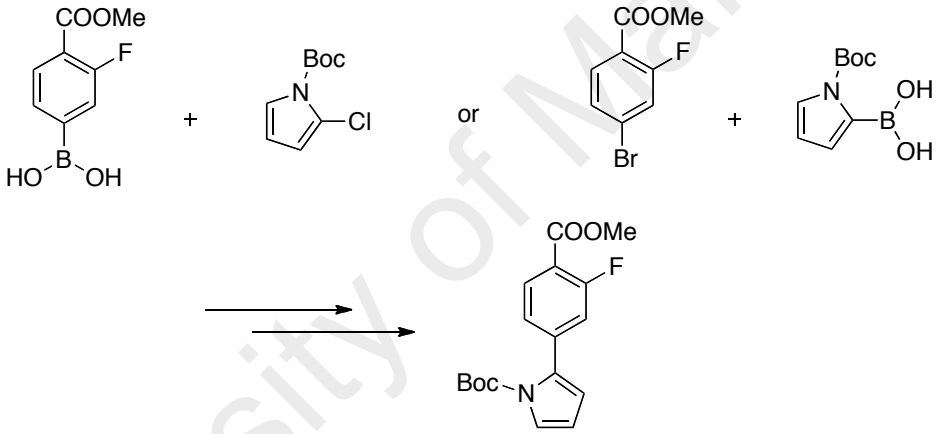

Scheme 2.9. Carbon-carbon bond formation via Suzuki coupling reaction.

Boronate ester serves as an alternative boron source in the Suzuki coupling reaction where bis(pinacolato)diboron is widely used in a palladium complex-catalysed reaction (Scheme 2.10) (Miyaura & Suzuki, 1979, 1995; Miyaura, Yamada, & Suzuki, 1979).

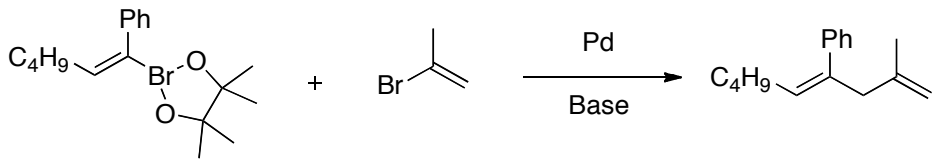

Scheme 2.10. Boronate ester used as starting materials in Suzuki Coupling.

2.4 Amide Coupling Reaction

Amides and peptides compounds are common features in natural products as well as in many bioactive synthetic compounds. Carboxamide in particular, appears to be important in functional group in bioactive compounds due to its stability, neutrality and hydrogen-bond donor acceptor capability (Montalbetti & Falque, 2005). Thus, methods and strategies towards amide formation reaction have been growing tremendously to enhance its applications and addressing its challenges (Han & Kim, 2004).

One general distinctive amide coupling reaction involves activation of a carboxylic acid moiety and an amine moiety, as shown in Scheme 2.11 (Valeur & Bradley, 2009).

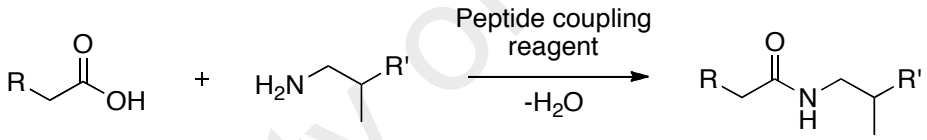

Scheme 2.11. Amide bond formation via coupling reagent reaction.

Carboxamide can also be produced in high yield from carboxylic acid through a reaction with ammonium chloride and EDCI with HOBt as additive in the presence of Hunig's base, as shown in Scheme 2.12 (Wang & McMurray, 1999; Gruver e*t al*., 2008; Kalgutkar e*t al*., 2008).

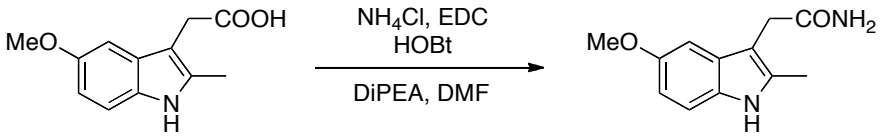

Scheme 2.12. Conversion of carboxylic acid moiety to carboxamide.

There is an abundance of coupling reagents to generate amide bonds ranging from aminiums, carbodiimides, phosphoniums, uroniums, and others reported such as dicyclohexylcarbodiimide (DCC), *N,N′*-diisopropylcarbodiimide (DIC) (Valeur & Bradley, 2009), 1-ethyl-3-(3-dimethylaminopropyl)carbodiimide (EDCI.HCl) (Nakajuma & Ikada, 1995), 1-hydroxybenzotriazole (HOBt) (Carpino, 1993), and 1-[bis(dimethylamino)methylene]-1H-1,2,3-triazolo[4,5-b]pyridinium 3-oxide hexafluoro phosphate (HATU) (Figure 2.3) (Albericio, 2004).

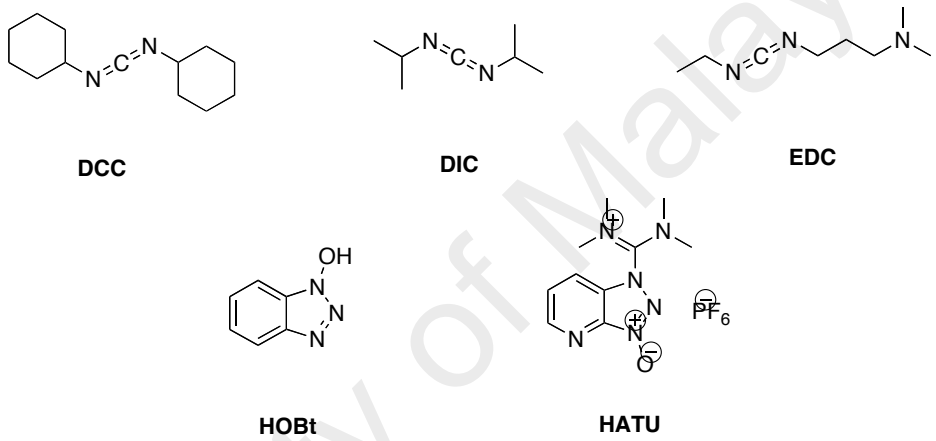

Figure 2.3. Common coupling reagents available in amide bond reaction.

2.5 Nitro Reduction

Arylnitro compounds can be reduced to arylamine compounds. Countless methods have been reported on this reduction process. Mild nitro reduction conditions with high yield reaction have been employed by Kroemer and co-workers using zinc dust in aqueous medium, as illustrated in Scheme 2.13 (Kroemer e*t al*., 2006).

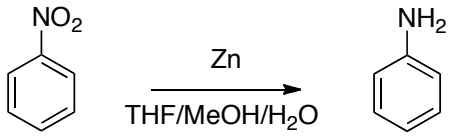

Scheme 2.13. Aryl nitro reduction to aryl amine.

In a similar manner, as shown in Scheme 2.14, Gamble and co-workers reported an attractive approach to aryl nitro reduction by ultrasonic irradiation using iron as reducing agent under acidic condition. The desired aryl amine was obtained in a shorter reaction time (Gamble e*t al*., 2007).

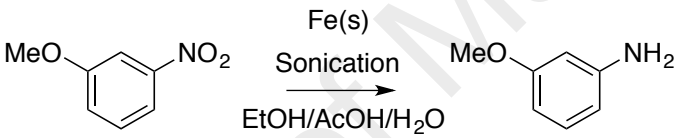

Scheme 2.14. Aryl nitro reduction via sonication reaction.

CHAPTER 3: DESIGN OF HITS-TO-LEAD BENZIMIDAZOLE

3.1 Molecular Docking

Veliparib and brequinar are two drugs that work independently on PARP-1 and DHODH enzymes, respectively. Using information on these two drugs such as their interactions with residues of both enzymes would be viable in designing a new drug that can act as a dual inhibitor towards both the PARP-1 as well as the DHODH enzymes. The approach that we have taken in our attempt to design a compound that could be a potential inhibitor for both DHODH and PARP-1 involves molecular docking, synthesis of the compounds and subsequent screening for their activities, as depicted in Figure 3.1.

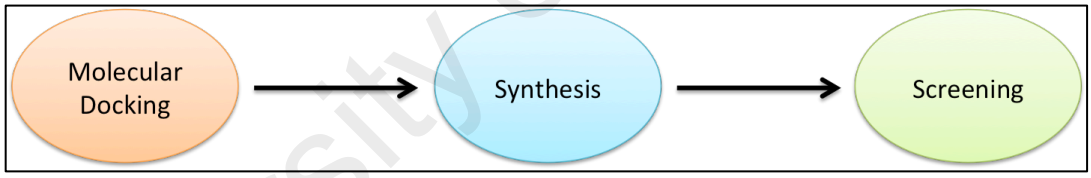

Figure 3.1. Workflow of project for PARP-1 and DHODH dual inhibitors.

3.2 Molecular Docking Methodology

The molecular docking studies of PARP-1 and DHODH were done at Aurigene Discovery Technologies Ltd, Bangalore, India. Here, 2D structures of the ligands were sketched using ChemBioDraw Ultra 12.0 program and then converted into their 3D format with the *LigPrep* utility of Schrodinger Software Suite 2014-1. Similarly the protein-ligand complexes, obtained from the Protein Data Bank in the pdb format (pdb ID: 4IGH for DHODH and 4HHZ for PARP-1), were prepared using the *Protein Preparation Wizard* utility of the software. The hydrogen atoms were added, bond

orders assigned, missing side-chains filled, and water molecules outside the active site deleted. Restrained minimization was done on the structures to relieve the strain and steric clashes that may occur in the protein-ligand complexes.

Using the *Glide* module of the Schrodinger Software, the active site was defined by constructing a receptor grid spanning amino acid residues within a distance of around 10Å from the co-crystallized ligand in the protein complexes. Some key hydrogen-bonding constraints (like with residues Gln-47 & Arg-136 in DHODH and with Gly-202 & Ser-243 in PARP-1) were also defined while generating the receptor grid to be employed in the protein-ligand docking.

The prepared ligands (in sdf format) and protein structures (as receptor grids) were supplied as input to the *Glide* module of the software for docking. During *Glide* docking, extra precision (XP) mode was employed. The protein was kept as rigid, while the ligands were given full flexibility in addition to sampling nitrogen inversions and ring conformations. However, the amide torsions were restricted to the trans-conformation only. Other parameters include adding *Epik* state penalties to docking score, rewarding intramolecular hydrogen bonds, and enhancing planarity of the conjugated pi groups. The docking protocol was set to report at least 10 poses per ligand, which were finally viewed and analyzed within the protein active site for desired interactions, using the *maestro* viewer of the Schrodinger Software Suite, or PyMol.

3.3 Molecular Docking Results on Known Inhibitors

Initial studies were conducted with known PARP inhibitors to obtain some structural insights. Eight known PARP inhibitors (Kinoshita e*t al*., 2004; Iwashita e*t al*., 2005;

Ishida e*t al*., 2006; Barkalow e*t al*., 2007; Donawho e*t al*., 2007; Miyashiro e*t al*., 2009; Gandhi e*t al*., 2010; Penning e*t al*., 2010) shown in Figure 3.2, were chosen and docked onto PARP-1 enzyme (pdb ID: 4HHZ), as illustrated in Figure 3.3 and Figure 3.4.

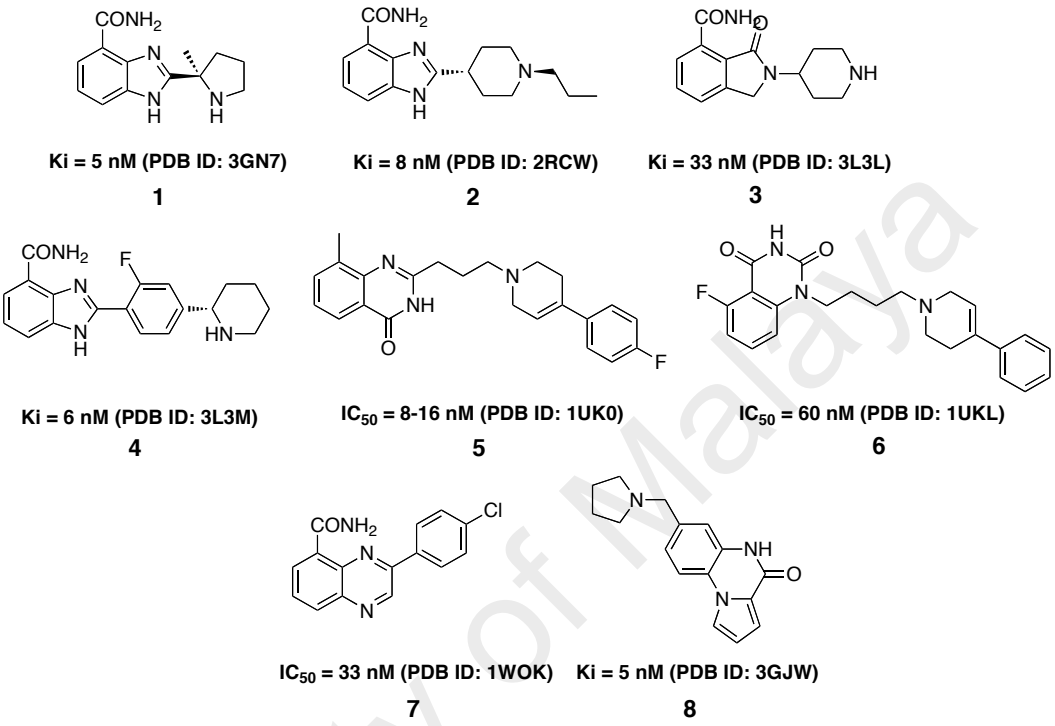

Figure 3.2. Structures of known PARP-1 inhibitors.

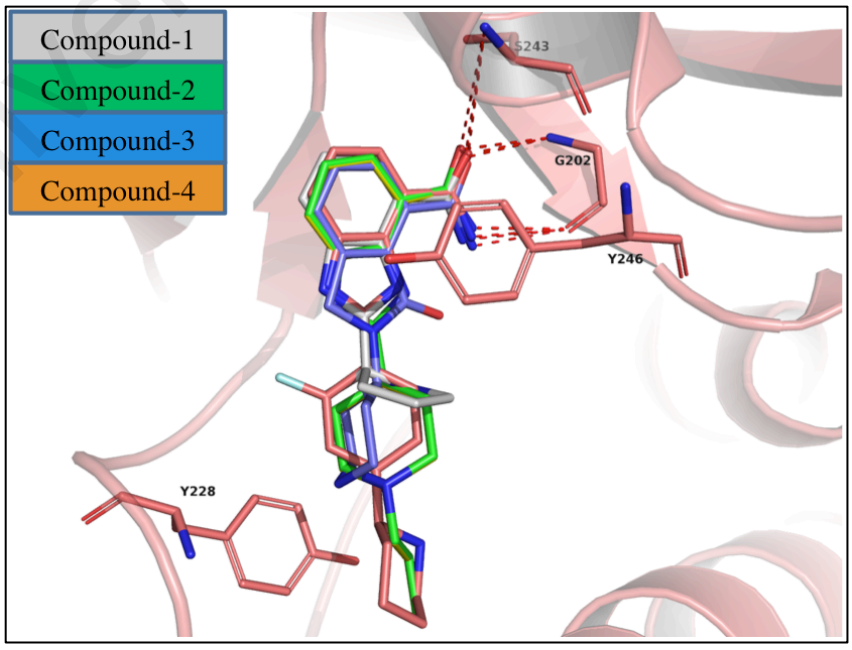

Figure 3.3. X-Ray co-crystal of compounds **1-4** overlaid on PARP-1 enzyme.

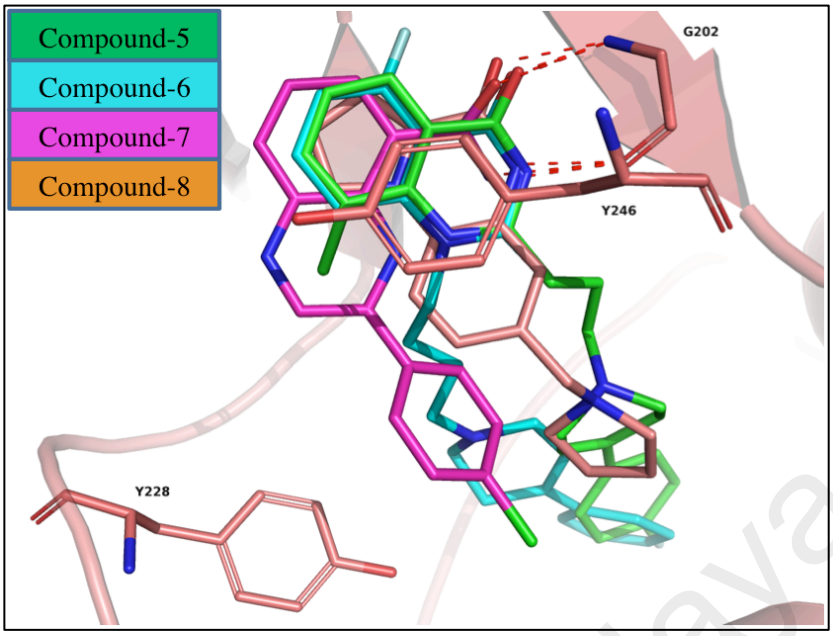

Figure 3.4. X-Ray co-crystal of compounds **5-8** overlaid on PARP-1 enzyme.

As for DHODH inhibitors, brequinar and compound **4Sc**, shown in Figure 3.5 (Leban e*t al*., 2004, 2005, 2006) were selected and docked inside DHODH enzyme (pdb ID: 4IGH) and superpositioned to one another as preliminary studies, as shown in Figure 3.6.

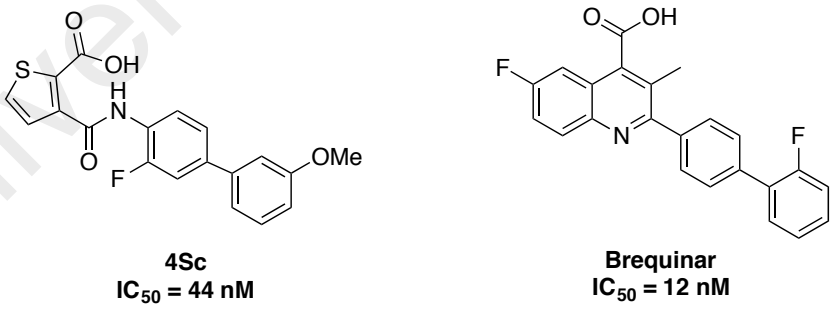

4Sc
IC_{50} = 44 nM

Brequinar
IC_{50} = 12 nM

Figure 3.5. Selected structures of known DHODH inhibitors of compound **4Sc** and brequinar.

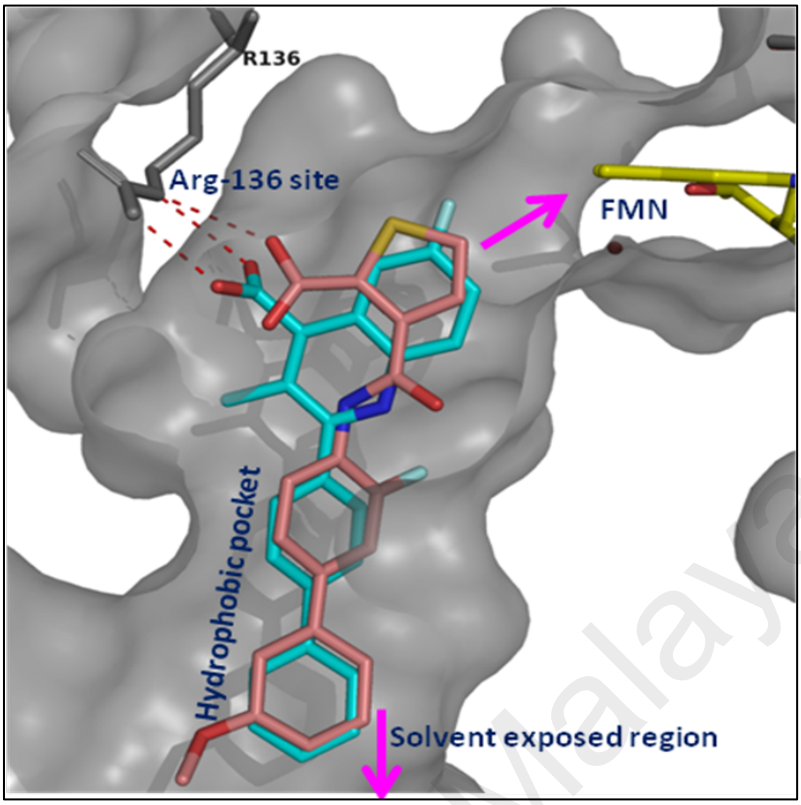

Figure 3.6. Binding mode of brequinar (cyan) and compound **4Sc** (orange) superimposed in DHODH enzyme (pdb ID: 4IGH).

3.4 Molecular Docking Discussion on Known Inhibitors

From the illustrations of Figure 3.3 depicted above, each compound **1**-**4** showed similar binding pose in the binding site of PARP-1 enzyme where the carboxamide of the benzimidazole scaffold creates three hydrogen bonds between two key amino acid residues Ser-243, (C=O to H-O Ser-243) and Gly-202 backbone, (C=O to N-H Gly-202 and N-H to C=O Gly-202) in the nicotinamide binding site. Also observed was π-π stacking interaction with Tyr-246 residue. Compounds **5**-**8** in Figure 3.4 showed only two hydrogen bonds with the amide backbone of Gly-202 amino acid residue, and π-π stacking interaction with Tyr-246 residue with each compound, demonstrating different poses in the catalytic site. A consensus pharmacophore has been disclosed in relation to become PARP-1 inhibitor (Costantino e*t al*., 2001; Tonelli e*t al*., 2004; Jagtap & Szabo,

2005; Zhu e*t al*., 2008; Refaat, 2010; Curtin & Szabo, 2013; Steffen e*t al*., 2013; Zhu e*t al*., 2013), as shown in Figure 3.7.

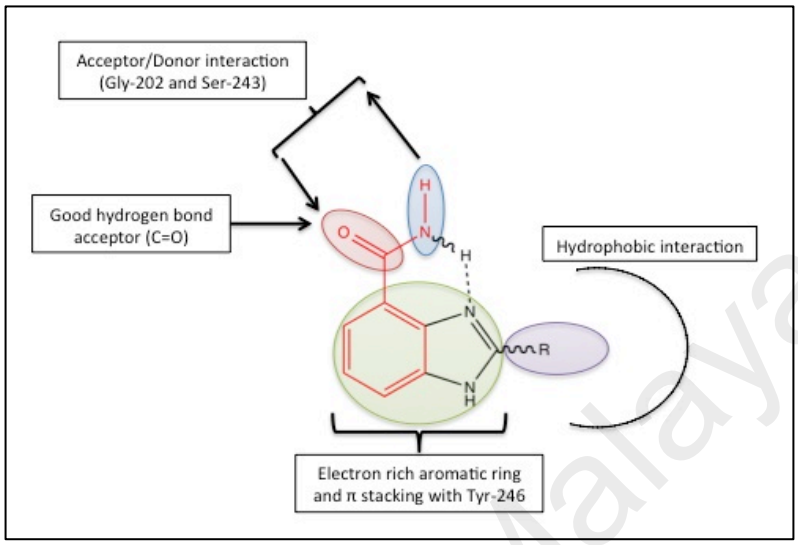

Figure 3.7. A consensus pharmacophore query for PARP-1 inhibitor.

Three key features were found to be optimal for PARP-1 binding, restricting the rotation of a carboxamide group attached at C-4 position with one NH locked achieved by intramolecular hydrogen bond, an aromatic ring and side-chain extended towards the hydrophobic region.

As in the binding mode of brequinar (discussed in previous section, Chapter 1), compound **4Sc** also adopts the "brequinar-like" conformation where carboxylic acid of the thiophene ring interacts with Arg-136 and Gln-47 residue side chains (Figure 3.7). However, it is likely that compound **4Sc** is capable of displaying a "nonbrequinar-like" conformation whereby hydrogen bond interaction with Tyr-356 and a water molecule mediated with Tyr-147 was observed when the thiophene ring were rotated at 180^{o} (Figure 3.8). This seems to suggest that compound **4Sc** exhibits a dual binding mode (Baumgartner e*t al*., 2006). In nature interactions between protein and ligand, identification of subsites can be explored. Each subsite (Figure 3.8) consists of specific

functional groups responsible, and could potentially be a stabiliser for interactions occurring with each functional group introduced by plausible inhibitor.

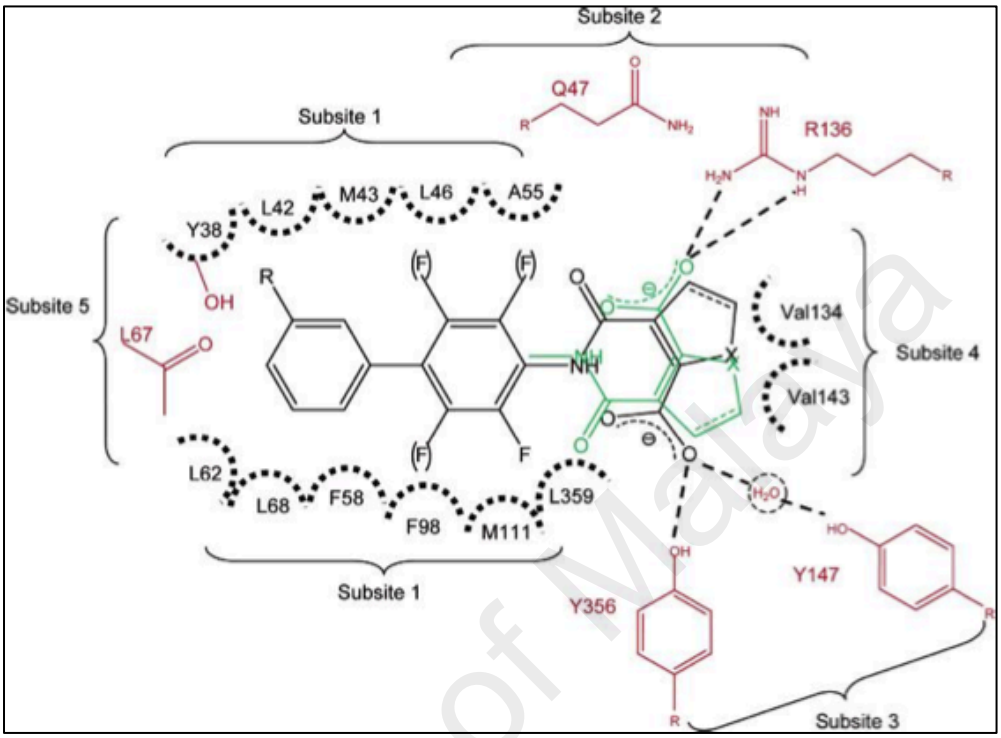

Figure 3.8. Five subsites of a DHODH inhibitor binding site. Black dotted lines in subsite one are mainly responsible for hydrophobic interactions where two more remotely hydrophobic site are located at subsite four of the binding pocket. Plausible hydrogen bond interactions are shown in black dashed lines found in subsite two and three. Subsite five is polar in nature anchored by hydroxyl group of Tyr-38 and Leu-62. Other alternative binding mode of the inhibitor is coded in green. Reprinted with permission (Baumgartner e*t al*., 2006).

From the information obtained, three important pharmacophores were outlined (Hansen e*t al*., 2004; Das e*t al*., 2013). They are; (i) free carboxylic acid of the quinolone/aromatic ring as the head group, (ii) potential electron withdrawing-donating effect on the quinolone/aromatic ring and (iii) side-chain extension towards the hydrophobic pocket.

Compound **I1** (Figure 3.9), developed by Aurigene Discovery Technologies Ltd. were then docked with DHODH enzyme (pdb ID: 4IGH) and the interactions were studied.

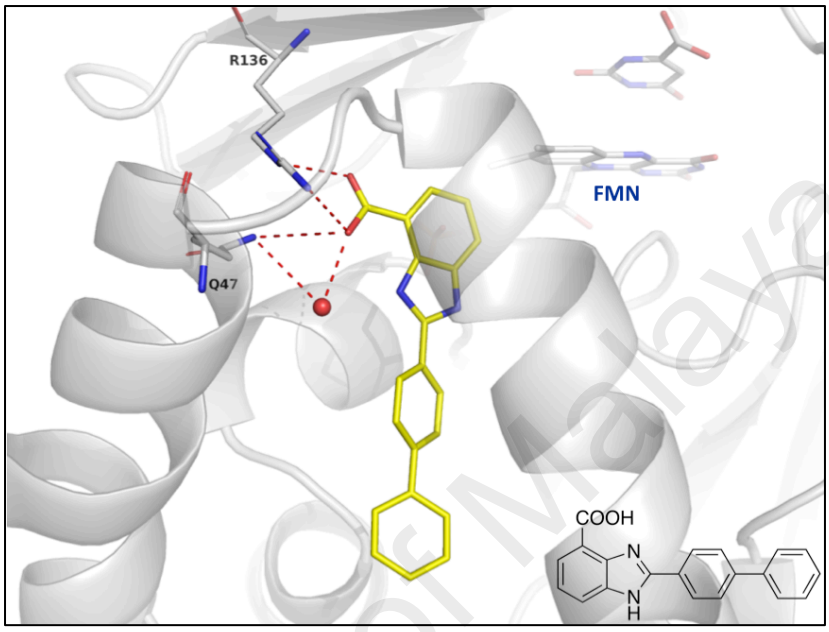

Figure 3.9. Binding mode of compound **I1** on DHODH enzyme (pdb ID: 4IGH).

Our findings demonstrate that the binding mode of compound **I1** substantially possess a 'brequinar-like' interactions and is located at the ubiquinone binding site with an IC_{50} value of 750 nM. The carboxylic acid head group of the inhibitor makes hydrogen bond interactions towards the back bone of Arg-136 and Glu-47 amino acid residues. Additional interactions with one water molecule were also observed, depicted as red circle in Figure 3.9.

As we come closer in understanding and obtaining better insights of the pharmacophores discussed, some similarities and close relationship between the PARP-1 and DHODH inhibitor pharmacophores can be observed. Both enzymes seem to be in need of electron rich aromatic ring and side-chain that extends out to the hydrophobic

pocket while only the head group either carboxamide in Veliparib or carboxylic acid in Brequinar differs in each particular inhibitor, respectively. With all the information gathered, the compounds, as depicted in Table 3.1, are proposed to serve as hits-to-lead in order to achieve our objective in searching for a dual inhibitor for PARP-I and DHODH. The compounds proposed to be synthesised and screened for their biological activity.

Table 3.1. Proposed compounds to be synthesised.

Entry	Compound	Structure
1	9a[a]	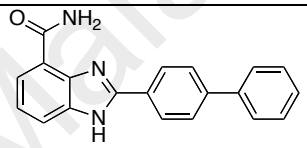
2	9b	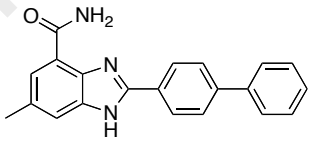
3	9c[b]	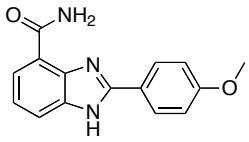
4	9d	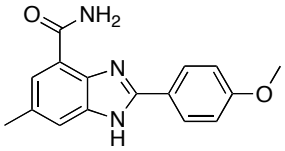
5	9e[b]	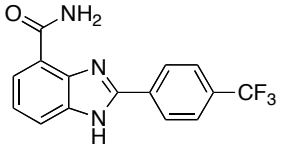
6	9f	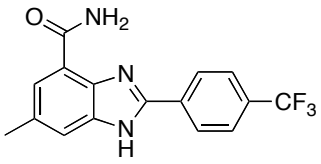

Table 3.1 continued

7	**9g**	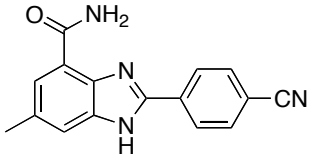
8	**9h**	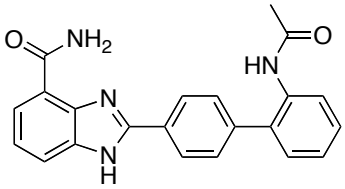
9	**9i**	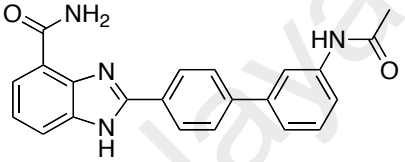
10	**9j**	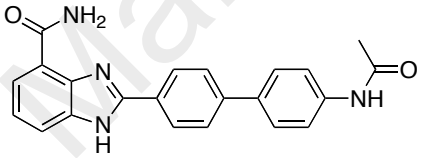
11	**10a**[a]	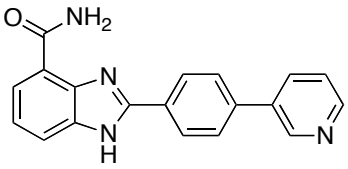
12	**10b**	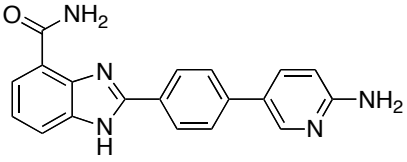
13	**10c**	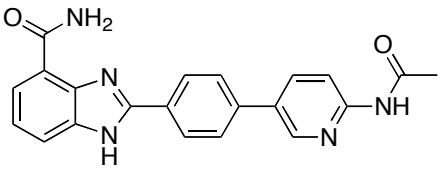
14	**10d**[a]	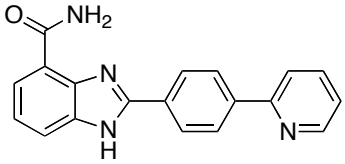
15	**10e**	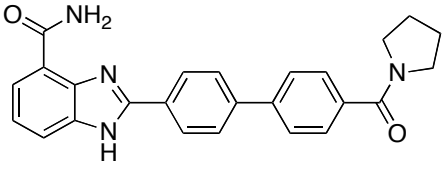

Table 3.1 continued

16	**10f**	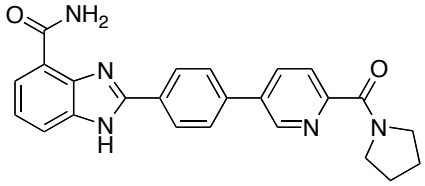
17	**10g**	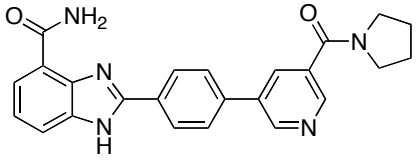
18	**10h**	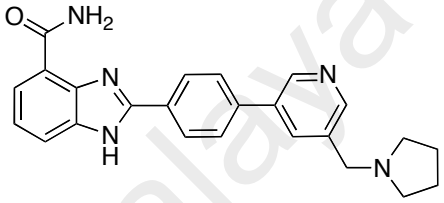
19	**11a**	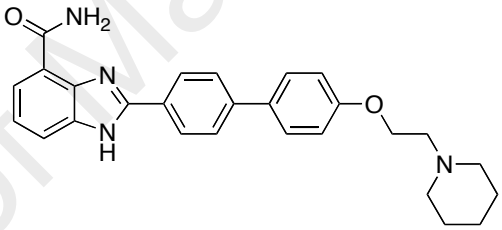
20	**11d**	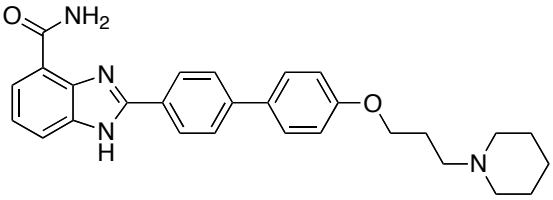
21	**11c**	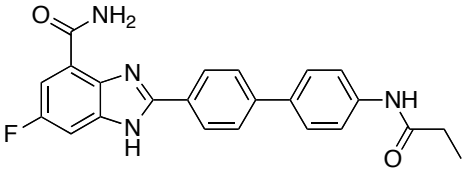
22	**11d**	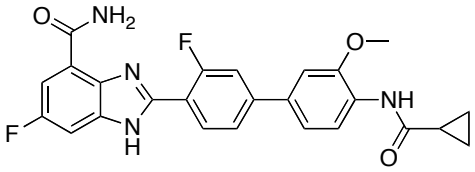
23	**11e**	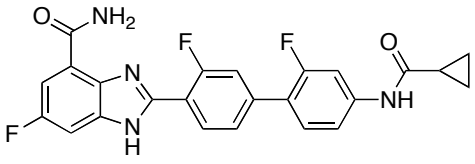

Table 3.1 continued

25	**7b**	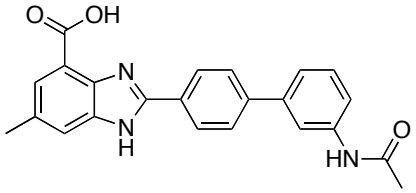
26	**7c**	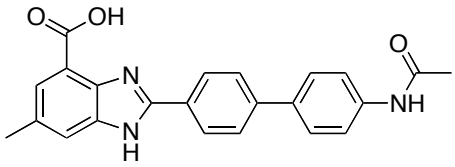
27	**7d**	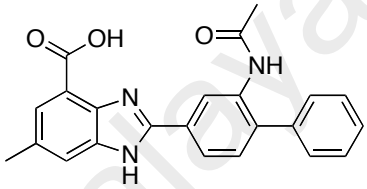
28	**7e**	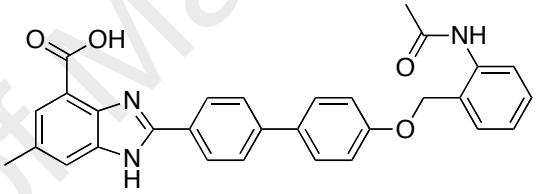
29	**7f**	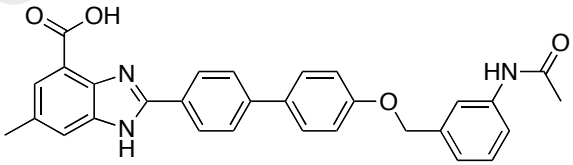
30	**7g**	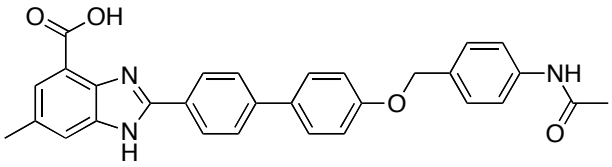

[a]Compounds reported by Tong and group (Tong e*t al*., 2009).
[b]Compounds reported by White and group (White e*t al*., 2000).

CHAPTER 4: SYNTHESIS OF BENZIMIDAZOLE DERIVATIVES

4.1 General

Chemicals that were used in all syntheses were purchased from Merck, Sigma-Aldrich and/or provided by Aurigene Discovery Technologies Limited. All melting points were taken on a Stuart Melting Point SMP 30 melting point apparatus. NMR spectra were obtained from Bruker AVN 400, JEOL Lambda 400, JEOL ECA 400 and JEOL 270. Semi-preparative HPLC was performed on Waters Binary Pump 1525, Waters Photodiode Array Detector 2998 with Merck Chromolith® Performance Reverse-phase C-18 column (100-4.6mm). High Resolution Mass Spectrometry was recorded with Agilent 1200 Series / Agilent Technologies 6530 Q-TOF (ESI) with Agilent Zorbax C-18 column. ^{1}H, ^{13}C and MS analyses were used to characterize all the target compounds. Thin Layer Chromatography (TLC) was carried out by using aluminium sheets TLC silica 60 F_{254} purchased from Merck. Flash Column Chromatography using silica gel (40-60 μm) were purchased from Merck, Mallinckrodt and Analisa Resources Sdn. Bhd. Anhydrous tetrahydrofuran (THF) used were purified through the PureSolv solvent purification system and dichloromethane (CH_2Cl_2) were distilled from CaH_2 prior to use. Other anhydrous solvents and also reagents used were purchased from Merck and Sigma-Aldrich.

4.2 Retrosynthetic Analysis

The approach involved making a series of compounds containing benzimidazole scaffold with various functional groups at three different positions (C-2, C-4 and C-6) of the benzimidazole, as illustrated in Figure 4.1. Initially work is to focus on the

preparation of various side chains that is eventually connected to the tail-end of the benzimidazole core as shown in Figure 4.1 (in blue).

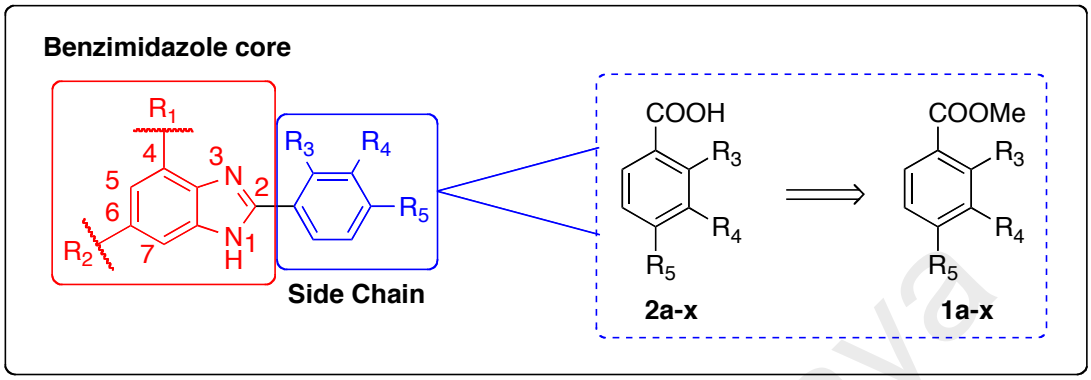

Figure 4.1. Three positions functional group variation on the benzimidazole scaffold.

Scheme 4.1 describes the retrosynthetic analysis of the benzimidazole ring construction. Two routes have been employed in order to accomplish the benzimidazole ring formation. The retrosynthesis analysis on the right hand side in Scheme 4.1 shows a functional group interconversion from a carboxylic acid (**D**) to the target amide (**E**). Functional group interconversion of the ester (**C**) presumably will lead to the carboxylic acid (**D**). Retrosynthesis of the ester (**C**) shows a disconnection of the imidazole ring, which could be achieved through intramolecular cyclisation of ester (**B**). The ester (**B**) could be obtained from the diaminobenzoate (**A**).

Retrosynthesis on the left hand side illustrates a shorter route involving a intramolecular cyclisation of the amide (**F**) to form the target amide (**G**). The amide (**F**) could be prepared from an amide coupling reaction between the diamine (**E**) and the carboxylic acid (**2**).

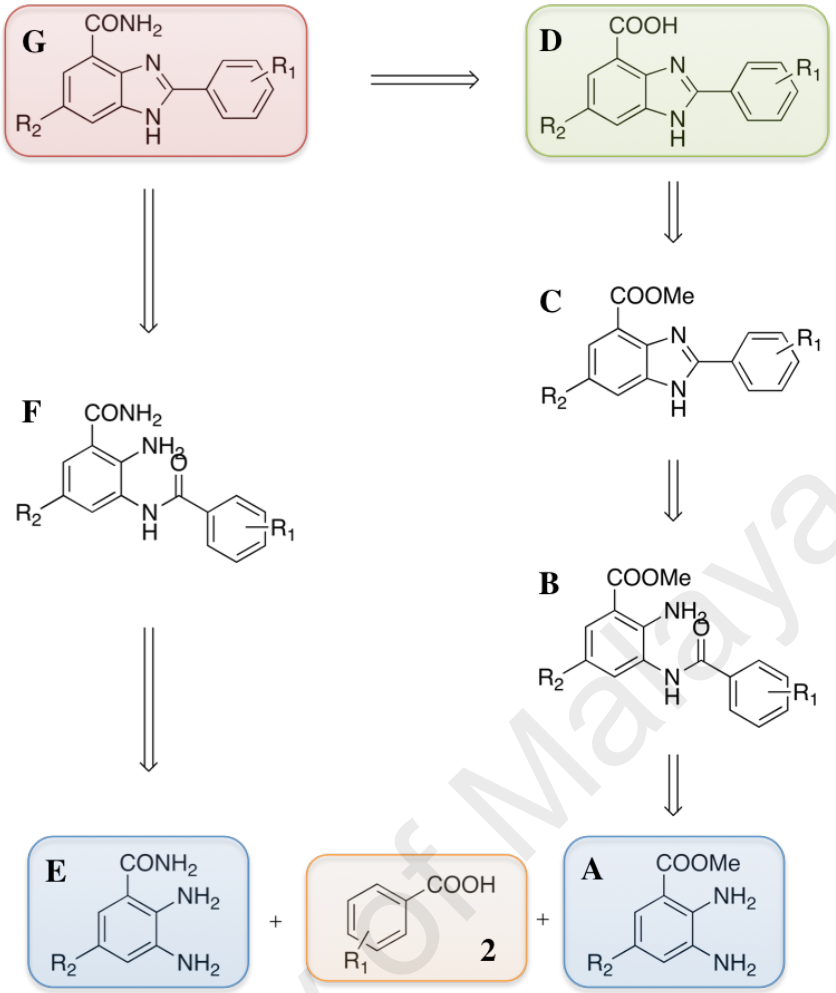

Scheme 4.1. Retrosynthesis of benzimidazole.

4.3 Synthesis of Benzimidazole Derivative Side Chains

As mentioned in Chapter 3, 30 different benzimidazole derivatives have been designed for biological testing. The differences in these compounds lie mainly in the carboxyl substituent on the C-2 position of the benzimidazole scaffold. These carboxyl substituents were prepared from carboxylic acids (**2**), where different groups were placed at the *ortho*, *meta,* and *para*-position. The carboxylic acids (**2**) were, in turn, prepared by saponification of the corresponding ester (**1**) (Figure 4.1), as shown in Table 4.1 (Compounds **2a-x**).

Table 4.1. Side chain compounds.

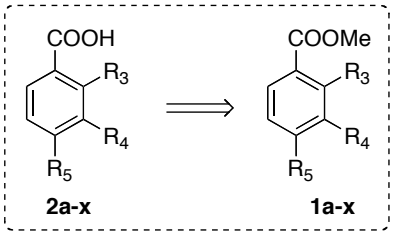

Entry	Structure	Entry	Structure
2a	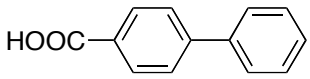	**2m**	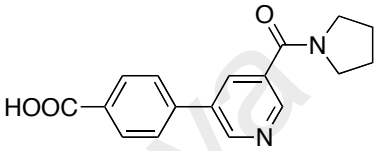
2b	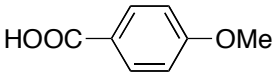	**2n**	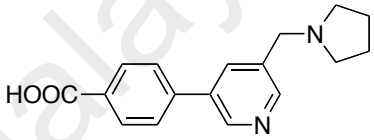
2c	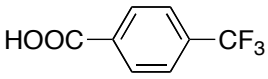	**2o**	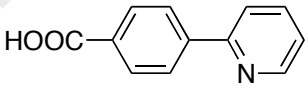
2d	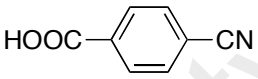	**2p**	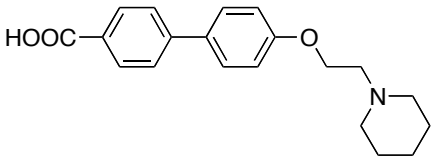
2e	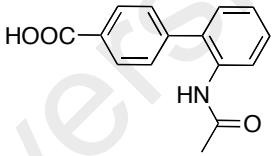	**2q**	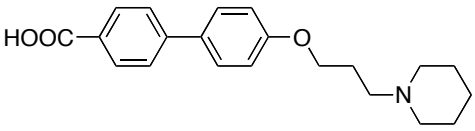
2f	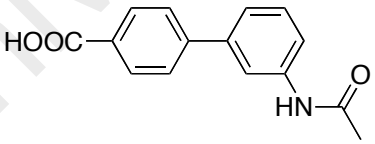	**2r**	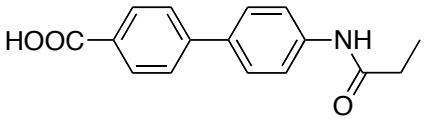
2g	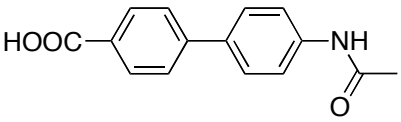	**2s**	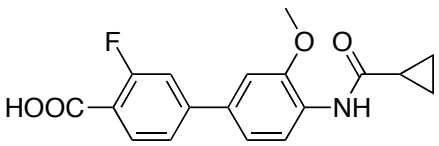
2h	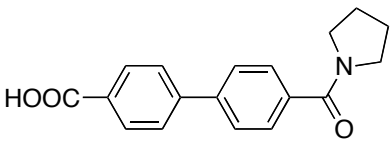	**2t**	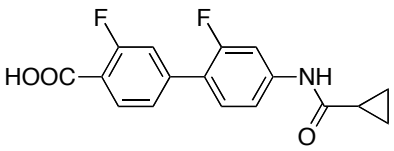

Table 4.1 continued

2i	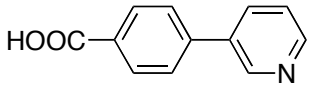	**2u**	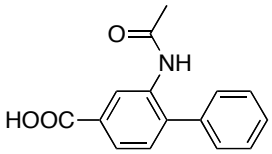
2j	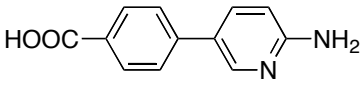	**2v**	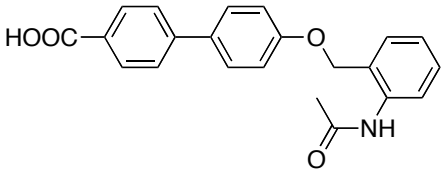
2k	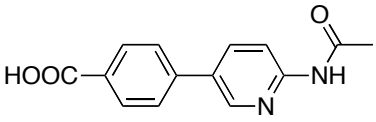	**2w**	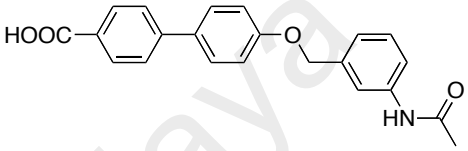
2l	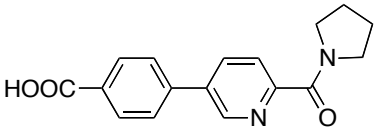	**2x**	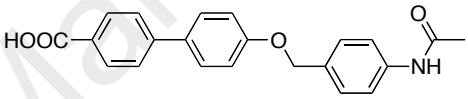

Eleven carboxylic acid side chains (Figure 4.2), used in this work (Compounds **2a**, **2b**, **2c**, **2d**, **2e**, **2f**, **2g**, **2o**, **2w**), were provided by Aurigene Discovery Technologies Ltd.

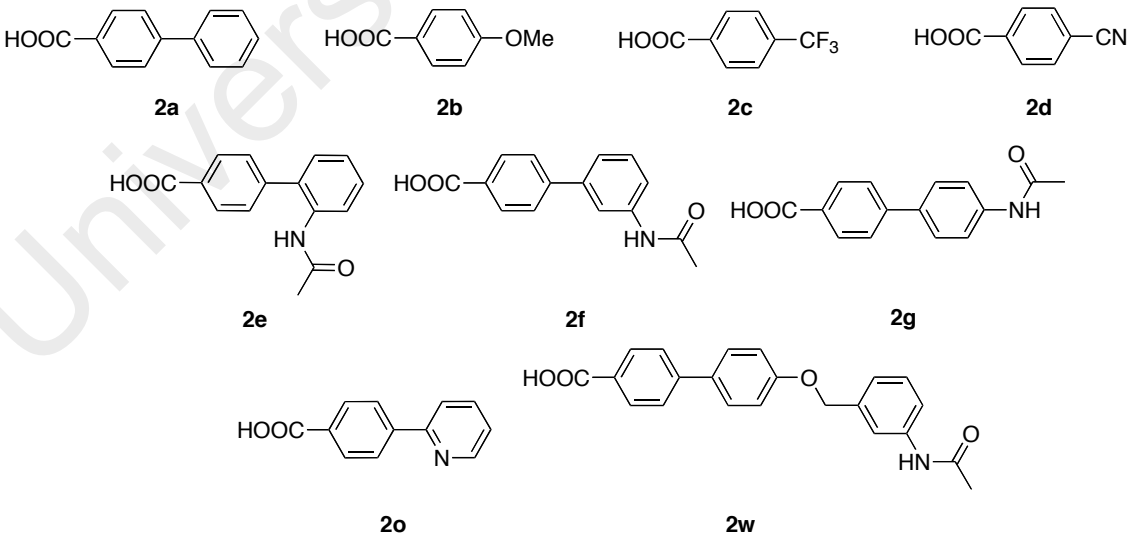

Figure 4.2. Compounds provided by Aurigene Discovery Technologies Ltd.

Table 4.2. List of starting materials used in the synthesis.

Entry	Structure / Name of Molecule	Entry	Structure / Name of Molecule
A1	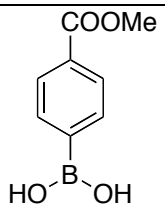 (4-(Methoxycarbonyl)phenyl) boronic acid	**C4**	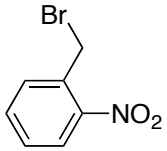 1-(Bromomethyl)-2-nitrobenzene
A2	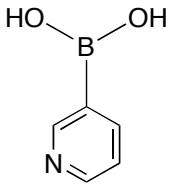 Pyridin-3-ylboronic acid	**C5**	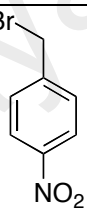 1-(Bromomethyl)-4-nitrobenzene
A3	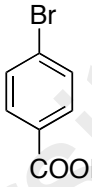 4-Bromobenzoic acid	**D1**	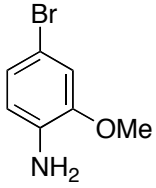 4-Bromo-2-methoxyaniline
A4	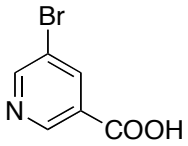 5-Bromonicotinic acid	**D2**	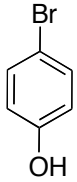 4-Bromophenol
A5	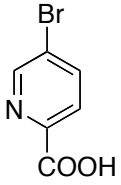 5-Bromopicolinic acid	**D3**	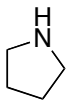 Pyrrolidine

Table 4.2 continued

A6	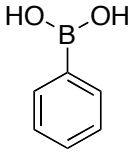 Phenylboronic acid	**D4**	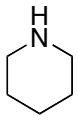 Piperidine
B1	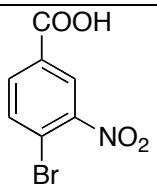 4-Bromo-3-nitrobenzoic acid	**D5**	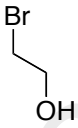 2-Bromoethanol
B2	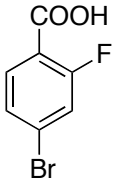 4-Bromo-2-fluorobenzoic acid	**D6**	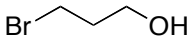 3-Bromopropan-1-ol
B3	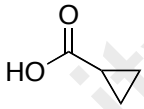 Cyclopropanecarboxylic acid	**E1**	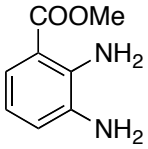 Methyl 2,3-diaminobenzoate
B4	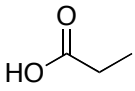 Propionic acid	**E2**	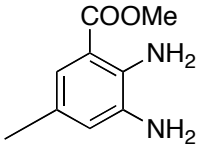 Methyl 2,3-diamino-5-methylbenzoate
C1	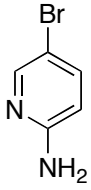 5-Bromopyridin-2-amine	**E3**	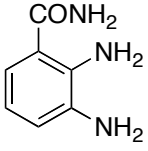 2,3-Diaminobenzamide

Table 4.2 continued

C2	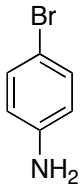 4-Bromoaniline	**E4**	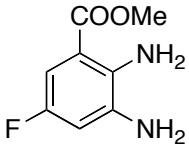 Methyl 2,3-diamino-5-fluorobenzoate
C3	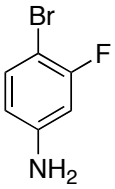 4-Bromo-3-fluoroaniline	**F1**	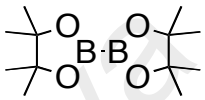 *Bis*(pinacolato)diboron

*Starting materials were obtained from Aurigene Discovery Technologies Ltd. (India).

The remaining carboxylic acids (Compounds **2h**, **2i**, **2j**, **2k**, **2l**, **2m**, **2n**, **2p**, **2q**, **2r**, **2s**, **2t**, **2u**, **2v**, **2x**), shown in Table 4.1, were synthesised using various methods. Prior to the synthesis, the compounds were categorized into groups according to similarities in the functional groups, as illustrated in Figure 4.3 (Refer to appendix A1 for spectra). This was done since the synthetic strategies being carried out were presumed to be the same for the compounds within the same group. With the exception of Group 1 (provided by Aurigene), the synthetic strategies for the preparation of Groups 2-6 compounds are described below;

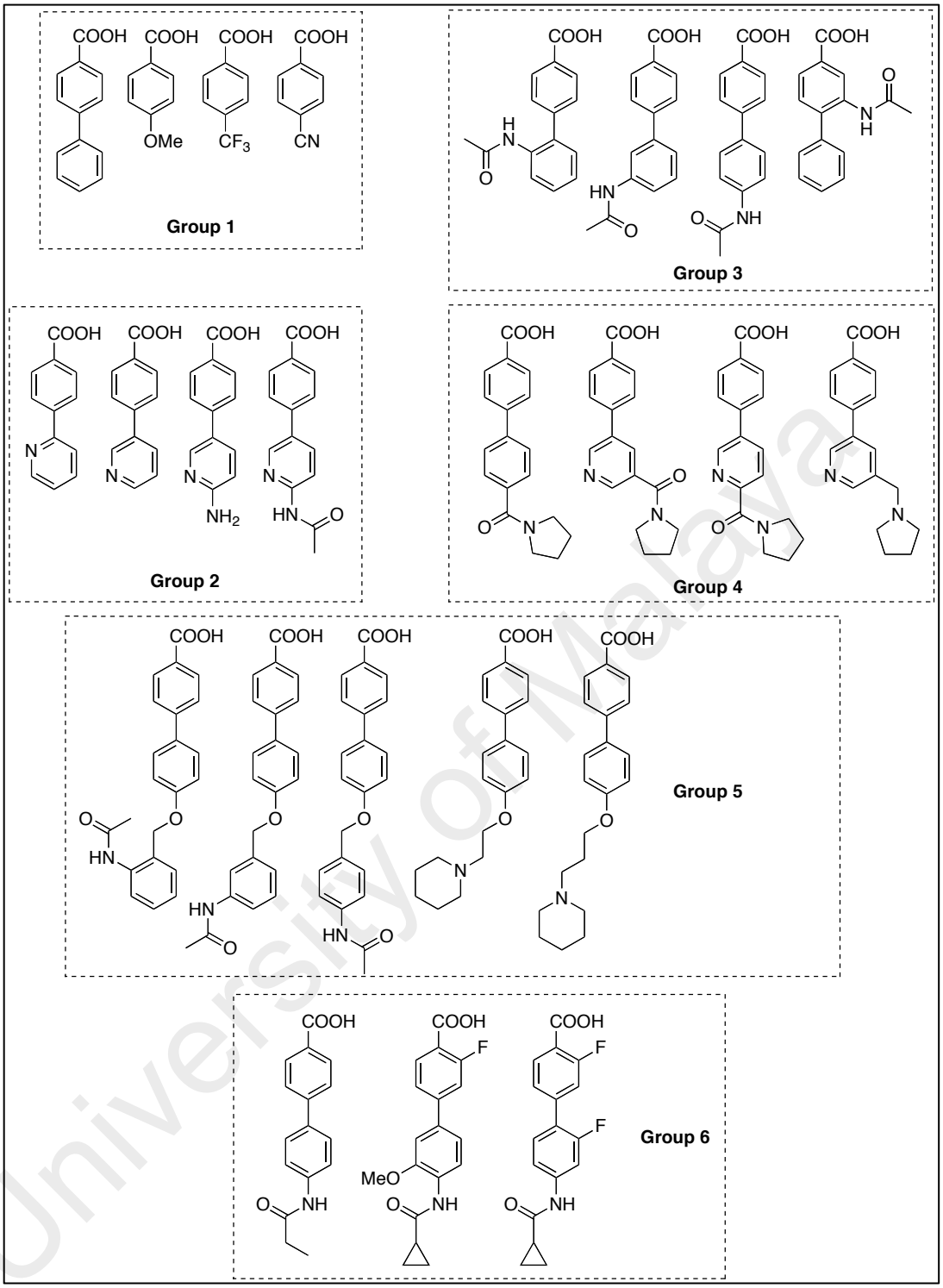

Figure 4.3. Carboxylic acid side chains divided into groups.

4.3.1 Synthesis of Carboxylic Acids in Group 2

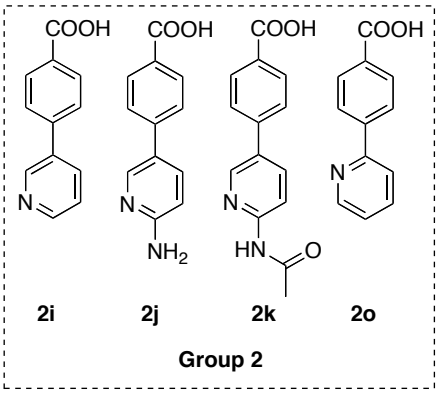

Figure 4.4. Compounds of Group 2.

4.3.1.1 Synthesis of 4-(pyridin-3-yl)benzoic acid, 2i

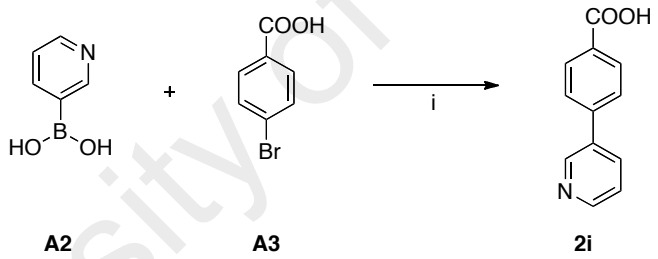

Procedure:

(i) $Pd(PPh_3)_2Cl_2$ (0.28 g, 0.40 mmol) was taken into the mixture of 1,4-dioxane (30 mL) and water (10 mL) and then degassed with N_2 gas for 10 minutes. 4-bromobenzoic acid (**A3**) (1.00 g, 4.03 mmol) and pyridin-3-ylboronic acid (**A2**) (0.59 g, 4.83 mmol) was added to the reaction mixture and again degassed for another 10 minutes before adding CS_2CO_3 (4.26 g, 12.07 mmol), then the resulting mixture was degassed for 5 minutes and heated to 80°C for 4 hours. After completion of the reaction, which was monitored by TLC, it was filtered through celite pad, and the filtrate was concentrated to remove 1,4-dioxane. The

residue was diluted with water and washed with EtOAc. Acidifying the aqueous phase with 10% HCl to pH 2 resulted solids that were filtered and dried under vacuum to obtain 4-(pyridin-3-yl)benzoic acid (**2i**) as light yellow solid in 59% yield (0.47 g, 2.38 mmol), and used without further purification. $\mathbf{R_f}$ (EtOAc:Hex; 1:1; v/v) 0.0. **^{1}H NMR (400 MHz, DMSO-*d*$_6$): δ 8.97 (s, 1H), 8.64 (d, *J*=8.0, 1H), 8.07 (d, *J*=8.5, 2H), 7.88 (d, *J*=8.5, 2H), 7.53 (dd, *J*=4.8, 7.5, 1H).**

4.3.1.2 Synthesis of methyl 4-(6-aminopyridin-3-yl)benzoate, 1j-1

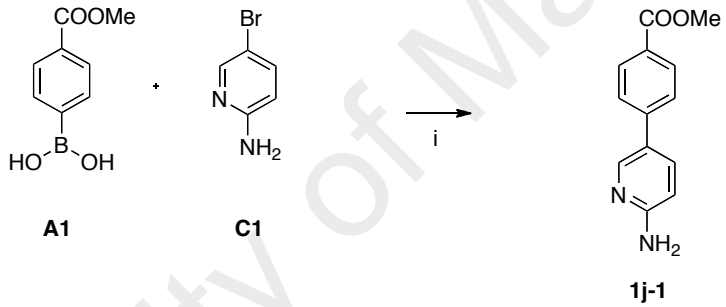

Procedure

(i) To a solution of 1,4-dioxane (20 mL) and water (5 mL), was added CS_2CO_3 (3.06 g, 8.67 mmol) and left to stir through N_2 gas bubbling for 10 minutes. (4-(methoxycarbonyl)phenyl)boronic acid (**A1**) (0.62 g, 3.47 mmol) and 5-bromopyridin-2-amine (**C1**) (0.50 g, 2.89 mmol) were then added to the mixture and allowed to dissolve completely, followed by $Pd(PPh_3)_2Cl_2$ (0.41 g, 0.58 mmol) and stirred for additional 10 minutes. The reaction mixture was set to reflux at 100°C for about 3 hours. After completion of the reaction (monitored by TLC), 1,4-dioxane was removed *in vacuo*. The residues were extracted with EtOAc, washed with water and brine followed by drying over $MgSO_4$ and concentrated. The crude residue was then purified by column chromatography

(CH_2CL_2:MeOH; 9:1; v/v) to afford the desired product methyl 4-(6-aminopyridin-3-yl)benzoate (**1j-1)** as yellow solid in 54% yield (0.36 g, 1.56 mmol). **R_f** (EtOAc:Hex; 3:7; v/v) 0.20. **^{1}H NMR (400 MHz, DMSO-*d*$_6$): δ 8.36 (s, 1H), 7.97 (d, *J*= 8.5, 2H), 7.79 (dd, *J*=2.4, 8.5, 1H), 7.73 (d, *J*=8.5, 2H), 6.54 (d, *J*=8.5, 1H), 6.25 (s, NH_2), 3.86 (s, 3H).**

4.3.1.3 Synthesis of 4-(6-aminopyridin-3-yl)benzoic acid, 2j

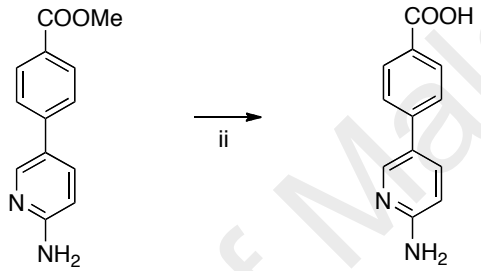

1j-1 **2j**

Procedure

(ii) Compound **1j-1** (0.36 g, 1.56 mmol) was dissolved in MeOH:THF (6 mL; 1:1; v/v), followed LiOH (0.11 g, 4.79 mmol) dissolved in water (3 mL) were added and the reaction mixture was stirred for 24 hours. The reaction mixture progress was monitored by TLC. Upon reaction completion, solvents were removed *in vacuo*. The pH of the resulting mixture was adjusted to 2 with 10% HCl to obtain the desired product 4-(6-aminopyridin-3-yl)benzoic acid (**2j**) as light brown solid in 95.5% yield (0.32 g, 1.49 mmol). **R_f** (EtOAc:Hex; 3:7; v/v) 0.0. **^{1}H NMR (400 MHz, DMSO-*d*$_6$): δ 8.42 (s, 1H), 8.35 (dd, *J*=1.9, 9.3, 1H), 8.27 (bs, NH_2), 8.02 (d, *J*=8.3, 2H), 7.81 (d, *J*=8.3, 2H), 7.13 (d, *J*=9.3, 1H).**

4.3.1.4 Synthesis methyl 4-(6-acetamidopyridin-3-yl)benzoate, 1k-1

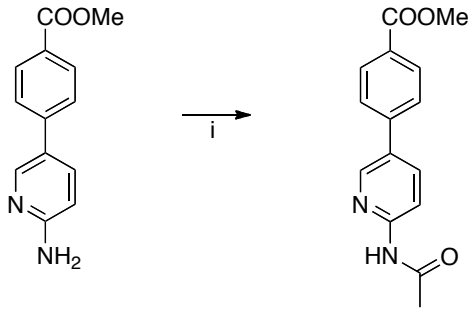

1j-1 **1k-1**

Procedure

(i) To a stirred solution of compound **1j-1** (0.40 g, 1.75 mmol) in dichloromethane (25 mL), triethylamine (0.70 mL, 5.25 mmol) was added and the mixture was cooled to 0°C. Acetyl chloride (AcCl, 0.18 mL, 2.62 mmol) was then added dropwise and the reaction was brought to room temperature while stirring (about 4 hours). Progress of the reaction was monitored by TLC. Water was added to quench the reaction and the mixture was extracted with dichloromethane. The organic phase was then washed with water, brine and dried over $MgSO_4$. The reaction proceeded to the next step without further purification. Crude compound containing methyl 4-(6-acetamidopyridin-3-yl)benzoate (**1k-1**) obtained was 0.62 g. $\mathbf{R_f}$ (EtOAc:Hex; 3:7; v/v) 0.3. **^{1}H NMR (400 MHz, $CDCl_3$): δ 8.53 (d, *J*=2.2, 1H), 8.31 (d, *J*=8.7, 1H), 8.29 (s, NH), 8.13 (d, *J*=8.3, 2H), 7.95 (dd, *J*=2.2, 8.8, 1H), 7.63 (d, *J*=8.5, 2H), 3.95 (s, 3H), 2.25 (s, 3H).**

4.3.1.5 Synthesis of 4-(6-acetamidopyridin-3-yl)benzoic acid, 2k

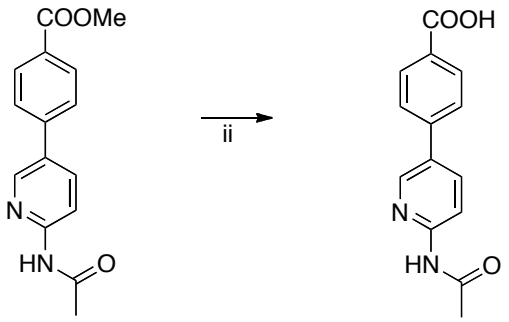

1k-1 **2k**

Procedure

(ii) Compound **1k-1** (0.62 g, 2.27 mmol) was dissolved in MeOH:THF (6 mL, 1:1; v/v), followed by the addition of LiOH (54 mg, 2.25 mmol) in water (3 mL), and the reaction mixture was allowed to stir overnight. Progress of the reaction was monitored by TLC. Upon completion reaction, solvents were removed *in vacuo*. The resulting aqueous mixture was adjusted to pH 2 with 10% HCl to obtain the desired product 4-(6-acetamidopyridin-3-yl)benzoic acid (**2k**), as light brown powder in 69% yield (0.41 g, 1.58 mmol). $\mathbf{R_f}$ (EtOAc:Hex; 3:7; v/v) 0.0. **^{1}H NMR (400 MHz, DMSO-d_6): δ 10.65 (s, 1H), 8.70 (s, 1H), 1.88-1.86 (s, 2H overlap), 8.01 (d, *J*=8.5, 2H), 7.83 (d, *J*=8.3, 2H), 2.11 (s, 3H).**

Compound **2i** was synthesised in one-step through a Suzuki coupling reaction of the pyridinylboronic acid (**A2**) and the 4-bromocarboxylic acid (**A3**) in 59% yield (Scheme 4.2).

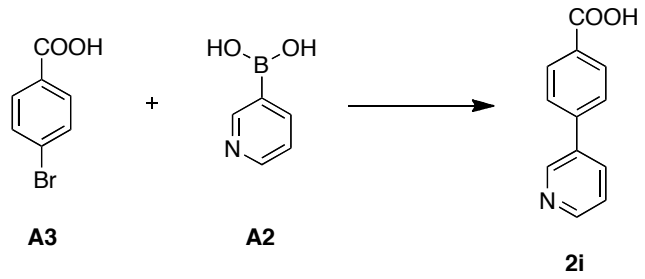

Scheme 4.2. Synthesis strategy for compound **2i**.

As shown in Scheme 4.3, Suzuki coupling of the phenylboronic ester (**A1**) with the 5-bromopyridin-2-amine (**C1**) gave the intermediate compounds (**1j-1**). Saponification of **1j-1** gave the compounds **2j**, while compound **2k** was obtained after N-acetylation and subsequent saponification of **1j-1** in decent yields (approximately 51.6%).

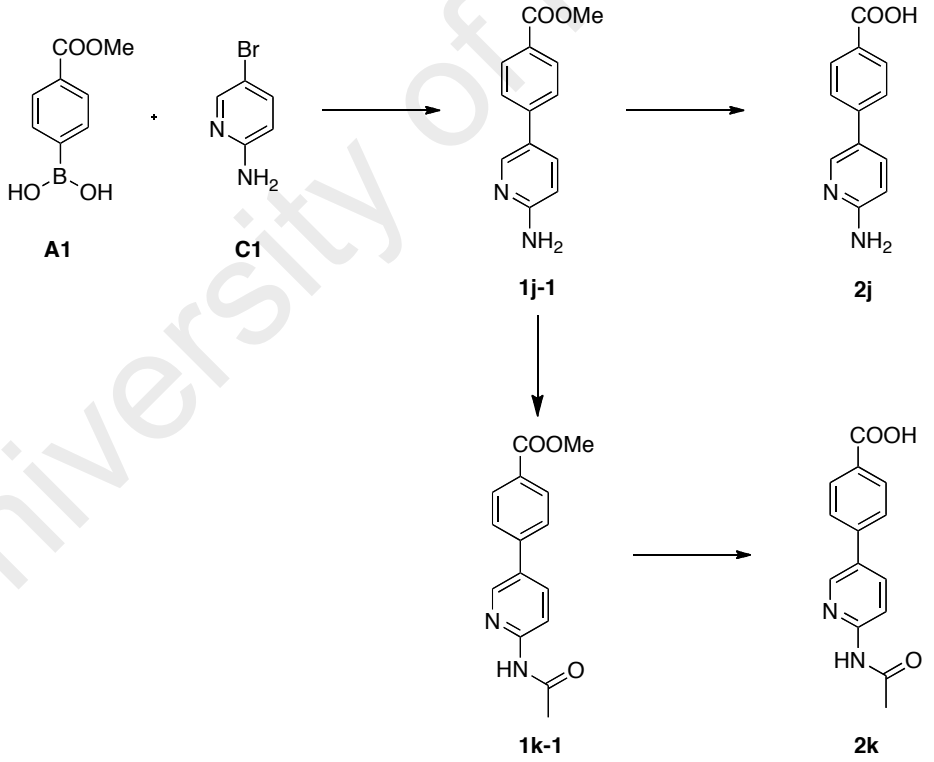

Scheme 4.3. Synthetic strategy for compounds **2j** and **2k**.

4.3.2 Synthesis of Carboxylic Acids in Group 3

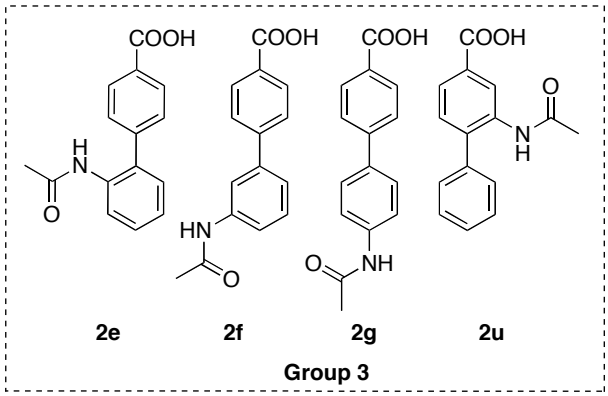

Figure 4.5. Compounds of Group 3.

4.3.2.1 Synthesis of 4-bromo-3-nitrobenzoate, B1a

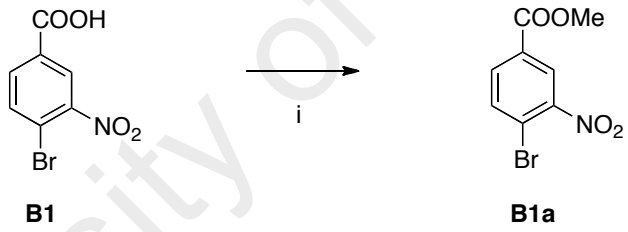

Procedure

(i) 4-Bromo-3-nitrobenzoic acid (**B1**) (0.50 g, 2.03 mmol) was added to a solution of MeOH (50 mL) dissolved with EDCI (0.51 g, 2.64 mmol). Afterwards, DiPEA (0.53 mL) was added and left to stir at room temperature for 2 hours. Upon completion of reaction, MeOH was removed *in vacuo* and the solids were washed with water, filtered and dried to afford methyl 4-bromo-3-nitrobenzoate (**B1a**) as light yellow solid in 77% yield (0.41 g, 1.56 mmol), and used for next step with no further purification. **R_f** (EtOAc:Hex; 3:7; v/v) 0.4. **^{1}H NMR (400 MHz, $CDCl_3$): δ 8.47 (d, *J*=1.9, 1H), 8.07 (dd, *J*=1.9, 8.5, 1H), 7.84 (d, *J*=8.2, 1H), 3.97 (s, 3H).**

4.3.2.2 Synthesis of 3-amino-4-bromobenzoate, B1b

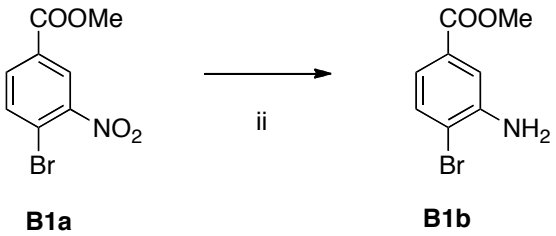

B1a **B1b**

Procedure

(ii) To a mixture of acetic acid/ethanol/water (5 mL, 2:2:1, v/v), was added compound **B1a** (0.10 g, 0.38 mmol). Reduced iron powder (0.11 g, 1.92 mmol) was introduced and the resulting mixture was sonicated at 30°C for 15 minutes, with TLC analysis monitoring to assess the reaction progress. The reaction mixture was filtered through celite and washed with EtOAc. The filtrate was treated with saturated aqueous $NaHCO_3$, where the basic layer was further extracted with EtOAc (3x), washed with water, brine, dried under $MgSO_4$ and concentrated to give methyl 3-amino-4-bromobenzoate (**B1b**) as yellow solid in 85% (0.08 g, 0.03 mmol), which was used without purification. $\mathbf{R_f}$ (EtOAc:Hex; 3:7; v/v) 0.38. **^{1}H NMR (400 MHz, $CDCl_3$): δ 7.37 (d, *J*=8.2, 1H), 7.34 (d, *J*=1.7, 1H), 7.16 (dd, *J*=1.9, 8.3, 1H), 4.18 (bs, NH_2), 3.79 (s, 3H).**

4.3.2.3 Synthesis of methyl 2-amino-[1,1'-biphenyl]-4-carboxylate, 1u-1

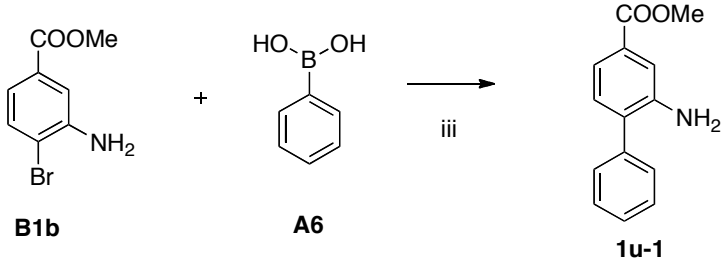

B1b **A6** **1u-1**

Procedure

(iii) To a solution of 1,4-dioxane (20 mL) and water (5 mL) was added CS_2CO_3 (0.66 g, 1.87 mmol), and left to stir with bubbling (degassed) under N_2 gas for 10 minutes. Phenylboronic acid (**A6**) (0.17 g, 1.41 mmol) and compound **B1b** (0.22 g, 0.94 mmol) were then added to the mixture and allowed to dissolve completely followed by addition of $Pd(PPh_3)_2Cl_2$ (0.13 g, 0.19 mmol) and stirring for additional 10 minutes. The reaction mixture was set to reflux at 100°C for about 2 hours. Upon completion of reaction monitored by TLC, 1,4-dioxane was removed *in vacuo* and extracted with EtOAc, washed with water, brine followed by drying over $MgSO_4$ and concentration. The crude residue was then purified by column chromatography (EtOAc:Hex; 3:1; v/v) to afford the desired product methyl 2-amino-[1,1'-biphenyl]-4-carboxylate (**1u-1**), as yellow-orange liquid in 77% yield (0.16 g, 0.72 mmol). $\mathbf{R_f}$ (EtOAc:Hex; 3:7; v/v) 0.2. **^{1}H NMR (400 MHz, $CDCl_3$): δ 7.48-7.43 (m, 7H), 7.17 (d, *J*=7.8, 1H), 3.90 (s, 3H), 3.87 (bs, NH_2).**

4.3.2.4 Synthesis of methyl 2-acetamido-[1,1'-biphenyl]-4-carboxylate, 1u-2

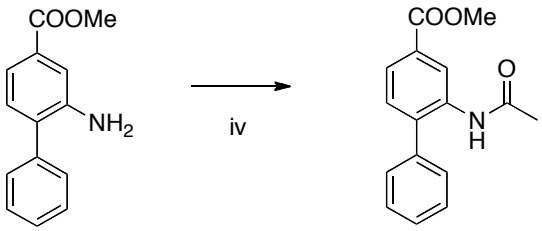

1u-1 **1u-2**

Procedure

(iv) To a stirred solution of compound **1u-1** (0.15 g, 0.54 mmol) in dichloromethane (20 mL), triethylamine (0.22 mL, 1.62 mmol) was added and cooled to 0°C.

Acetyl chloride (AcCl) (0.09 g, 1.08 mmol) was then added dropwise and the reaction was left to stir for additional 2 hours to room temperature. Progress of the reaction was monitored by TLC. Water was added to quench the completed reaction and extracted with dichloromethane. The organic phase was then washed with water, brine and dried over $MgSO_4$ to afford methyl 2-acetamido-[1,1'-biphenyl]-4-carboxylate (**1u-2**) as light yellow solid in 95% yield (0.17 g, 0.63 mmol) which were used without further purification. $\mathbf{R_f}$ (EtOAc:Hex; 3:7; v/v) 0.3. **^{1}H NMR (400 MHz, $CDCl_3$): δ 8.87 (s, 1H), 7.86 (d, *J*=4.8, 1H), 7.50 (d, *J*=7.6, 2H), 7.46 (d, *J*=7.2, 1H), 7.37 (d, *J*=6.8, 2H), 7.32 (d, *J*=8.4, 1H), 7.14 (bs, NH), 3.93 (s, 3H), 2.10 (s, 3H).**

4.3.2.5 Synthesis of 2-acetamido-[1,1'-biphenyl]-4-carboxylic acid, 2u

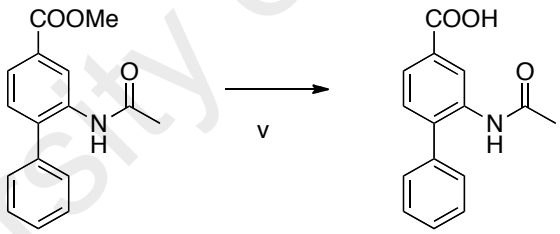

1u-2 **2u**

Procedure

(v) Compound **1u-2** (0.17 g, 0.63 mmol) was dissolved in MeOH:THF (4 mL, 1:1, v/v) followed by the addition of LiOH (0.02 g, 0.94 mmol) in water (2 mL) and the reaction mixture was allowed to stir overnight. Upon reaction completion, solvents were removed *in vacuo*. pH of the resulting aqueous mixture was adjusted to 2 with 10% HCl to obtain the desired product 2-acetamido-[1,1'-biphenyl]-4-carboxylic acid (**2u**), as white solid in 81% (0.14 g, 0.54 mmol). $\mathbf{R_f}$

(EtOAc:Hex; 3:7; v/v) 0.0. **^{1}H NMR (400 MHz, DMSO-d_6): δ 13.03 (bs, 1H), 9.39 (s, NH), 8.05 (s, 1H), 7.82 (d, *J*=8.8, 1H), 7.49-7.38 (m, 6H), 1.91 (s, 3H).**

Compounds **2e**, **2f**, and **2g** in Group 3 were synthesised directly from the phenylboronic ester (**A1**) with the various *o*-, *m*- and *p*-substituted bromoaniline (**C6**, **C7** and **C8**), respectively (Scheme 4.4) (Provided by Aurigene).

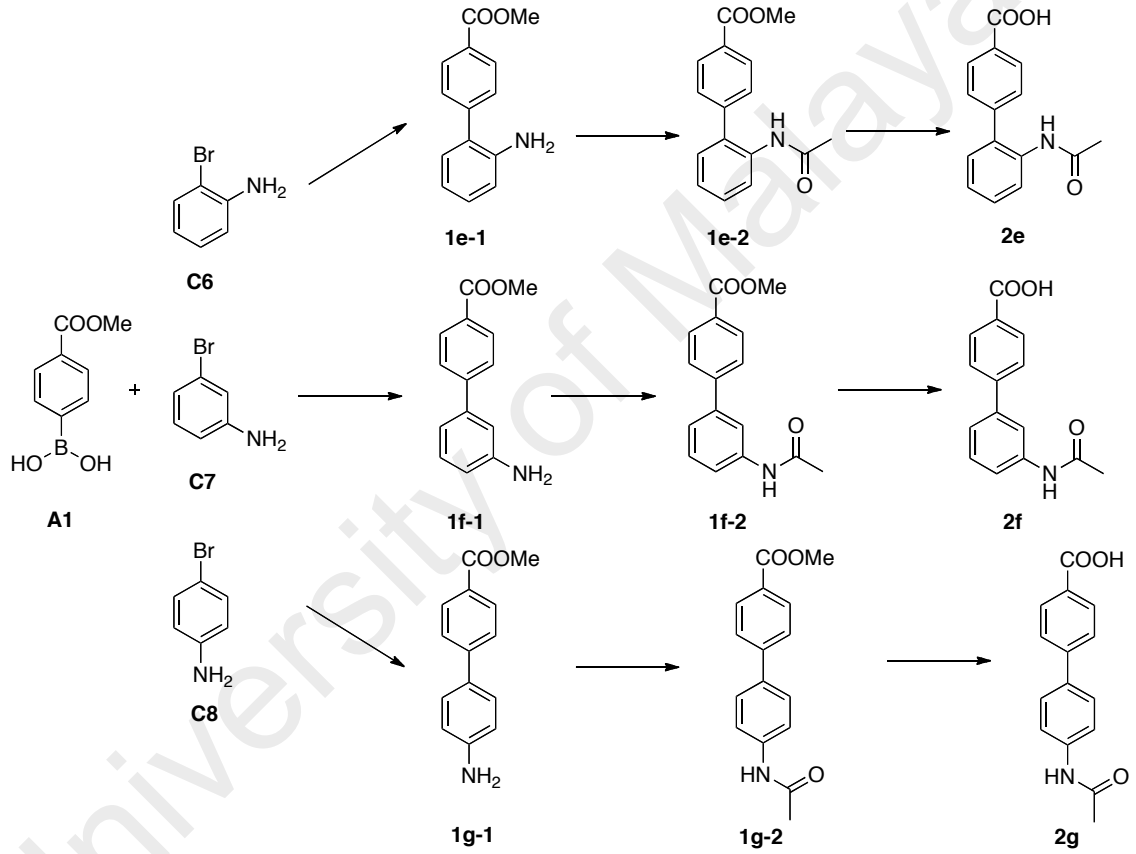

Scheme 4.4. Synthetic strategy for compounds **2e**, **2f** and **2g**.

Attempts on Suzuki coupling between phenylboronic acid and 4-bromo-3-nitrobenzoic acid (**B1**) did not result in the desired compound **1u-3**, as shown in Scheme 4.5.

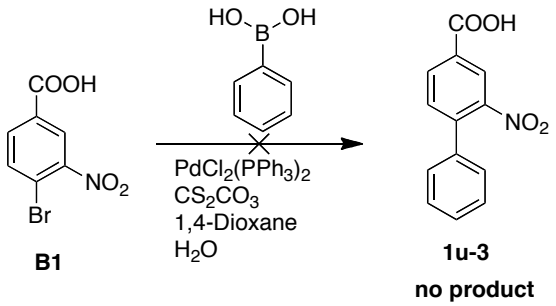

Scheme 4.5. Synthetic strategy for compound **1u-3**.

Thus, different strategy was used where the carboxylic acid (**B1**) was first protected as an ester, and then subjected to both Suzuki and Ullman coupling, as shown in Scheme 4.6 below. However, Suzuki reaction gave less than 10% yield of the desired product, while no product was obtained under the Ullman condition.

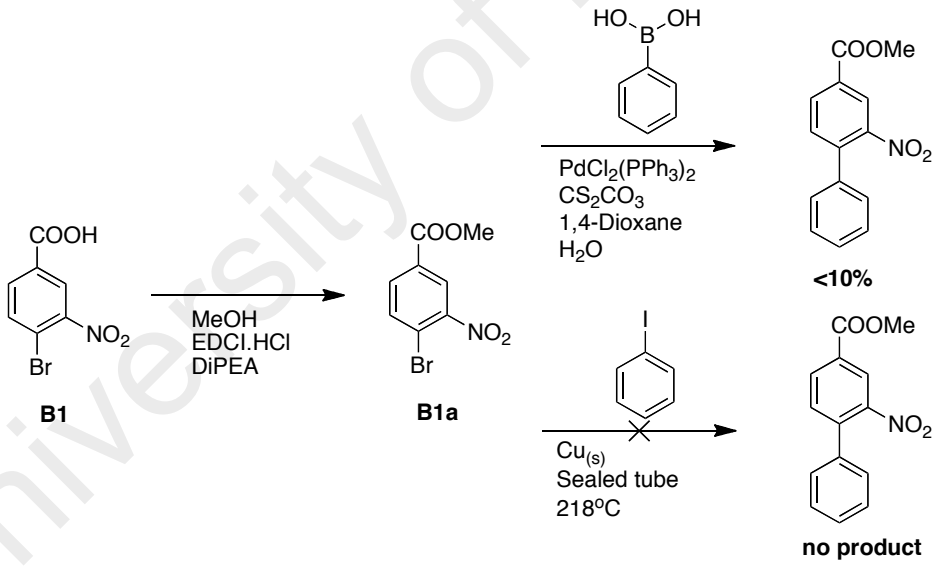

Scheme 4.6. Esterification of **B1** followed by Suzuki coupling and Ullman coupling.

Although Suzuki coupling has been reported to work well with many substrates, including nitrobenzenes, the reaction did not proceed well when the reaction was performed. Thus, **B1** was firstly esterified, and then reduce the nitro group to an amino group following the procedure of Gamble and co-workers (Gamble *et al*., 2007). Here, 5 equivalents of iron powder were added to the methyl 4-bromo-3-nitrobenzoate (**B1a**) in

a mixture of ethanol, glacial acetic acid and water. The reaction mixture was then subjected to ultrasonic condition for 15 minutes to give the methyl 3-amino-4-bromobenzoate (**B1b**) in quantitative yield. This fast reaction may be due to the high-energy effects of acoustic cavitation of the ultrasound, with the iron surface continuously been cleaned and activated by glacial acetic acid (Gamble *et al*., 2007). Dehalogenation was not observed during the aryl nitro reduction (Scheme 4.7).

The corresponding methyl 3-amino-4-bromobenzoate (**B1b**) was subjected to Suzuki coupling reaction with phenylboronic acid, as shown in Scheme 4.7. This reaction proceeded well, producing the methylamino biphenyl carboxylate (**1u-1**) in 77% yield. N-acetylation and saponification of the methylamino biphenyl carboxylate (**1u-1**) gave the desired N-acetyl biphenyl carboxylic acid (**2u**) in about 59% yield in 3 steps from the methylamino biphenyl carboxylate (**1u-1**).

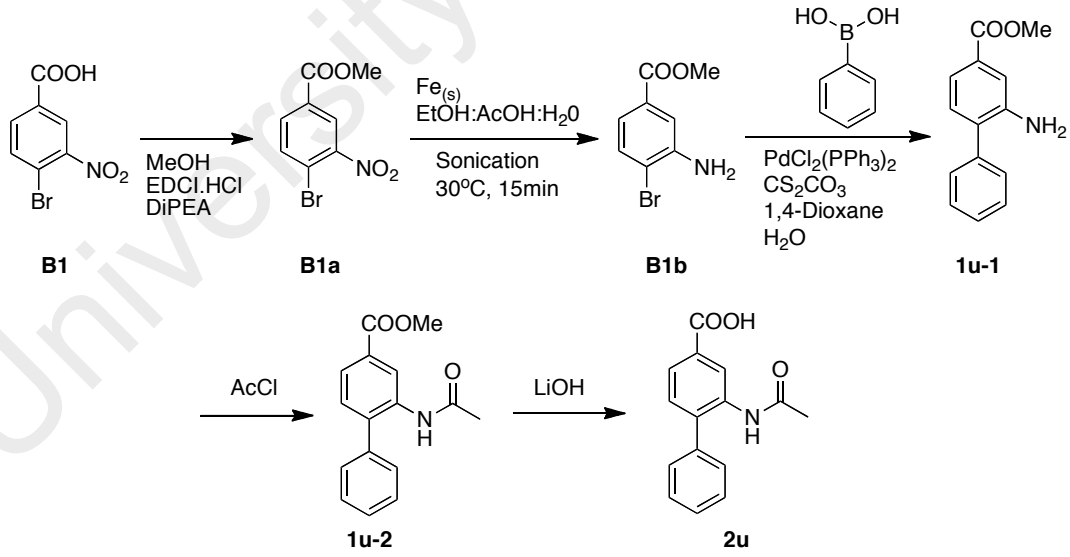

Scheme 4.7. Alternative route in preparing compound **2u**.

4.3.3 Synthesis of Carboxylic Acids in Group 4

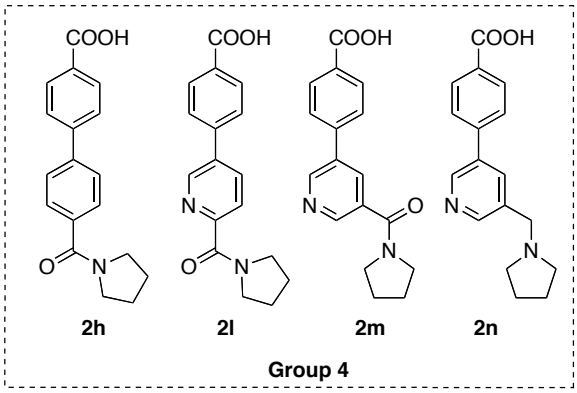

Figure 4.6. Compounds of Group 4.

4.3.3.1 Synthesis of (4-bromophenyl)(pyrrolidin-1-yl)methanone, 1h-1

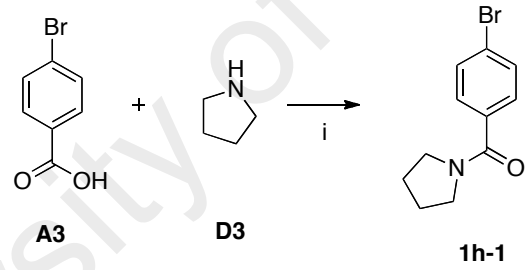

Procedure

(i) 4-bromobenzoic acid (**A3**) (1.00 g, 4.95 mmol), pyrrolidine (**D3**) (0.53 g, 7.42 mmol), EDCI (0.94 g, 4.95 mmol) and HOBt (0.67 g, 4.95 mmol) was added to a solution of DMF (6 mL) followed by DiPEA (1 mL). The resulting mixture was then allowed to stir at room temperature for 3 hours. Upon completion of the reaction, water (80 mL) was added to the reaction mixture and solids obtained was filtered and dried, affording (4-bromophenyl)(pyrrolidin-1-yl)methanone (**1h-1)** as yellow solid in 80% yield (1.01 g, 3.96 mmol). $\mathbf{R_f}$ (EtOAc:Hex; 3:7; v/v) 0.3. **^{1}H NMR (400 MHz, $CDCl_3$): δ 7.66 (d, *J*=8.2, 2H),**

7.18 (d, *J*=8.2, 2H), 3.53 (t, *J*=6.9, 2H), 3.32 (t, *J*=6.3, 2H), 1.88-1.84 (m, 2H), 1.82-1.77 (m, 2H).

4.3.3.2 Synthesis of methyl 4'-(pyrrolidine-1-carbonyl)-[1,1'-biphenyl]-4-carboxylate, 1h-2

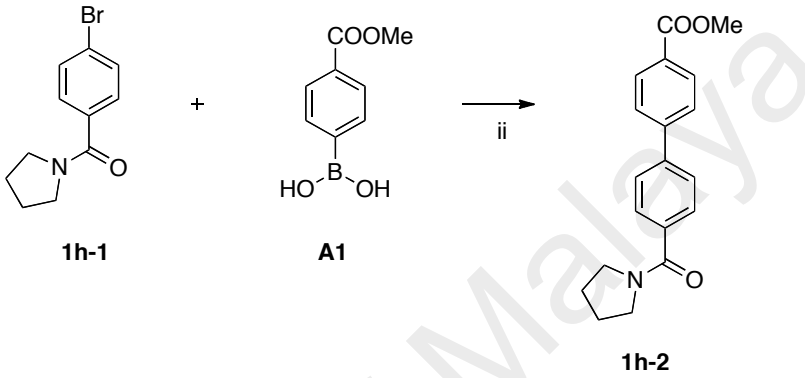

Procedure

(ii) To a solution of 1,4-dioxane (35 mL) and water (10 mL), was added CS_2CO_3 (4.15 g, 0.01 mol), and left to stir bubbling (degassed) under N_2 gas for 10 minutes. (4-(methoxycarbonyl)phenyl)boronic acid (**A1**) (0.84 g, 4.70 mmol) and compound **1h-1** (1.00 g, 3.92 mmol) was then added to the mixture and allowed to dissolve completely, followed by *bis*(triphenylphosphine) palladium(II)dichloride $Pd(PPh_3)_2Cl_2$ (0.55 g, 0.78 mmol), and stirred for additional 10 minutes. Reaction mixture was set to refluxed at 100°C for about 4 hours. After completion of the reaction monitored by TLC, 1,4-dioxane was removed *in vacuo*, extracted with EtOAc, washed with water and brine followed by drying over $MgSO_4$ and concentrated. The crude residue was then purified by column chromatography (EtOAc:Hex; 3:1; v/v) to afford desired product methyl 4'-(pyrrolidine-1-carbonyl)-[1,1'-biphenyl]-4-carboxylate (**1h-2)** as light yellow solid in 68% yield (0.83 g, 2.66 mmol). $\mathbf{R_f}$ (EtOAc:Hex; 3:7; v/v) 0.2. **^{1}H NMR**

(400 MHz, $CDCl_3$): δ 8.12 (d, *J*=8.0, 2H), 7.68-7.63 (m, 6H), 3.95 (s, 3H), 3.68 (t, *J*=6.4, 2H), 3.49 (t, *J*=6.8, 2H), 2.00-1.96 (m, 2H), 1.93-1.89 (m, 2H).

4.3.3.3 Synthesis of product 4'-(pyrrolidine-1-carbonyl)-[1,1'-biphenyl]-4-carboxylic acid, 2h

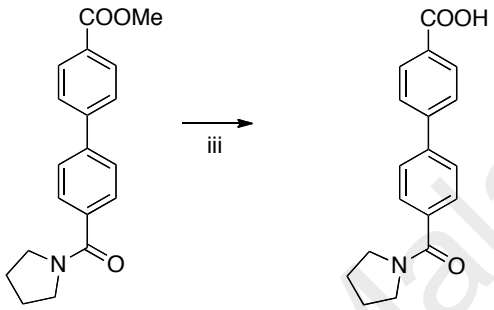

1h-2 **2h**

Procedure

(iii) Compound of **1h-2** (0.80 g, 2.58 mmol) was dissolved in MeOH:THF (8 mL; 1:1; v/v), followed by the addition of LiOH (0.18 g, 7.72 mmol) in water (4 mL), and the reaction mixture was allowed to stir overnight. Upon reaction completion, solvents were removed *in vacuo*. The resulting aqueous mixture pH was adjusted to 2 with 10% HCl to obtain the desired product 4'-(pyrrolidine-1-carbonyl)-[1,1'-biphenyl]-4-carboxylic acid (**2h**) as pale yellow solid in 90% yield (0.69 g, 2.32 mmol). $\mathbf{R_f}$ (EtOAc:Hex; 3:7; v/v) 0.0. **^{1}H NMR (400 MHz, $CDCl_3$): δ 8.17 (d, *J*=6.8, 2H), 7.70-7.64 (m, 6H), 3.68 (t, *J*=6.4, 2H), 3.49 (t, *J*=6.0, 2H), 2.01-1.96 (m, 2H), 1.92-1.89 (m, 2H).**

4.3.3.4 Synthesis of compound 2l

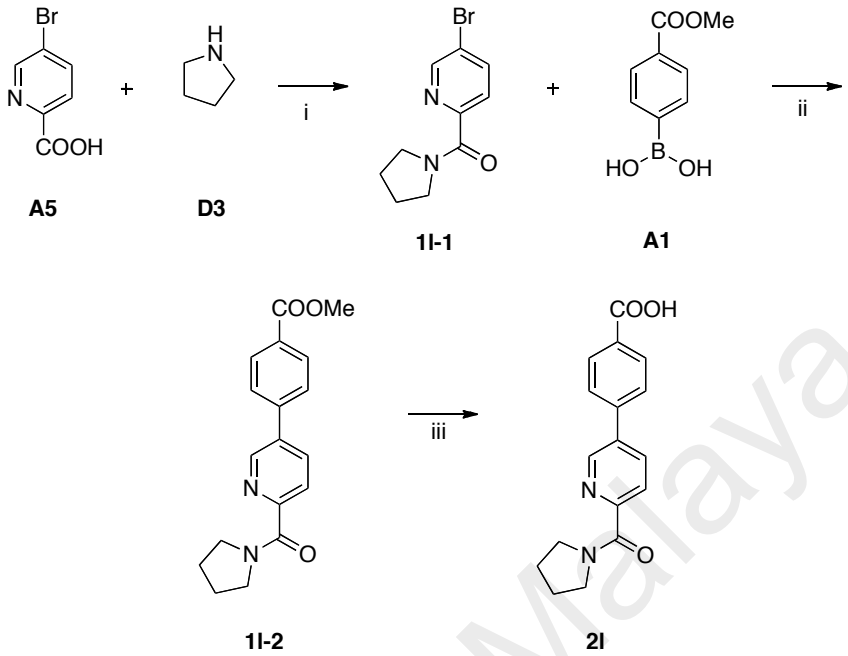

(i) EDCI, HOBt, DMF, DiPEA; (ii) $Pd(PPh_3)_2Cl_2$, CS_2CO_3, 1,4-Dioxane, H_2O, 100°C; (iii) $LiOH/H_2O$, MeOH/THF.

Procedure

Compounds **1l-1**, **1l-2** and **2l** were prepared in a similar fashion as compound **2h**.

(a) Spectral data for (5-bromopyridin-2-yl)(pyrrolidin-1-yl)methanone, **1l-1**

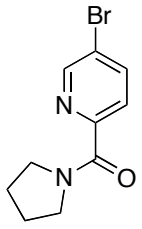

1l-1

Yellow solid in 85% yield (1.07 g, 4.21 mmol). $\mathbf{R_f}$(EtOAc:Hex; 3:7; v/v) 0.3. **^{1}H NMR (400 MHz, $CDCl_3$): δ 8.64 (dd, *J*=0.7, 2.3, 1H), 7.93 (dd, *J*=2.3, 8.4, 1H), 7.78 (dd, *J*=0.7, 8.4, 1H), 3.76 (t, *J*=6.8, 2H), 3.67 (t, *J*=7.0, 2H). 1.95-1.91 (m, 4H).**

(b) Spectral data for methyl 4-(6-(pyrrolidine-1-carbonyl)pyridin-3-yl)benzoate, **1l-2**

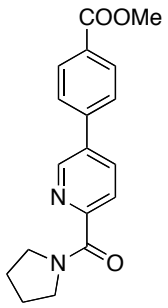

1l-2

Light yellow solid in 70% yield (0.85 g, 2.74 mmol). $\mathbf{R_f}$ (EtOAc:Hex; 3:7; v/v) 0.2. **^{1}H NMR (400 MHz, $CDCl_3$): δ 8.84 (dd, *J*=0.7, 2.3, 1H), 8.16 (d, *J*=8.5, 2H), 8.03 (dd, *J*=2.3, 8.1, 1H), 7.96 (dd, *J*=0.7, 8.1, 1H), 7.69 (d, *J*=8.5, 2H), 3.95 (s, 3H), 3.82 (t, *J*=6.7, 2H), 3.71 (t, *J*=6.9, 2H), 1.97-1.93 (m, 4H).**

(c) Spectral data for 4-(6-(pyrrolidine-1-carbonyl)pyridin-3-yl)benzoic acid, **2l**

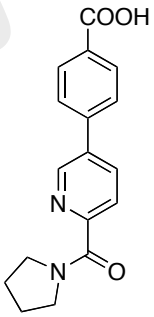

2l

Pale yellow solid in 93% yield, (0.71 g, 2.39 mmol). $\mathbf{R_f}$ (EtOAc:Hex; 3:7; v/v) 0.0. **^{1}H NMR (400 MHz, CH_3OD): δ 8.95 (s, 1H), 8.32 (d, *J*=8.3, 1H), 8.16 (d, *J*=8.3, 2H), 7.89 (d, *J*=8.3, 1H), 7.84 (d, *J*=7.8, 2H), 3.70-3.65 (m, 4H), 1.97 (m, 4H).**

4.3.3.5 Synthesis of compound 2m

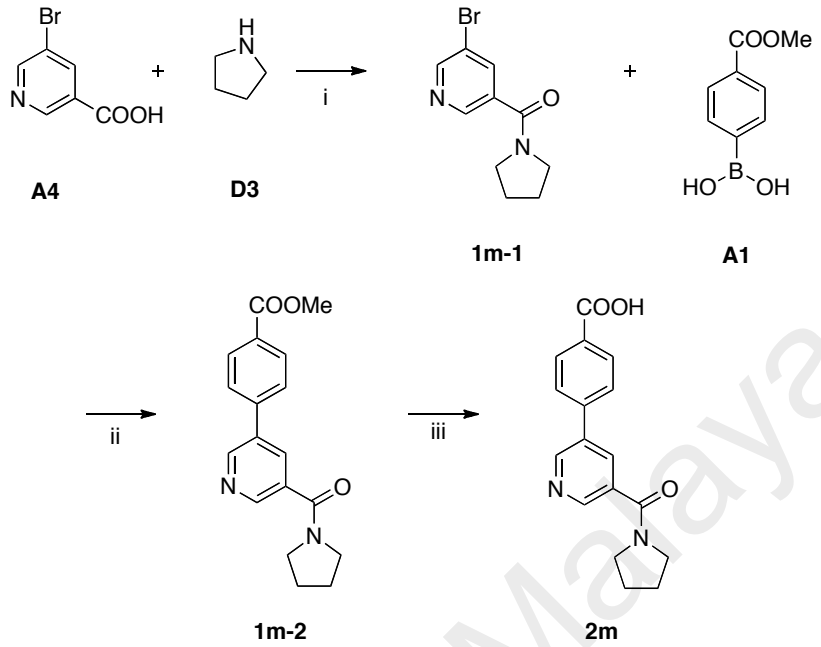

(i) EDCI, HOBt, DMF, DiPEA; (ii) $Pd(PPh_3)_2Cl_2$, CS_2CO_3, 1,4-Dioxane, H_2O, 100°C; (iii) $LiOH/H_2O$, MeOH/THF.

Procedure

Compounds **1m-1**, **1m-2** and **2m** were prepared in a similar fashion as compound **2h**.

(a) Spectral data for (5-bromopyridin-3-yl)(pyrrolidin-1-yl)methanone, **1m-1**

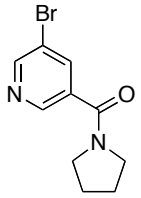

1m-1

Yellow solid in 80% yield (1.01 g, 3.96 mmol). $\mathbf{R_f}$(EtOAc:Hex; 3:7; v/v) 0.3. **^{1}H NMR (400 MHz, $CDCl_3$): δ 8.64 (d, *J*=2.3, 1H), 8.61 (d, *J*=1.8, 1H), 7.94 (t, *J*=2.1, 1H), 3.57 (t, *J*=6.9, 2H), 3.39 (t, *J*=6.3, 2H), 1.93-1.82 (m, 4H).**

(b) Spectral data for methyl 4-(5-(pyrrolidine-1-carbonyl)pyridin-3-yl)benzoate, **1m-2**

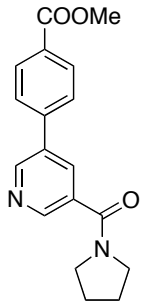

1m-2

Light yellow solid in 68% yield (0.83 g, 2.66 mmol). $\mathbf{R_f}$ (EtOAc:Hex; 3:7; v/v) 0.2. **^{1}H NMR (400 MHz, $CDCl_3$): δ 8.92 (d, *J*=2.0, 1H), 8.79 (d, *J*=1.7, 1H), 8.16 (d, *J*=8.4, 2H), 8.10 (t, *J*=1.6, 1H), 7.68 (d, *J*=8.4, 2H), 3.69 (t, *J*=6.8, 2H), 3.95 (s, 3H), 3.52 (t, *J*=6.4, 2H), 2.05-1.91 (m, 4H).**

(c) Spectral data for 4-(5-(pyrrolidine-1-carbonyl)pyridin-3-yl)benzoic acid, **2m**

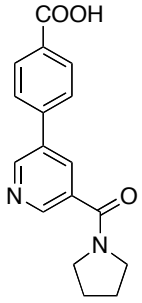

2m

Pale yellow solid in 90% yield (0.69 g, 2.32 mmol). $\mathbf{R_f}$ (EtOAc:Hex; 3:7; v/v) 0.0. **^{1}H NMR (400 MHz, CD_3Cl + CD_3OD): δ 8.99 (d, *J*=2.1, 1H), 8.86 (d, *J*=1.8, 1H), 8.21 (d, *J*=8.4, 2H), 8.20 (t, *J*=1.4, 1H), 7.70 (d, *J*=8.3, 2H), 3.72 (t, *J*=6.8, 2H), 3.55 (t, *J*=6.4, 2H), 2.04-1.94 (m, 4H).**

4.3.3.6 Synthesis of methyl 5-bromonicotinate, A4-1

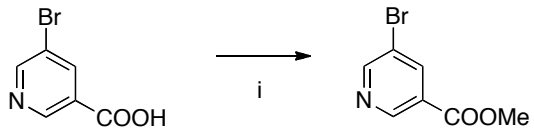

A4 **A4-1**

Procedure

(i) 5-Bromonicotinic acid (**A4**) (5.00 g, 0.02 mol) was added to a solution of MeOH (50 mL) dissolved with EDCI (4.99 g, 0.03 mol). Afterwards, DiPEA (6 mL) was added and left to stir at room temperature for 2 hours. Upon completion of reaction, MeOH was removed *in vacuo,* and the solids were washed with water, filtered and dried to afford methyl 5-bromonicotinate (**A4-1**) as light yellow solid in 95% yield, (5.11 g, 0.02 mol). $\mathbf{R_f}$ (EtOAc:Hex; 3:7; v/v) 0.4 and **proceeded to next step without further purification.**

4.3.3.7 Synthesis of (5-bromopyridin-3-yl)methanol, A4-2

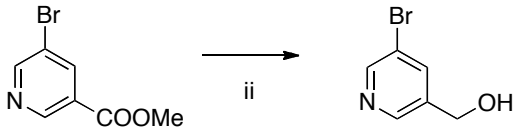

A4-1 **A4-2**

Procedure

(ii) In a round bottom flask equipped with a magnetic stir bar, MeOH (6 mL) and compound **A4-1** (1.62 g, 7.50 mmol) were added and left to stir for 10 mins. To the mixture, a solution of $NaBH_4$ (0.70 g, 0.02 mol) in H_2O solution was added

dropwise and continued to stir at room temperature, and refluxed for 5 hours. Water was added to the reaction mixture was acidified with 10% HCl, followed by ethyl acetate extraction and purified with EtOAc:MeOH (10:1; v/v), yielding (5-bromopyridin-3-yl)methanol (**A4-2**) as yellow oil in 48% yield (0.68 g, 3.60 mmol). **R_f** (EtOAc:Hex; 3:7; v/v) 0.1**. ^{1}H NMR (400 MHz, $CDCl_3$): δ 8.47 (d, *J*=2.4, 1H), 8.39 (d, *J*=1.4, 1H), 7.88 (s, 1H), 4.68 (s, 2H).**

4.3.3.8 Synthesis of 5-bromonicotinaldehyde, A4-3

A4-2 **A4-3**

Procedure

(iii) **A4-2** (0.68 g, 3.60 mmol) dissolved in dichloromethane (DCM) (10 mL) was added to a suspension of Dess-Martin Periodinane (DMP) solution, 15% (11.7 mL, 5.40 mmol) at 0°C, and the mixture was stirred to room temperature. After reaction completion, judged by TLC, sufficient amount of $NaHCO_3$ was added to destroy the excess of oxidant. The mixture was diluted with dichloromethane, and the aqueous layer was extracted with dichloromethane (3x). Combined organic layer extracts were washed with water, brine, dried over $MgSO_4$ and concentrated to yield product 5-bromonicotinaldehyde (**A4-3**) as light yellow solid in 84% yield (0.56 g, 3.00 mmol), and used without further purification. **R_f** (EtOAc:Hex; 3:7; v/v) 0.3**. ^{1}H NMR (400 MHz, $CDCl_3$): δ 10.08 (s, 1H), 8.99 (s, 1H), 8.91 (s, 1H), 8.30 (s, 1H).**

4.3.3.9 Synthesis of methyl 4-(5-formylpyridin-3-yl)benzoate, 1n-1

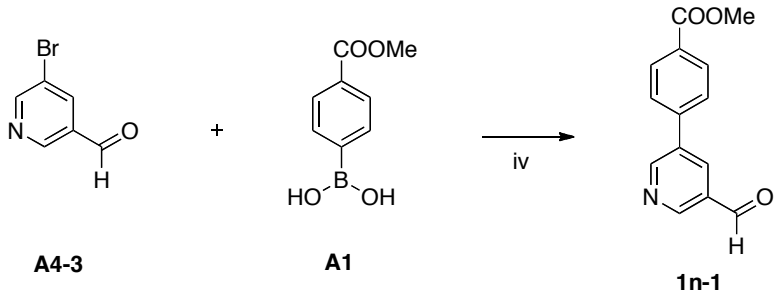

A4-3 **A1** **1n-1**

Procedure

(iv) To a solution of 1,4-dioxane (15 mL) in water (2 mL) was added CS_2CO_3 (3.42 g, 9.69 mmol) and left to stir bubbling (degassed) under N_2 gas for 10 minutes. (4-(methoxycarbonyl)phenyl)boronic acid (**A1**) (0.63 g, 3.52 mmol) and compound **A4-3** (0.60 g, 3.23 mmol) were then added to the mixture and allowed to dissolve completely, followed by $Pd(PPh_3)_2Cl_2$ (0.23 g, 0.32 mmol) and stirred for additional 10 minutes. The reaction mixture was set to reflux at 100°C for about 5 hours. After completion of reaction, monitored by TLC, 1,4-dioxane iwas removed *in vacuo* and extracted with EtOAc, washed with water, brine followed by drying over $MgSO_4$ and then concentrated. The crude residue was then purified by column chromatography (EtOAc:Hex; 5:1; v/v) to afford desired product methyl 4-(5-formylpyridin-3-yl)benzoate (**1n-1**) as white solid in 53% yield (0.42 g, 1.74 mmol). $\mathbf{R_f}$(EtOAc:Hex; 3:7; v/v) 0.2**. ^{1}H NMR (270 MHz, $CDCl_3$): δ 10.10 (s, 1H), 8.99 (s, 2H), 8.27 (s, 1H), 8.06 (d, *J*=11.9, 2H), 7.60 (d, *J*=11.9, 2H).**

4.3.3.10 Synthesis of methyl 4-(5-(pyrrolidin-1-ylmethyl)pyridin-3-yl)benzoate, 1n-2

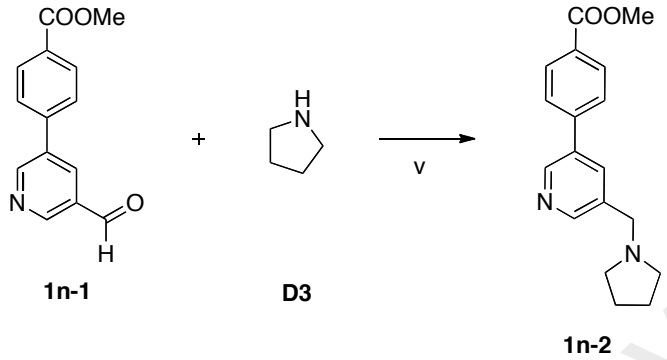

Procedure

(v) Compound **1n-1** (1.00 g, 4.15 mmol) and pyrolidine (**D3**) (0.38 mL, 4.51 mmol) were mixed together in 1,2-dichloroethane (DCE) (10 mL), and then further treated with sodium triacetoxyborohydride ($Na(OAc)_3BH$) (1.30 g, 6.13 mmol), which was stirred for 2 hours at room temperature under N_2 gas. The reaction mixture was quenched with saturated $NaHCO_3$ aqueous, and extracted with EtOAc, washed with water and dried over $MgSO_4$. The organic phase were concentrated and purified with EtOAc:Hex (5:1; v/v) to yield the product, methyl 4-(5-(pyrrolidin-1-ylmethyl)pyridin-3-yl)benzoate (**1n-2**), as brownish sticky gel in 45% yield (0.55 g, 1.86 mmol). $\mathbf{R_f}$ (EtOAc:Hex; 1:2; v/v) 0.1. **^{1}H NMR (270 MHz, CD_3OD): δ 8.78 (d, *J*=2.8, 1H), 8.60 (d, *J*=2.4, 1H), 8.16 (s, 1H), 8.04 (d, *J*=11.9, 2H), 7.73 (d, *J*=12.3, 2H), 4.04 (s, 2H), 3.87 (s, 3H), 2.90 (s, 4H), 1.92 (bs, 4H).**

4.3.3.11 Synthesis of 4-(5-(pyrrolidin-1-ylmethyl)pyridin-3-yl)benzoic acid, 2n

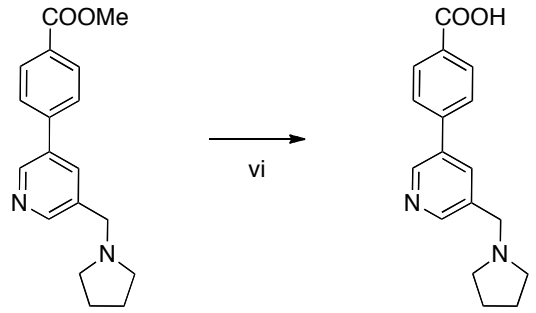

1n-2 **2n**

Procedure

(vi) Compound **1n-2** (0.55 g, 1.86 mmol) was dissolved in MeOH:THF (10 mL, 1:1; v/v), followed by the addition of LiOH (0.26 g, 11.15 mmol) in water (5 mL), and the reaction mixture was allowed to stir overnight. Upon reaction completion, solvents were removed *in vacuo*. pH of th resulting aqueous was adjusted to 2 with 10% HCl to obtain the desired product 4-(5-(pyrrolidin-1-ylmethyl)pyridin-3-yl)benzoic acid (**2n**) as light brown solid in 95% yield (0.51 g, 1.79 mmol), that was filtered, dried and used without further purification. $\mathbf{R_f}$ (EtOAc:Hex; 3:7; v/v) 0.0. **^{1}H NMR (270 MHz, CD_3OD): δ 8.86 (d, *J*=2.8, 1H), 8.74 (d, *J*=2.8, 1H), 8.41 (s, 1H), 7.95 (d, *J*=12.3, 2H), 7.62 (d, *J*=12.3, 2H), 4.55 (s, 2H), 2.13 (bs, 4H), 1.93 (s, 4H).**

Compounds **2h**, **2l** and **2m** in Group 4 were synthesised, first through amide-bond formation, followed by Suzuki coupling and subsequent saponification, as shown in Scheme 4.8.

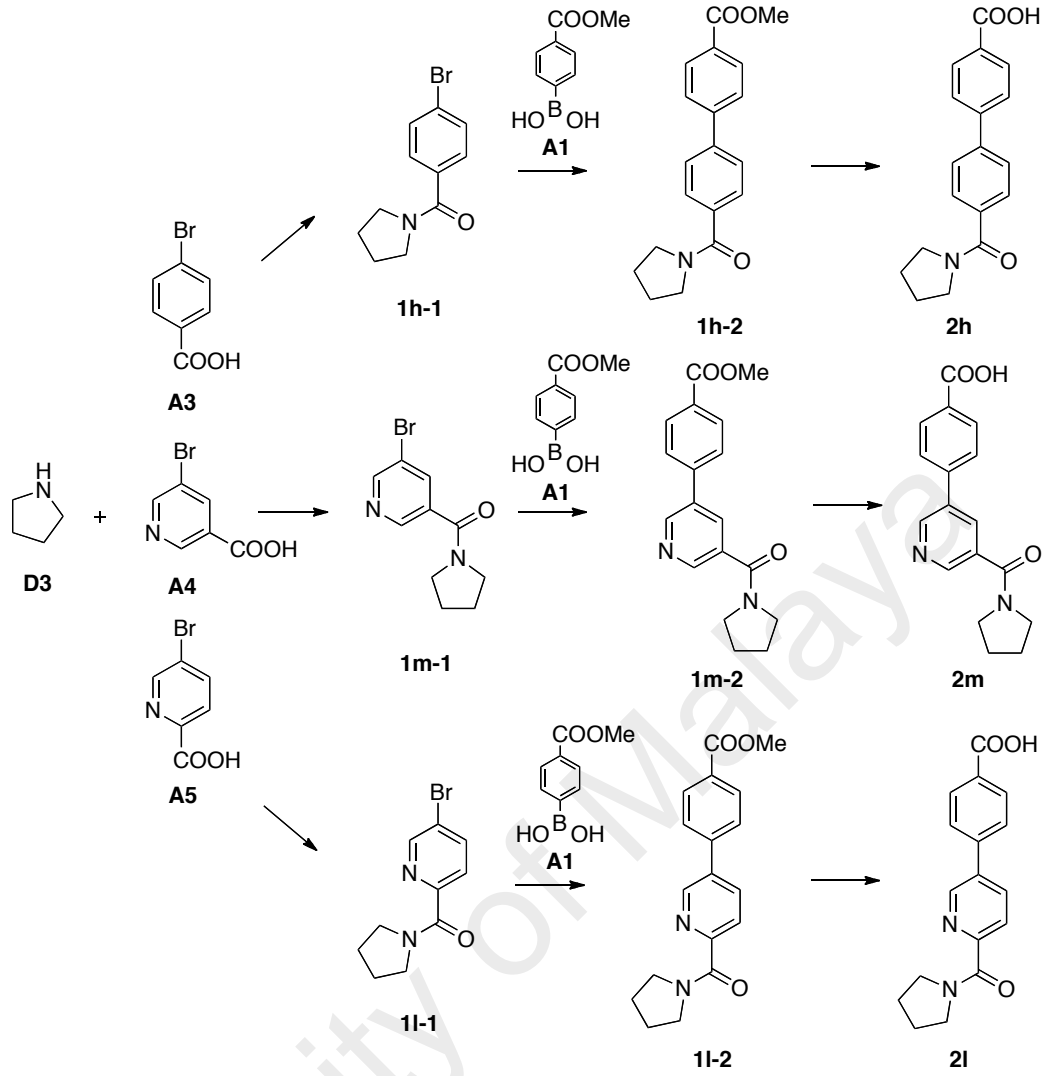

Scheme 4.8. Synthetic strategy for compounds **2h**, **2l** and **2m**.

Compound **2n** was obtained in a slightly different manner where, the ester **A4-1** was reduced to the alcohol **A4-2** first. This alcohol was then reoxidised to the aldehyde (**A4-3**), which was then subjected to the Suzuki coupling reaction with phenylboronic ester (**A1**). The aldehyde (**1n-1**) was treated to a reductive amination with pyrrolidine, and subsequent saponification of the ester (**1n-2**) gave the desired product in 26% overall yield (Scheme 4.9).

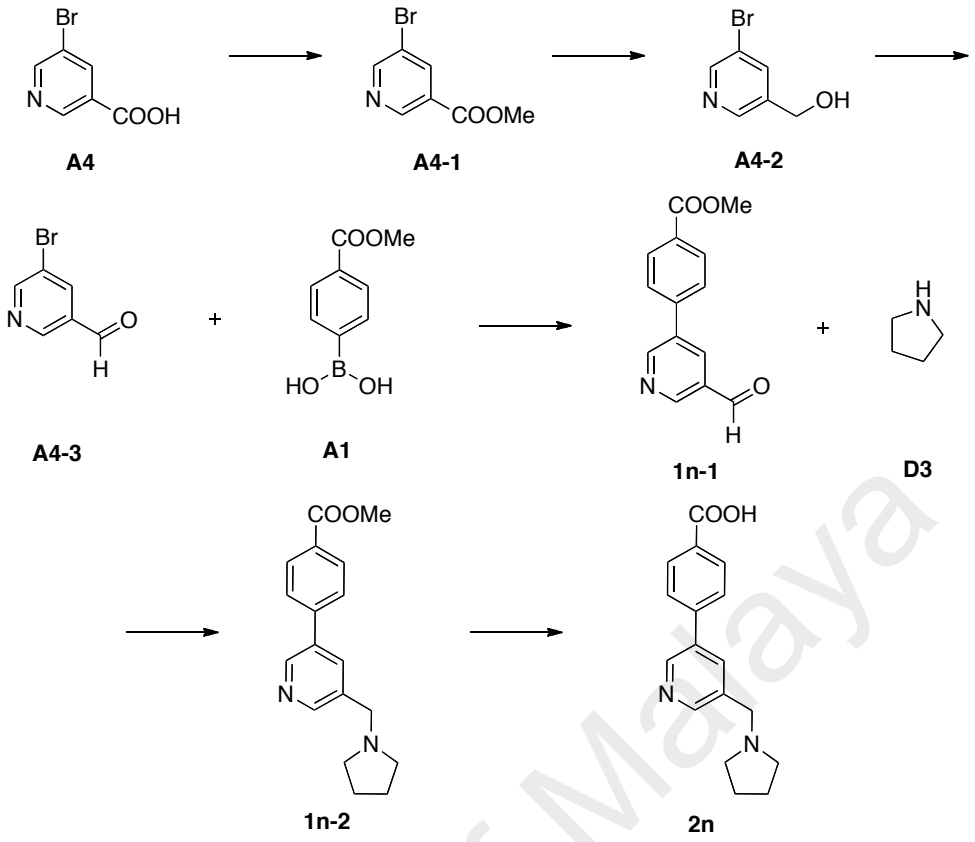

Scheme 4.9. Synthetic strategy for compound **2n**.

4.3.4 Synthesis of Carboxylic Acids in Group 5

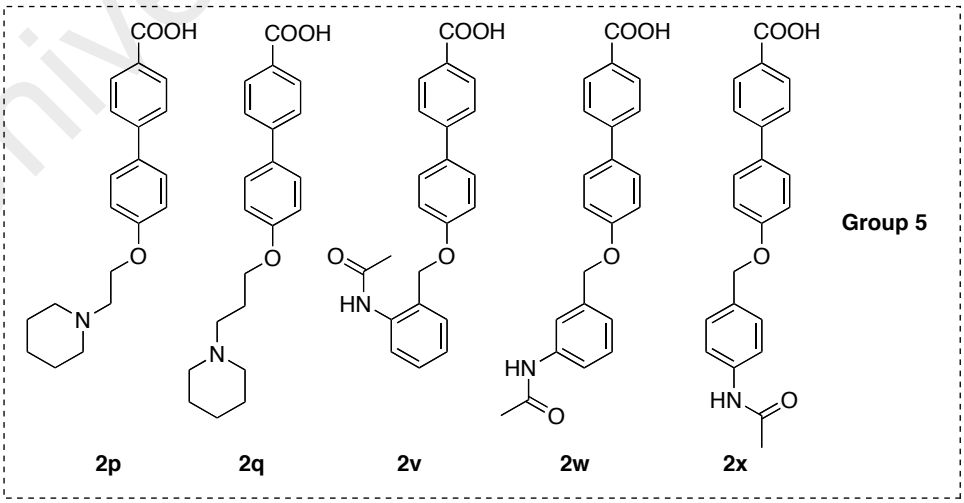

Figure 4.7. Compounds of Group 5.

4.3.4.1 Synthesis of compounds 2p and 2q

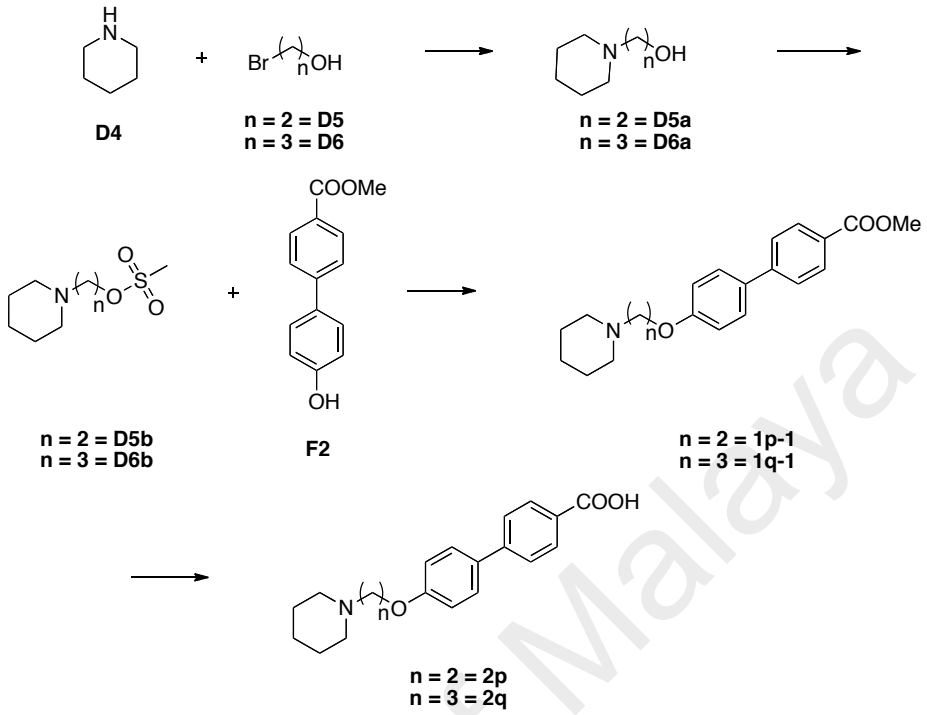

(i) neat, reflux, 60°C; (ii) MsCl, TEA, DCM, 0°C; (iii) K_2CO_3, DMF, 60°C; (iv) $LiOH/H_2O$, THF.

Scheme 4.10. Synthetic strategy for compounds **2p** and **2q**.

4.3.4.2 Synthesis of 3-(piperidin-1-yl)propan-1-ol, D6a

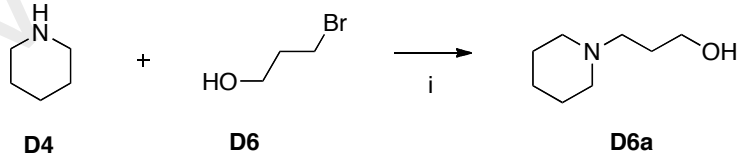

Procedure

(i) Piperidine (**D4**) (2.18 mL, 0.02 mol) was refluxed at 60°C, followed by dropwise addition of 2-bromoethanol (**D6**) (1.00 mL, 0.01 mol) in 1 hour with continuous stirring and monitoring by TLC analysis. The compounds was extracted with diethyl ether and concentrated to afford crude compound 3-

(piperidin-1-yl)propan-1-ol (**D6a**) as light orange solid in 82% yield (1.30 g, 9.08 mmol). The compound was further used without any purification. Synthesis of 2-(piperidin-1-yl)ethanol (**D5a**) requires the same procedure by using 3-bromopropanol (**D5**) and piperidine (**D4**) as starting materials. $\mathbf{R_f}$ (EtOAc:Hex; 3:7; v/v) 0.25. **^{1}H NMR (400 MHz, $CDCl_3$): δ 3.73 (t, *J*=5.1, 2H), 2.49 (t, *J*=5.6, 2H), 2.37 (bs, 4H), 1.62 (q, *J*=5.3, 2H), 1.50 (q, *J*=5.6, 4H), 1.36 (bs, 2H).**

(a) Spectral data for 2-(piperidin-1-yl)ethanol, **D5a**

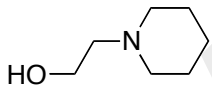

Light orange powder in 90% yield (1.64 g, 0.01 mol). **^{1}H NMR (400 MHz, $CDCl_3$): δ 3.61 (t, *J*=5.2, 2H), 2.48 (t, *J*=5.6, 2H), 2.41 (bs, 4H), 1.61-1.55 (m, 2H), 1.46-1.45 (bm, 2H).**

4.3.4.3 Synthesis of 3-(piperidin-1-yl)propyl methanesulfonate, D6b

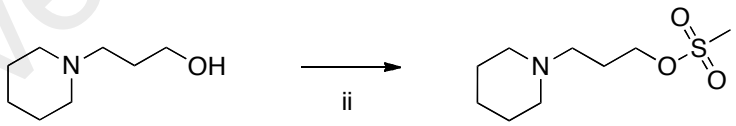

D6a **D6b**

Procedure

(ii) To a solution of **D6a** (1.80 g, 0.01 mol) in dichloromethane (35 mL) was added triethylamine (2 mL), followed by dropwise addition of methanesulfonyl chloride (MsCl) (0.79 mL, 0.02 mol) at 0°C. The mixture was allowed to stir for 30 minutes and another additional 1 hour stir at room temperature. The resulting mixture was diluted with EtOAc after it was concentrated, washed with water,

brine, dried over $MgSO_4$ and concentrated. Flash chromatography of EtOAc:Hex (1:5; v/v) elution gave purified compound of 3-(piperidin-1-yl)propyl methanesulfonate (**D6b)** as orange liquid in 13% yield (0.37 g, 1.67 mmol). Synthesis of 2-(piperidin-1-yl)ethyl methanesulfonate (**D5b**) required the same procedure by using **D5a** as starting material where **D5b** was then used without any purification for the next step. $\mathbf{R_f}$ (EtOAc:Hex; 3:7; v/v) 0.3. **^{1}H NMR (400 MHz, DMSO-d_6): δ 4.12 (t, *J*=8.2, 2H), 3.39 (bt, *J*=5.8, 6H – Overlap H_2O), 2.42 (q, *J*=8.2, 2H), 2.29 (s, 3H), 1.62 (bm, 4H), 1.41 (m, 2H).**

(a) Spectral data for 2-(piperidin-1-yl)ethyl methanesulfonate, **D5b**

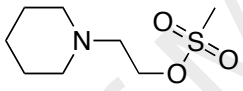

Reaction proceed to next step without purification.

4.3.4.4 Synthesis of methyl 4'-(3-(piperidin-1-yl)propoxy)-[1,1'-biphenyl]-4-carboxylate, 1q-1

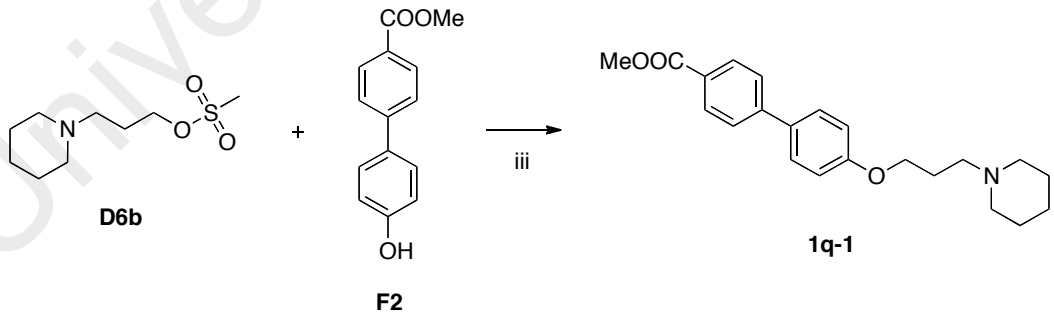

Procedure

(iii) In a round bottom flask equipped with a magnetic stirrer, methyl 4'-hydroxy-[1,1'-biphenyl]-4-carboxylate (**F2**) (0.35 g, 1.52 mmol) was dissolved in DMF (6 mL) and K_2CO_3 (0.42 g, 3.04 mmol) was added to the mixture. Mesylated

compound **D6b** (0.37 g, 1.67 mmol) was later added to the mixture and left to stir at 60°C until completion of the reaction. The reaction mixture was then extracted with EtOAc. The organic layer was washed with water, brine and dried over $MgSO_4$ to obtain the product, methyl 4'-(3-(piperidin-1-yl)propoxy)-[1,1'-biphenyl]-4-carboxylate (**1q-1**), as light yellow solid in 63% yield (0.34 g, 0.95 mmol), which was used without further purification for the next step. To obtain methyl 4'-(2-(piperidin-1-yl)ethoxy)-[1,1'-biphenyl]-4-carboxylate (**1p-1**), the same procedure was employed by using **D5b** as the starting material. $\mathbf{R_f}$ (EtOAc:Hex; 3:7; v/v) 0.35. **^{1}H NMR (400 MHz, $CDCl_3$): δ 8.04 (d, *J*=8.3, 2H), 7.61 (d, *J*=8.3, 2H), 7.55 (d, *J*=8.7, 2H), 6.98 (d, *J*=8.7, 2H), 4.05 (t, *J*=6.3, 2H), 2.49 (t, *J*=7.8, 2H), 2.41 (bs, 4H), 2.00 (q, *J*=6.6, 2H), 1.59 (q, *J*=5.6, 4H), 1.44 (bm, 2H).**

(a) Spectral data for methyl 4'-(2-(piperidin-1-yl)ethoxy)-[1,1'-biphenyl]-4-carboxylate, **1p-1**

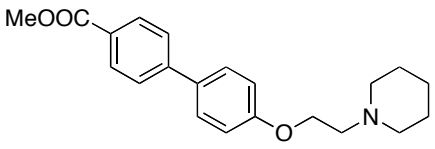

Light yellow powder in 60% yield (0.44 g, 1.31 mmol). **^{1}H NMR (400 MHz, $CDCl_3$): δ 8.07 (d, *J*=8.8, 2H), 7.61 (d, *J*=8.0, 2H), 7.56 (d, *J*=8.8, 2H), 6.99 (d, *J*=8.8, 2H), 4.16 (t, *J*=6.4, 2H), 2.80 (t, *J*=6.4, 2H), 2.53 (bs, 4H), 1.65-1.59 (m, 2H), 1.47-1.145 (bm, 2H).**

4.3.4.5 Synthesis of 4'-(3-(piperidin-1-yl)propoxy)-[1,1'-biphenyl]-4-carboxylic acid, 2q

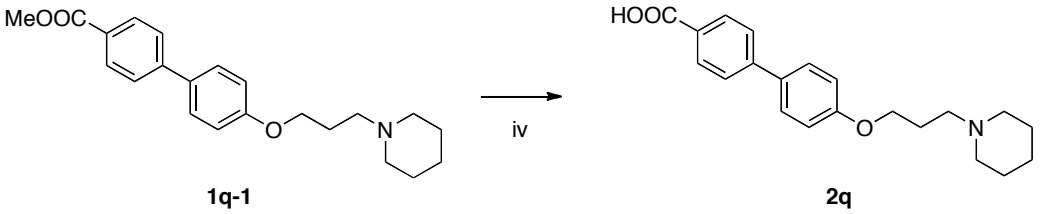

1q-1 **2q**

Procedure

(iv) Compound **1q-1** (0.30 g, 0.85 mmol) was dissolved in THF:MeOH (6 mL; 1:1; v/v), followed by the addition of LiOH (40 mg, 1.69 mmol) in water (3 mL), and the reaction mixture was allowed to stir overnight. Upon reaction completion, solvents were removed *in vacuo*. pH of the resulting aqueous mixture was adjusted to 2 with 10% HCl to obtain the desired product 4'-(3-(piperidin-1-yl)propoxy)-[1,1'-biphenyl]-4-carboxylic acid (**2q**) as white solid in 99% yield (0.29 g, 0.84 mmol), and used for next step without further purification. 4'-(2-(piperidin-1-yl)ethoxy)-[1,1'-biphenyl]-4-carboxylic acid (**2p**) was obtained with the same procedure by using **1p-1** as the starting material. $\mathbf{R_f}$ (CH_2Cl_2:MeOH; 10:1; v/v) 0.0. **^{1}H NMR (400 MHz, DMSO-d_6): δ 7.97 (d, *J*=8.0, 2H), 7.74 (d, *J*=7.9, 2H), 7.68 (d, *J*=8.3, 2H), 7.05 (d, *J*=8.3, 2H), 4.10 (t, *J*=5.8, 2H), 2.96 (bm, 6H), 2.14 (bs, 2H), 1.72 (bs, 4H), 1.50 (bs, 2H).**

(a) Spectral data for 4'-(2-(piperidin-1-yl)ethoxy)-[1,1'-biphenyl]-4-carboxylic acid, **2p**

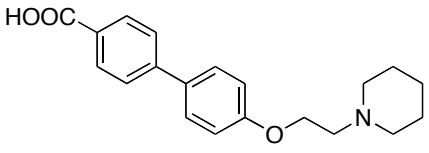

White powder in 97% yield (0.37 g, 1.14 mmol). **^{1}H NMR (400 MHz, CD_3Cl): δ 8.17 (d, *J*=8.0, 2H), 7.68 (d, *J*=7.6, 2H), 7.56 (d, *J*=8.4, 2H), 6.99 (d, *J*=8.8, 2H), 4.20 (t, *J*=6.0, 2H), 2.89 (t, *J*=5.2, 2H), 2.64 (bs, 4H), 1.70-1.65 (m, 4H), 1.50 (bm, 2H).**

4.3.4.6 Preparation of compounds 2v and 2x

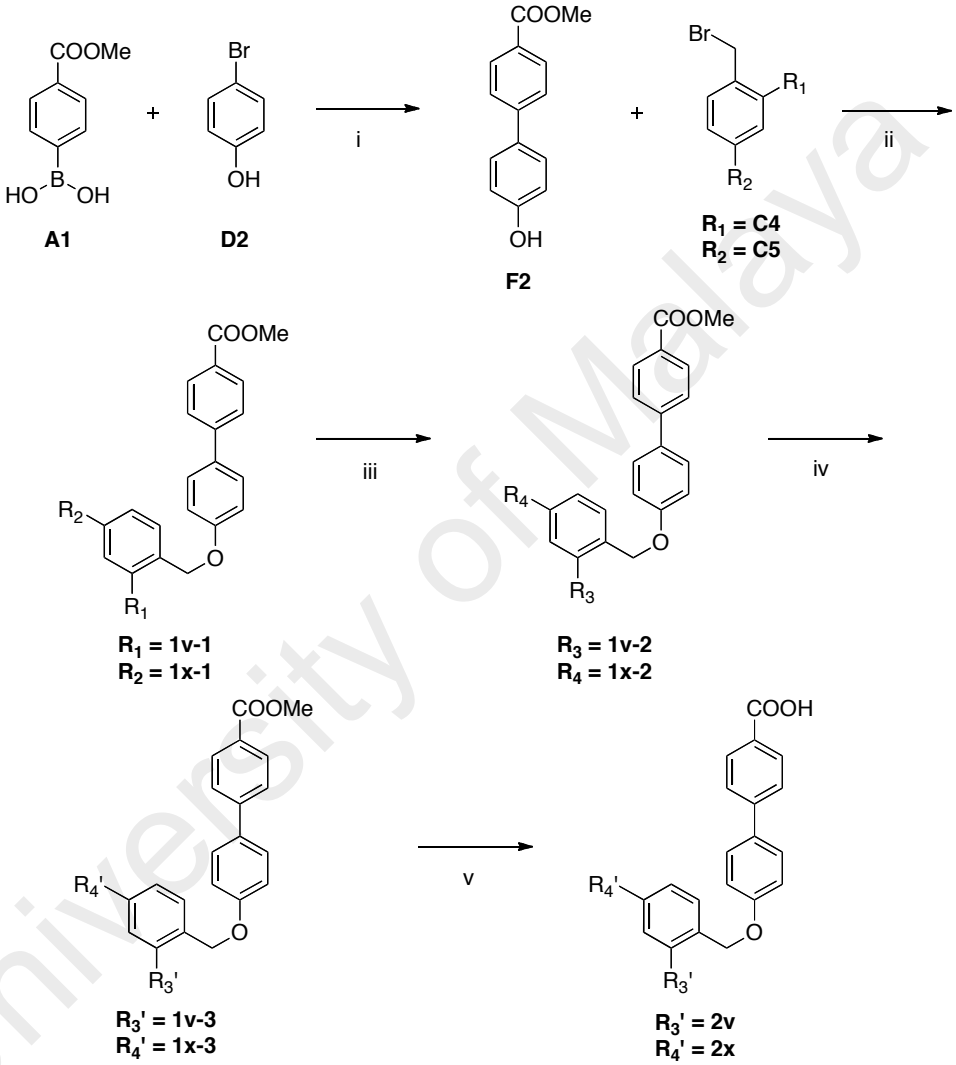

(i) $Pd(PPh_3)_2Cl_2$, CS_2CO_3, 1,4-Dioxane, H_2O, 100°C; (ii) K_2CO_3, DMF; (iii) Zn, NH_4Cl, THF, H_2O; (iv) AcCl, DCM, TEA, 0°C; (v) $LiOH/H_2O$, THF.

Compound	R_1	R_2	R_3	R_4	R_3'	R_4'
2v	NO_2	H	NH_2	H	NHAc	H
2x	H	NO_2	H	NH_2	H	NHAc

4.3.4.7 Synthesis of methyl 4'-hydroxy-[1,1'-biphenyl]-4-carboxylate, F2

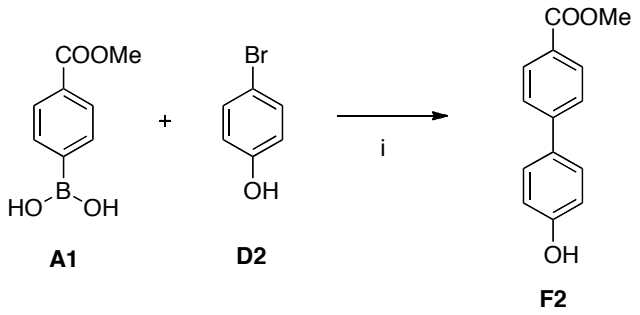

Procedure

(i) To a solution of 1,4-dioxane (60 mL) and water (15 mL) was added CS_2CO_3 (13.58 g, 0.04 mol) and left to stir bubbling (degassed) under N_2 gas for 10 minutes. (4-(methoxycarbonyl)phenyl)boronic acid (**A1**) (5.00 g, 0.03 mol) and 4-bromophenol (**D2**) (5.76 g, 0.03 mol) was then added to the mixture and allowed to dissolve completely followed by addition of $Pd(PPh_3)_2Cl_2$ (0.39 g, 0.56 mmol) and stirring for additional 10 minutes. Reaction mixture was set to reflux at 100°C for about 4 hours. After reaction completion monitored by TLC, 1,4-dioxane was removed *in vacuo* and extracted with EtOAc, washed with water, brine followed by drying over $MgSO_4$ and concentrated to afford crude residue (5.28 g), which was recrystallized in acetone-methanol solution to obtain product of methyl 4'-hydroxy-[1,1'-biphenyl]-4-carboxylate (**F2**) as white powder in 70% yield (4.44 g, 0.02 mol). $\mathbf{R_f}$ (EtOAc:Hex; 3:7; v/v) 0.3. **^{1}H NMR (400 MHz, $CDCl_3$): δ 8.07 (d, *J*=8.4, 2H), 7.61 (d, *J*=7.9, 2H), 7.52 (d, *J*=8.8, 2H), 6.93 (d, *J*=8.8, 2H), 3.93 (s, 3H).**

4.3.4.8 Synthesis of methyl 4'-((4-nitrobenzyl)oxy)-[1,1'-biphenyl]-4-carboxylate, 1x-1

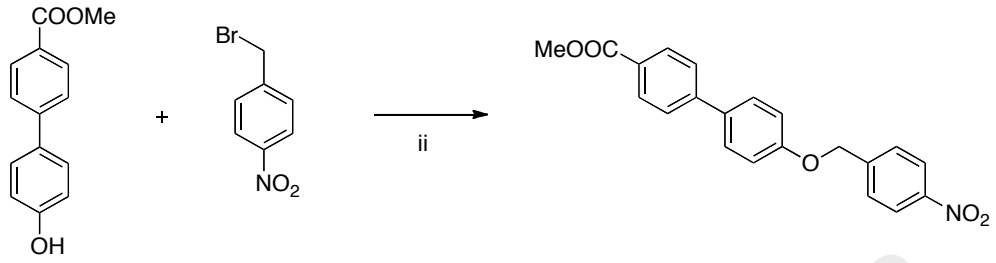

F2 **C5** **1x-1**

Procedure

(ii) In a round bottom flask equipped with a magnetic stir bar, compound **F2** (0.80 g, 3.51 mmol) was dissolved in DMF (10 mL) and K_2CO_3 (1.00 g, 7.24 mmol) was added to the mixture. 1-(bromomethyl)-4-nitrobenzene (**C5**) (0.76 g, 3.50 mmol) was later added to the mixture and left to stir at room temperature for 2 hours. Water was added upon reaction completion to obtain methyl 4'-((4-nitrobenzyl)oxy)-[1,1'-biphenyl]-4-carboxylate (**1x-1**) as white powder in 99% yield (1.26 g, 3.46 mmol) which was filtered and used without further purification. To obtain methyl 4'-((2-nitrobenzyl)oxy)-[1,1'-biphenyl]-4-carboxylate (**1v-1**), the exact procedure was employed by using 1-(bromomethyl)-2-nitrobenzene (**C4**) as the starting materials. $\mathbf{R_f}$ (EtOAc:Hex; 3:7; v/v) 0.35. **^{1}H NMR (400 MHz, $CDCl_3$): δ 8.26 (d, *J*=8.5, 2H), 8.08 (d, *J*=8.5, 2H), 7.63 (d, *J*=7.9, 2H), 7.61 (d, *J*=8.2, 2H), 7.58 (d, *J*=8.8, 2H), 7.05 (d, *J*=8.0, 2H), 5.23 (s, 2H), 3.93 (s, 3H).**

(a) Spectral data for methyl 4'-((2-nitrobenzyl)oxy)-[1,1'-biphenyl]-4-carboxylate, **1v-1**

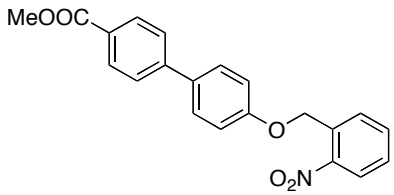

White solid in 98% yield (1.25 g, 3.44 mmol). **^{1}H NMR (400 MHz, $CDCl_3$): δ 8.12 (d, *J*=8.3, 1H), 8.01 (d, *J*=8.7, 2H), 7.86 (d, *J*=9.3, 1H), 7.63 (t, *J*=8.8, 1H), 7.55 (d, *J*=8.5, 2H), 7.52 (d, *J*=9.0, 2H), 7.44 (t, *J*=8.0, 1H), 7.01 (d, *J*=8.7, 2H), 6.87 (impurities), 5.48 (s, 2H), 3.86 (s, 3H).**

4.3.4.9 Synthesis of methyl 4'-((4-aminobenzyl)oxy)-[1,1'-biphenyl]-4-carboxylate, 1x-2

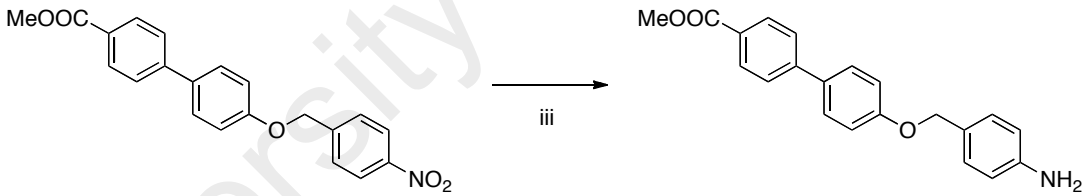

1x-1 **1x-2**

Procedure

(iii) To a solution of tetrahydrofuran (100 mL) mixed with water (10 mL) was added ammonium chloride (0.88 g, 0.16 mol), compound **1x-1** (0.60 g, 1.65 mmol), followed by excess amount of zinc powder (0.54 g, 8.25 mmol). Reaction mixture was stirred at room temperature overnight. Water was added after reaction was completed, filtered through celite and dried over $MgSO_4$. Organic phase was concentrated to afford the desired product of methyl 4'-((4-aminobenzyl)oxy)-[1,1'-biphenyl]-4-carboxylate (**1x-2**) as pale yellow powder

in 99% yield (0.54 g, 1.63 mmol) with no further purification. To obtain methyl 4'-((2-aminobenzyl)oxy)-[1,1'-biphenyl]-4-carboxylate (**1v-2**), the exact procedure was employed by using **1v-1** as the starting materials. $\mathbf{R_f}$ (EtOAc:Hex; 3:7; v/v) 0.0. **^{1}H NMR (400 MHz, DMSO-d_6 + MeOD): δ 7.98 (d, *J*=8.5, 2H), 7.74 (d, *J*=8.5, 2H), 7.65 (d, *J*=8.7, 2H), 7.09 (d, *J*=8.3, 2H), 7.06 (d, *J*=8.8, 2H), 6.55 (d, *J*=8.3, 2H), 4.90 (s, 2H), 3.84 (s, 3H).**

(a) Spectral data for methyl 4'-((2-aminobenzyl)oxy)-[1,1'-biphenyl]-4-carboxylate, **1v-2**

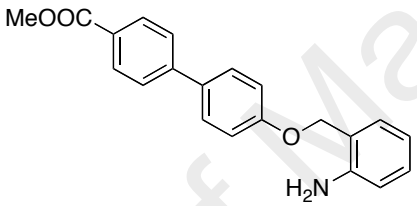

White solid in 99% yield (0.820 g, 2.459 mmol).

Reaction proceeded to next step without purification based on similar TLC profile as compound **1x-2**.

4.3.4.10 Synthesis of methyl 4'-((4-acetamidobenzyl)oxy)-[1,1'-biphenyl]-4-carboxylate, 1x-3

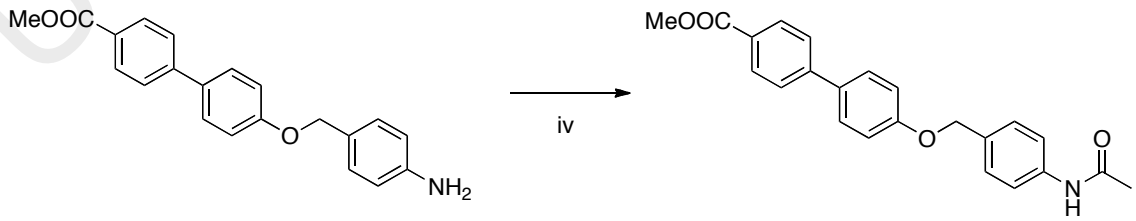

1x-2 **1x-3**

Procedure

(iv) To a stirred solution of compound **1x-2** (0.62 g, 1.86 mmol) in dichloromethane (25 mL), triethylamine (0.78 mL, 5.58 mmol) was added and cooled to 0°C. Acetyl chloride (AcCl) (0.26 mL, 3.72 mmol) was then added dropwise and the reaction was left to stir for additional 2 hours to room temperature. Progress of the reaction was monitored by TLC. Water was added to quench the completed reaction and extracted with dichloromethane. The organic phase was then washed with water, brine and dried over $MgSO_4$. Flash chromatography of CH_2Cl_2:MeOH (9:1, v/v) elution gave purified compound methyl 4'-((4-acetamidobenzyl)oxy)-[1,1'-biphenyl]-4-carboxylate (**1x-3**) as light yellow solid in 85% yield (0.59 g, 1.58 mmol). The same procedure was followed for compound methyl 4'-((2-acetamidobenzyl)oxy)-[1,1'-biphenyl]-4-carboxylate (**1v-3**) by using **1v-2** as the starting material. **R_f** (EtOAc:Hex; 3:7; v/v) 0.2. **^{1}H NMR (400 MHz, DMSO-d_6): δ 9.98 (s, NH), 7.98 (d, *J*=7.0, 2H), 7.77 (d, *J*=8.3, 2H), 7.68 (d, *J*=8.9, 2H), 7.58 (d, *J*=7.3, 2H), 7.37 (d, *J*=8.0, 2H), 7.10 (d, *J*=8.7, 2H), 5.07 (s, 2H), 3.85 (s, 3H), 2.02 (s, 3H).**

(a) Spectral data for methyl 4'-((2-acetamidobenzyl)oxy)-[1,1'-biphenyl]-4-carboxylate, **1v-3**

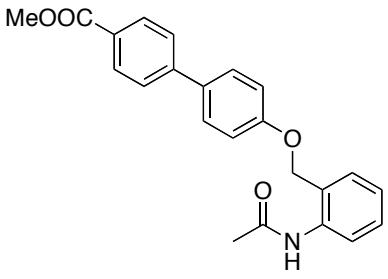

Light yellow solid in 85% yield (0.77 g, 2.04 mmol). **^{1}H NMR (400 MHz, $CDCl_3$): δ 8.01 (d, *J*=8.8, 2H), 7.97 (t overlap, *J*=7.6, 1H), 7.53 (t overlap, *J*=7.6, 4H), 7.32 (t,**

***J*=8.0, 1H), 7.28 (d, *J*=7.2, 1H), 7.08 (t, *J*=8.0, 1H), 7.02 (d, *J*=8.8, 2H), 5.06 (s, 2H), 3.86 (s, 3H), 2.10 (s, 3H).**

4.3.4.11 Synthesis of 4'-((4-acetamidobenzyl)oxy)-[1,1'-biphenyl]-4-carboxylic acid, 2x

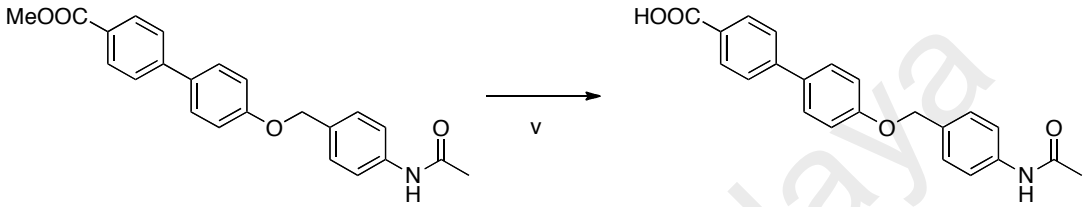

1x-3 **2x**

Procedure

(v) Compound **1x-3** (0.30 g, 0.80 mmol) was dissolved in THF (20 mL) followed by the addition of LiOH (0.96 g, 4.00 mmol) in water (10 mL) and the reaction mixture was allowed to stir overnight. Upon reaction completion, solvents were removed *in vacuo*. pH of the resulting aqueous mixture was adjusted to 2 with 10% HCl to obtain the desired product 4'-((4-acetamidobenzyl)oxy)-[1,1'-biphenyl]-4-carboxylic acid (**2x**), as light yellow powder in 95% yield (0.28 g, 0.76 mmol), and proceeded to next step without further purification. The same procedure was followed for compound 4'-((2-acetamidobenzyl)oxy)-[1,1'-biphenyl]-4-carboxylic acid (**2v**) by using **1v-3** as the starting material. $\mathbf{R_f}$ (EtOAc:Hex; 3:7; v/v) 0.0. **^{1}H NMR (400 MHz, DMSO-d_6): δ 10.03 (s, NH), 7.88 (d, *J*=8.4, 2H), 7.60 (d, *J*=4.4, 2H), 7.58 (d, *J*=4.0, 2H), 7.51 (d, *J*=8.4, 2H), 7.37 (d, *J*=8.4, 2H), 7.06 (d, *J*=8.8, 2H), 5.05 (s, 2H), 2.03 (s, 3H).**

(a) Spectral data for 4'-((2-acetamidobenzyl)oxy)-[1,1'-biphenyl]-4-carboxylic acid, **2v**

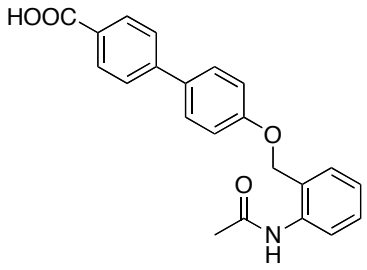

White solid in 92% yield (0.62 g, 1.72 mmol). **^{1}H NMR (400 MHz, DMSO-d_6): δ 8.38 (bs, NH), 7.99 (d, *J*=8.3, 2H), 7.74 (t, *J*=7.3, 1H), 7.51 (t overlap, *J*=8.8, 4H), 7.32-7.27 (m, 2H), 7.10 (t, *J*=6.8, 1H), 7.00 (d, *J*=8.3, 2H), 5.05 (s, 2H), 2.08 (s, 3H).**

Group 5 compounds consisted of **2p**, **2q**, **2v**, **2w** and **2x**. For compounds **2p** and **2q**, initial alkylation of piperidine under neat thermal condition gave the substituted piperidinyl compounds **D5a** and **D6a**, respectively. Protection of the hydroxyl group with methanesulfonyl chloride, followed by Williamson synthesis and saponification with lithium hydroxide furnished the desired carboxylic acid **2p** and **2q** (Scheme 4.10). Some decomposition was encountered in the preparation of compound **D5b**. This may be due to the low carbon number in the alkyl chain making the mesylated compound unstable, which decomposed during the acidic workup. Thus, in the preparation of compound **1p-1**, the Williamson ether synthesis was carried through without isolation of the mesylated intermediate.

As for compounds **2v**, **2w** and **2x**, Suzuki coupling reaction of phenylboronic ester (**A1**) with 4-hydroxybromobenzene (**D2**) gave the methyl 4-hydroxy biphenyl carboxylate (**F2**). Williamson ester synthesis of the methyl 4-hydroxy biphenyl carboxylate (**F2**) with *o*-, *m*-, and *p*-bromomethylnitrobenzene gave the compounds **1v-1**, **1w-1** and **1x-1,** respectively. Reduction of the nitro group using zinc dust in a mixture

of ammonium chloride, tetrahydrofuran and water on compounds **1v-1**, **1w-1** and **1x-1**, followed by N-acetylation and saponification gave the desired compounds **2v**, **2w** and **2x**, as shown in Scheme 4.11.

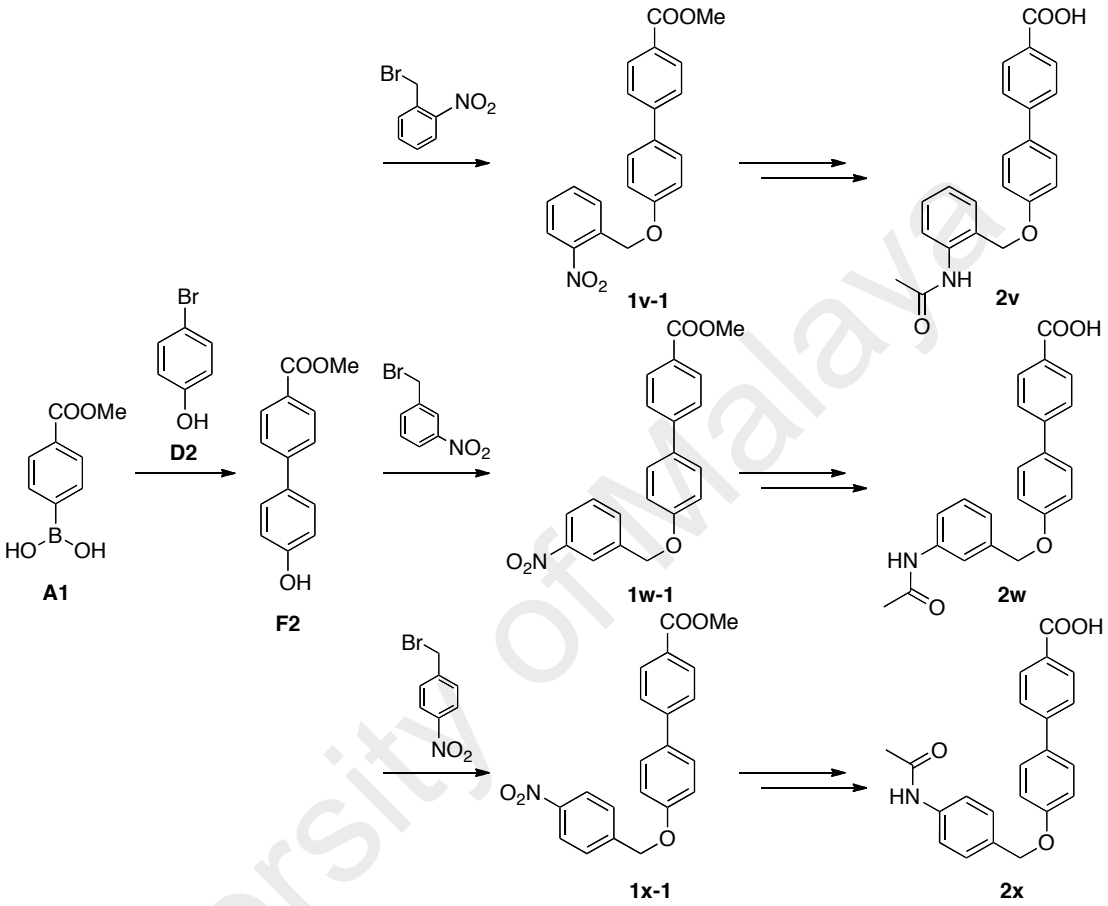

Scheme 4.11. Synthetic strategy for compounds **2v**, **2w** and **2x**.

4.3.5 Synthesis of Carboxylic Acids in Group 6

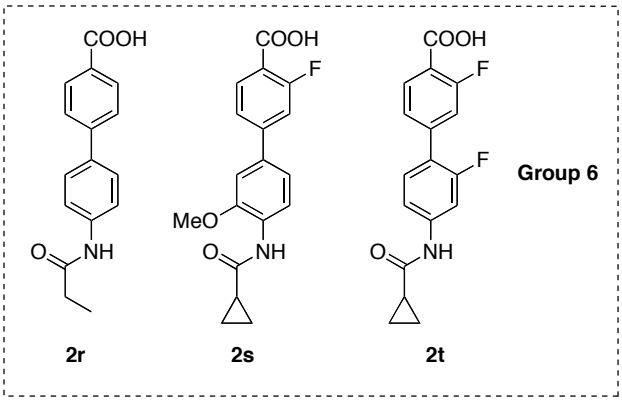

Figure 4.8. Compounds of Group 6.

4.3.5.1 Synthesis of product Methyl 4'-amino-[1,1'-biphenyl]-4-carboxylate, 1r-1

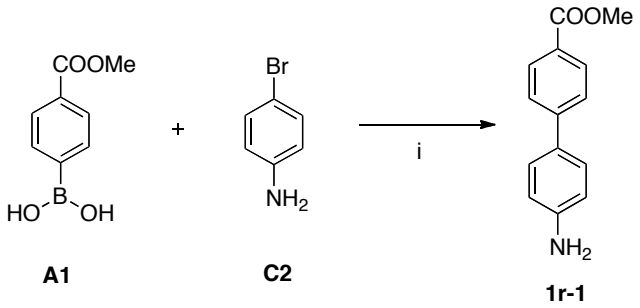

Procedure

(i) To a solution of 1,4-dioxane (30 mL) and water was added CS_2CO_3 (6.4 g, 18.00 mmol), and left to stir bubbling (degassed) under N_2 gas for 10 minutes. (4-(methoxycarbonyl)phenyl)boronic acid (**A1**) (1.00 g, 6.00 mmol) and 4-bromoaniline (**C2**) (0.83 g, 4.80 mmol) were then added to the mixture and allowed to dissolve completely, followed by addition of $Pd(PPh_3)_2Cl_2$ (0.42 g, 0.60 mmol) and stirring for an additional 10 minutes. The reaction mixture was set to reflux at 100°C for about 2-4 hours. After completion of the reaction monitored by TLC, 1,4-dioxane was removed under reduced pressure and extracted with EtOAc (3x) and washed with water, brine followed by drying over $MgSO_4$ and then concentrated. The crude residue was then purified by column chromatography (EtOAc:Hex; 3:1; v/v) to afford the desired product, methyl 4'-amino-[1,1'-biphenyl]-4-carboxylate (**1r-1**), as yellow solid in 50% yield, (0.55 g, 2.42 mmol). $\mathbf{R_f}$ (EtOAc:Hex; 3:7; v/v) 0.3. **^{1}H NMR (400 MHz, $CDCl_3$): δ 8.05 (d, *J*=8.5, 2H), 7.59 (d, *J*=8.5, 2H), 7.46 (d, *J*=8.5, 2H), 6.76 (d, *J*=8.7, 2H), 3.92 (s, 3H), 3.81 (bs, NH_2).**

4.3.5.2 Synthesis of methyl 4'-propionamido-[1,1'-biphenyl]-4-carboxylate, 1r-2

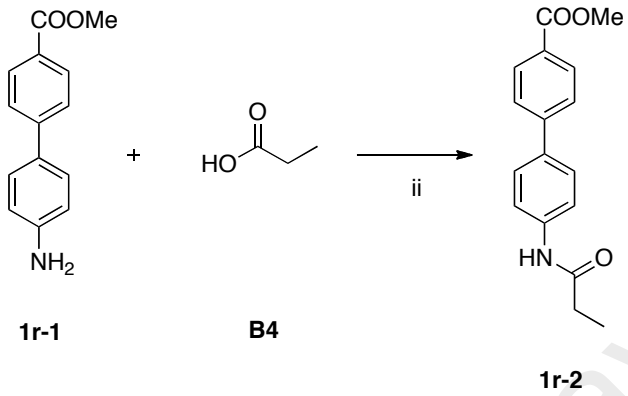

1r-1 **B4** **1r-2**

Procedure

(ii) To a round bottom flask equipped with a magnetic stirrer, was added compound **1r-1** (0.46 g, 2.02 mmol), propionic acid (**B4**) (1.53 mL, 2.02 mmol) and HATU (1.00 g, 2.63 mmol), dissolved in DMF (6 mL) and stirred under N_2 gas atmosphere. Afterwards, DiPEA (2 mL) was added to the mixture and the reaction mixture was left to stir for 3 hours. Water (100 mL) was then added to the reaction mixture, filtered and dried to afford methyl 4'-propionamido-[1,1'-biphenyl]-4-carboxylate (**1r-2**) as light yellow solid in 80% yield (0.46 g, 1.62 mmol), which were used for the next step without purification. $\mathbf{R_f}$ (EtOAc:Hex = 3:7; v/v) 0.15. **^{1}H NMR (400 MHz, $CDCl_3$): δ 8.08 (d, *J*=8.0, 2H), 7.64-7.53 (m, 6H), 7.21 (bs, NH), 3.93 (s, 3H), 2.43 (dd, *J*=7.9, 15.5, 2H), 1.27 (t, *J*=7.2, 3H).**

4.3.5.3 Synthesis of methyl 4'-propionamido-[1,1'-biphenyl]-4-carboxylic acid, 2r

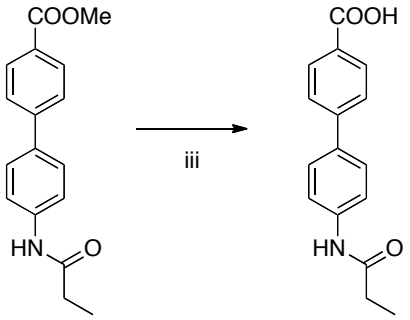

1r-2 **2r**

Procedure

(iii) Compound **1r-2** (0.46 g, 1.62 mmol) was dissolved in THF (40 mL), followed by the addition of LiOH (0.19 g, 8.11 mmol) in water (20 mL) and the reaction mixture was allowed to stir overnight. Upon completion of reaction, solvents were removed *in vacuo*. pH of the resulting aqueous mixture was adjusted to 2 with 10% HCl to obtain the desired product, 4'-propionamido-[1,1'-biphenyl]-4-carboxylic acid (**2r**) as pale brown solid in 93% yield (0.41 g, 1.52 mmol) and used without purification for next step. $\mathbf{R_f}$(EtOAc:Hex; 2:1; v/v) 0.0. **^{1}H NMR (400 MHz, DMSO-d_6): δ 10.02 (s, NH), 7.98 (d, *J*=8.3, 2H), 7.65 (d, *J*=8.3, 2H), 7.72 (d, *J*=9.3, 2H) 7.67 (d, *J*=8.5, 2H), 2.34 (dd, *J*=7.5, 15.1, 2H), 1.08 (t, *J*=7.6, 3H).**

4.3.5.4 Synthesis of 2-methoxy-4-(4,4,5,5-tetramethyl-1,3,2-dioxaborolan-2-yl)aniline, D1a

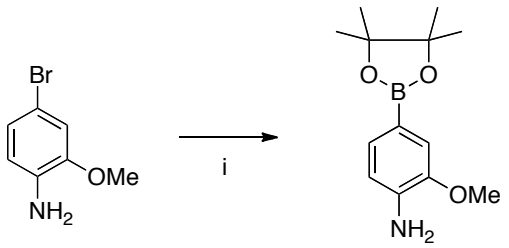

D1 **D1a**

Procedure

(i) To a solution of 1,4-dioxane (30 mL) was added [1-1'-bis(diphenylphosphino)ferrocene]dichloropalladium ($Pd(dppf)Cl_2$) (0.40 g, 0.49 mmol) and degassed for 10 minutes, followed by the addition of KOAc (0.97 g, 9.89 mmol). 4-bromo-2-methoxyaniline (**D1**) (1.00 g, 4.95 mmol) and bis(pinacolato)diboron (1.89 g, 7.42 mmol) was added to the mixture, degassed for another 10 minutes and then refluxed at 80°C. The reaction mixture was filtered through celite and extracted with EtOAc, washed with water, brine, dried over $MgSO_4$ and concentrated to afford the crude product, which was purified by flash column chromatography with EtOAc:Hex (3:7; v/v) to yield product of 2-methoxy-4-(4,4,5,5-tetramethyl-1,3,2-dioxaborolan-2-yl)aniline (**D1a**) as brown liquid in 88% yield (1.08 g, 4.35 mmol). $\mathbf{R_f}$ (EtOAc:Hex; 3:7; v/v) 0.3. **^{1}H NMR (400 MHz, $CDCl_3$): δ 7.33 (d, *J*=7.9, 1H), 7.24 (s, 1H), 6.72 (d, *J*=7.6, 1H), 3.91 (s, 3H), 1.36 (s, 12H).**

4.3.5.5 Synthesis of methyl 4-bromo-2-fluorobenzoate, B2a

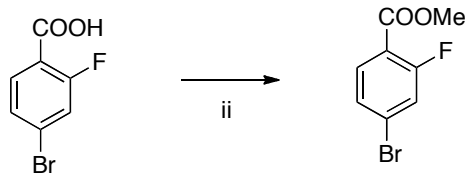

B2 **B2a**

Procedure

(ii) 4-Bromo-2-fluorobenzoic acid (**B2**) (1.00 g, 4.56 mmol) was added to a solution of MeOH (100 mL) dissolved with EDCI (0.92 g, 4.82 mmol). Afterwards, DiPEA (1.20 mL, 5.94 mmol) was added and left to stir at room temperature for 2 hours. Upon completion of the reaction, MeOH was removed *in vacuo* and the solids were washed with water, filtered and dried to afford methyl 4-bromo-2-fluorobenzoate (**B2a**) as light yellow solid in 67% (0.71 g, 3.06 mmol). This was used for the next step without purification. $\mathbf{R_f}$ (EtOAc:Hex; 3:7; v/v) 0.4. **^{1}H NMR (400 MHz, $CDCl_3$): δ 7.82-7.77 (m, 1H), 7.35-7.29 (m, 2H), 3.89 (s, 3H).**

4.3.5.6 Synthesis of methyl 4'-amino-3-fluoro-3'-methoxy-[1,1'-biphenyl]-4-carboxylate, 1s-1

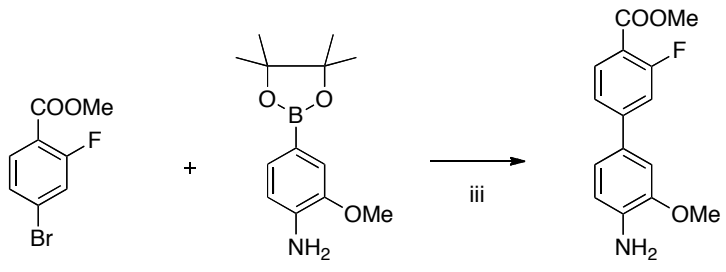

B2a **D1a** **1s-1**

Procedure

(iii) To a solution of 1,4-dioxane (30 mL) and water (10 mL), was added CS_2CO_3 (3.79 g, 0.01 mol) and left to stir bubbling (degassed) under N_2 gas for 10 minutes. Compound **D1a** (0.89 g, 3.58 mmol) and compound **B2a** (1.00 g, 4.29 mmol) were then added to the mixture and allowed to dissolve completely followed by addition of $Pd(PPh_3)_2Cl_2$ (0.25 g, 0.36 mmol) and stirred for an additional 10 minutes. Reaction mixture was set to reflux at 100°C for about 4.5 hours. After reaction completion, monitored by TLC, 1,4-dioxane was removed *in vacuo* and extracted with EtOAc, washed with water, brine followed by drying over $MgSO_4$ and concentration. The crude residue was then purified by column chromatography (EtOAc:Hex; 3:7; v/v) to afford the desired product methyl 4'-amino-3-fluoro-3'-methoxy-[1,1'-biphenyl]-4-carboxylate (**1s-1**) as yellow solid in 60% yield (0.59 g, 2.14 mmol). $\mathbf{R_f}$ (EtOAc:Hex; 3:7; v/v) 0.2. **^{1}H NMR (400 MHz, $CDCl_3$): δ 7.88 (t, *J*=8.0, 1H), 7.31 (dd, *J*=2.0, 8.4, 1H), 7.23 (dd, *J*=2.0, 12.8, 1H), 7.02 (dd, *J*=2.0, 8.0, 1H), 6.96 (d, *J*=2.0, 1H), 6.70 (d, *J*=8.4, 1H), 3.92 (bs, NH), 3.86 (s, 6H).**

4.3.5.7 Synthesis of methyl 4'-(cyclopropanecarboxamido)-3-fluoro-3'-methoxy-[1,1'-biphenyl]-4-carboxylate, 1s-2

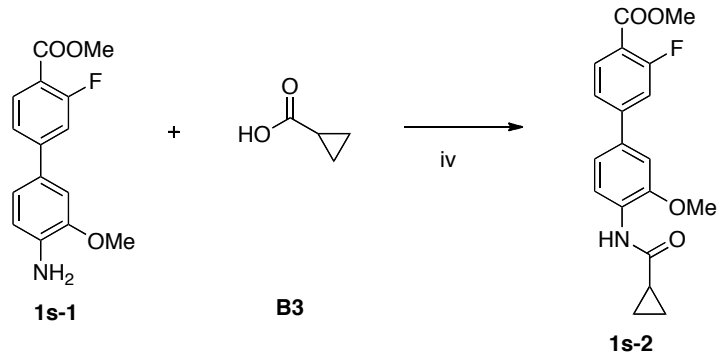

Procedure

(iv) To a round bottom flask equipped with a magnetic stirrer was added compound **1s-1** (0.50 g, 1.82 mmol), cyclopropanecarboxylic acid (**B3**) (0.14 mL, 1.82 mmol), and HATU (0.90 g, 2.36 mmol) dissolved in DMF (6 mL) and stirred under N_2 gas atmosphere. Afterwards, DiPEA (2 mL) was added to the mixture and reaction mixture was left to stir for 3 hours. Water (100 mL) was added to the reaction mixture, filtered and dried to afford methyl 4'-(cyclopropanecarboxamido)-3-fluoro-3'-methoxy-[1,1'-biphenyl]-4-carboxylate (**1s-2**) as light yellow solid in 90% yield (0.56 g, 1.63 mmol) which was used without further purification. $\mathbf{R_f}$ (EtOAc:Hex; 3:7; v/v) 0.3. **Reaction proceed to next step without purification.**

4.3.5.8 Synthesis of 4'-(cyclopropanecarboxamido)-3-fluoro-3'-methoxy-[1,1'-biphenyl]-4-carboxylic acid, 2s

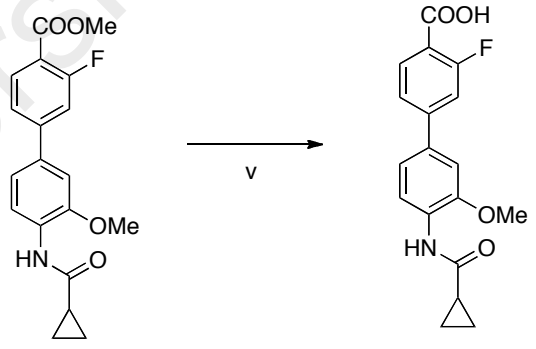

1s-2 **2s**

Procedure

(v) Compound of **1s-2** (0.50 g, 1.46 mmol) was dissolved in MeOH:THF (10 mL; 1:1; v/v), followed by addition of LiOH (0.17 g, 7.28 mmol) in water (5 mL), and the reaction mixture was allowed to stir overnight. Upon reaction completion monitored by TLC, solvents were removed *in vacuo*. pH of the

resulting aqueous mixture wass adjusted to 2 with 10% HCl to obtain the desired product, 4'-(cyclopropanecarboxamido)-3-fluoro-3'-methoxy-[1,1'-biphenyl]-4-carboxylic acid (**2s**) as white solid in 95% yield (0.45 g, 1.38 mmol), that was filtered and dried, used without further purification. $\mathbf{R_f}$ (EtOAc:Hex; 3:7; v/v) 0.0. **^{1}H NMR (400 MHz, CD_3OH): δ 8.00 (d, *J*=8.3, 1H), 7.93 (t, *J*=7.8, 1H), 7.51 (d, *J*=8.5, 1H), 7.45 (d, *J*=11.9, 1H), 7.29 (s, 1H), 7.24 (d, *J*=8.3, 1H), 3.99 (s, 3H), 1.86 (m, 1H), 0.96-0.95 (m, 2H), 0.87-0.85 (m, 2H).**

4.3.5.9 Synthesis of 3-fluoro-4-(4,4,5,5-tetramethyl-1,3,2-dioxaborolan-2-yl)aniline, C3a

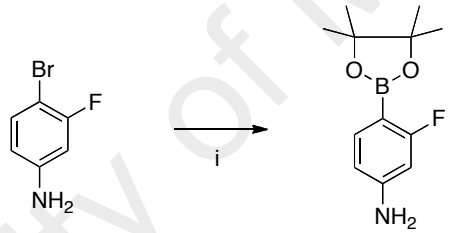

C3 **C3a**

Procedure

(i) To a solution of 1,4-dioxane (15 mL) was added [1-1'-bis(diphenylphosphino)ferrocene]dichloropalladium ($Pd(dppf)Cl_2$) (0.21 g, 0.26 mmol) and degassed for 10 minutes, followed by the addition of KOAc (0.52 g, 5.26 mmol). 4-bromo-3-fluoroaniline (**C3**) (0.50 g, 2.63 mmol) and bis(pinacolato)diboron (1.00 g, 3.94 mmol) was added to the mixture, degassed for another 10 minutes and then refluxed at 80°C. The reaction mixture was filtered through celite and extracted with EtOAc (3x), washed with water, brine, dried over $MgSO_4$ and concentrated to afford crude product, which afterwards purified by flash column chromatography with EtOAc:Hex (3:7; v/v) to yield

product of 3-fluoro-4-(4,4,5,5-tetramethyl-1,3,2-dioxaborolan-2-yl)aniline (**C3a**) as light brown solid in 99% yield (0.62 g, 2.61 mmol). $\mathbf{R_f}$ (EtOAc:Hex; 3:7; v/v) 0.3. **^{1}H NMR (400 MHz, $CDCl_3$): δ 7.15 (t, *J*=7.8, 1H), 6.36 (dd, *J*=2.7, 10.5, 1H), 6.26 (dd, *J*=2.7, 8.8, 1H), 3.55 (bs, NH_2), 1.25 (s, 12H).**

4.3.5.10 Synthesis of methyl 4'-amino-2',3-difluoro-[1,1'-biphenyl]-4-carboxylate, 1t-1

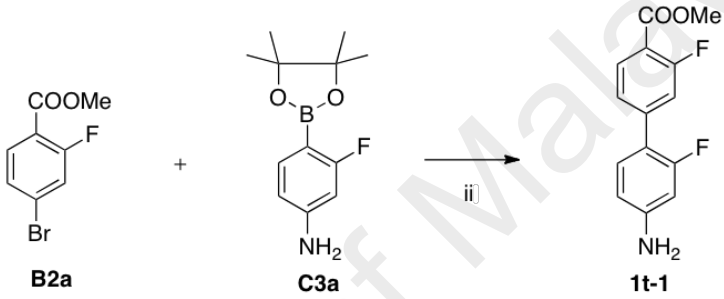

Procedure

(ii) To a solution of 1,4-dioxane (15 mL) and water (5 mL), was added CS_2CO_3 (1.58 g, 4.83 mmol), and left to stir bubbling (degassed) under N_2 gas for 10 minutes. Compound **C3a** (0.63 g, 2.66 mmol) and compound **B2a** (0.56 g, 2.42 mmol) were then added to the mixture and allowed to dissolve completely followed by addition of $Pd(PPh_3)_2Cl_2$ (0.20 g, 0.24 mmol) and stirring for an additional 10 minutes. The reaction mixture was set to reflux at 100°C for about 4 hours. After completion of reaction monitored by TLC, 1,4-dioxane was removed *in vacuo* and extracted with EtOAc, washed with water, brine followed by drying over $MgSO_4$ and concentration. The crude residue was then purified by column chromatography (EtOAc:Hex; 3:7; v/v) to afford desired product methyl 4'-amino-2',3-difluoro-[1,1'-biphenyl]-4-carboxylate (**1t-1**) as yellow solid in 63% (0.41 g, 1.54 mmol). $\mathbf{R_f}$ (EtOAc:Hex; 3:7; v/v) 0.2. **^{1}H NMR (400**

MHz, CD_3OD): δ 7.90 (t, *J*=7.9, 1H), 7.38 (d, *J*=8.2, 1H), 7.31 (d, *J*=12.8, 1H), 7.26 (t, *J*=8.5, 1H), 6.54 (dd, *J*=2.1, 6.4, 1H), 6.46 (dd, *J*=2.1, 11.8, 1H), 3.89 (s, 3H).

4.3.5.11 Synthesis of methyl 4'-(cyclopropanecarboxamido)-2',3-difluoro-[1,1'-biphenyl]-4-carboxylate, 1t-2

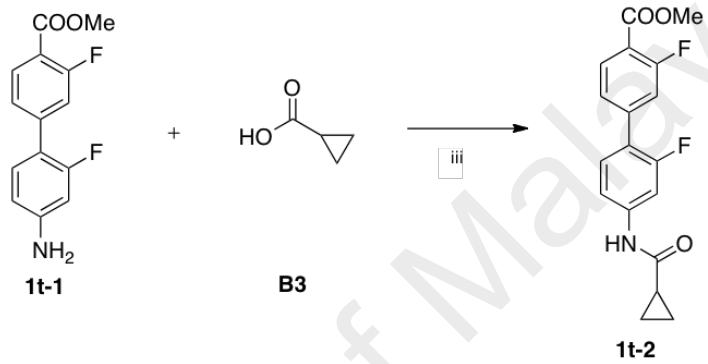

Procedure

(iii) To a round bottom flask equipped with a magnetic stirrer was added compound **1t-1** (0.37 g, 1.41 mmol), cyclopropanecarboxylic acid (**B3**) (0.11 mL, 1.41 mmol), HATU (0.70 g, 1.82 mmol) and dissolved in DMF (6 mL) with stirring under N_2 gas atmosphere. Afterwards, DiPEA (1 mL) was added to the mixture and reaction mixture was left to stir for 3 hours. Water (80 mL) was added to the reaction mixture, filtered and dried to afford methyl 4'-(cyclopropanecarboxamido)-2',3-difluoro-[1,1'-biphenyl]-4-carboxylate (**1t-2**) as light yellow solid in 92% yield (0.43 g, 1.30 mmol) which was then used without further purification. $\mathbf{R_f}$ (EtOAc:Hex; 1:1; v/v) 0.3. **^{1}H NMR (400 MHz, $CDCl_3$): δ 7.92 (t, *J*=8.0, 1H), 7.55 (d, *J*=12.9, 1H), 7.44 (s, 1H), 7.34-7.25 (m, 3H overlap), 1.47-1.45 (m, 1H overlap), 1.08-1.04 (m, 2H), 0.86-0.81 (m, 2H).**

4.3.5.12 Synthesis of 4'-(cyclopropanecarboxamido)-2',3-difluoro-[1,1'-biphenyl]-4-carboxylic acid, 2t

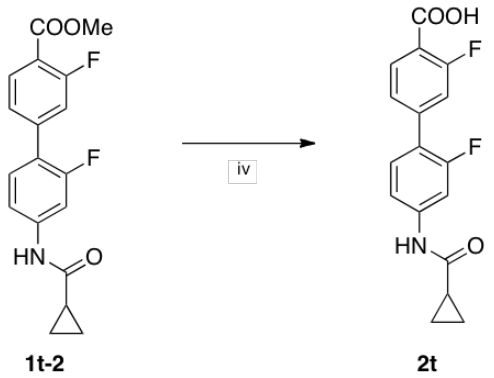

1t-2 **2t**

Procedure

(iv) Compound **1t-2** (0.43 g, 1.30 mmol) was dissolved in THF (20 mL), followed by addition of LiOH (0.16 g, 6.49 mmol) in water (20 mL), and the reaction mixture was allowed to stir overnight. Upon reaction completion, solvents were removed *in vacuo*. pH of the resulting aqueous mixture was adjusted to 2 with 10% HCl to obtain the desired product 4'-(cyclopropanecarboxamido)-2',3-difluoro-[1,1'-biphenyl]-4-carboxylic acid (**2t**) as light yellow solid in 99% yield (0.41 g, 1.29 mmol). $\mathbf{R_f}$ (EtOAc:Hex; 1:1; v/v) 0.0. **^{1}H NMR (400 MHz, DMSO-d_6): δ 10.55 (s, NH), 7.92 (t, *J*=8.0, 1H), 7.72 (d, *J*=13.6, 1H), 7.57 (t, *J*=8.8, 1H), 7.48 (s, 1H), 7.45 (s, 1H), 7.40 (d, *J*=8.3, 1H), 1.79-1.76 (m, 1H), 0.84-0.82 (m, 4H).**

Group 6 involves three compounds, **2r**, **2s** and **2t**. Similar strategies as in preparation of previous compounds, involving Suzuki coupling, amide coupling and saponification were employed. However, slight differences for preparation of compounds, **2s** and **2t** were encountered, whereby their starting materials, 4-bromo-2-methoxyaniline (**D1**)

and 4-bromo-3-floroaniline (**C3**), were first subjected to the Miyaura borylation before the Suzuki coupling reaction, as shown in Scheme 4.12.

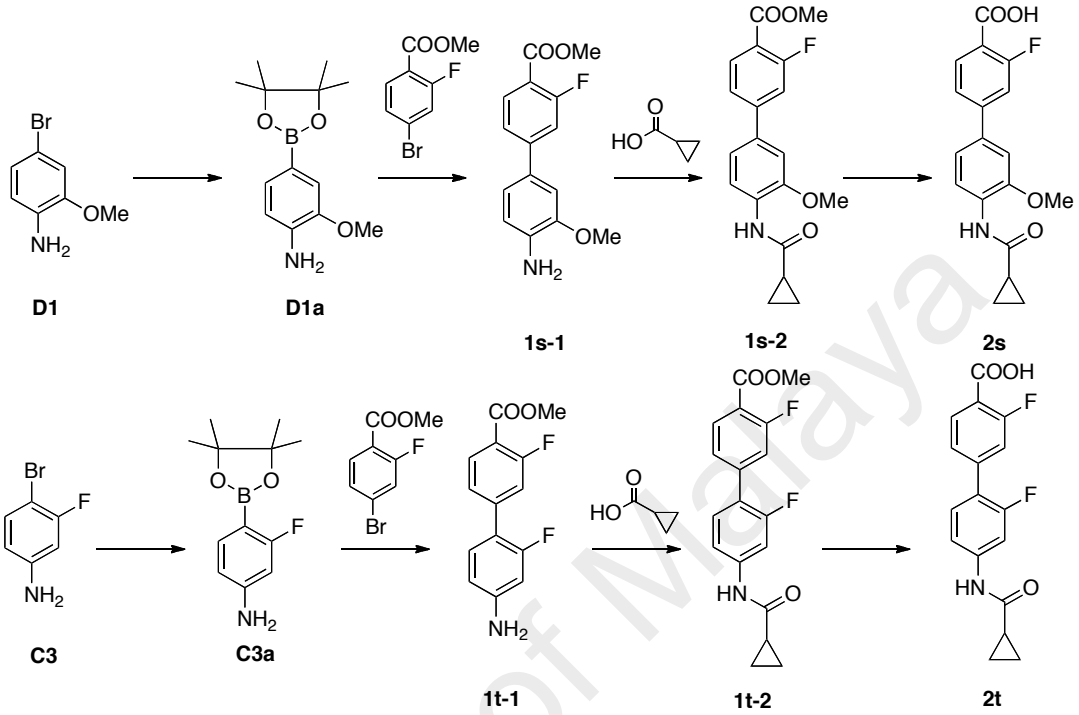

Scheme 4.12. Synthetic strategy for compounds **2s** and **2t**.

In summary, all of the side chain compounds were synthesised in good to excellent yield. Suzuki coupling reactions were used extensively in order to link carbon-carbon bond.

4.4 Synthesis of Benzimidazole Derivatives

Benzimidazole compounds serve a wide range of therapeutic effects, as described in the previous chapters. There is a plethora of organisations involved in the pursuit of benzimidazole as either PARP-1, or DHODH inhibitor (White e*t al*., 2000; Zhu e*t al*., 2008; Penning e*t al*., 2009; Tong e*t al*., 2009; Romero-Castro e*t al*., 2011). We

continued our study on benzimidazoles with carboxylic acid side chains as the starting materials as shown in the Scheme 4.13 below, and linking these compounds to obtain benzimidazole as PARP-1 and DHODH inhibitors.

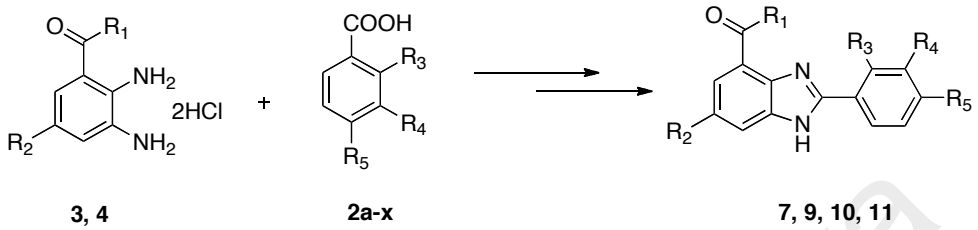

3, 4 **2a-x** **7, 9, 10, 11**

Scheme 4.13. General benzimidazole synthesis route.

There are various ways to prepare benzimidazole compounds reported in the literature. Penning and co-workers described a convenient method in synthesising the scaffold, as illustrated in Scheme 4.14 (Penning e*t al*., 2008, 2010).

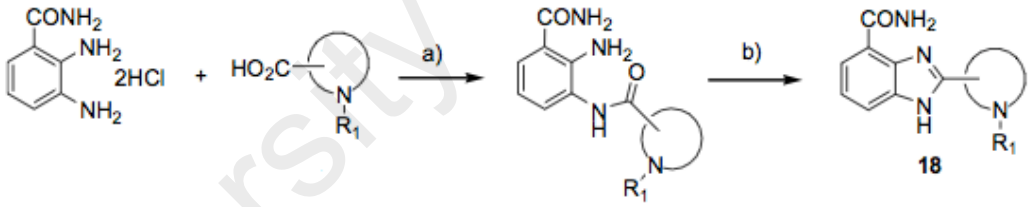

Scheme 4.14. Reagents and conditions: a) CDI, DMF, pyridine; b) AcOH, heat. Synthetic procedure reported by Penning and co-workers (Penning e*t al*., 2008, 2010).

Zhu and co-workers (Zhu e*t al*., 2013) also reported a procedure to prepare a benzimidazole derivative where the benzene ring is substituted with a pyridine ring, as shown in Scheme 4.15. Here, they coupled the diaminonicotinamide with 3-pipecolinic acid and PyBOP or $SOCl_2$, which then underwent cyclisation in acetic acid (Zhu e*t al*., 2013).

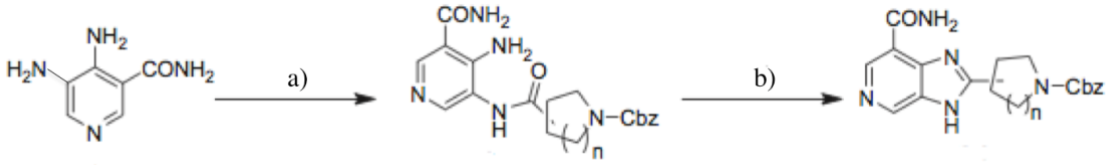

Scheme 4.15. Reagents and conditions: a) PyBOP, 3-pipecolinic acid, DiPEA, DMF, rt, 12h; b) AcOH, 160°C, in an autoclave, 24h. Synthetic procedure reported by Zhu and co-workers (Zhu e*t al*., 2013).

In this work, four compounds, **E1**, **E2**, **E3** and **E4** were used, as shown in Table 4.2, as the starting materials for benzimidazole compounds. The general synthesis scheme is shown in Scheme 4.16.

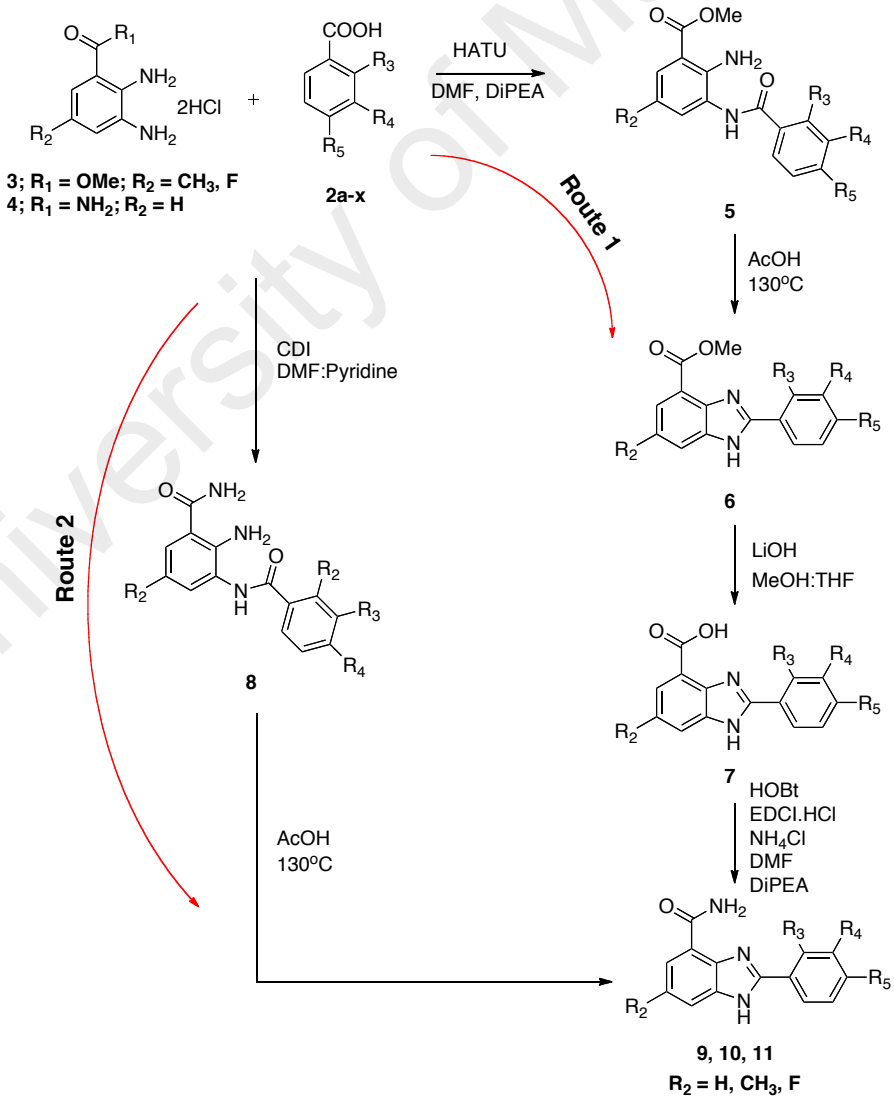

Scheme 4.16. General synthesis route for benzimidazole compounds.

4.4.1 Synthesis of Benzimidazole Derivatives via Route 1

4.4.1.1 General procedure for synthesis of 5

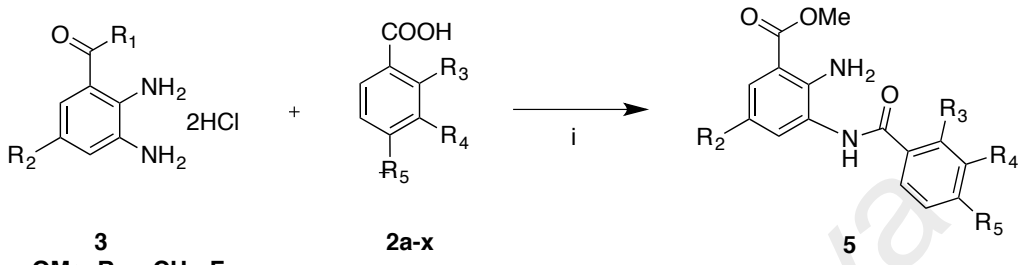

3
R_1 = OMe; R_2 = CH_3, F

2a-x

5

Procedure

(i) To a round bottom flask equipped with a magnetic stir bar was added diamine benzoate (**3**; R_2 = CH_3; F) (1.00 mmol), carboxylic acid **2a-x** (1.00 mmol), and HATU (1.30 mmol), dissolved in DMF (6 mL) and stirred under N_2 gas. DiPEA (2 mL) was then added to the mixture and the reaction mixture was left to stir for 3 hours. Water (100 mL) was added to the reaction mixture, filtered and dried to afford **5**, which was used without further purification. **R_f** (EtOAc:Hex; 3:7; v/v) 0.3.

4.4.1.2 General procedure for synthesis of 6

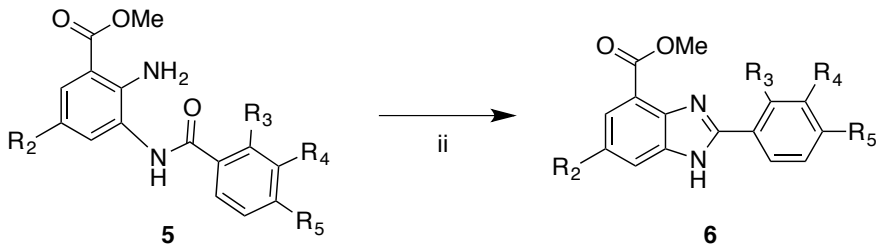

5
R_2 = CH_3, F

6

Procedure

(ii) Compound **5** was dissolved in acetic acid (AcOH) (10 mL) and refluxed at 130°C until reaction was fully completed under TLC analysis monitoring. Flash column chromatography with EtOAc:Hex (3:1; v/v) elution yielded purified compound **6**. $\mathbf{R_f}$ (EtOAc:Hex; 3:1; v/v) 0.32.

4.4.1.3 General procedure for synthesis of 7

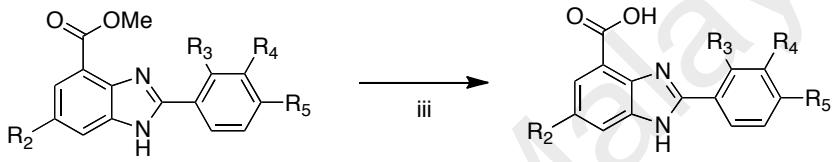

6
R_2 = CH_3, F

7

Procedure

(iii) Compound **6** was dissolved in a mixture of MeOH:THF (1:1; v/v), followed by addition of $LiOH.H_2O$ (3-5 eq) and the reaction mixture was allowed to stir overnight. Upon reaction completion, solvents were removed *in vacuo*. pH of the resulting aqueous mixture was adjusted to 2 with 10% HCl to obtain the desired product **7**, which was filtered, dried and used without further purification. $\mathbf{R_f}$ (EtOAc:Hex; 3:7; v/v) 0.0**.**

4.4.1.4 General procedure for synthesis of 9, 10 and 11

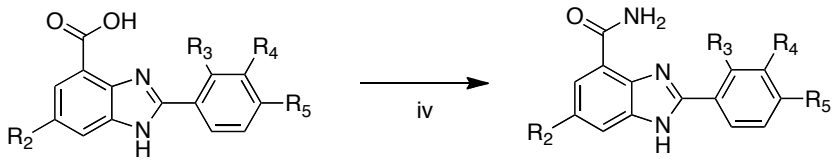

7
R_2 = CH_3, F

9, 10, 11

Procedure

(iv) To a solution of DMF (6 mL) was added EDCI.HCl (2 mmol), HOBt (2.00 mmol), NH_4Cl (5.00 mmol), and compound **7** (1.00 mmol) followed by DiPEA (1 mL), and was left to stir overnight until reaction was completed, judged by TLC analysis. Water (100 mL) was added to the reaction mixture after which the resulting product was filtered and dried to afford compound **9, 10** and **11**. $\mathbf{R_f}$ (EtOAc:Hex; 3:7; v/v) 0.15.

The carboxylic acids of **2a-x** were subsequently coupled with diamine **3** and **4** to furnish compounds **5** and **8**, respectively, as illustrated in Scheme 4.16. Two different routes were employed to prepare the benzimidazole compounds. The first route (route 1) involves coupling of diamine **3** using standard 1-[bis(dimethylamino)methylene]-1H-1,2,3-triazolo[4,5-b]pyridinium 3-oxide hexafluorophosphate (HATU) in dimethylformamide (DMF), and the presence of *N,N*-diisopropylethylamine (DiPEA) as base (Zhu e*t al*., 2012) for the formation of **5**. Subsequent thermal cyclisation of **5** in acetic acid (AcOH) gave the intermediate **6**. Saponification of the ester **6** with lithium hydroxide (LiOH) provided the carboxylic acid derivatives **7a-g** (Table 4.3), which were subsequently converted to the corresponding carboxamide benzimidazole derivatives **9a-j, 10a-h** and **11a-e** with hydroxybentzotriazole (HOBt) and 1-ethyl-3-(3-dimethylaminopropyl)carbodiimide (EDCI.HCl).

4.4.2 Synthesis of Benzimidazole Derivatives via Route 2

4.4.2.1 General procedure for synthesis of 8

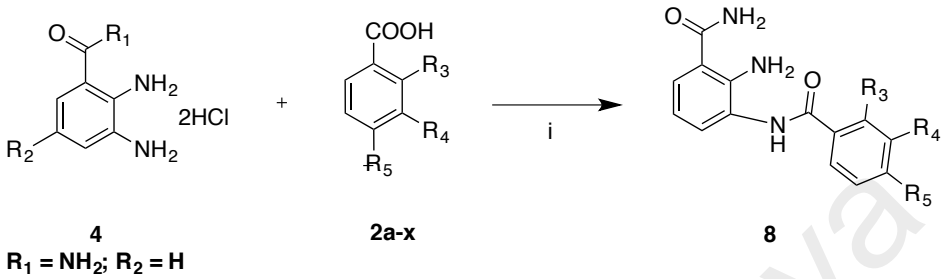

4
$R_1 = NH_2$; $R_2 = H$

2a-x

8

Procedure

(i) To a solution of DMF:pyridine (1:1; v/v) was added compound **2a-x** (0.90 mmol) and 1,1'-Carbonyldiimidazole (**CDI**) (0.90 mmol) and stirred at 60°C under N_2 gas atmosphere for 3 hours. After the reaction mixture is cooled down to room temperature, 2,3-diaminobenzamide **4** (1.00 mmol) was added and left to stir overnight until the completion of the reaction, monitored by TLC analysis. Water (100 mL) was added and the resulting product of **8** was filtered and dried without further purification. $\mathbf{R_f}$ (EtOAc:Hex; 1:1; v/v) 0.3.

4.4.2.2 General procedure for synthesis of 9, 10 and 11

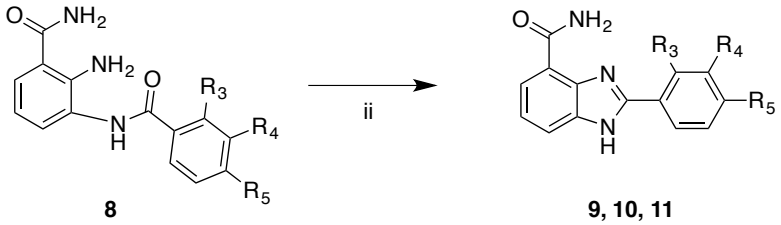

8

9, 10, 11

Procedure

(ii) Compound **8** was dissolved in acetic acid (AcOH) (10 mL) and refluxed at 130°C until reaction was fully completed under TLC analysis monitoring. Flash column chromatography with EtOAc:Hex (3:1; v/v) elution yielded purified compound **9, 10** and **11**. $\mathbf{R_f}$ (EtOAc 100%) 0.33.

Compounds **9a-j, 10a-h** and **11a-e** (Table 4.4) could also be prepared via an alternative route (Route 2), as shown in Scheme 4.16. Reacting 2,3-diaminobenzamide **4** with 1,1'-carbonyldiimidazole (CDI) in pyridine and dimethylformamide (DMF) (1:1, v/v) with **2a-x** gave the amide **8**, which could be then be cyclised to the benzimidazole **9** by refluxing in AcOH, as reported by Penning and co-workers (Penning e*t al*., 2009).

Table 4.3. Chemical structures of synthesised benzimidazole carboxylic acid derivatives.

Entry	Compound	Entry	Compound
7a	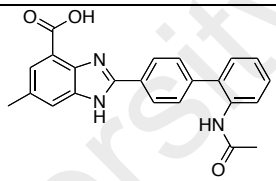	**7e**	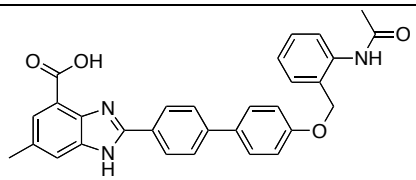
7b	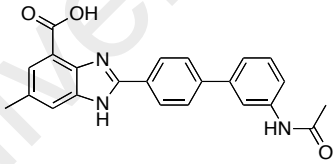	**7f**	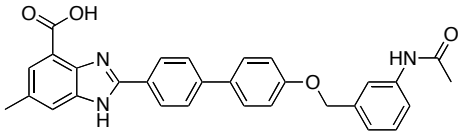
7c	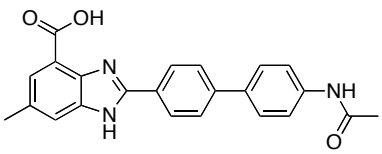	**7g**	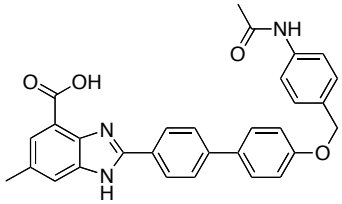
7d	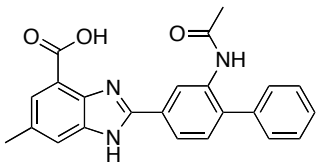		

4.4.3 NMR Data for Compounds 7a-g (Refer to Appendix A2 for spectra)

(i) 2-(2'-acetamido-[1,1'-biphenyl]-4-yl)-6-methyl-1*H*-benzimidazole-4-carboxylic acid, **7a**

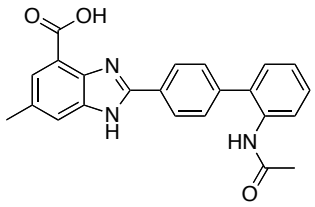

^{1}H NMR (270MHz, CD_3OD): δ 8.03 (d, *J*=8.3, 2H), 7.84 (s, 1H), 7.53 (d, *J*=8.3, 1H), 7.40 (d, *J*=8.3, 2H), 7.38 (d, *J*=5.9, 1H), 7.30-7.21 (m, 3H), 2.33 (s, 3H), 1.88 (s, 3H). ^{13}C NMR (67MHz, CD_3OD): δ 172.44, 167.62, 154.55, 145.16, 142.97, 138.17, 135.47, 133.25, 131.39, 130.50, 129.48, 128.58, 128.52, 128.46, 127.96, 127.44, 124.14, 115.25, 22.92, 21.29. HRMS (ESI) calculated for $C_{23}H_{19}N_3O_3$ $(M+H)^+$: 386.1504, found 386.1510

(ii) 2-(3'-acetamido-[1,1'-biphenyl]-4-yl)-6-methyl-1*H*-benzimidazole-4-carboxylic acid, **7b**

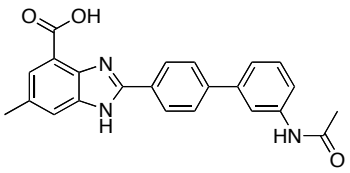

^{1}H NMR (270MHz, DMSO-d_6): δ 10.08 (s, NH), 8.37 (d, *J*=8.1, 2H), 7.97 (s, 1H), 7.76 (d, *J*=8.4, 2H), 7.70 (s, 1H), 7.65 (s, 1H), 7.60 (bs, 1H), 7.41 (s, 1H), 7.39 (s, 1H), 2.46 (s, 3H), 2.07 (s, 3H). ^{13}C NMR (67MHz, DMSO-d_6): δ

168.67, 166.83, 152.52, 141.74, 140.04, 139.82, 129.53, 128.60, 128.12, 126.91, 125.80, 121.57, 118.67, 117.32, 24.12, 21.02. HRMS (ESI) calculated for $C_{23}H_{19}N_3O_3$ $(M+H)^+$: 386.1504, found 386.1502

(iii) 2-(4'-acetamido-[1,1'-biphenyl]-4-yl)-6-methyl-1*H*-benzimidazole-4-carboxylic acid, **7c**

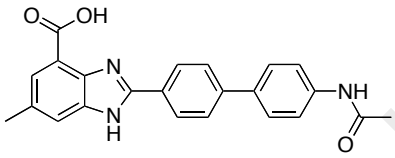

^{1}H NMR (400MHz, DMSO-d_6): δ 10.28 (s, NH), 8.33 (d, *J*=8.3, 2H), 7.91 (d, *J*=8.0, 2H), 7.83 (s, 1H), 7.81 (s, 1H), 7.75 (d, *J*=9.0, 2H), 7.72 (d, *J*=8.8, 2H), 2.50 (s, 3H), 2.06 (s, 3H). ^{13}C NMR (100MHz, DMSO-d_6): δ 169.10, 166.12, 151.38, 143.58, 139.96, 135.99, 134.90, 133.14, 131.05, 129.69, 128.22, 127.49, 126.71, 123.07, 119.71, 119.44, 117.08, 24.23, 21.12. HRMS (ESI) calculated for $C_{23}H_{19}N_3O_3$ $(M+H)^+$: 386.1504, found 386.1499

(iv) 2-(2-acetamido-[1,1'-biphenyl]-4-yl)-6-methyl-1*H*-benzimidazole-4-carboxylic acid, **7d**

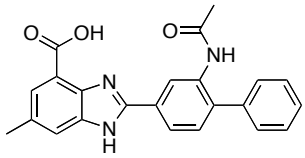

^{1}H NMR (400MHz, DMSO-d_6): δ 9.52 (s, NH), 8.40 (s, 1H), 8.22 (d, *J*=7.8, 1H), 7.74 (s, 1H), 7.71 (s, 1H), 7.52 (d, *J*=8.1, 1H), 7.49-7.46 (m, 5H), 1.95 (s,

3H). ^{13}C NMR (100MHz, DMSO-d_6): δ 169.06, 166.51, 151.76, 139.21, 138.29, 135.32, 132.22, 130.79, 128.66, 128.55, 127.73, 127.55, 127.05, 126.43, 125.49, 116.10, 22.97, 20.98. HRMS (ESI) calculated for $C_{23}H_{19}N_3O_3$ $(M+H)^+$: 386.1504, found 386.1505

(v) 2-(4'-((2-acetamidobenzyl)oxy)-[1,1'-biphenyl]-4-yl)-6-methyl-1*H*-benzimidazole-4-carboxylic acid, **7e**

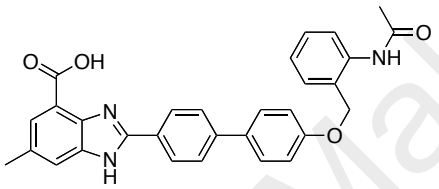

^{1}H NMR (400MHz, DMSO-d_6): δ 9.66 (s, NH), 8.40 (d, *J*=8.5, 2H), 7.96 (d, *J*=7.9, 2H), 7.89 (bs, 2H), 7.80 (d, *J*=8.5, 2H), 7.47 (d, *J*=7.3, 1H), 7.43 (d, *J*=7.9, 1H), 7.30 (t, *J*=7.9, 1H), 7.20 (t, *J*=7.3, 1H), 7.12 (d, *J*=8.5, 2H), 5.16 (s, 2H), 2.54 (s, 3H), 2.07 (s, 3H). ^{13}C NMR (100MHz, DMSO-d_6): δ 168.71, 165.65, 158.94, 150.77, 144.10, 135.75, 130.88, 130.76, 130.04, 129.97, 129.49, 128.71, 128.33, 128.02, 126.44, 125.42, 125.30, 121.20, 118.51, 117.25, 115.50, 66.24, 23.31, 20.87. HRMS (ESI) calculated for $C_{30}H_{25}N_3O_4$ $(M+H)^+$: 492.1923, found 492.1929

(vi) 2-(4'-((3-acetamidobenzyl)oxy)-[1,1'-biphenyl]-4-yl)-6-methyl-1*H*-benzimidazole-4-carboxylic acid, **7f**

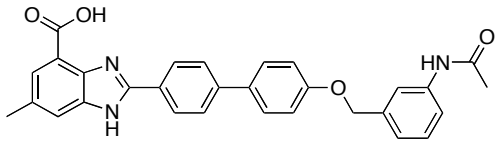

^{1}H NMR (400MHz, DMSO-d_6): δ 10.26 (s, NH), 8.40 (d, *J*=8.3, 2H), 7.89 (d, *J*=8.3, 2H), 7.84 (s, 1H), 7.83 (s, 1H), 7.78 (s, 1H), 7.73 (d, *J*=8.5, 2H), 7.60 (d, *J*=8.0, 1H), 7.31 (t, *J*=7.8, 1H), 7.13 (d, *J*=10.2, 1H), 7.10 (d, *J*=8.8, 2H), 5.12 (s, 2H), 2.51 (s, CH_3), 2.09 (s, CH_3). ^{13}C NMR (100MHz, DMSO-d_6): δ 168.66, 165.72, 158.89, 150.65, 143.78, 139.67, 137.47, 135.24, 134.37, 130.83, 129.99, 129.80, 128.86, 128.41, 128.23, 126.34, 122.19, 121.55, 118.62, 118.08, 117.09, 115.46, 115.42, 69.42, 24.12, 20.96. HRMS (ESI) calculated for $C_{30}H_{25}N_3O_4$ $(M+H)^+$: 492.1923, found 492.1922

(vii) 2-(4'-((4-acetamidobenzyl)oxy)-[1,1'-biphenyl]-4-yl)-6-methyl-1*H*-benzimidazole-4-carboxylic acid, **7g**

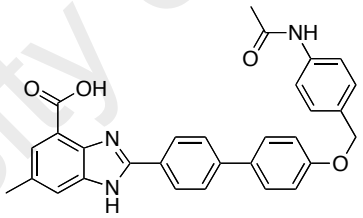

^{1}H NMR (400MHz, DMSO-d_6): δ 10.30 (s, NH), 8.34 (d, *J*=8.5, 2H), 7.88 (d, *J*=8.5, 2H), 7.78 (bs, 2H), 7.75 (d, *J*=8.8, 2H), 7.60 (d, *J*=8.5, 2H), 7.38 (d, *J*=8.5, 2H), 7.12 (d, *J*=8.8, 2H), 5.09 (s, 2H), 2.03 (s, CH_3). ^{13}C NMR (100MHz, DMSO-d_6): δ 168.41, 166.14, 158.77, 151.65, 143.06, 139.09, 133.69, 131.29, 131.14, 129.11, 128.48, 128.14, 127.34, 126.37, 124.12, 120.01, 118.95, 116.60, 115.50, 69.18, 24.11, 20.91. HRMS (ESI) calculated for $C_{30}H_{25}N_3O_4$ $(M+H)^+$: 492.1923, found 492.1928

Table 4.4[a,b]. Chemical structures of synthesised benzimidazole carboxamide derivatives.

Entry	Product	Entry	Product	Entry	Product
9a[a]	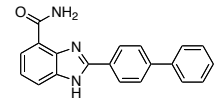	**10a**[a]	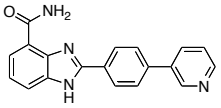	**11a**	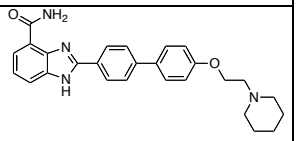
9b	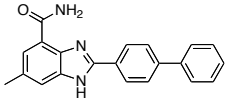	**10b**	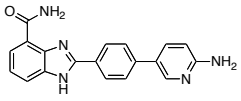	**11b**	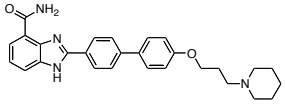
9c[b]	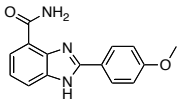	**10c**	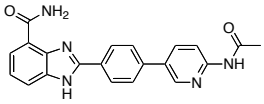	**11c**	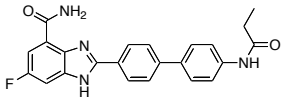
9d	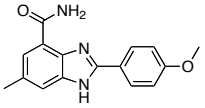	**10d**[a]	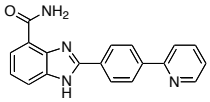	**11d**	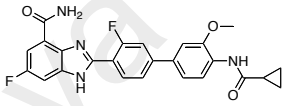
9e[b]	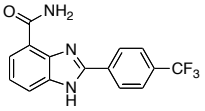	**10e**	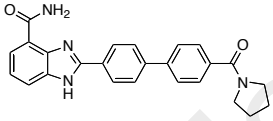	**11e**	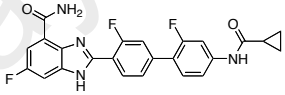
9f	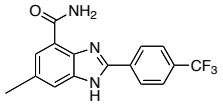	**10f**	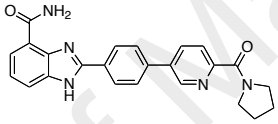		
9g	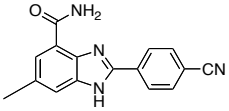	**10g**	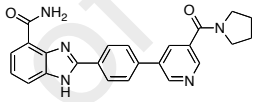		
9h	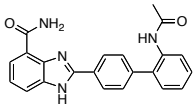	**10h**	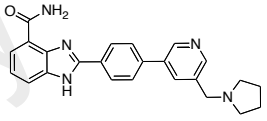		
9i	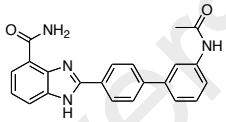				
9j	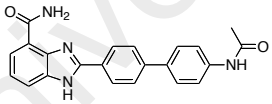				

[a]Compounds reported by Tong and group (Tong e*t al*., 2009).
[b]Compounds reported by White and group (White e*t al*., 2000).

4.4.4 NMR Data for Compounds 9a-j, **10a-h** and **11a-e (Refer to Appendix A3 for spectra)**

(i) 2-([1,1'-biphenyl]-4-yl)-1*H*-benzimidazole-4-carboxamide, **9a**

(Tong e*t al*., 2009)

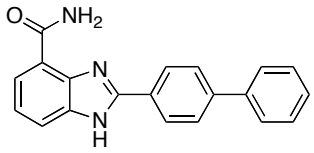

^{1}H NMR (400MHz, DMSO-d_6): δ 9.39 (s, NH), 8.32 (d, *J*=7.8, 2H), 7.90 (d, *J*=7.8, 3H overlap), 7.77 (d, *J*=7.8, 3H overlap), 7.51 (t, *J*=7.4, 2H), 7.41 (t, *J*=7.4, 1H), 7.35 (t, *J*=7.9, 1H). ^{13}C NMR (100MHz, DMSO-d_6): δ 166.44, 151.17, 142.19, 141.66, 139.21, 135.51, 129.23, 128.23, 128.12, 127.60, 127.44, 126, 89, 123.16, 122.58, 122.41, 115.22. HRMS (ESI) calculated for $C_{20}H_{15}N_3O$ $(M+H)^+$: 314.1293, found 314.1294

(ii) 2-([1,1'-biphenyl]-4-yl)-6-methyl-1*H*-benzimidazole-4-carboxamide, **9b**

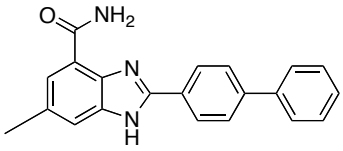

^{1}H NMR (400MHz, DMSO-d_6): δ 13.29 (s, $CONH_2$), 9.34 (s, NH), 8.31 (d, *J*=7.1, 2H), 7.91 (d, *J*=8.1, 1H), 7.79 (d, *J*=7.8, 2H), 7.72 (s, 1H), 7.54 (s, 1H), 7.51 (t, *J*=7.8, 2H), 7.43 (t, *J*=7.3, 1H). ^{13}C NMR (100MHz, DMSO-d_6): δ 166.33, 151.19, 141.89, 139.83, 139.18, 135.76, 132.02, 129.14, 128.23, 128.11,

127.37, 127.33, 126.80, 124.39, 121.87, 114.82, 21.34. HRMS (ESI) calculated for $C_{21}H_{17}N_3O$ $(M+H)^+$: 328.1449, found 328.1461

(iii) 2-(4-methoxyphenyl)-1*H*-benzimidazole-4-carboxamide, **9c**

(White e*t al*., 2000)

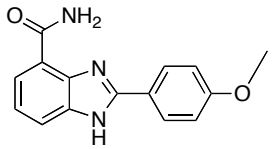

^{1}H NMR (270MHz, DMSO-d_6): δ 13.25 (s, $CONH_2$), 9.44 (s, NH), 8.21 (d, *J*=8.6, 2H), 7.89 (d, *J*=7.3, 1H), 7.73 (d, *J*=7.8, 1H), 7.34 (t, *J*=7.8, 1H), 7.16 (d, *J*=8.6, 2H), 3.87 (s, 3H). ^{13}C NMR (67MHz, DMSO-d_6): δ 166.41, 161.19, 152.11, 141.66, 135.35, 128.59, 122.73, 122.09, 121.92, 121.56, 114.73, 114.55, 55.41. HRMS (ESI) calculated for $C_{15}H_{13}N_3O_2$ $(M+H)^+$: 268.1085, found 268.1081

(iv) 2-(4-methoxyphenyl)-6-methyl-1*H*-benzimidazole-4-carboxamide, **9d**

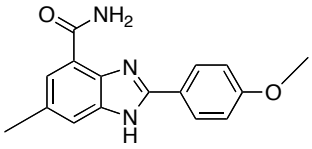

^{1}H NMR (270MHz, DMSO-d_6): δ 12.99 (s, $CONH_2$), 9.28 (s, NH), 8.09 (d, *J*=8.9, 2H), 7.61 (s, 1H), 7.41 (s, 1H), 7.07 (d, *J*=8.9, 2H), 3.79 (s, 3H), 2.41 (s, 3H). ^{13}C NMR (67MHz, DMSO-d_6): δ 166.33, 161.03, 151.59, 139.84, 135.63,

131.35, 128.39, 123.97, 121.72, 121.53, 114.52, 114.47, 55.41, 21.25. HRMS (ESI) calculated for $C_{16}H_{15}N_3O_2$ $(M+H)^+$: 282.1242, found 282.1239

(v) 2-(4-(trifluoromethyl)phenyl)-1*H*-benzimidazole-4-carboxamide, **9e**

(White e*t al*., 2000)

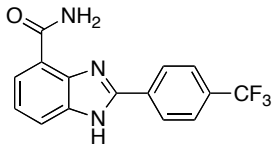

^{1}H NMR (400MHz, DMSO-d_6): δ 13.68 (s, $CONH_2$), 9.28 (s, NH), 8.47 (d, *J*=8.1, 2H), 7.99 (d, *J*=7.8, 2H), 7.91 (d, *J*=7.6, 1H), 7.79 (d, *J*=8.1, 1H), 7.41 (t, *J*=7.8, 1H). ^{13}C NMR (100MHz, DMSO-d_6): δ 165.99, 150.43, 141.33, 135.50, 132.92, 130.45, 130.06, 127.60, 126.10, 123.43, 123.02, 122.84, 115.33. HRMS (ESI) calculated for $C_{15}H_{10}N_3F_3O$ $(M+H)^+$: 306.0853, found 306.0855

(vi) 6-methyl-2-(4-(trifluoromethyl)phenyl)-1*H*-benzimidazole-4-carboxamide, **9f**

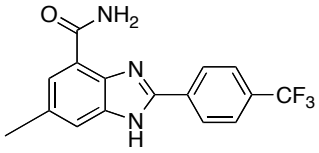

^{1}H NMR (400MHz, DMSO-d_6): δ 13.52 (bs, $CONH_2$), 9.24 (s, NH), 8.44 (d, *J*=8.1, 2H), 7.96 (d, *J*=8.1, 2H), 7.74 (s, 1H), 7.57 (s, 1H), 2.47 (s, 3H). ^{13}C NMR (100MHz, DMSO-d_6): δ 166.09, 149.81, 139.51, 135.78, 133.10, 132.54, 130.16, 129.84, 128.14, 127.42, 126.00, 122.72, 122.19, 115.19, 21.25. HRMS (ESI) calculated for $C_{16}H_{12}N_3F_3O$ $(M+H)^+$: 320.1010, found 320.1009

(vii) 2-(4-cyanophenyl)-6-methyl-1*H*-benzimidazole-4-carboxamide, **9g**

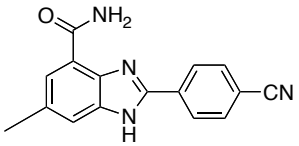

^{1}H NMR (400MHz, DMSO-d_6): δ 13.45 (bs, $CONH_2$), 9.29 (s, NH), 8.31 (d, *J*=9.7, 2H), 8.06 (d, *J*=7.3, 2H), 7.72 (d, *J*=1.8, 1H), 7.55 (d, *J*=1.7, 1H). ^{13}C NMR (100MHz, DMSO-d_6): δ 167.81, 166.67, 151.10, 140.12, 136.18, 135.99, 132.81, 132.15, 128.72, 127.03, 125.12, 122.48, 115.45, 21.77. HRMS (ESI) calculated for $C_{16}H_{12}N_4O$ $(M+H)^+$: 277.1089, found 277.1092

(viii) 2-(2'-acetamido-[1,1'-biphenyl]-4-yl)-1*H*-benzimidazole-4-carboxamide, **9h**

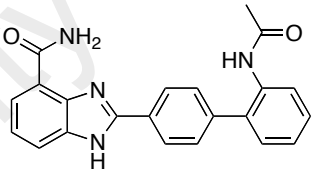

^{1}H NMR (270MHz, CD_3OD): δ 8.19 (d, *J*=8.3, 2H), 7.92 (d, *J*=7.8, 1H), 7.68 (d, *J*=7.8, 1H), 7.52 (d, *J*=8.3, 2H), 7.48 (d, *J*=8.1, 1H), 7.36-7.30 (m, 3H), 7.22 (t, *J*=7.5, 1H), 1.98 (s, 3H). ^{13}C NMR (67MHz, CD_3OD): δ 172.54, 153.64, 143.00, 138.24, 135.64, 131.40, 130.63, 129.55, 129.47, 128.45, 128.08, 127.97, 124.39, 123.50, 123.27, 122.56, 118.58, 22.90. HRMS (ESI) calculated for $C_{22}H_{18}N_4O_2$ $(M+H)^+$: 371.1507, found 371.1505

(viii) 2-(3'-acetamido-[1,1'-biphenyl]-4-yl)-1*H*-benzimidazole-4-carboxamide, **9i**

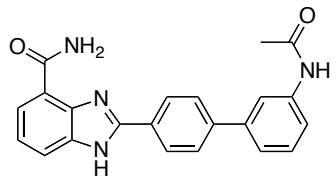

^{1}H NMR (400MHz, DMSO-d_6): δ 13.49 (s, $CONH_2$), 10.10 (s, NH), 9.38 (s, NH), 8.33 (d, *J*=8.3, 2H), 7.99 (s, 1H), 7.88 (d, *J*=7.7, 1H), 7.83 (d, *J*=8.3, 2H), 7.74 (d, *J*=7.8, 1H), 7.60 (s, 1H), 7.42 (d, *J*=4.8, 2H), 7.34 (t, *J*=7.8, 1H), 2.07 (s, CH_3). ^{13}C NMR (100MHz, DMSO-d_6): δ 168.56, 166.22, 151.60, 142.07, 141.55, 140.02, 139.66, 135.41, 129.48, 128.17, 127.54, 127.26, 123.02, 122.42, 121.54, 118.35, 117.28, 115.05, 24.07. HRMS (ESI) calculated for $C_{22}H_{18}N_4O_2$ $(M+H)^+$: 371.1507, found 371.1509

(x) 2-(4'-acetamido-[1,1'-biphenyl]-4-yl)-1*H*-benzimidazole-4-carboxamide, **9j**

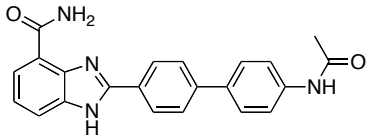

^{1}H NMR (270MHz, DMSO-d_6): δ 8.32 (d, *J*=8.4, 2H), 8.22 (d, *J*=7.8, 1H), 8.14 (d, *J*=8.1, 1H), 7.93 (d, *J*=8.4, 2H), 7.75 (d, *J*=8.6, 2H), 7.69 (d, *J*=8.6, 2H), 7.54 (bs, 1H), 2.21 (s, 3H). ^{13}C NMR (100MHz, CD_3OD): δ 168.98, 167.10, 153.10, 142.02, 139.85, 133.94, 129.92, 129.04, 128.67, 127.79, 127.48, 126.84, 126.31, 125.17, 122.55, 119.85, 116.65, 24.54. HRMS (ESI) calculated for $C_{22}H_{18}N_4O_2$ $(M+H)^+$: 371.1507, found 371.1508

(xi) 2-(4-(pyridin-3-yl)phenyl)-1*H*-benzimidazole-4-carboxamide, **10a**

(Tong e*t al*., 2009)

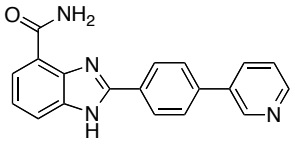

^{1}H NMR (400MHz, DMSO-d_6): δ 13.51 (bs, $CONH_2$), 9.37 (s, NH), 9.02 (s, 1H), 8.63 (d, *J*=4.6, 1H), 8.38 (d, *J*=8.1, 2H), 8.21 (d, *J*=8.3, 1H), 8.00 (d, *J*=8.1, 2H), 7.90 (d, *J*= 7.1, 1H), 7.80 (s, 1H), 7.77 (d, *J*=8.1, 1H), 7.55 (dd, *J*=4.8, 8.0, 1H), 7.37 (t, *J*=7.6, 1H). ^{13}C NMR (100MHz, DMSO-d_6): δ 166.12, 151.38, 149.01, 147.72, 142.78, 141.49, 138.97, 135.37, 134.61, 134.21, 128.72, 127.58, 123.97, 123.04, 122.47, 115.03. HRMS (ESI) calculated for $C_{19}H_{14}N_4O$ $(M+H)^+$: 315.1245, found 315.1234

(xii) 2-(4-(6-aminopyridin-3-yl)phenyl)-1*H*-benzimidazole-4-carboxamide, **10b**

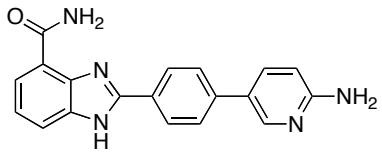

^{1}H NMR (400MHz, DMSO-d_6): δ 13.39 (s, $CONH_2$), 9.39 (s, NH), 8.39 (s, 1H), 8.27 (d, *J*=8.3, 2H), 7.88-7.79 (m, 4H), 7.74 (d, *J*=8.3, 1H), 7.35 (t, *J*=7.6, 1H), 6.58 (d, *J*=8.7, 1H), 6.28 (s, NH_2). ^{13}C NMR (100MHz, DMSO-d_6): δ 166.21, 159.46, 151.83, 145.83, 141.58, 140.06, 135.48, 135.36, 127.46, 126.75, 125.65, 122.89, 122.70, 122.28, 114.90, 108.16. HRMS (ESI) calculated for $C_{19}H_{15}N_5O$ $(M+H)^+$: 330.1354, found 330.1348

(xiii) 2-(4-(6-acetamidopyridin-3-yl)phenyl)-1*H*-benzimidazole-4-carboxamide, **10c**

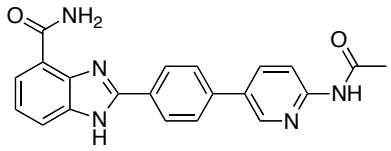

^{1}H NMR (400MHz, DMSO-d_6): δ 13.48 (s, $CONH_2$), 10.67 (s, NH), 9.38 (s, NH), 8.77 (s, 1H), 8.34 (d, *J*=8.0, 2H), 8.21 (s, 2H), 7.97 (d, *J*=8.0, 2H), 7.89 (d, *J*=7.3, 1H), 7.81-7.75 (m, 1H), 7.36 (t, *J*=8.0, 1H), 2.13 (s, 3H). ^{13}C NMR (100MHz, DMSO-d_6): δ 169.96, 166.70, 152.32, 152, 03, 146.42, 142.03, 139.24, 136.72, 135.88, 130.42, 128.63, 128.06, 127.39, 123.54, 122.91, 115.54, 113.72, 24.46. HRMS (ESI) calculated for $C_{21}H_{17}N_5O_2$ $(M+H)^+$: 372.1460, found 372.1461

(xiv) 2-(4-(pyridin-2-yl)phenyl)-1*H*-benzimidazole-4-carboxamide, **10d**

(Tong e*t al*., 2009)

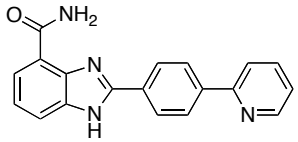

^{1}H NMR (270MHz, DMSO-d_6): δ 9.37 (s, NH), 8.71 (d, *J*=3.8, 1H), 8.37 (d, *J*=8.4, 2H), 8.30 (d, *J*=8.6, 2H), 8.07 (d, *J*=8.1, 1H), 7.93 (dd, *J*=1.3, 7.5, 1H), 7.87 (d, *J*=7.6, 1H), 7.76 (d, *J*=7.6, 1H), 7.40 (dd, *J*=4.6, 6.7, 1H), 7.32 (t, *J*=7.8, 1H). ^{13}C NMR (67MHz, DMSO-d_6): δ 166.28, 155.02, 151.79, 149.72, 149.67, 140.25, 137.42, 128.76, 127.22, 127.10, 123.14, 122.87, 122.29, 122.18, 120.61,

115.62. HRMS (ESI) calculated for $C_{19}H_{14}N_4O$ $(M+H)^+$: 315.1245, found 315.1251

(xv) 2-(4'-(pyrrolidine-1-carbonyl)-[1,1'-biphenyl]-4-yl)-1*H*-benzimidazole-4-carboxamide, **10e**

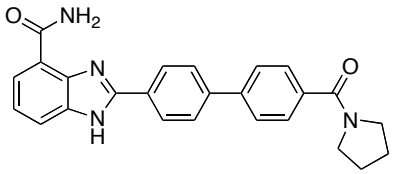

^{1}H NMR (400MHz, DMSO-d_6): δ 9.38 (bs, NH), 8.37 (d, *J*=8.4, 2H), 7.96 (d, *J*=8.4, 2H), 7.90 (d, *J*=7.2, 1H), 7.84 (d, *J*=8.4, 2H), 7.78 (d, *J*=8.0, 1H), 7.65 (d, *J*=8.0, 2H), 7.37 (t, *J*=7.2, 1H), 3.51-3.48 (m, 4H), 1.90-1.83 (m, 4H). ^{13}C NMR (100MHz, DMSO-d_6): δ 168.34, 166.79, 152.07, 141.63, 140.77, 137.14, 128.99, 128.75, 128.43, 128.36, 128.08, 127.94, 127.16, 127.05, 123.48, 122.92, 115.68, 49.10, 46.51, 26.53, 24.44. HRMS (ESI) calculated for $C_{25}H_{22}N_4O_2$ $(M+H)^+$: 411.1820, found 411.1817

(xvi) 2-(4-(6-(pyrrolidine-1-carbonyl)pyridin-3-yl)phenyl)-1*H*-benzimidazole-4-carboxamide, **10f**

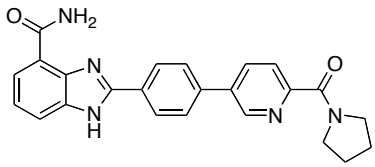

^{1}H NMR (400MHz, DMSO-d_6): δ 9.03 (bs, NH), 8.66 (bs, 1H), 8.37 (d, *J*=8.6, 2H), 8.33 (s, 1H), 8.07 (d, *J*=8.6, 2H), 7.95 (d, *J*=7.7, 1H), 7.90 (d, J=8.1, 1H),

7.83 (bs, 1H), 7.53 (t, J=8.1, 1H), 3.62 (m, 2H), 3.49 (m, 2H), 1.82 (m, 4H). ^{13}C NMR (100MHz, DMSO-d_6): δ 166.90, 165.35, 153.71, 151.07, 146.51, 140.53, 136.24, 134.03, 133.79, 129.98, 128.10, 125.30, 124.89, 124.25, 122.28, 117.00, 49.02, 46.97, 26.53, 23.98. HRMS (ESI) calculated for $C_{24}H_{21}N_5O_2$ $(M+H)^+$: 412.1773, found 412.1761

(xvii) 2-(4-(5-(pyrrolidine-1-carbonyl)pyridin-3-yl)phenyl)-1*H*-benzimidazole-4-carboxamide, **10g**

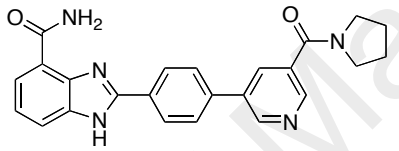

^{1}H NMR (400MHz, DMSO-d_6): δ 9.22 (s, 1H), 8.90 (s, 1H), 8.80 (bs, NH), 8.71 (s, 1H), 8.37 (d, *J*=8.1, 2H), 8.07 (d, *J*=8.1, 2H), 7.91 (d, *J*=7.7, 1H), 7.86 (d, *J*=8.6 ,1H), 7.47 (t, J=8.1, 1H), 3.48-3.43 (m, 4H), 1.82-1.79 (m, 4H). ^{13}C NMR (100MHz, DMSO-d_6): δ 167.20, 164.47, 150.96, 144.55, 143.21, 138.35, 138.20, 136.65, 135.39, 134.44, 129.64, 128.42, 126.31, 124.98, 124.76, 122.06, 117.21 49.18, 46.67, 26.19, 24.24. HRMS (ESI) calculated for $C_{24}H_{21}N_5O_2$ $(M+H)^+$: 412.1773, found 412.1765

(xviii) 2-(4-(5-(pyrrolidin-1-ylmethyl)pyridin-3-yl)phenyl)-1*H*-benzimidazole-4-carboxamide, **10h**

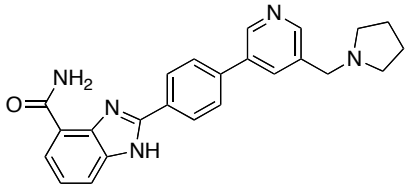

^{1}H NMR (400MHz, CD_3OD): δ 8.79 (s, 1H), 8.52 (s, 1H), 8.26 (d, *J*=8.3, 2H), 8.15 (s, 1H), 7.92 (bd, 1H), 7.83 (d, *J*=8.3, 2H), 7.71, (bd, *J*=7.5, 1H), 3.84 (s, 2H), 2.69 (bs, 4H), 1.87 (bs, 4H). ^{13}C NMR (67MHz, CD_3OD): δ 68.45, 57.61, 55.03, 24.10, 22.13. HRMS (ESI) calculated for $C_{24}H_{23}N_5O$ $(M+H)^+$: 398.1980, found 398.1989

(xix) 2-(4'-(2-(piperidin-1-yl)ethoxy)-[1,1'-biphenyl]-4-yl)-1*H*-benzimidazole-4-carboxamide, **11a**

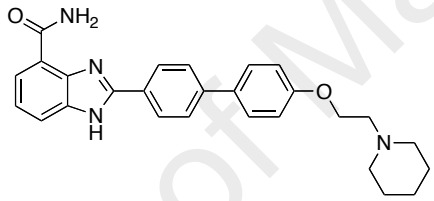

^{1}H NMR (400MHz, DMSO-d_6): δ 13.61 (bs, $CONH_2$), 9.42 (s, NH), 8.28 (d, *J*=7.5, 2H), 7.87 (d, *J*=6.8, 1H), 7.77 (d, *J*=8.3, 2H), 7.73 (d, *J*=7.5, 1H), 7.63 (d, *J*=8.3, 2H), 7.31 (t, *J*=7.5, 1H), 6.98 (d, *J*=8.3, 2H), 4.06 (t, *J*=5.3, 2H), 2.68 (t, *J*=5.3, 2H), 1.46 (t, *J*=5.3, 4H), 1.31 (bs, 2H). ^{13}C NMR (100MHz, DMSO-d_6): δ 166.88, 159.01, 152.30, 142.30, 135.97, 131.92, 130.43, 129.52, 128.37, 128.01, 127.82, 127.38, 127.08, 126.86, 123.44, 122.78, 115.54, 65.75, 57.51, 54.67, 25.66, 24.08, 21.74. HRMS (ESI) calculated for $C_{27}H_{28}N_4O_2$ $(M+H)^+$: 441.2290, found 441.2291

(xx) 2-(4'-(3-(piperidin-1-yl)propoxy)-[1,1'-biphenyl]-4-yl)-1*H*-benzimidazole-4-carboxamide, **11b**

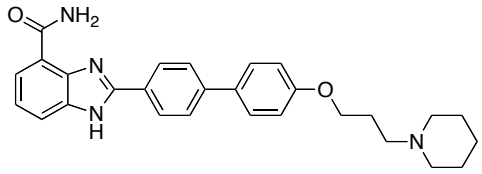

^{1}H NMR (400MHz, DMSO-d_6): δ 13.67 (s, $CONH_2$), 9.39 (bs, NH), 8.33 (d, *J*=8.3, 1H), 7.96 (d, *J*=8.0, 2H), 7.85 (bs, 1H), 7.72 (d, *J*=8.0, 2H), 7.66 (d, *J*=8.3, 2H), 7.33 (bs, 1H), 7.03 (d, *J*=8.5, 2H), 4.09 (bs, 2H), 2.92 (bs, 2H), 2.11 (bs, 2H), 1.70 (bs, 4H), 1.48 (bs, 2H) . ^{13}C NMR (100MHz, DMSO-d_6): δ 167.35, 158.64, 143.68, 131.43, 129.95, 129.35, 128.12, 126.06, 115.05, 65.44, 53.83, 52.57, 24.12, 23.27, 22.21. HRMS (ESI) calculated for $C_{28}H_{30}N_4O_2$ $(M+H)^+$: 455.2446, found 455.2441

(xxi) 6-fluoro-2-(4'-propionamido-[1,1'-biphenyl]-4-yl)-1*H*-benzimidazole-4-carboxamide, **11c**

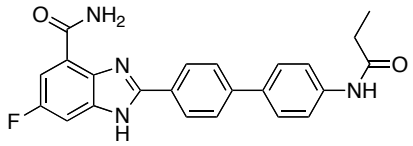

^{1}H NMR (400MHz, DMSO-d_6): δ 10.03 (s, NH), 9.35 (s, NH), 8.27 (d, *J*=8.0, 2H), 7.86 (d, *J*=8.3, 2H), 7.24 (bs, 4H), 7.59 (s, 1H), 7.57 (s, 1H), 2.34 (q, *J*=7.6, 2H), 1.08 (t, *J*=7.6, 3H). ^{13}C NMR (100MHz, DMSO-d_6): δ 172.38, 165.20, 158.47, 152.47, 141.81, 139.54, 133.45, 128.27, 127.58, 127.36, 127.16, 126.82,

125.98, 123.31, 119.53, 110.30, 101.68, 29.68, 9.75. HRMS (ESI) calculated for $C_{23}H_{19}N_4F_1O_2$ $(M+H)^+$: 403.1570, found 403.1575

(xxii) 2-(4'-(cyclopropanecarboxamido)-3-fluoro-3'-methoxy-[1,1'-biphenyl]-4-yl)-6-fluoro-1*H*-benzimidazole-4-carboxamide, **11d**

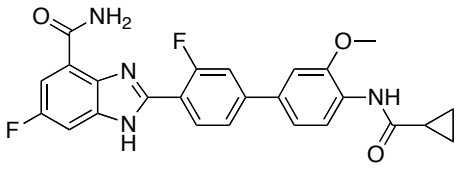

^{1}H NMR (400MHz, DMSO-d_6): δ 9.53 (s, NH), 9.27 (s, NH), 8.33 (t, *J*=8.0, 1H), 8.10 (d, *J*=8.3, 1H), 7.87 (d, *J*=12.9, 1H), 7.78 (dd, *J*=1.7, 8.3, 1H), 7.60 (bm, 2H), 7.44 (s, 1H), 7.37 (dd, *J*=1.9, 8.5, 1H), 3.98 (s, 3H), 2.12 (m, 1H), 0.80-0.76 (m, 4H). ^{13}C NMR (100MHz, DMSO-d_6): δ 172.08, 164.84, 160.48, 158.06, 149.56, 148.05, 144.20, 137.53, 135.84, 133.15, 130.55, 128.27, 123.45, 122.98, 121.81, 118.87, 115.17, 114.18, 110.60, 109.48, 101.92, 55.97, 14.26, 7.44. HRMS (ESI) calculated for $C_{25}H_{20}N_4F_2O_3$ $(M+H)^+$: 463.1581, found 463.1572

(xxiii) 2-(4'-(cyclopropanecarboxamido)-2',3-difluoro-[1,1'-biphenyl]-4-yl)-6-fluoro-1*H*-benzimidazole-4-carboxamide, **11e**

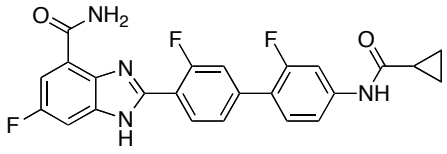

^{1}H NMR (400MHz, DMSO-d_6): δ 10.60 (s, NH), 9.26 (s, NH), 8.35 (t, J=7.8, 1H), 7.99-7.60 (m, 5H), 7.43 (s, 1H), 7.41 (s, 1H), 1.80-1.75 (m, 1H), 0.84-0.81 (m, 4H). ^{13}C NMR (100MHz, DMSO-d_6): δ 172.46, 165.10, 160.45, 160.42, 158.00, 157.97, 147.99, 141.44, 141.32, 138.44, 130.82, 130.50, 125.30, 124.05, 120.11, 116.39, 115.77, 115.27, 110.78, 106.43, 102.10, 14.84, 7.75. HRMS (ESI) calculated for $C_{24}H_{17}N_4F_3O_2$ $(M+H)^+$: 451.1381, found 451.1378

In conclusion, the methods employed were very convenient, easy and safe to handle. All compounds were obtained in high yield and purity.

CHAPTER 5: PARP-1 AND DHODH INHIBITION STUDIES

5.1 Pharmacological evaluation

Biological assay studies on PARP-1 and DHODH were carried out at Aurigene Discovery Technologies Ltd. (Malaysia). These assays were independently done on PARP colometric assay and DHODH enzymatic assay.

5.1.1 Poly (ADP-ribose) Polymerase (PARP) Colorimetric Assay

Inhibitory effects of compounds **7a-g, 9a-j, 10a-h** and **11a-e** on PARP-1 activity were measured using HT Universal Colorimetric PARP assay kit Histone-coated Strip Wells, Trevigen, Gaithersburg, MD, USA. The assays were carried out by quantifying the incorporation of biotinylated poly (ADP-ribose) onto histone proteins in 96-well plates. In brief, 10 µL of PARP-1 enzyme (0.25 U) was pre-incubated with 15 µL of tested compounds in rehydrated histone-coated wells, followed by addition of 25 µL of PARP cocktail mixture containing 2 µL of 10x PARP cocktail, 2 µL of 10x activated DNA and 21 µL of 1x PARP buffer into the wells. After 60 minutes of incubation, the wells were washed twice with 1x PBS + 0.1% Triton X-100, followed by 1x PBS. 50 µL of 1x Strep-HRP was then added and incubated for 60 minutes. The wells were washed again as in the previous step. 50 µL of pre-warmed TACS-Sapphire substrate was added and the mixture incubated for 15 minutes in dark. The reactions were terminated with 50 µL of 0.2 M HCl. The absorbance readings were taken at 450 nm using VICTORTM X5, Multimode Plate Reader. IC_{50} values were determined by fitting the activity data at different concentrations of the compounds to sigmoidal dose-response curve fitting program, using GraphPad Prism software version 6.00.

5.1.2 Dihydroorotate Dehydrogenase (DHODH) Enzymatic Assay

Compounds **7a-g, 9a-j, 10a-h** and **11a-e** were evaluated for their potency to inhibit DHODH in a coupled enzymatic spectrophotometric assay. The assay is based on the decrease in absorbance at 610 nm, resulting from the oxidation of L-dihydroorotic acid (L-DHO), facilitated by the reduction of 2,6-dichloroindophenol (DCIP) and decylclubiquinone (DUQ) (Baldwin e*t al*., 2005). The decrease in absorbance at 610 nm is proportional to the reduction of DCIP. The assay buffer was 50 mM TrisHcl, 150 mM MKCL and 0.8% Triton, pH 8.0. 100 µL reaction mixture was used in 96-well plates at room temperature. A mixture of 82 µL of enzyme (25 ng) in buffer and 5 µL of test compounds were pre-incubated for 30 minutes, and the reaction was started by adding 13 µL of substrate mixture (20 mM of L-DHO, 2 mM of DuQ and 2 mM of DCIP). The final concentration of DMSO used was 1%. Lastly, the absorbance of mixture in each well was measured at 610 nm, using a VICTOR X5 (Waltham, MA, USA) at every 10 minutes for 1 hour. IC_{50} values were determined from the dose response plot using GraphPad Prism software version 6.00.

Preliminary activities for both PARP and DHODH assay were measured at 10 µM concentrations of the synthesized compounds (**7a-g, 9a-j, 10a-h** and **11a-e**) with veliparib and brequinar as reference inhibitors (Table 5.1). The biological assay results tabulated in Table 5.1 show a number of compounds with good inhibitory activity either in PARP-1, or DHODH assay, in correlation with the functional groups attached to the compound.

Table 5.1. PARP-1 and DHODH inhibition by benzimidazole derivatives. The activity is expressed as percent inhibition at 10 µM or IC_{50} values.

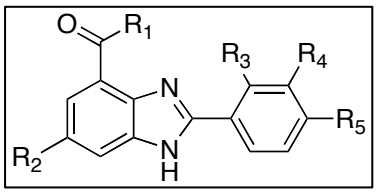

Entry	R_1	R_2	R_3	R_4	R_5	PARP IC_{50} (µM) / % Inhibition at 10 µM	DHODH IC_{50} (µM) / % Inhibition at 10 µM
Veliparib (ABT-888)				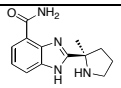		0.005	-
Brequinar				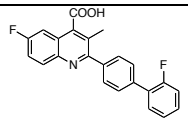		-	0.012
9a[a]	NH_2	H	H	H		0.714	9.80
9b	NH_2	CH_3	H	H		28%	7.80
9c[b]	NH_2	H	H	H	-OCH_3	N.A	N.A
9d	NH_2	CH_3	H	H		N.A	N.A
9e[b]	NH_2	H	H	H	-CF_3	N.A	N.A
9f	NH_2	CH_3	H	H		N.A	N.A
9g	NH_2	CH_3	H	H	-CN	N.A	N.A
9h	NH_2	H	H	H		0.14	51%
9i	NH_2	H	H	H	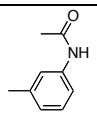	0.46	42%
9j	NH_2	H	H	H	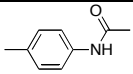	16%	56%
10a[a]	NH_2	H	H	H		0.022	19%
10b	NH_2	H	H	H	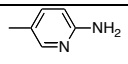	0.032	20%
10c	NH_2	H	H	H	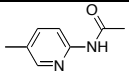	0.049	46%
10d[a]	NH_2	H	H	H		0.083	28%
10e	NH_2	H	H	H	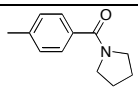	0.31	20%

Table 5.1 continued

10f	NH_2	H	H	H	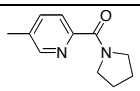	0.12	26%
10g	NH_2	H	H	H	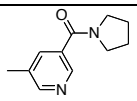	0.29	28%
10h	NH_2	H	H	H	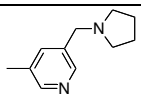	0.061	55%
11a	NH_2	H	H	H	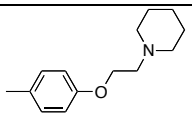	0.72	31%
11b	NH_2	CH_3	H	H	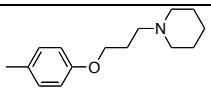	2.28	N.A
11c	NH_2	F	H	H	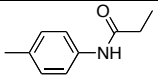	1.72	12%
11d	NH_2	F	F	H	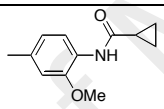	0.98	23%
11e	NH_2	F	F	H	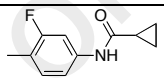	0.084	48%
7a	OH	CH_3	H	H		N.A	32%
7b	OH	CH_3	H	H	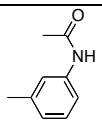	N.A	1.38
7c	OH	CH_3	H	H	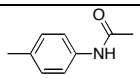	N.A	0.21
7d	OH	CH_3	H	NHAc		N.A	47%
7e	OH	CH_3	H	H	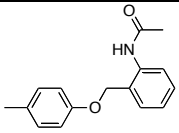	10.63	0.30
7f	OH	CH_3	H	H	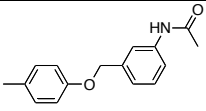	N.A	0.028
7g	OH	CH_3	H	H	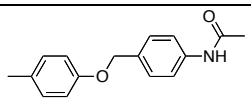	44%	0.013

*N.A. – Not active

A library of diversified compounds (as shown in Table 5.1) were designed and synthesised by substituting various electron-donating and electron-withdrawing groups on the benzimidazole scaffold and their biological activities were evaluated for the two targets, PARP-1 and DHODH. The objective was to develop an inhibitor that is active towards both on PARP-1 and DHODH enzymes. The designed compounds were docked onto PARP-1 (pdb ID: 4HHZ) and DHODH (pdb ID: 4IGH) enzymes, and their interactions with the active site residues of both enzymes were analyzed in order to understand their activities with the two targets.

Compound **I1** (Figure 5.1) was reported by Thunuguntla and co-workers to inhibit DHODH (Thunuguntla e*t al*., 2010) activity with an IC_{50} value of 0.75 µM. Replacing the carboxylic acid substituent at C-4 position of the benzimidazole ring in compound **I1** with amide functionality as in compound **9a** resulted in an improved activity with PARP-1 enzyme (IC_{50} value of 0.71 µM). However, at the same time, the potency of compound **9a** towards DHODH enzyme was observed to decrease to 9% inhibition at 10 µM. This seemes to indicate that the -COOH group at C-4 position is required for DHODH activity, while the -$CONH_2$ substituent is needed for PARP-1 activity.

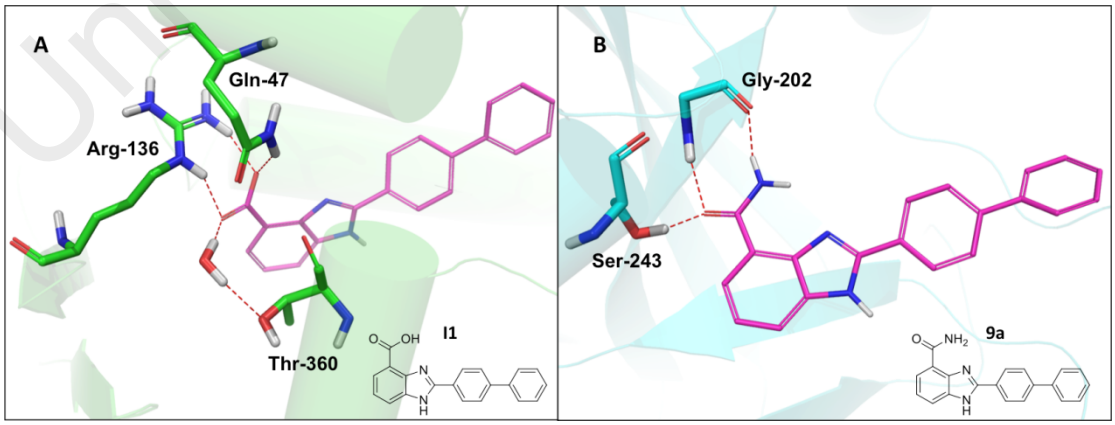

Figure 5.1. (A) shows the docking mode of compound **I1** on DHODH enzyme (pdb ID: 4IGH). (B) shows the docking mode of compound **9a** docked on PARP-1 enzyme (pdb ID: 4HHZ). Figures were generated with PyMol.

5.2 Biological Evaluation of Synthesised Compounds

5.2.1 Biological Evaluation of Synthesised Compounds on PARP-1 Enzyme

The parent benzimidazole compound, **9a** (Figure 5.2) showed activity towards PARP-1 at IC_{50} value of 0.71 μM.

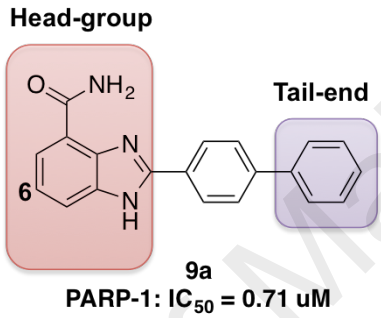

Figure 5.2. Compound **9a**.

To test possible hydrophobic site for interaction at the active pocket, the hydrogen at C-6 of the benzimidazole head-group was substituted with a methyl group (compound **9b**). This change led to a reduction in activity by about 28% compared to compound **9a**.

Investigation on the influence of substituents in the tail of the benzimidazole compound, using compound **9a** as the parent template were carried out. The biphenyl group in **9a** was replaced with the 4-methoxyphenyl and 4-triflourophenyl to give compounds **9c** and **9e**, respectively. No activity was observed with both compounds on PARP-1 enzyme. Two other compounds, **9d** and **9f** (Figure 5.3) were tested on PARP-1 enzyme assay. Neither compound showed any activity activities towards the PARP-1 enzyme. Another compound, **9g** (Figure 5.3), with methyl substituent on C-6 of the head-group and 4-cynophenyl at the tail-end was tested for PARP-1 activity and

similarly, no activity was observed. Thus, it can be concluded that the C-6 position of the head-group must not be a methyl, and that the biphenyl group is necessary at the tail-end.

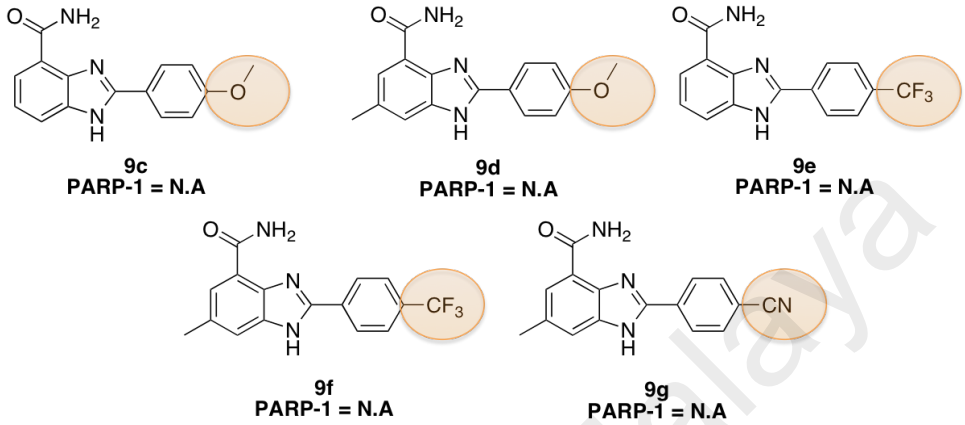

Figure 5.3. Compounds **9c**, **9d**, **9e**, **9f** and **9g**.

Three compounds, **9h**, **9i** and **9j**, with an acetamide functionality at the *ortho*, *meta* and *para*-positions of the second phenyl ring in the biphenyl tail-end of the benzimidazole were synthesized and screened, as shown in Figure 5.4.

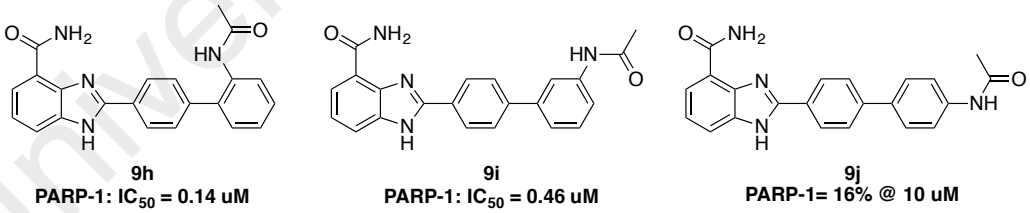

Figure 5.4. Compounds **9h**, **9i** and **9j**.

Compound **9h** gave an IC_{50} value of 0.14 µM in PARP-1 activity, while compound **9i** showed a decreased in activity against PARP-1 with an IC_{50} value of 0.46 µM. Both compounds **9h** and **9i** showed better inhibitory activity towards PARP-1 compared to compound **9a**. However, compound **9j**, with the acetamide at the *para*-position of the biphenyl ring, displayed poorer PARP-1 activity with only 16% inhibition at 10 µM.

The presence of an electron-donating acetamide group seems to increase the PARP-1 activity, in the first instance, as seen with compounds **9h** and **9i**.

As shown in the surface model (Figure 5.5, A), compound **9h** fits exactly into the active pocket of the enzyme. This would enable good interactions between functional groups of the ligand with the active site of the PARP-1 enzyme. Two hydrogen-bond interactions were observed between compound **9h**, with Ser-243 (C=O to O-H Ser, 2.2 Å) and Gly-202 (N-H to C=O Gly, 2.1 Å). Intramolecular hydrogen-bond interaction between the -NH of the carboxamide group with the imidazole nitrogen helped to put the carboxamide group in place for a good interaction between this group and the Ser-243 and Gly-202 residues. In addition, a water-mediated hydrogen bonding interaction between the acetamide group of the site of the ligand with the Arg-217 (C=O to H-O-H, 2.4 Å to N-H Arg, 2.4 Å) residue of the enzyme was also observed, as shown in Figure 5.5 (B).

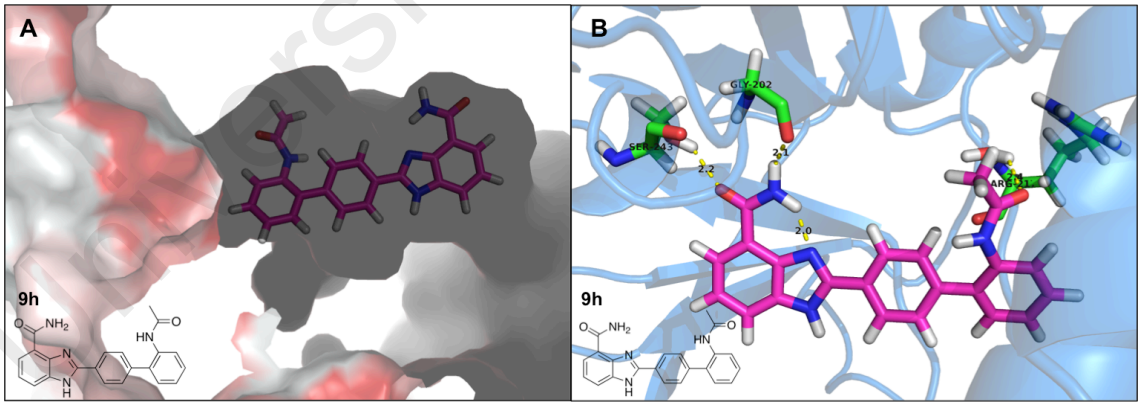

Figure 5.5. (A) shows the ligand interaction of compound **9h** towards hydrophobicity surface. Red color indicates the hydrophobic surface of the enzyme (pdb ID: 4HHZ). (B) illustrates the docking mode of compound **9h** on PARP-1 enzyme (pdb ID: 4HHZ). Hydrogen bonds are highlighted in yellow dash. Figures were generated with PyMol.

For compound **9i**, the ligand seems to still fit into the active pocket of the enzyme. The lower activity observed with **9i** compare to **9h**, presumably is due to the lost of some interactions between the ligand and the residues in the active pocket of the

enzyme. The H-bond interactions between the carboxamide head-group with Ser-243 and Gly-202 are still observed with compound **9i**, as shown in Figure 5.6. However, unlike in compound **9h**, there is no H-bond interaction between the amide functionality at the tail-end of the ligand (compound **9i**) with Arg-217. This may be the cause of the reduced activity observed between compound **9i** and PARP-1 enzyme.

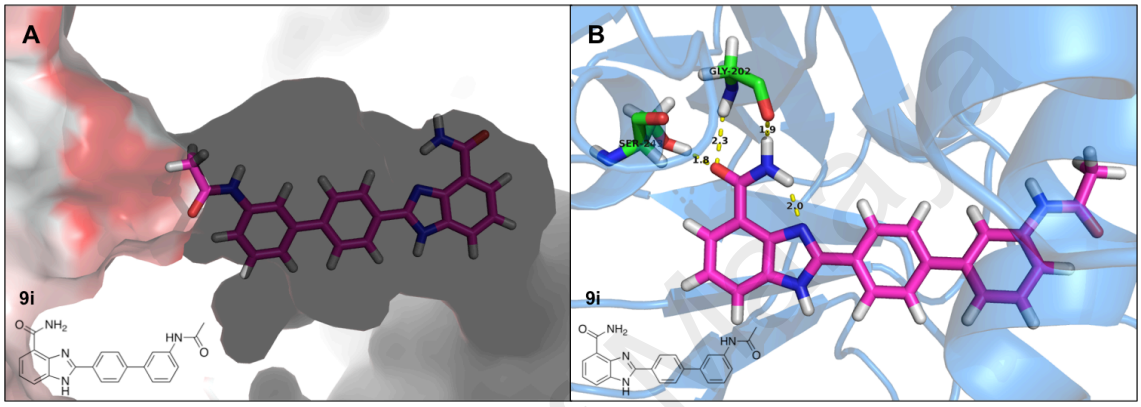

Figure 5.6. (A) shows the ligand interaction of compound **9i** towards hydrophobicity surface. Red color indicates the hydrophobic surface of the enzyme (pdb ID: 4HHZ). (B) illustrates the docking mode of compound **9i** on PARP-1 enzyme (pdb ID: 4HHZ). Hydrogen bonds are highlighted in yellow dash. Figures were generated with PyMol.

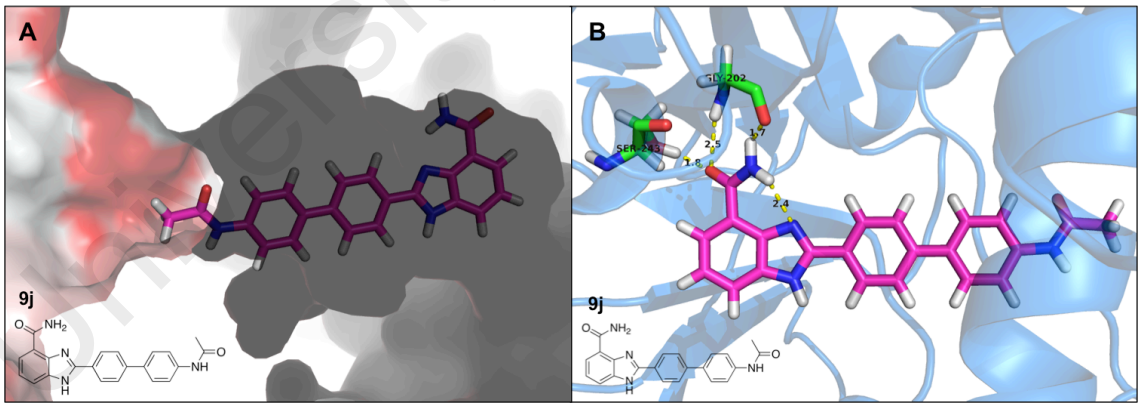

Figure 5.7. (A) shows the ligand interaction of compound **9j** towards hydrophobicity surface. Red color indicates the hydrophobic surface of the enzyme (pdb ID: 4HHZ). (B) illustrates the docking mode of compound **9j** on PARP-1 enzyme (pdb ID: 4HHZ). Hydrogen bonds are highlighted in yellow dash. Figures were generated with PyMol.

A drastic lost in activity, however, was observed with compound **9j**, although similar H-bond interactions were observed between the carboxamide head-group of **9j** with Ser-243 and Gly-202. As seen in the model shown in Figure 5.7, the tail-end of this ligand is

linear rather than "bent" as in compounds **9h** and **9i**. The linear tail-end of compound **9j** seems to be pushed out of the cavity of the active pocket of the enzyme, as shown in Figure 5.7, possibly affecting the activity of the compound against PARP-1 enzyme.

Thus, it can be conclude that the position of amide at the tail-end of the ligand is important for activity. When it is in the *ortho*-position, it was able to form added interaction with Arg-271. However, in the *meta*-position, the amide group is distant from the Arg-217 residue, and is not enable to form any H-bond interaction. This is more distinctly observed in the case where the amide group is placed in the *para*-position.

It has been reported by Tong and co-workers that replacing the second benzene ring with a pyridine showed increase in activity, compared to compound **9a**. Compound **10a** (Tong e*t al*., 2009) was reported to inhibit the PARP-1 enzyme activity with a K_i value of 0.95 nM. Thus, extension of this study was done by introducing heteroaromatic moiety to replace the second benzene ring at the tail-end of the benzimidazole structure. Using compound **10a** as reference, compounds **10b** and **10c** were synthesised and tested for activity with PARP-1 enzyme (Figure 5.8).

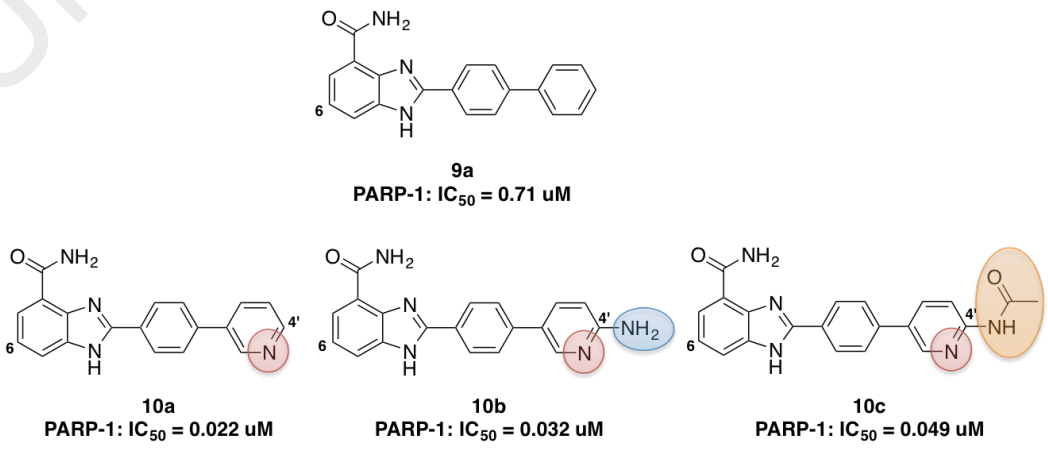

Figure 5.8. Compounds **9a**, **10a**, **10b** and **10c**.

The activity of compound **10a** with PARP-1 was observed to give an IC_{50} value of 0.022 μM. This is an increase of approximately 14-folds in activity for compound **10a**, compared to that of compound **9a** (IC_{50} = 0.71 μM). Presumably, the more polar pyridinyl group in compound **10a** led to repulsion between the residues Tyr-49, Ala-101, Asp-105, Ala-219 and Ala-223, pushing the ligand more inwards into the active pocket of PARP-1 (Figure 5.9). This resulted in a stronger H-bond interaction between the carboxamide head-group with Ser-243 and Gly-202 of PARP-1 enzyme (Compound **10a** H-bonds length, C=O to H-O Ser, 1.7 Å; C=O to N-H Gly, 1.7 Å and N-H to C=O Gly, 1.7 Å. Compound **9a** H-bonds length, C=O to H-O Ser, 1.6 Å; C=O to N-H Gly, 2.1 Å and N-H to C=O Gly, 1.7 Å) (Figure 5.10).

Adding an amino group on the pyridinyl ring as in compound **10b** resulted in slight reduction of activity observed with PARP-1 enzyme (IC_{50} = 0.032 μM). Examination of the model as shown in Figure 5.11 revealed the amino group to be outside the cavity of the active pocket of the enzyme. This also plausibly affected the H-bond interaction between the carboxamide head-group and the residues Ser-243 (C=O to H-O Ser, 2.0 Å) and Gly-202 (C=O to N-H Gly, 2.1 Å; N-H to C=O Gly, 1.8 Å) of the PARP-1 enzyme.

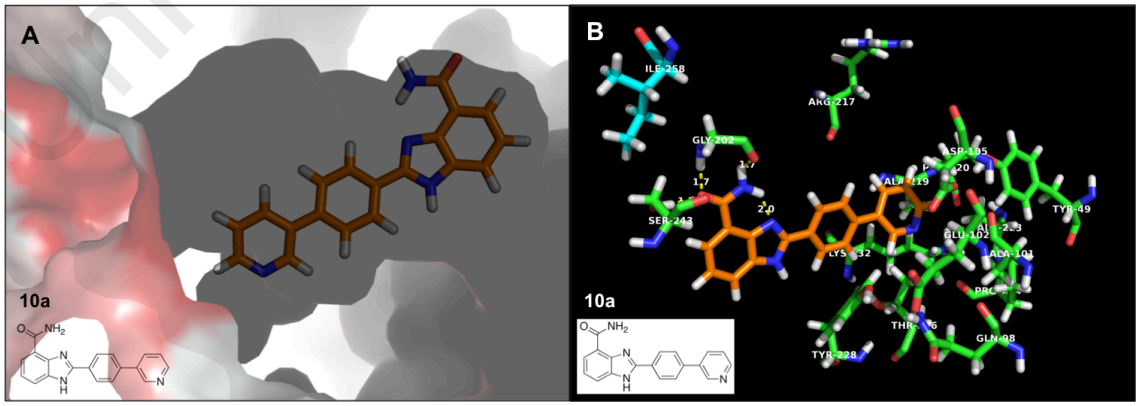

Figure 5.9. (A) shows the hydrophobic interactions of compound **10a** on PARP-1 enzyme (pdb ID: 4HHZ). Red color indicates hydrophobic surface. (B) illustrates the docking mode of compound **10a** on PARP-1 enzyme (pdb ID: 4HHZ). Hydrogen bonds are highlighted as yellow dash. Figures were generated with PyMol.

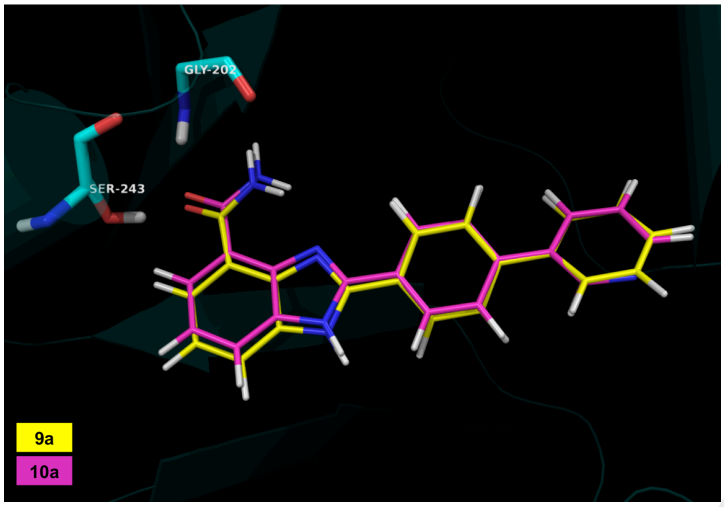

Figure 5.10. Superposition of compounds **9a** and **10a** on PARP-1 enzyme (pdb ID: 4HHZ). Figure was generated with PyMol.

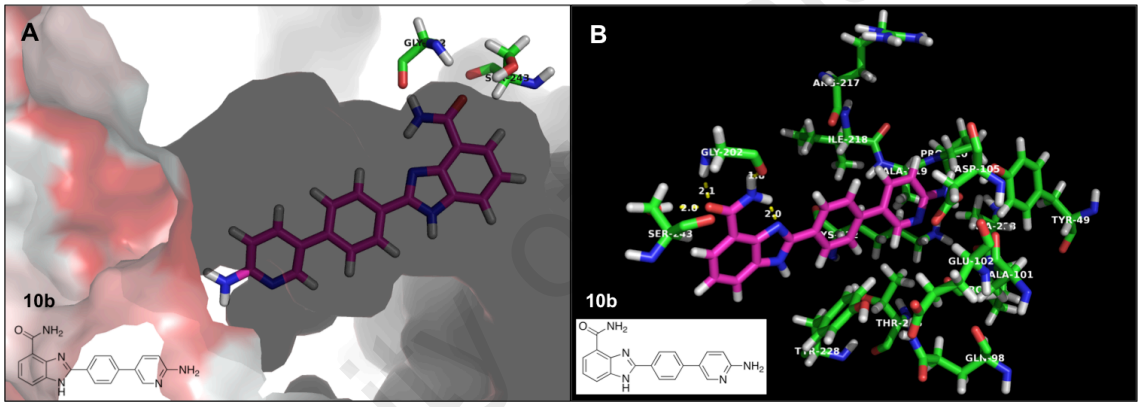

Figure 5.11. (A) shows the hydrophobic interactions of compound **10b** on PARP-1 enzyme (pdb ID: 4HHZ). Red color indicates hydrophobic surface. (B) illustrates the docking mode of compound **10b** on PARP-1 enzyme (pdb ID: 4HHZ). Hydrogen bonds are highlighted as yellow dash. Figures were generated with PyMol.

For compound **10c**, where the amino group (in compound **10b**) was replaced with an acetamide group, the PARP-1 activity was observed with an IC_{50} value of 0.049 µM. The acetamide group was observed to reside outside the cavity of the active pocket of the PARP-1 enzyme (Figure 5.12, A). Furthermore, the hydrophobic interactions at the tail-end of the compound occurred with different residues than that of all previous compounds studied (Figure 5.12, B). Here, the interactions of the tail-end group of the ligand were observed with the residues Ile-45, Leu-108, Asp-109, Gly-233, Ile-234, instead of the usual Gln-98, Ala-101, Glu-102, Pro-224, Lys-232 and Ile-258. In

addition, poorer H-bond interactions were observed between the carboxamide head-group with Ser-243 (C=O to H-O Ser, 2.1 Å) and Gly-202 (N-H to C=O Gly, 2.4 Å).

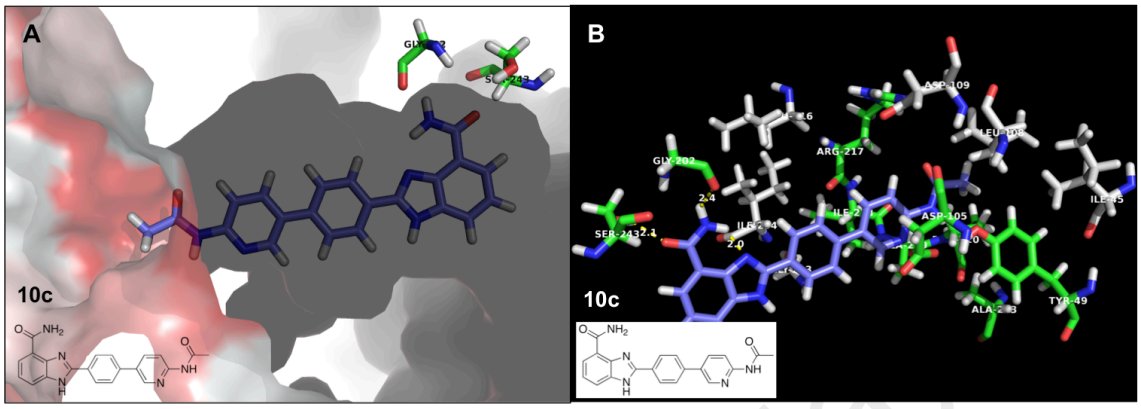

Figure 5.12. (A) shows the hydrophobic interactions of compound **10c** on PARP-1 enzyme (pdb ID: 4HHZ). Red color indicates hydrophobic surface. (B) illustrates the docking mode of compound **10c** on PARP-1 enzyme (pdb ID: 4HHZ). Hydrogen bonds are highlighted as yellow dash. Figures were generated with PyMol.

Compounds **10a**, **10b** and **10c** all contained the pyridinyl ring in the tail-end group with the nitrogen atom in the 3rd position. Investigation on the importance of the nitrogen atom position in the pyridinyl ring for PARP-1 activity was carried out. Compound **10d** was prepared with the nitrogen atom of pyridinyl ring at the 2nd position (Figure 5.13). Biological assay of compound **10d** indicated a 4-fold reduction in activity compared to compound **10a**.

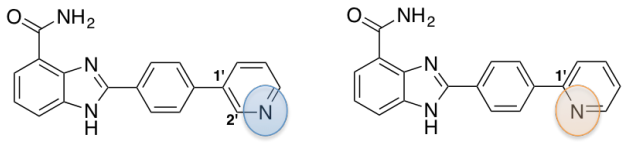

Figure 5.13. Compounds **10a** and **10d**.

However, docking studies did not indicate much difference to explain the significant difference that was observed in the assay. Extra hydrophobic interactions between

compound **10a** and the amino acid residues of PARP-1 were observed compared to those of compound **10d** (Figure 5.14). Table 5.2 shows the amino acids that interacted with compounds **10a** and **10d**. Perhaps it is these added interactions that resulted in better activity observed for compound **10a**.

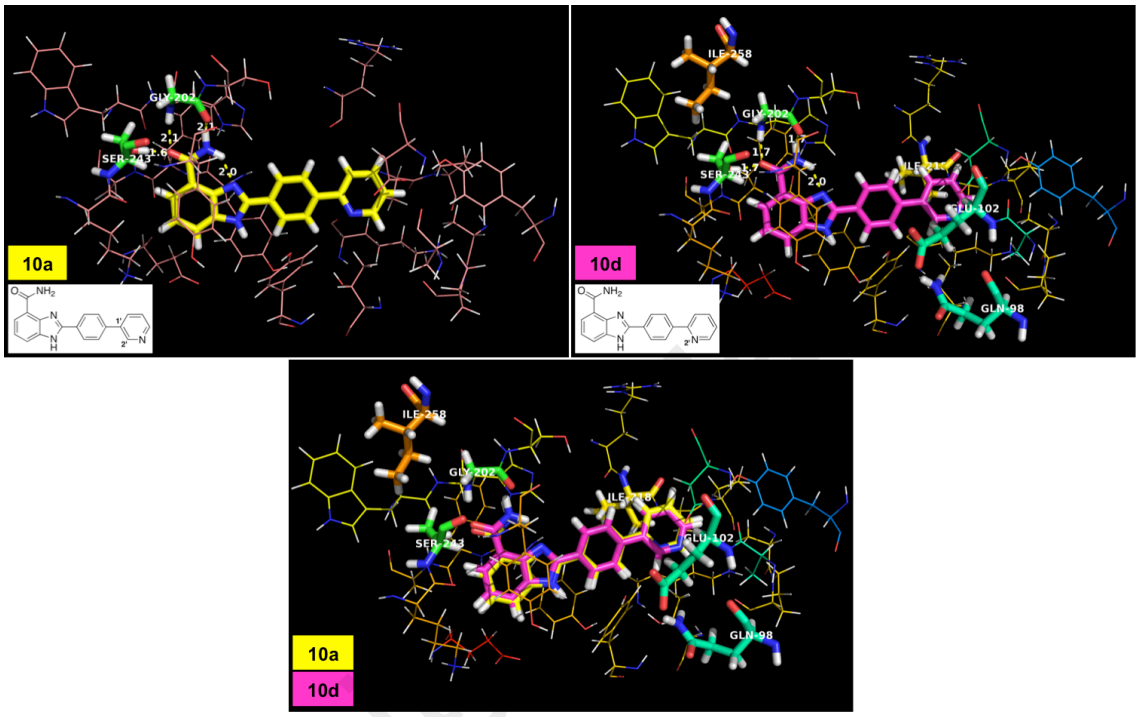

Figure 5.14. (A) and (B) illustrates the docked pose of compounds **10a** and **10d** on PARP-1 enzyme, respectively. Hydrogen bonds are highlighted as yellow dash. (C) shows the superposition of compounds **10a** and **10d** on PARP-1 enzyme (pdb ID: 4HHZ). Figures were generated with PyMol.

Table 5.2. Ligand-amino acid interactions (close contact) in the active pocket of PARP-1 enzyme for compounds **10a** and **10d**.

	10a		**10d**	
Amino Acids (Found)	Ala-101	Phe-236	Ala-101	Phe-236
	Ala-219	Pro-220	Ala-219	Pro-220
	Ala-223	Pro-224	Ala-223	Pro-224
	Ala-237	Ser-203	Ala-237	Ser-203
	Arg-217	Thr-226	Arg-217	Thr-226
	Asp-105	Trp-200	Asp-105	Trp-200
	Glu-327	Tyr-228	Glu-327	Tyr-228

Table 5.2 continued

Amino Acids (Found)	His-201 Lys-232 Lys-242	Tyr-235 Tyr-246 Tyr-49	His-201 Lys-232 Lys-242	Tyr-235 Tyr-246 Tyr-49
	*Gln-98 *Ile-218	*Glu-102 *Ile-258		

*Additional amino acid residue interaction.

In addition, the hydrogen bond length calculated for compound **10d** (1.6 Å C=O to H-O Ser-243, 2.1 Å C=O to N-H Gly-202 and 2.1 Å N-H to C=O Gly-202) were longer compared to compound **10a** (1.7 Å C=O to H-O Ser-243, 1.7 Å C=O to N-H Gly-202 and 1.7 Å N-H to C=O Gly-202). The intramolecular hydrogen bond length between the two compounds was found to be identical at 2.0 Å. Lesser number of contacts between **10d** with amino acid residues in the active pocket of PARP-1 was observed, which resulted in lower interactions towards these hydrophobic residues. In addition, longer hydrogen bond length was observed between the head group of the compound **10d** with Ser-243 and Gly-202. These findings could potentially be the major factor for activity reduction in compound **10d** compared to compound **10a**.

Investigation on another group of compounds involving pyrrolidinone substituents at the tail-end of the benzimidazole compound were carried out. These compounds are shown in Figure 5.15.

Compound **10e** exhibited an IC_{50} value of 0.31 μM in PARP-1 activity. This is an increase in activity for PARP-1 inhibition compared to that observed with compound **9a** (IC_{50} = 0.71 μM). As shown in Figure 5.16, the interactions between the enzyme and the head-group of compound **10e** are similar to that of compound **9a**, as well as all other ligands described earlier. However, the tail-end of compound **10e** is longer than that of

compound **9a**, as shown in Figure 5.17. Presumably, the extra length of compound **10e** (observed in the model in Figure 5.17) led to added hydrophobic interactions between **10e** and the enzyme, which may explain the better activity observed in **10e** compared to compound **9a** (Figure 5.18).

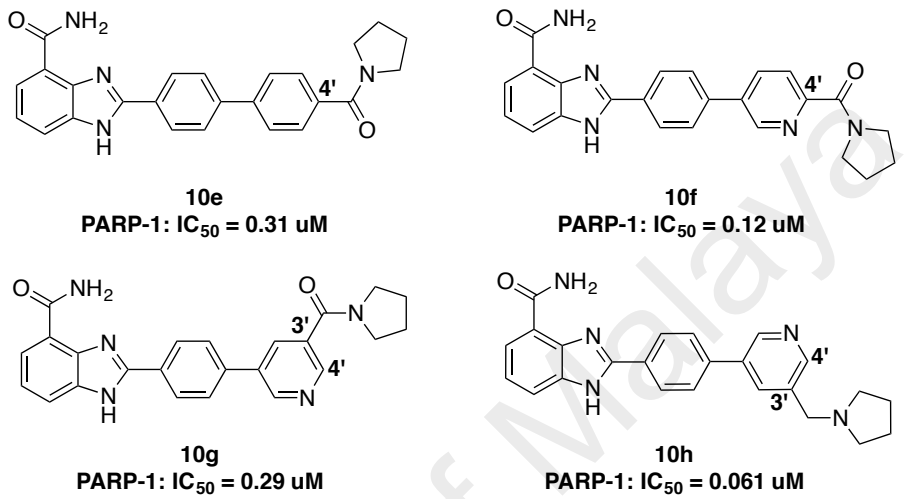

Figure 5.15. Compounds **10e**, **10f**, **10g** and **10h**.

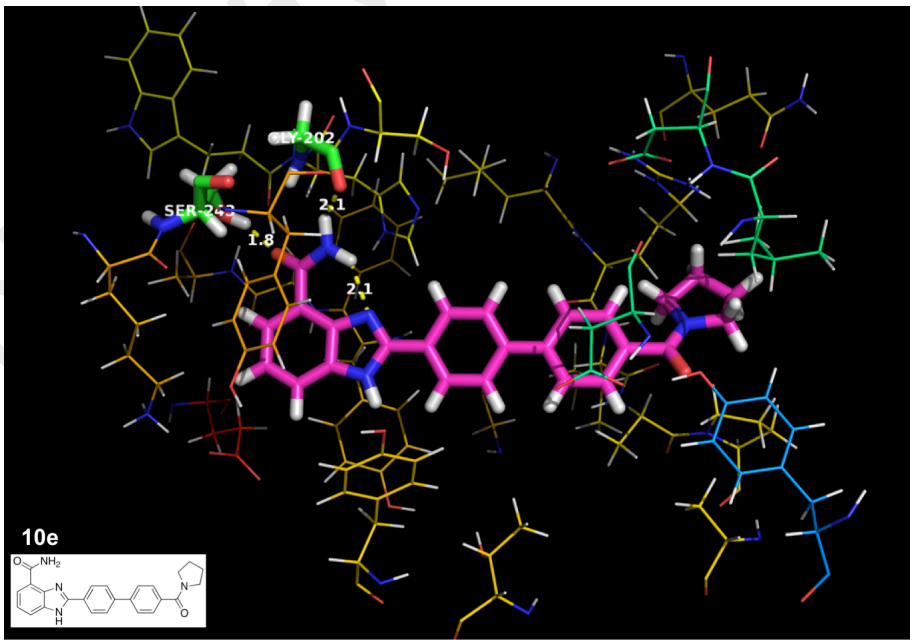

Figure 5.16. Docked pose of compound **10e** on PARP-1 enzyme (pdb ID: 4HHZ). Hydrogen bonds are highlighted in yellow dash. Figure was generated with PyMol.

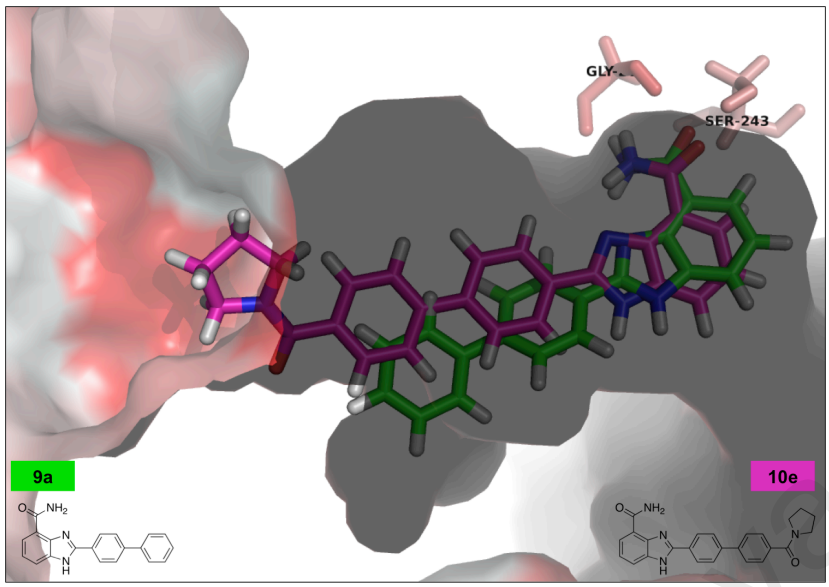

Figure 5.17. Ligand interaction of compounds **9a** and **10e** towards hydrophobicity surface. Red color shows the hydrophobic surface of the enzyme (pdb ID: 4HHZ). Figure was generated with PyMol.

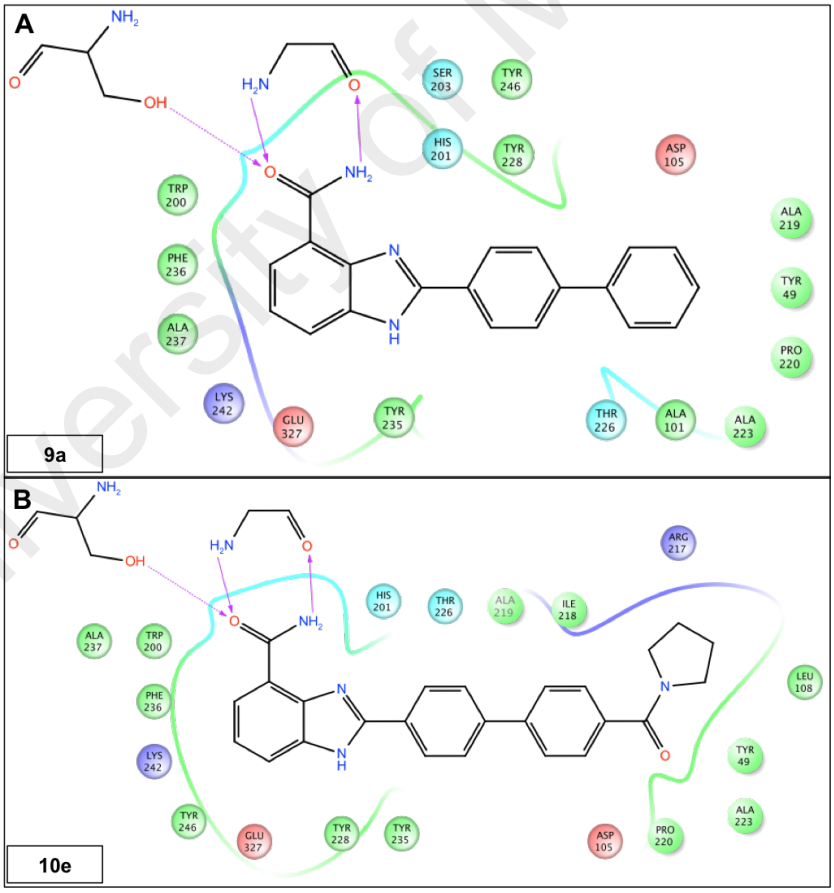

Figure 5.18. (A) and (B) shows the ligand interactions on PARP-1 enzyme with compounds **9a** and **10e**, respectively (pdb ID: 4HHZ). Red circle indicates negative charged residues, cyan indicates polar residues, green indicates hydrophobic residues, purple indicates positive charged residues. Cutoff was at 4.00 Å. Figures were generated with Maestro Schrodinger software.

Compound **10f** showed an IC_{50} value of 0.12 μM. This is an almost 3-fold increase in activity compared to compound **10e**. The difference between compound **10f** and **10e** lies in the tail-end where the second aryl group is a pyridinyl ring instead of a phenyl ring (Figure 5.19). This increase in activity is expected, as similar increase in activity was observed with compound **10a** (described above) when the second phenyl ring was replaced with a pyridinyl ring. In addition, **10f** fits better into the cavity of the active pocket of the enzyme compared to **10e**. However, this increase in activity is not as significant compared to that of **10a**. Presumably, poorer fit of compound **10f** into the active site of the enzyme compared to **10a** due to the extra pyrrolidinone group affected the activity of compound **10f** (Figure 5.20).

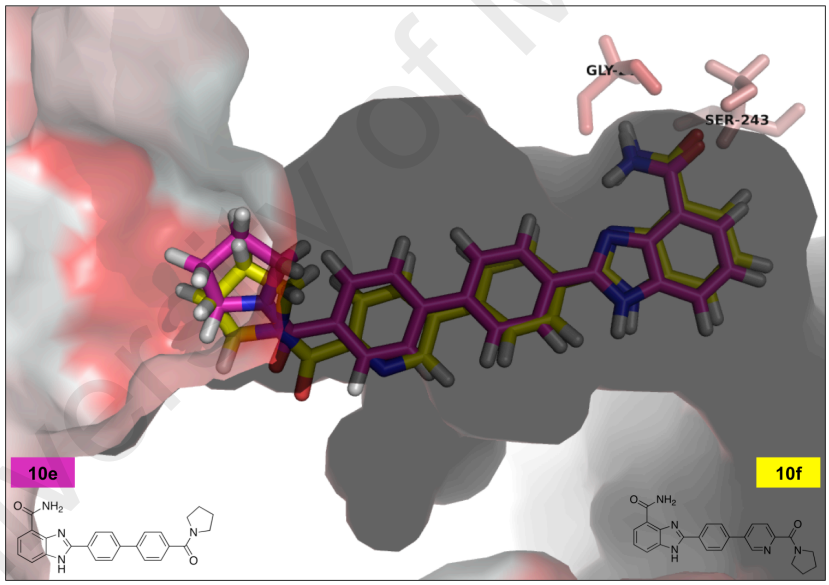

Figure 5.19. Ligand interaction of compounds **10e** and **10f** towards hydrophobicity surface. Red color indicates the hydrophobic surface of the enzyme (pdb ID: 4HHZ). Figure was generated with PyMol.

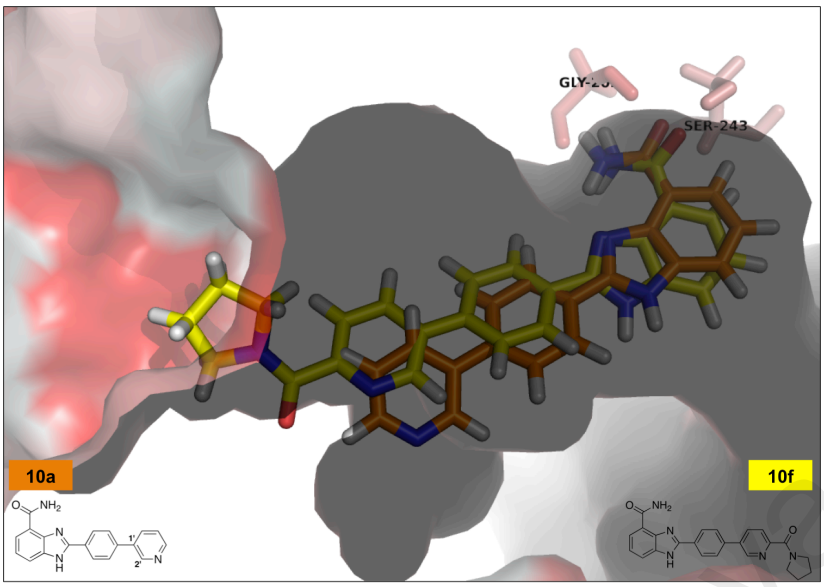

Figure 5.20. Ligand interaction of compounds **10a** and **10f** towards hydrophobicity surface. Red color indicates the hydrophobic surface of the enzyme (pdb ID: 4HHZ). Figure was generated with PyMol.

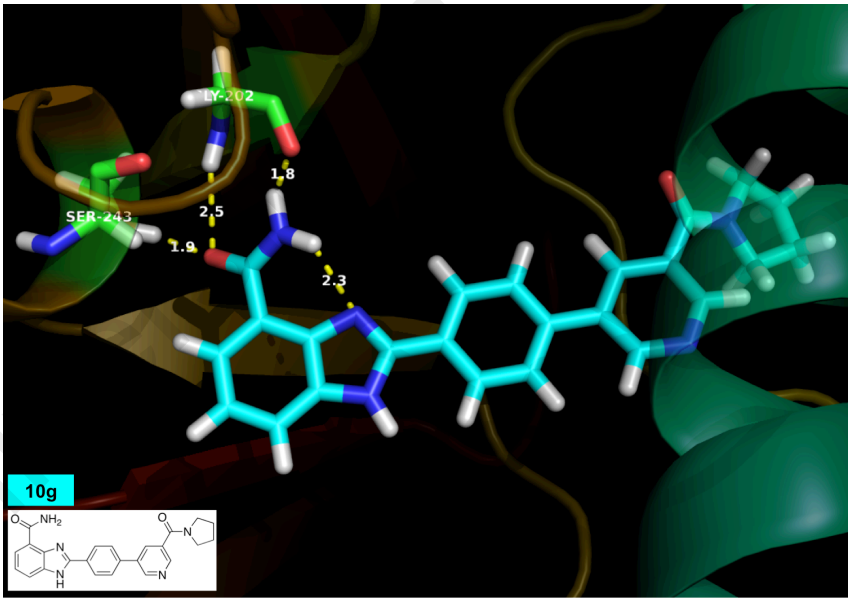

Figure 5.21. Docked pose of compound **10g** on PARP-1 enzyme (pdb ID: 4HHZ). Hydrogen bonds are highlighted in yellow dash. Figure was generated with PyMol.

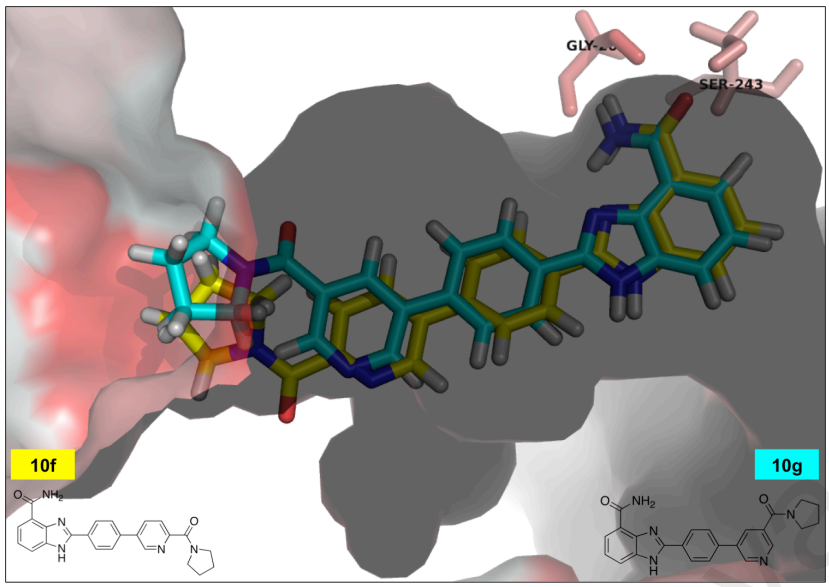

Figure 5.22. Ligand interaction of compounds **10f** and **10g** towards hydrophobicity surface. Red color indicates the hydrophobic surface of the enzyme (pdb ID: 4HHZ). Figure was generated with PyMol.

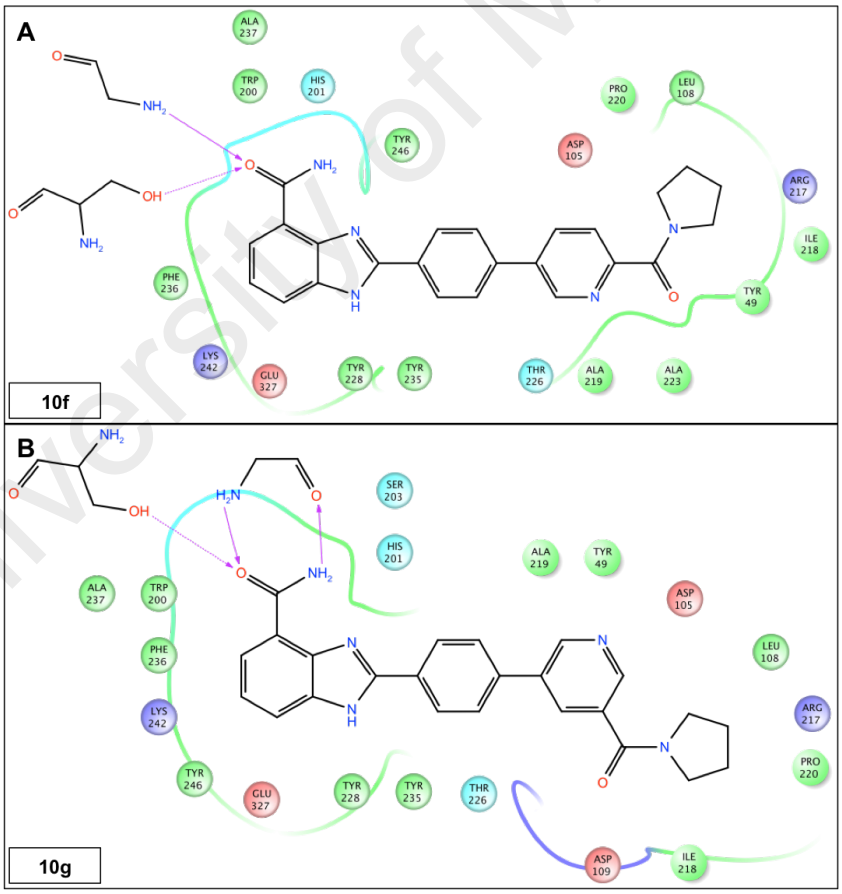

Figure 5.23. (A) and (B) shows the ligand interactions on PARP-1 enzyme with compounds **10f** and **10g**, respectively (pdb ID: 4HHZ). Red circle indicates negative charged residues, cyan indicates polar residues, green indicates hydrophobic residues, purple indicates positive charged residues. Cutoff was at 4.00 Å. Figures were generated with Maestro Schrodinger software.

Changing the pyrrolidinone group with a methylpyrrolidine group, as in compound **10h**, resulted in a significant increase in activity compared to compound **10g**. The IC_{50} value observed for compound **10h** was 0.061 μM. Perhaps, by removing the carbonyl group, there is an increase in hydrophobic interaction between the ligand and the active site of the enzyme (Figure 5.24). In addition, as shown in Figure 5.25, an additional ionic interaction between the nitrogen of the pyrrolidine and the residue Asp-109 is observed. Perhaps this led to the better activity observed with **10h**.

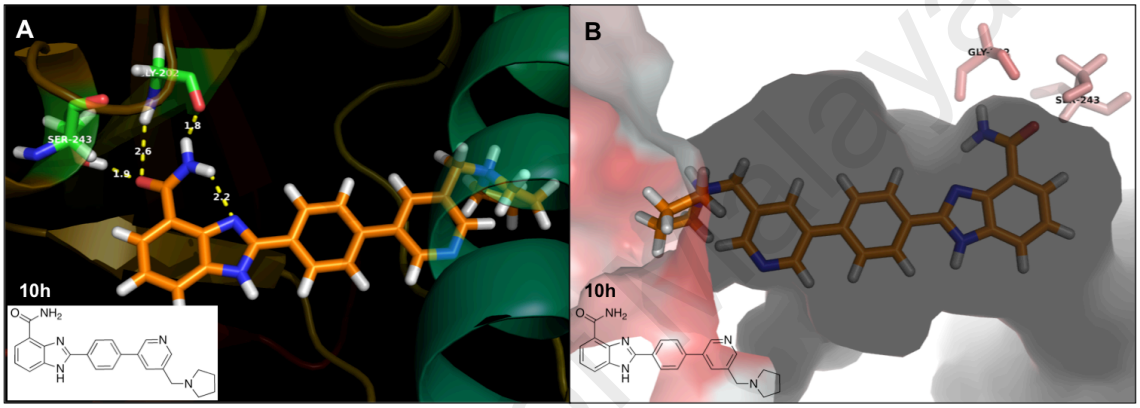

Figure 5.24. (A) illustrates the docking mode of compound **10h** on PARP-1 enzyme (pdb ID: 4HHZ). Hydrogen bonds are highlighted in yellow dash. (B) shows the ligand interaction of compound **10h** towards hydrophobicity surface. Red color indicates the hydrophobic surface of the enzyme (pdb ID: 4HHZ). Figures were generated with PyMol.

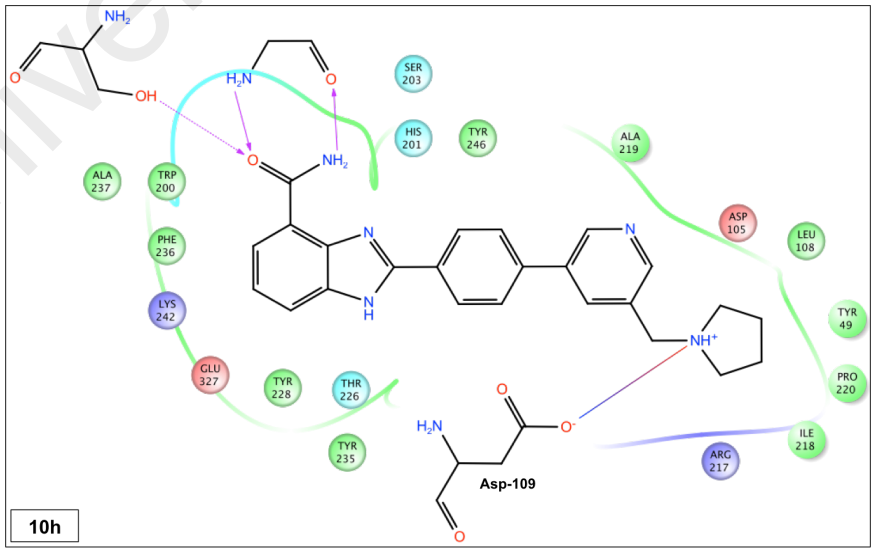

Figure 5.25. Ligand interaction of compound **10h** on PARP-1 enzyme (pdb ID: 4HHZ). Red circle indicates negative charged residues, cyan indicates polar residues, green indicates hydrophobic residues, purple indicates positive charged residues. Cutoff was at 4.00 Å. Figure was generated with Maestro Schrodinger software.

Table 5.3 shows a summary of the ligand-protein of compounds **10e**, **10f**, **10g** and **10h** towards the amino acid residues in the active pocket of the PARP-1 enzyme.

Table 5.3. Ligand-amino acid interactions (close contact) in active pocket of PARP-1 enzyme for compounds **10e**, **10f**, **10g** and **10h**.

	10e		**10f**		**10g**		**10h**	
Amino Acids (Found)	Ala-219	Lys-242	Ala-219	Lys-242	Ala-219	Lys-242	Ala-219	Lys-242
	Ala-223	Phe-236	Ala-223	Phe-236	-	Phe-236	-	Phe-236
	Ala-237	Pro-220	Ala-237	Pro-220	Ala-237	Pro-220	Ala-237	Pro-220
	Arg-217	Thr-226	Arg-217	Thr-226	Arg-217	Thr-226	Arg-217	Thr-226
	Asp-105	Trp-200	Asp-105	Trp-200	Asp-105	Trp-200	Asp-105	Trp-200
	Glu-327	Tyr-228	Glu-327	Tyr-228	Glu-327	Tyr-228	Glu-327	Tyr-228
	His-201	Tyr-235	His-201	Tyr-235	His-201	Tyr-235	His-201	Tyr-235
	Ile-218	Tyr-246	Ile-218	Tyr-246	Ile-218	Tyr-246	Ile-218	Tyr-246
	Leu-108	Tyr-49	Leu-108	Tyr-49	Leu-108	Tyr-49	Leu-108	Tyr-49
					*Asp-109		**Asp-109	
					*Ser-203		*Ser-203	

* Additional amino acid residue interaction.
** Ionic interaction of compound **10h** with amino acid residue.

In order to probe other possible interactions outside the cavity of the active pocket, compounds with longer substituent on the C-4' position of the biphenyl tail-end were prepared. Compounds **11a** and **11b** (Figure 5.26) were synthesised and screened for PARP-1 enzyme inhibitory activities. Results observed were as anticipated with compound **11a**, giving an IC_{50} value at 0.72 μM, while compound **11b** showed poor IC_{50} value at 2.28 μM.

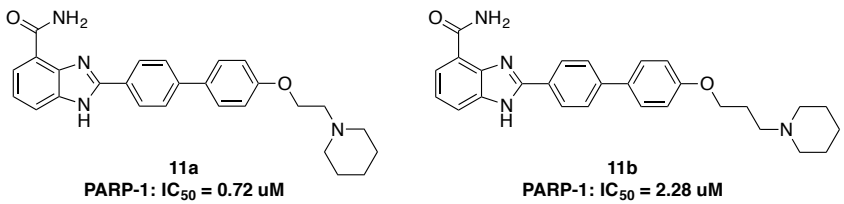

Figure 5.26. Compounds of **11a** and **11b**.

Adding an alkane piperidine substituent to the benzimidazole compound with an ether linkage seems to be unfavorable for PARP-1 activity. Our model showed this group to be entirely exposed towards the solvent site, which could presumably reduce the activity of the compound (Figure 5.27).

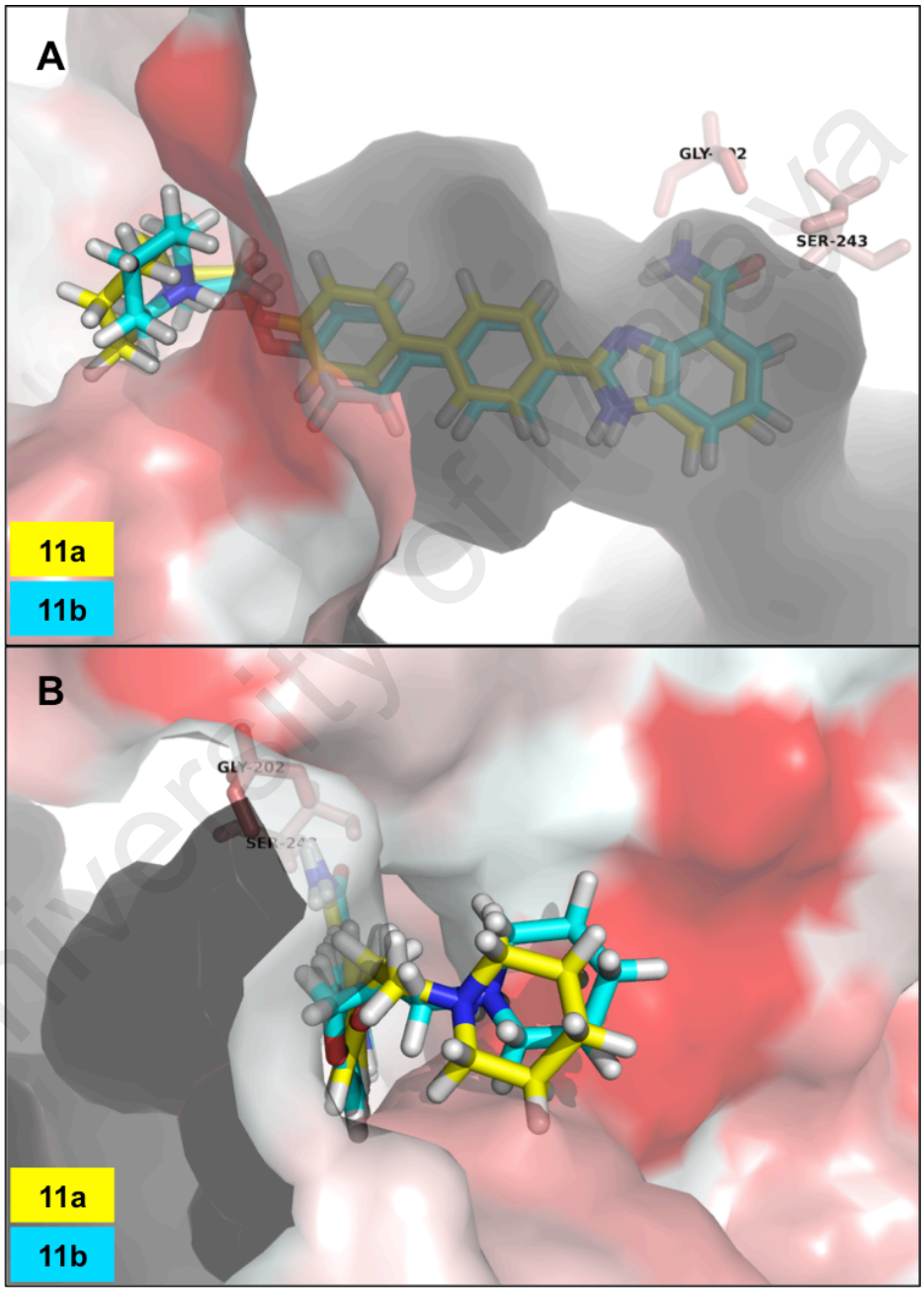

Figure 5.27. (A) and (B) illustrates the superposition of compounds **11a** and **11b** on PARP-1 enzyme, respectively, with hydrophobic interaction (pdb ID: 4HHZ). Red color indicates hydrophobic surface. Figures were generated with PyMol.

Fluorine and cyclopropane are bioisosteres for hydrogen and aromatic hydrocarbon, respectively. Many compounds have shown better activity when these isoteres were incorporated into the molecule. The unique properties of fluorine in a molecule often resulted in significant effect towards the bioactivity of the molecule. In such molecules, the hydrophobic interaction between the fluorinated ligand and the enzyme is enhanced, since the Van de Waals radius of hydrogen compared to fluorine increases from 1.20 to 1.35 Å. In addition, the high electronegativity of fluorine causes the carbon-fluorine bond to be polarized, which could affect the pose of the ligand in the active site of the enzyme.

Cyclopropane could also act as an isostere for an aryl group. Cyclopropane ring has a low molecular weight, and is low in lipophilicity. Thus, its presence in a molecule could presumably contribute to the potency of the molecule by enhancing its ADMET (adsorption, distribution, metabolism, excretion and toxicity) properties. In this work, cyclopropane was incorporated as cyclopropanecarboxamide in the hoping that the amido functionality could serve as a hydrogen bond donor and/or acceptor.

It would therefore be useful to investigate and study the effect of compounds with such functionality towards the PARP-1 inhibitory activity. Thus, compounds **11c**, **11d** and **11e** (Figure 5.28) were prepared by incorporating fluorine(s) and cyclopropane ring at various positions in the molecule.

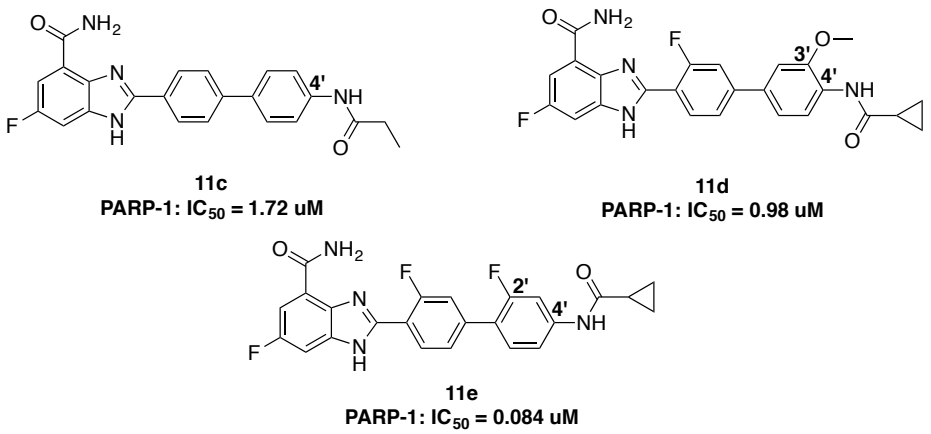

Figure 5.28. Compounds **11c**, **11d** and **11e**.

Fluoro group were placed at the C-6 position of the benzimidazole scaffold and a propionamide group were connected at the *para*-position of the biphenyl, as depicted in Figure 5.28 for compound **11c**. However, poor activity was observed for this compound at an IC_{50} value of 1.72 μM. From the model (Figure 5.29), it seemed that compound **11c** did not fit into the cavity as well as compound **10e**. The propionamide group seemed to be pushed into the lower surface of the cavity, possibly creating a high repulsion between the ligand and the surface of the cavity. Compound **10e** fitted better in the sense that it fits nicely within the hole of the cavity (Figure 5.29)

In compound **11d**, there is an additional fluoro substituent at the C-2 of the first phenyl ring of the biphenyl substituent in benzimidazole and a methoxy group at the C-3' position of the same biphenyl substituent. A much better activity, albeit still low, was observed for this compound (IC_{50} = 0.98 μM) (Figure 5.28).

The F-H bond (2.0 Å) between the amide hydrogen and the fluorine substituent on the phenyl ring helped to lock the conformation of the benzimidazole tail. This resulted in the cyclopropionamide group to be pushed away from the surface, fitting into the hole of the cavity better, as in compound **10e** (Figure 5.30).

Putting two fluoro groups into the molecule, such as in compound **11e**, resulted in an improved activity for compound **11e** with the IC_{50} value observed at 0.084 μM. The model in Figure 5.31 showed compound **11e** to fit nicely into the hole of the cavity. In addition, there were added hydrophobic interactions at the sites where both the fluoro substituents were placed

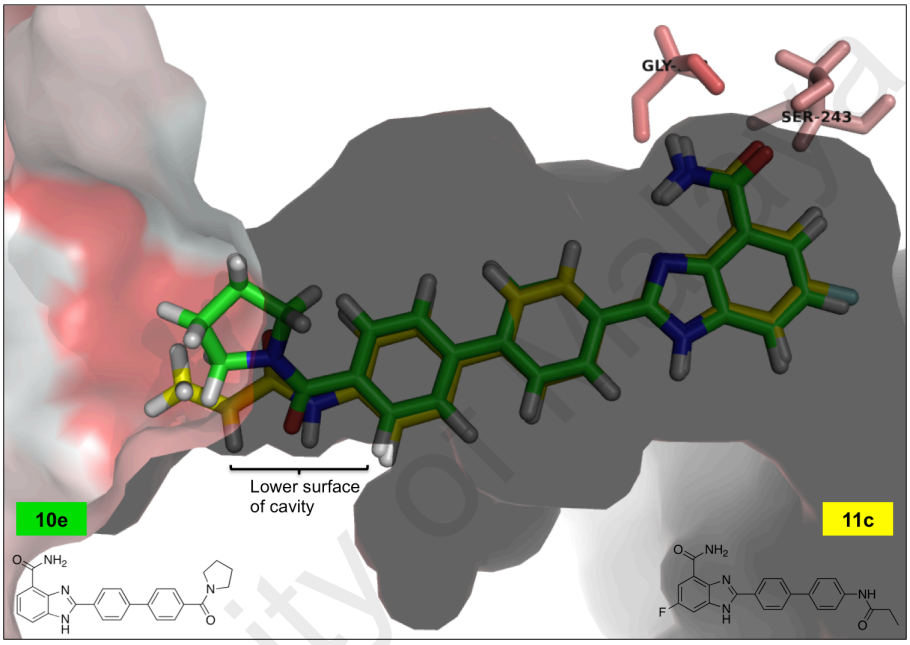

Figure 5.29. Superposition of compounds **10e** and **11c** on PARP-1 with hydrophobic interaction (pdb ID: 4HHZ). Red color indicates hydrophobic surface. Figure was generated with PyMol.

As for compounds **7a-g**, the docking mode of each compound on PARP-1 enzyme can be found in appendix B.

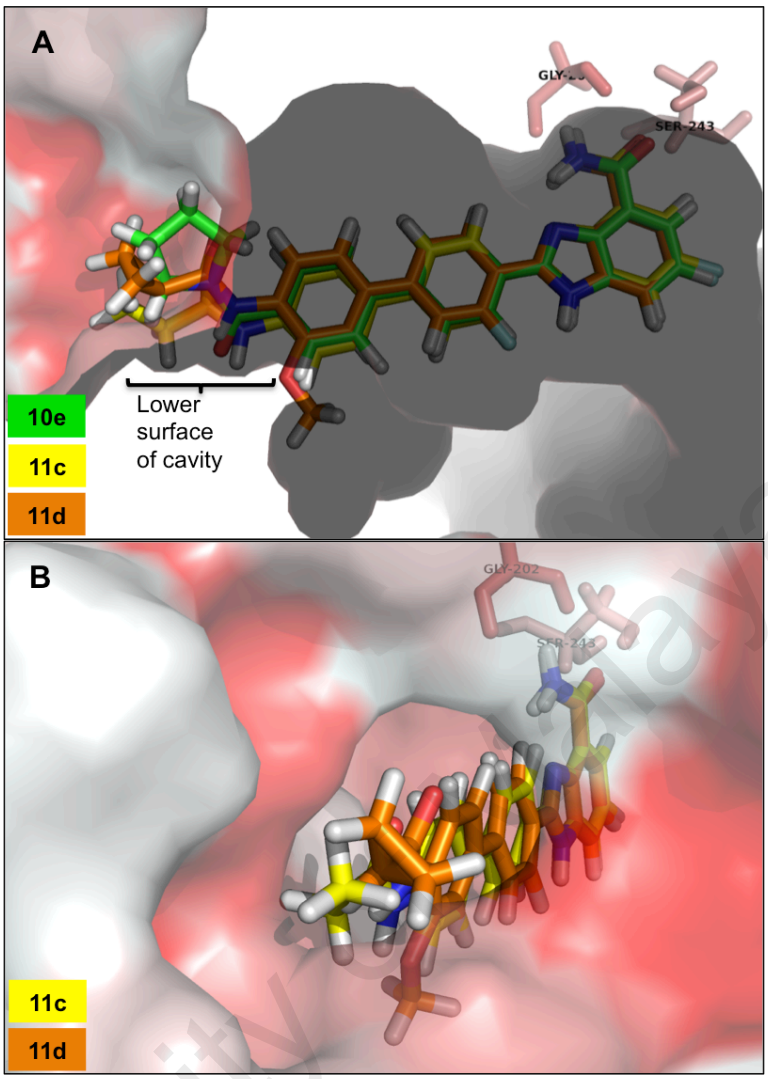

Figure 5.30. (A) illustrates the superposition of compounds **10e**, **11c** and **11d** on PARP-1 enzyme with hydrophobic interaction. (B) shows the tail-end group of the superimposed compounds **11c** and **11d** located at the cavity entrance of PARP-1 enzyme (pdb ID: 4HHZ). Red color indicates hydrophobic surface. Figures were generated with PyMol.

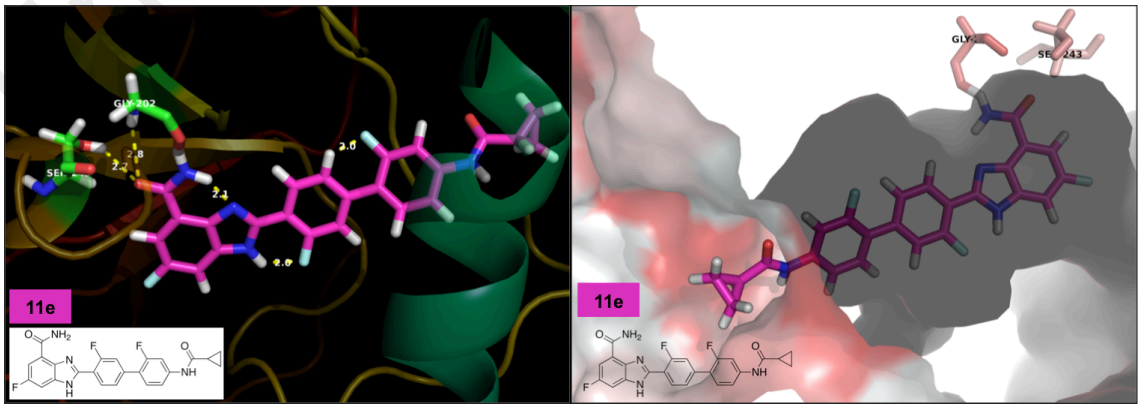

Figure 5.31. (A) illustrates the docked pose of compound **11e** on PARP-1 enzyme. (B) shows compound **11e** with hydrophobic interaction (pdb ID: 4HHZ). Red color indicates hydrophobic surface. Figures were generated with PyMol.

5.2.2 Biological Evaluation of Synthesised Compounds on DHODH Enzyme

The same synthesised compounds (Table 5.1) were then tested onto the second target, the DHODH enzyme. Liu and co-workers reported the brequinar analogue to have high affinity for human DHODH (Liu e*t al*., 2000). Co-crystallised brequinar analogue (Figure 5.32) in human DHODH showed an IC_{50} value of 0.007 μM (pdb ID: 1D3G).

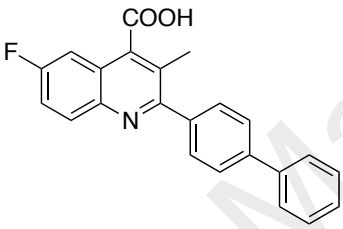

Brequinar analogue
DHODH IC_{50} = 0.007 uM

Figure 5.32. Structure of brequinar analogue.

Liu ascribed the high affinity in human DHODH observed with brequinar analogue to possibly be due to the interactions between the ligand and the enzyme. The fluoroquinoline carboxylate head-group of the analogue were observed to be buried deep inside the polar region of the active site of DHODH, while the two aromatic rings were in the hydrophobic region. The carboxylate form of the brequinar analogue formed hydrogen-bonding interactions with the residues Arg-136 and Gln-47 of DHODH. In addition, a water-mediated hydrogen bond between this carboxylate ligand and Thr-360 was also observed.

In addition, the fluorine group at C-6 position of the brequinar analogue interacted closely with the C-7 methyl of the FMN, while the quinoline ring formed a π-π stack with His-56 (Figure 5.33) (Liu e*t al*., 2000).

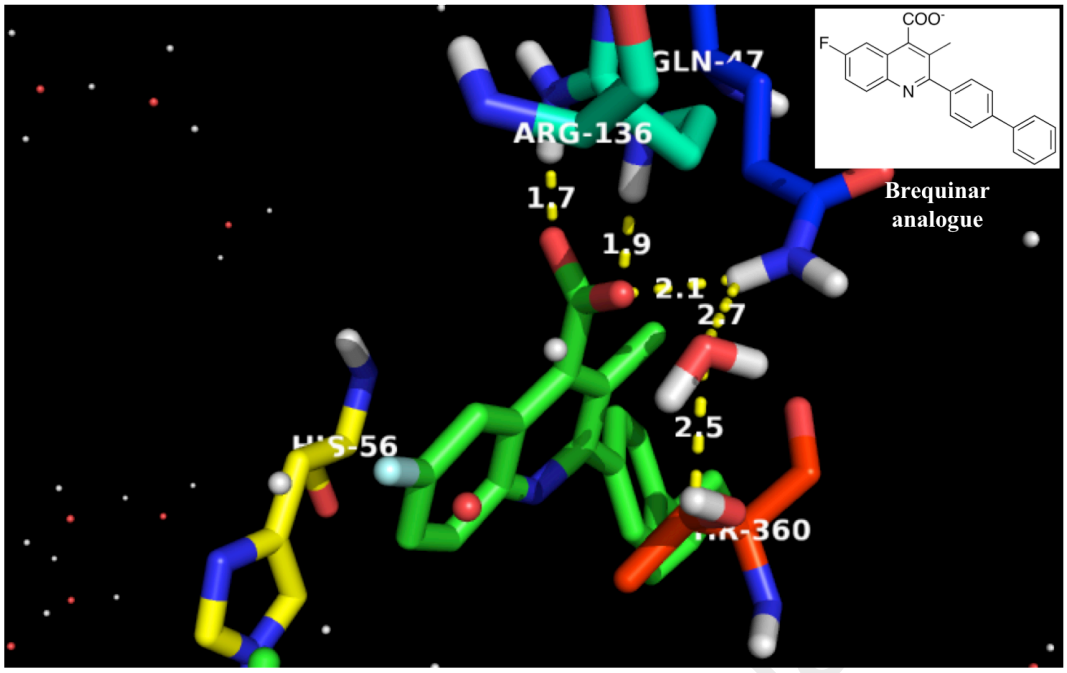

Figure 5.33. Brequinar analogue co-crystallised with DHODH (pdb ID: 1D3G). Hydrogen bonds are highlighted as yellow dash. Red and white sphere dots represents water molecules. Figure was generated with PyMol.

Compounds in Table 5.1, first evaluated against PARP-1 enzyme, were then subjected towards DHODH enzyme since the objective is to design a compound that could act as a dual inhibitor, towards PARP-1 and towards DHODH.

Evaluation of compounds **9a-g** (Figure 5.34) against DHODH enzyme was carried out. In this series (**9a-g**), the best activity observed was with compound **9b** with inhibition at an IC_{50} value of 9.80 µM. Compound **9a** showed 9% inhibition at 10 µM, while compounds **9c, 9f** and **9g** showed 1%, 11% and 5% inhibition at 10 µM, respectively, and considered to be inactive. However, compounds **9d** and **9e** were found to be inactive towards the enzyme.

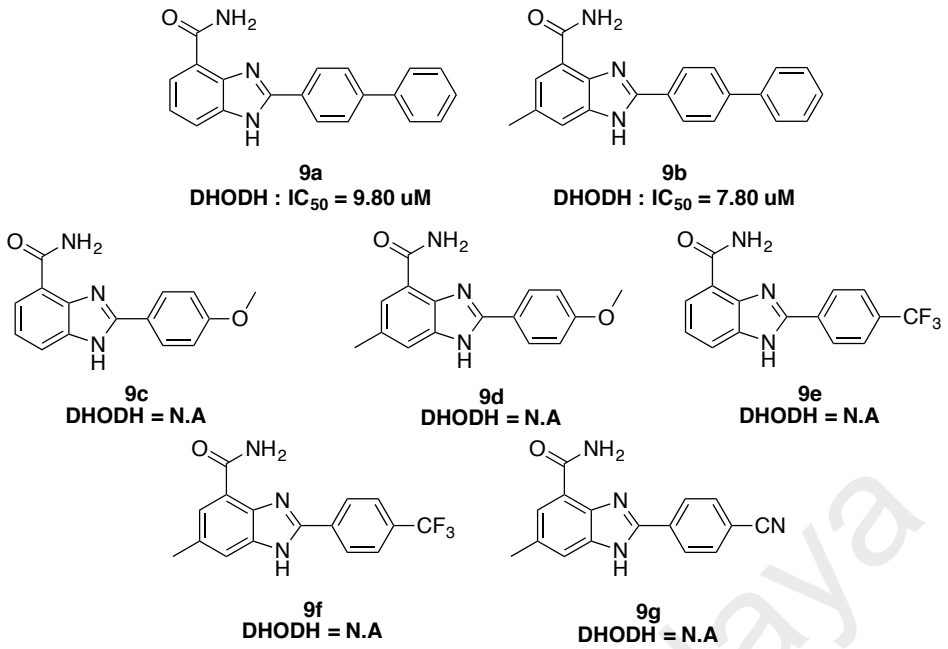

Figure 5.34. Compounds **9a-g**.

Compounds **9h**, **9i** and **9j** showed slight improvement in percent inhibition with values of 51%, 42% and 56% inhibition at 10 μM, respectively (Figure 5.35).

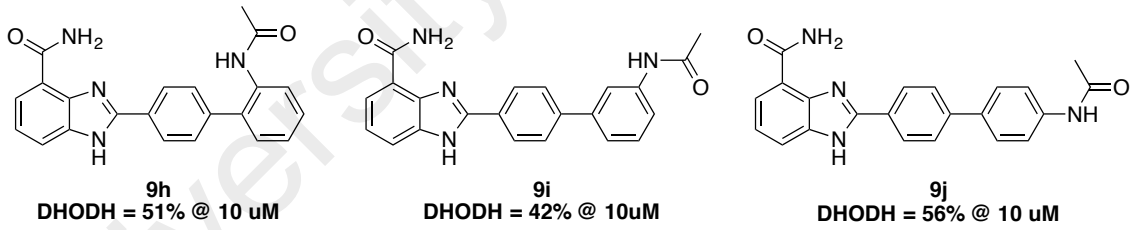

Figure 5.35. Compounds **9h**, **9i** and **9j**.

In order to understand the problem, we studied the co-crystallised structure of brequinar analogue with the DHODH enzyme (pdb ID: 1D3G) and compared this with the model of compounds **9h**, **9i** and **9j** docked onto DHODH enzyme (Figure 5.36), since these three compounds showed the best activities amongst the 9-series of compounds.

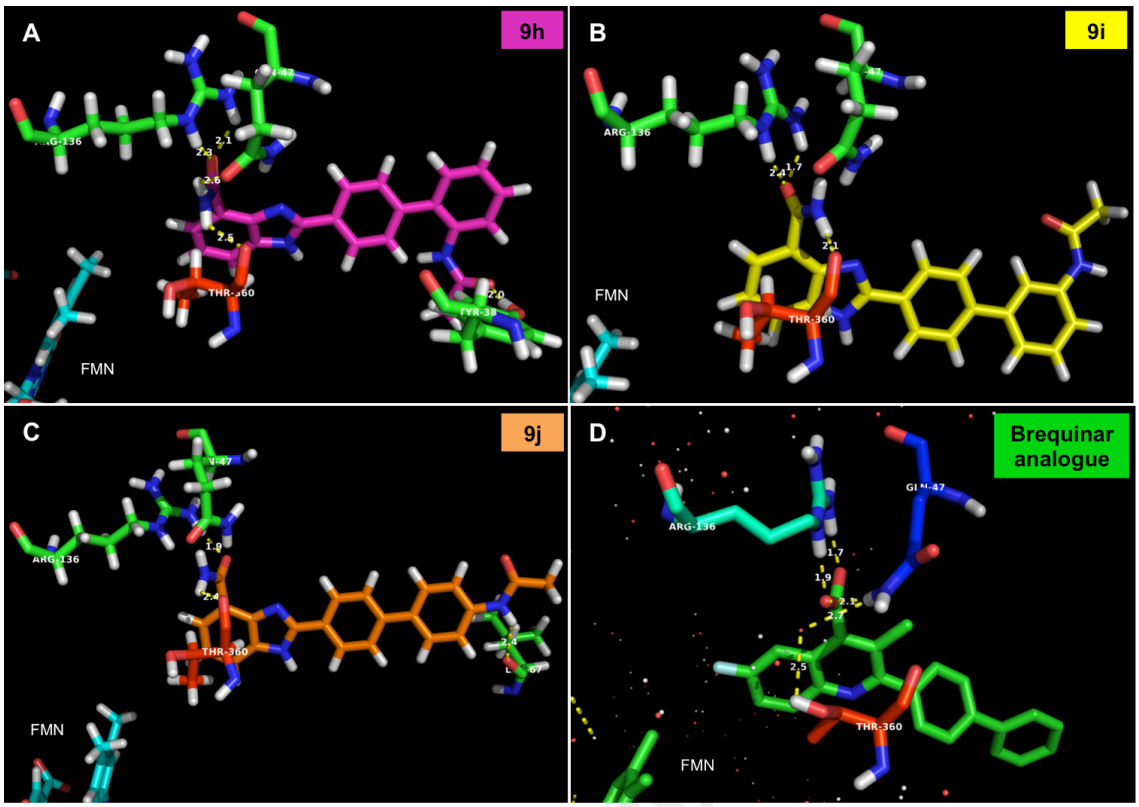

Figure 5.36. (A), (B), (C) and (D) illustrates the docked pose of compounds **9h**, **9i**, **9j** and brequinar analogue on DHODH enzyme (pdb ID: 4IGH), respectively. Hydrogen bonds are highlighted as yellow dash. Figures were generated with PyMol.

Several dissimilarities were observed between the interactions of compounds **9h**, **9i** and **9j** and the brequinar analogue. For compounds **9h**, **9i** and **9j**, the carbonyl oxygen of the carboxamide group of the ligand formed hydrogen-bonding with Arg-136. With the brequinar analogue, two hydrogen-bonding interactions were observed between the Arg-136 with the carboxylate group of the brequinar analogue. In addition, the amino hydrogen in the Gln-47 residue formed one hydrogen-bond with one of the carboxylate in the brequinar analogue. In the **9h**, **9i**, and **9j** models, this hydrogen-bond occurs between carbonyl oxygen of the Gln-47 residue and the amino hydrogen of the carboxamide head-group of the compound **9h** (Figure 5.37, A), but no H-bond interaction was observed with compounds **9i** (Figure 5.37, B) and **9j** (Figure 5.37, C) with Gln-47. This is shown (schematic diagram) in Figure 5.37.

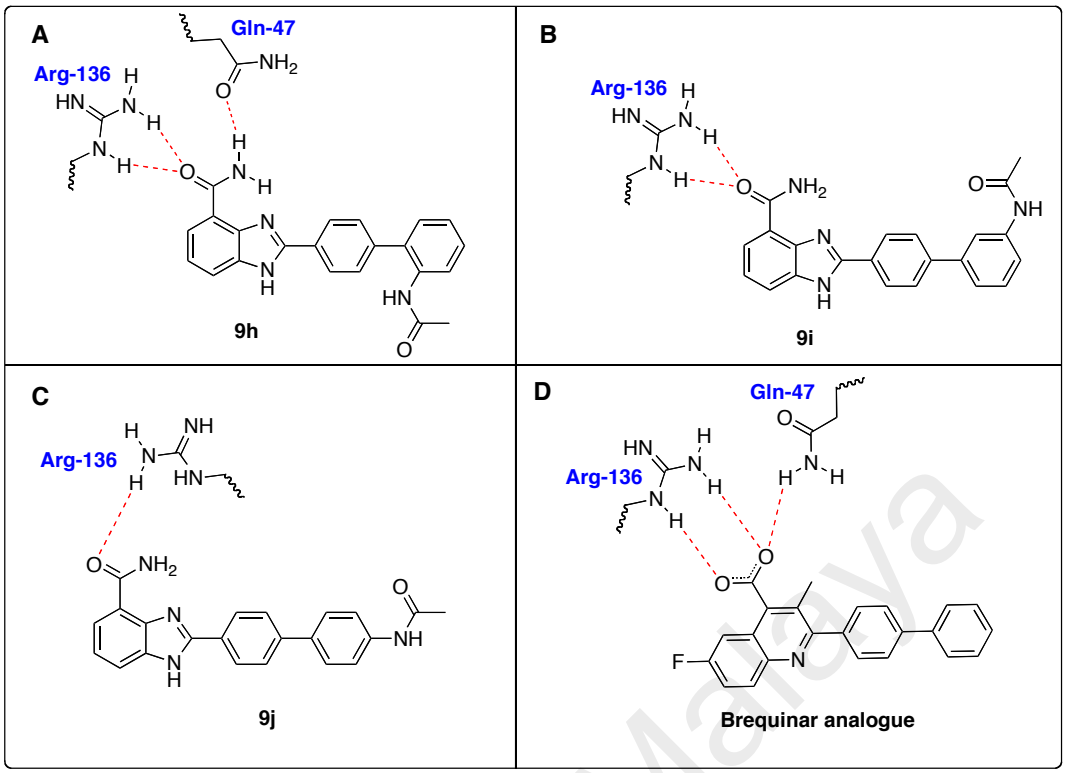

Figure 5.37. (A), (B), (C) and (D) illustrates the head-group of compounds **9h**, **9i**, **9j** and brequinar analogue interactions with DHODH enzyme, respectively. Hydrogen bonds are highlighted as red dash (pdb ID: 4IGH).

Unlike what is seen in the brequinar analogue-DHODH structure, no water-mediated H-bond was observed between compounds **9h**, **9i** and **9j** and Thr-360. Instead, the hydrogen bonding occurred between the amino hydrogen of the carboxamide and the carbonyl oxygen group of Thr-360 (Figure 5.38). The water molecule within the DHODH cavity is conserved and lies deep within the active pocket. It seems to play a crucial role in enhancing the activity of the ligand toward DHODH enzyme (Figure 5.39) (Liu e*t al*., 2000). The loss of this interaction with the compounds **9h**, **9i** and **9j** (as well as all the other 9-series compounds) would therefore contribute to the loss in activities, observed with these compounds.

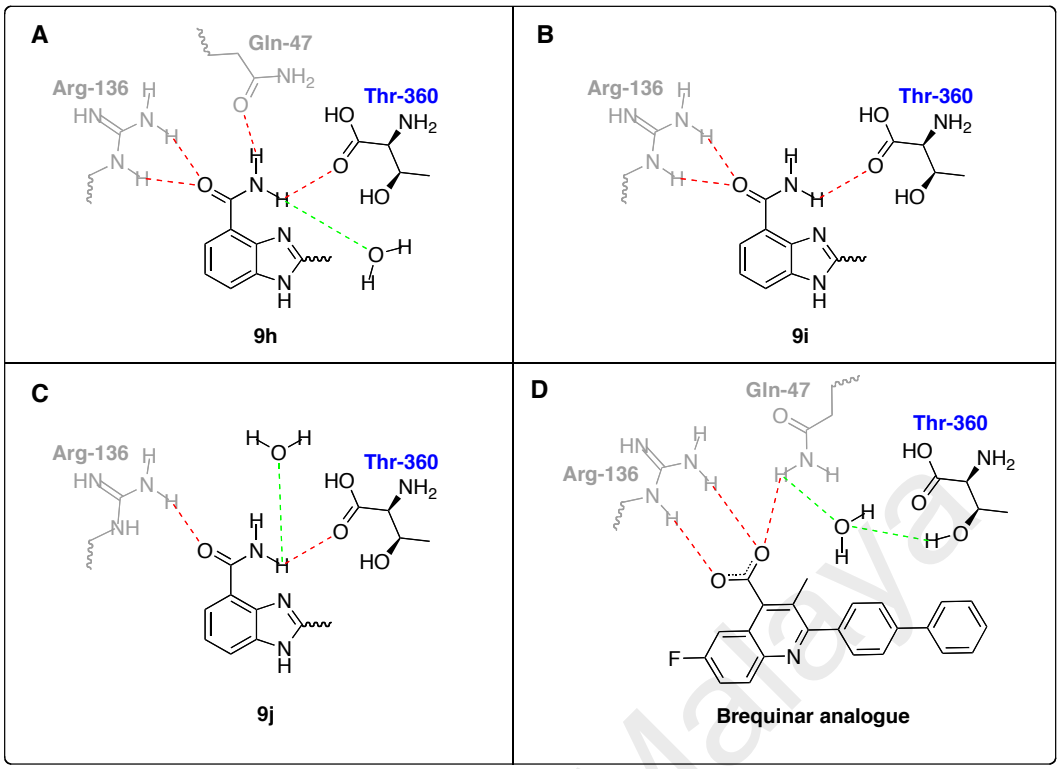

Figure 5.38. (A), (B), (C) and (D) illustrates the head-group of compounds **9h**, **9i**, **9j** and brequinar analogue interactions with DHODH enzyme, respectively. Hydrogen bonds to amino acid residues are highlighted as red dash. Hydrogen bond to a conserved water molecule is highlighted as green dash (pdb ID: 4IGH).

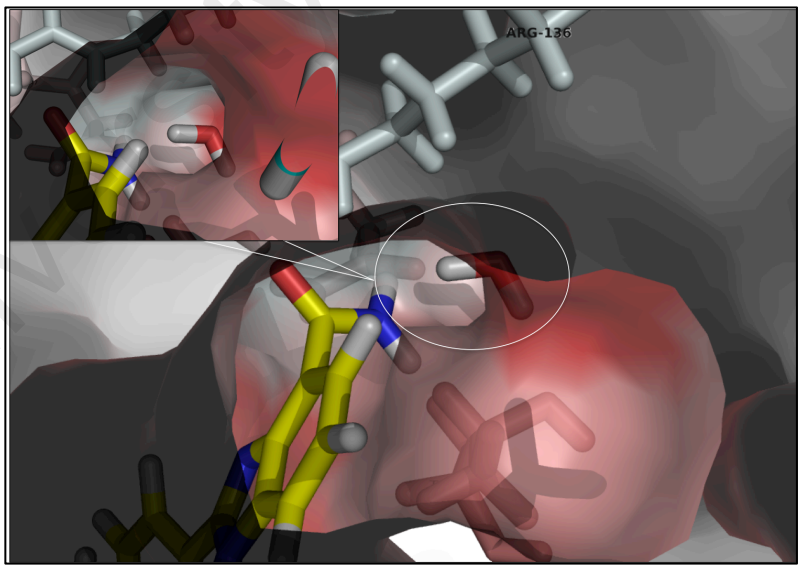

Figure 5.39. A conserved water molecule found deep inside the active site of DHODH enzyme (pdb ID: 4IGH). Figure was generated with PyMol.

Compounds **10a-h** (called the 10-series) and compounds **11a-e** (called the 11-series) were also tested as listed in Table 5.1. All the models for these compounds displayed

similar hydrogen bonding interactions as observed with the 9-series compounds. All of them showed similarly poor activity, at approximately 10-55% inhibition at 10 μM. The pictures of the models for all these compounds are shown in the appendix C.

Since the activities of benzimidazole carboxamide towards DHODH were observed to be very poor activity, consideration by replacing the carboxamide group at the C-3 position of the benzimidazole derivatives with a carboxyl substituent were made. This is to imitate the brequinar analogue where there is a good interaction between the carboxylate functionality with the important amino acid residues of DHODH. With this substituent, the compounds are expected to give better inhibitory activities towards DHODH. In addition, a methyl group was added at the C-6 position of the benzimidazole derivatives. The methyl substituent was placed at C-6 position to serve as a substituent for the fluorine in the brequinar analogue. By doing so, gaining some insights onto the interactions between the fluorine (in brequinar analogue) and FMN of the DHODH enzyme is hope to be observed. Compounds **7a-g** (7-series), were synthesised and tested for bioactivity with DHODH enzyme. Figure 5.40 shows the structure and bioactivity results for the compounds **7a-g**.

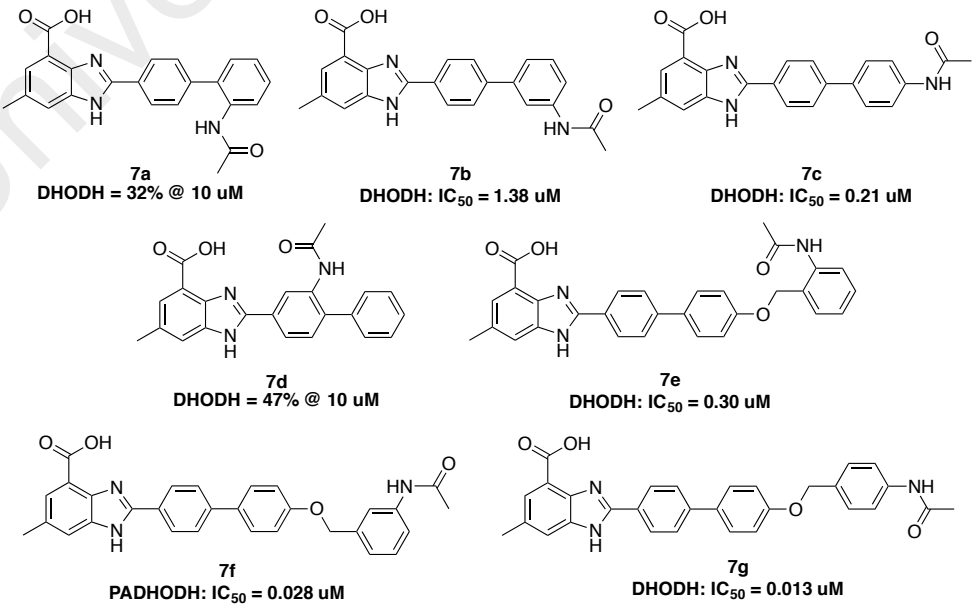

Figure 5.40. Compounds **7a-g**.

Of all the compounds in the 7-series, the best activities were observed with compounds **7f** and **7g** with IC_{50} values at 0.028 μM and 0.013 μM, respectively. All compounds in the 7-series displayed similar head-group interactions, where the carboxylate on the benzimidazole compounds interacted with the amino acid residues, Arg-136 and Gln-47 in DHODH (see appendix C). In addition, this carboxylate group formed a water-mediated H-bonding with the hydroxyl of Thr-360 moiety (Figure 5.41).

The difference in interaction between the compounds in this 7-series and DHODH enzymes lies in the tail-end of the molecule, presumably causing the difference in activities observed in these compounds. For **7f**, there is an added π-π interaction between the third phenyl ring of the ligand and the amino acid Tyr-38 of the DHODH enzyme, while compound **7g** has an additional H-bonding interaction between the amide group on the third ring of the tail-end of the benzimidazole derivative and Asp-34 of the DHODH enzyme as well as compound **7f**. These interactions are shown in Figure 5.42. Presumably, these additional interactions observed in **7f** and **7g** (but not with the other compounds) led to better activities observed with DHODH, compared to all other compounds in the 7-series.

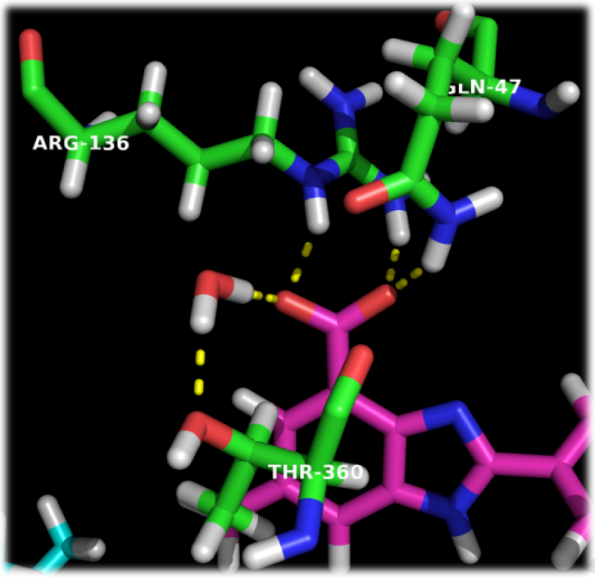

Figure 5.41. General head-group interactions for compounds **7a-g** (7-series) on DHODH enzyme. Hydrogen bond interactions are highlighted as yellow dash. Figure was generated with PyMol.

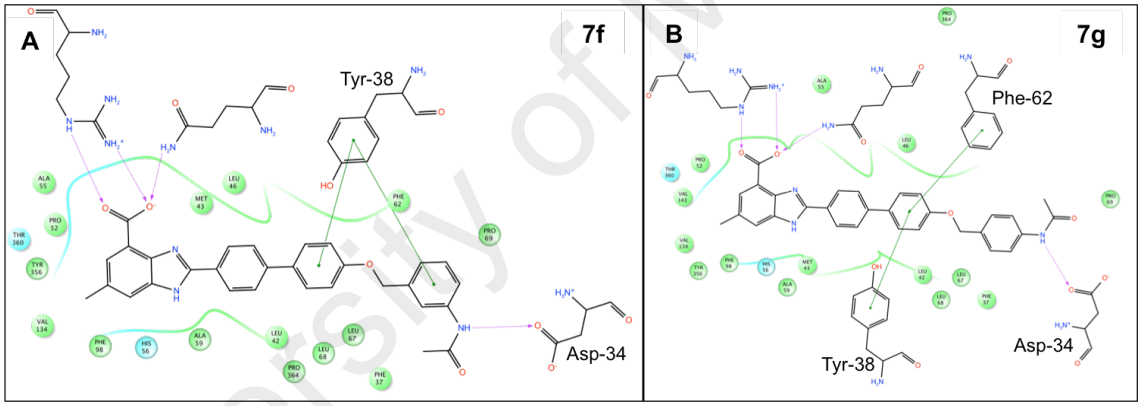

Figure 5.42. (A) and (B) illustrate interactions of compounds **7f** and **7g** on DHODH enzyme respectively (pdb ID: 4IGH). Hydrogen bonds are in pink arrow. π-π interactions are in green arrow. Red circle indicates negative charged residues, cyan indicates polar residues, green indicates hydrophobic residues, purple indicates positive charged residues. Cutoff was at 4.00 Å. Figures were generated with Maestro Schrodinger software.

Since aim of study is to search for a compound with dual inhibitory properties, towards both PARP-1 and DHODH enzymes, activity of the 7-series compounds towards PARP-1 were carried out.

From Table 5.1, compound **7e** is the only compound that indicated fair activities towards both DHODH and PARP-1with IC_{50} values of 10.63 µM for PARP-1, and 0.30

μM for DHODH. Compound **7e** comprised a carboxylate group at the C-3 position and a methyl substituent at the C-6 position of the benzimidazole scaffold. In addition, there is an acetamide group at the *ortho*-position of the third phenyl ring at the tail-end group compound (Figure 5.43). In comparison, the acetamide group in **7f** and **7g** is at the *meta*- and *para*-position of the compound, respectively. The activities for these two compounds, as discussed earlier, were good for DHODH, but not for PARP-1 enzyme (Figure 5.43).

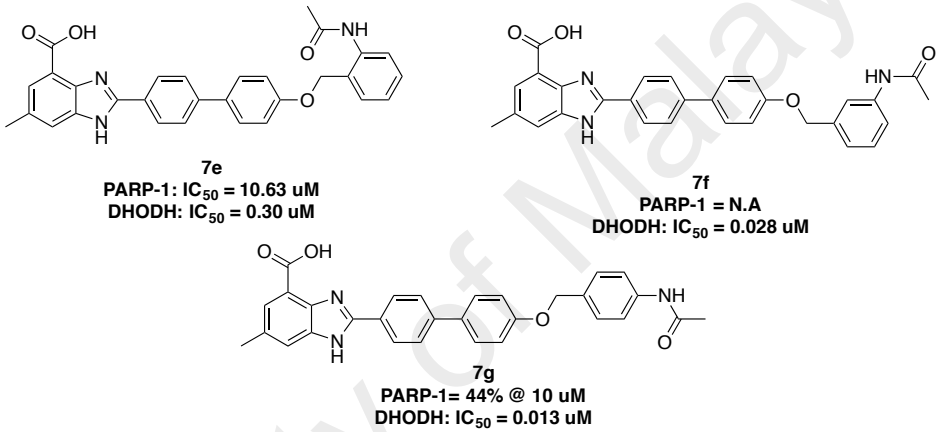

Figure 5.43. Compounds **7e**, **7f** and **7g**.

Model study of compound **7e**, docked into the PARP-1 enzyme indicated the carboxylate head-group of the benzimidazole scaffold to form a hydrogen-bonding interaction with Ser-203. In addition, the –NH of the acetamide group at the tail-end of this compound formed a hydrogen-bond with the carbonyl oxygen of Ile-218 (Figure 5.44). However, although same interactions were observed with the head-group of compounds **7f** and **7g** and Ser-203, no such H-bonds were observed at the tail-end with Ile-218. The H-bond interactions between tail-end of compound **7e** with Ile-218 in PARP-1 presumably played some role in increasing the activity of this compound towards PARP-1.

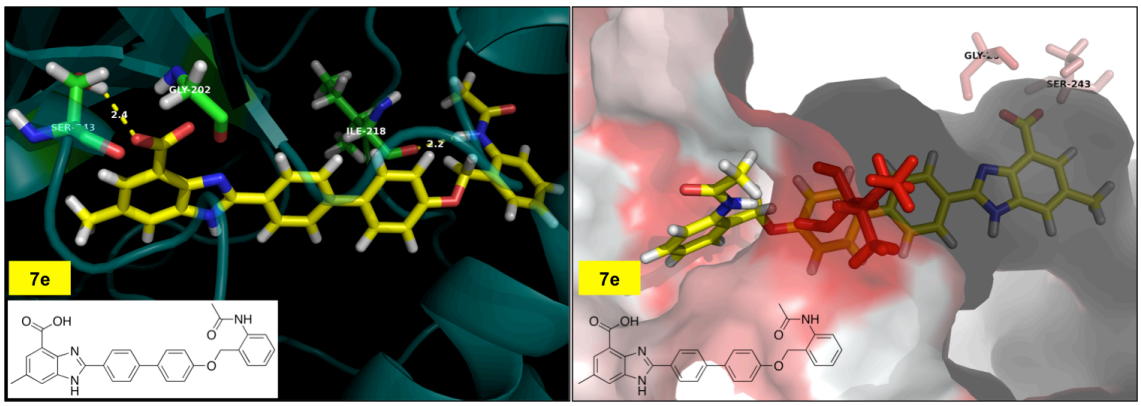

Figure 5.44. (A) shows the docked pose of compound **7e** on PARP-1 enzyme. Hydrogen bonds are highlighted as yellow dash. (B) illustrates compound **7e** on PARP-1 enzyme with hydrophobic surface interactions. Red color indicates hydrophobic surface (pdb ID: 4HHZ). Figures were generated with PyMol.

While good activities were observed with compounds **7f** and **7g** with DHODH giving IC_{50} values of 0.028 and 0.013 µM, respectively (Figure 5.43), compound **7e** did not show such good activity with an IC_{50} value of 0.30 µM. The head-group interactions of all the three compounds (**7e**, **7f** and **7g**) are the same where the carboxylate head-group formed hydrogen-bond interactions with Arg-136 and Gln-47, in addition to a water-mediated H-bond interaction with hydroxyl group of Thr-360 (Figure 5.45, A).

The difference between compound **7e** and compounds **7f** and **7g** lie in the tail-end interaction of these compounds with the DHODH enzyme where the amido group forms hydrogen-bonding interaction with Tyr-38 in compound **7e** while for compounds **7f** and **7g**, this hydrogen-bonding occurred with Asp-34 (Figure 5.42). Presumably, the hydrogen-bonding interaction with Asp-34 has some role to play in the activity of DHODH. Unfortunately, the findings could not be confirmed during this work.

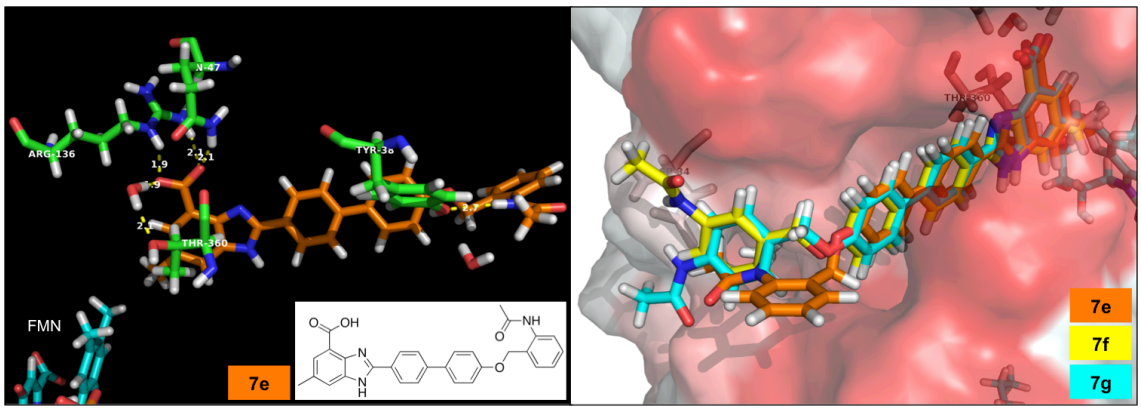

Figure 5.45. (A) shows the docked pose of compound **7e** on DHODH enzyme. Hydrogen bonds are highlighted as yellow dash. (B) illustrates superimposed of compounds **7e**, **7f** and **7g** on DHODH enzyme with hydrophobic surface interactions. Red color indicates hydrophobic surface (pdb ID: 4IGH). Figures were generated with PyMol.

Reviewing the activities for both PARP-1 and DHODH on all compounds tested revealed several compounds with relatively good activity values. These compounds are listed in Table 5.4 for PARP-1 and Table 5.5 for DHODH.

Table 5.4. Selected compounds with good activity for PARP-1 enzyme, and their ligand-amino acid interactions in the active pocket.

PARP-1 enzyme	**7e (IC_{50} = 10.63 µM)**		**9h (IC_{50} = 0.14 µM)**		**10h (IC_{50} = 0.061 µM)**		**11e (IC_{50} = 0.084 µM)**	
Head-group interactions	Gly-202 Ser-243		Gly-202 Ser-243		Gly-202 Ser-243		Gly-202 Ser-243	
Tail-end interactions	Ile-218		-		Asp-109 (ionic interaction)		Tyr-49	
Close contacts	Ala-219 Ala-237 Arg-217 Glu-327 His-201 Ile-333 Leu-108 Lys-242	Pro-220 Thr-226 Asp-105 Tyr-235 Tyr-246 Tyr-49 Tyr228	Ala-219 Ala-237 Arg-217 Asn-106 Asn-207 Asp-105 Asp-109 Glu-327 His-201	Ile-211 Leu-108 Lys-242 Pro-220 Ser-203 Thr-226 Tyr-235 Tyr-246 Tyr-49	Ala-219 Ala-237 Arg-217 Asp-105 Glu-327 His-201 Ile-218 Leu-108 Lys-242	Phe-236 Pro-220 Ser-203 Thr-226 Trp-200 Tyr-228 Tyr-235 Tyr-246 Tyr-49	Ala-219 Arg-217 Asp-105 His-201 Leu-108 Lys-242	Pro-220 Ser-203 Thr-226 Tyr-228 Tyr-235 Tyr-246

Table 5.5. Selected compounds with good activity for DHODH enzyme, and their ligand-amino acid interactions in the active pocket.

DHODH enzyme	**7e (IC_{50} = 0.30 µM)**		**9h (51% at 10 µM)**		**10h (55% at 10 µM)**		**11e (48% at 10 µM)**	
Head-group interactions	Gln-47 Arg-136		Gln-47 Arg-136 Thr-360		Gln-47 Arg-136 Thr-360		Gln-47 Arg-136 Thr-360	
Tail-end interactions	Tyr-38		Tyr-38		Tyr-38		Leu-67	
Close contacts	Ala-55 Ala-59 Asp-34 His-56 Leu-42 Leu-46 Leu-67 Leu-68 Leu359 Met-43	Phe-62 Phe-98 Pro-364 Pro-52 Pro-69 Tyr-147 Tyr-356 Tyr-38 Val-134 Val-143	Ala-55 Ala-59 His-56 Leu-42 Leu-46 Leu-50 Leu-58 Leu-67 Leu-68 Met-111	Met-43 Phe-62 Phe-98 Pro-364 Pro-52 Thr-63 Tyr-356 Tyr-38 Val 134 Val-143	Pro-52 Val-134 Tyr356 Val-143 Phe-98 His-56 Ala-55 Met-43	Leu-46 Phe-62 Tyr-38 Leu-42 Ala-59 Leu-58 Pro-364 Phe-37	Ala-55 Ala-59 His-56 Leu-42 Leu-46 Leu-67 Leu-68	Met-43 Phe-62 Phe-98 Pro-364 Pro-52 Tyr-356 Tyr-38
p-p interactions	Tyr-38 Phe-62		Phe-62		Phe-62		Tyr-38 Phe-62	
Other interactions	H-O-H – Thr-360		-		-		-	

Out of these compounds, three compounds indicated good inhibitory activities for both PARP-1 and DHODH. These compounds are **7e**, **10h** and **11e**. Unfortunately, there was no relationship that we could identify to connect these compounds with the relatively good activities observed for both enzymes. For PARP-1, the carboxamide at C-3 and hydrogen and/or fluorine at C-6 in the head-group of the benzimidazole scaffold are essential for good activity. For good DHODH activity, on the other hand, a carboxylic acid head-group at the C-3 and a methyl group at the C-6 position of the head-group of the benzimidazole scaffold are required. However, a methyl substituent at C-6 of the benzimidazole scaffold is detrimental for PARP-1 activity.

The biphenyl ring at the tail end of the benzimidazole scaffold is equally important for both PARP-1 and DHODH inhibitory activity. However, it seemed that the determining functionality for both PARP-1 and DHODH activities lie in the head-group of the benzimidazole scaffold. Compounds **7e**, **10h** and **11e** seemed to exhibit relatively good activities for both enzymes, and could potentially be used as a template to further search for a lead compound with dual properties.

A diagram summarizing the important functionalities in the benzimidazole scaffold for both PARP-1 and DHODH enzyme activities is shown in Figure 5.46.

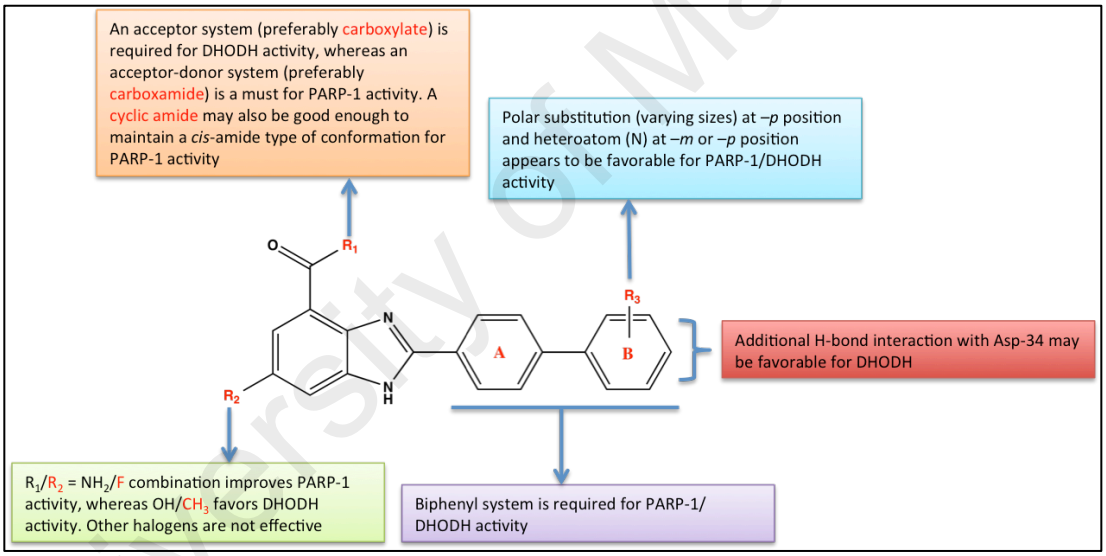

Figure 5.46. Summary of the SAR (structural-activity relationship) points for possible dual inhibition of PARP-1 and DHODH enzymes.

CHAPTER 6: CONCLUSION AND FUTURE WORK

6.1 Conclusion

Studies of various benzimidazole derivatives as prospective inhibitors for both PARP-1 and DHODH enzymes were conducted. All the benzimidazole compounds have been synthesized in good to excellent yields. These benzimidazole compounds have been tested for inhibitory activities against PARP-1 and DHODH enzymes.

Compounds **9h**, **10b**, **10c**, **10f**, **10h** and **11e,** were observed to give good activities with PARP-1 enzyme while compounds **7b**, **7e**, **7f** and **7g** showed good activities with DHODH enzymes.

SAR and bioactivity results indicated that carboxamide group on C-3 and hydrogen and/or fluorine at C-6 of the benzimidazole scaffold are important for PARP-1 enzyme inhibitory activity, while carboxylate group on C-3 and methyl group at C-6 of the same benzimidazole scaffold are important functionalities for DHODH enzyme activities. However, at the tail-end of the benzimidazole scaffold, the biphenyl ring is observed to play an essential role for enhancing bioactivities in both PARP-1 and DHODH enzymes. The results also indicated that the interactions of the head-group of the benzimidazole ligand are more important in influencing the activity of both enzymes.

There are, however, some indications of dual inhibitions observed with some compounds, such as compounds **9h**, **10h**, and **11e**, although they show much better activity with PARP-1 enzyme than with DHODH. Compound **7e** also indicated activities towards both PARP-1 and DHODH enzymes. However, unlike compounds

9h, **10h** and **11e**, compound **7e** showed better activity towards DHODH than PARP-1. These compounds could then be used to assist in designing other molecules with dual inhibition properties towards PARP-1 and DHODH.

6.2 Future Work

For the results obtained in the study, compounds **7e**, **9h**, **10h** and **11e** indicated dual activities towards PARP-1 and DHODH. These compounds could be used as template to design other molecules, which may show better activities towards both enzymes.

As discussed, one of the essential groups for activity towards PARP-1 could be the C-6 fluorine on the benzimidazole scaffold. It was also observed that a fluorine group at this position could interact with the C-7 methyl group of the FMN in the DHODH enzyme. So, perhaps, putting fluorine on compounds, such as **7e**, **9h** and **10h** could help to increase the activities of these compounds towards DHODH.

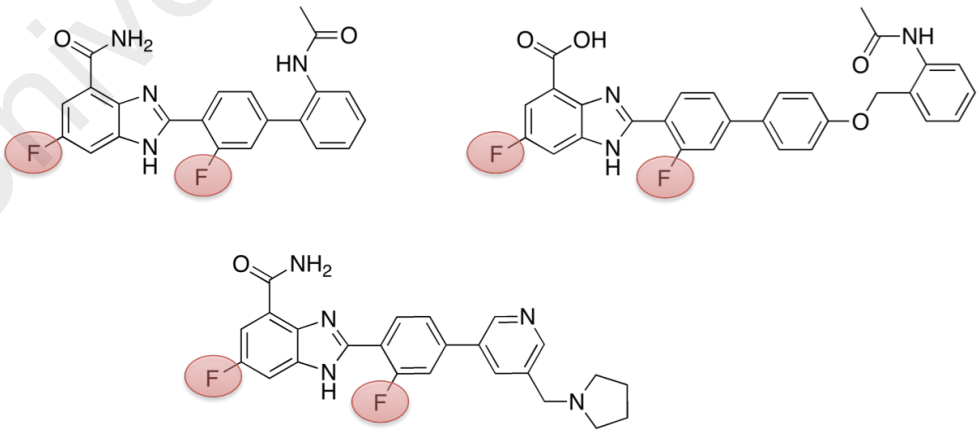

As for compound **11e**, perhaps by substituting the cyclopropane of the cyclopropionamide to a isoxazole, a cyano hydroxyl, hydroxamic acid groups and other potential functional groups could possibly help to enhance the activities towards both PARP-1 and DHODH enzymes.

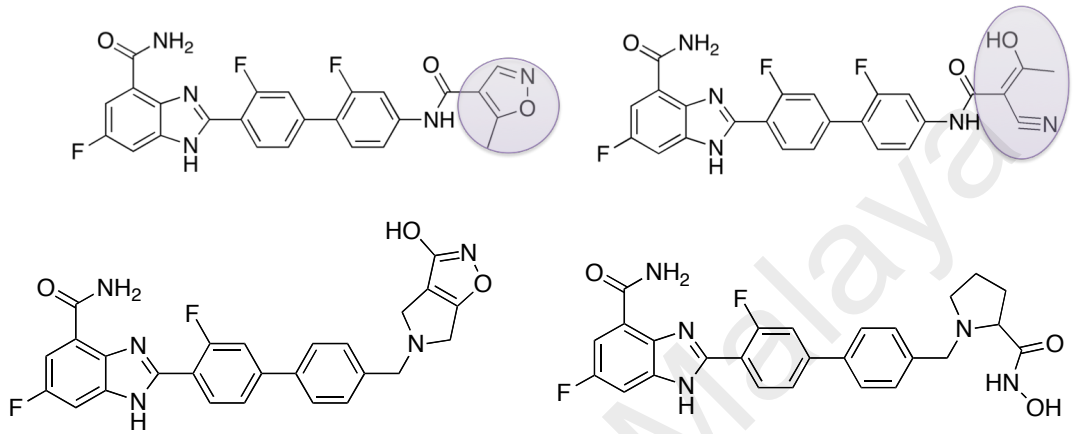

REFERENCES

Albericio, F. (2004). Developments in peptide and amide synthesis. *Current Opinion in Chemical Biology, 8*(3), 211-221.

Allison, A. C. (2000). Immunosuppressive drugs: the first 50 years and a glance forward. *Immunopharmacology, 47*(2–3), 63-83.

Ame, J. C., Spenlehauer, C., & de Murcia, G. (2004). The PARP superfamily. *Bioessays, 26*(8), 882-893.

Ancheta, P. B., Dumilon, R. A., Venturina, V. M., Cerbito, W. A., Dobson, R. J., LeJambre, L. F., Villa, E. C., & Gray, G. D. (2004). Efficacy of benzimidazole anthelmintics in goats and sheep in the Philippines using a larval development assay. *Veterinary Parasitology, 120*(1–2), 107-121.

Antoniou, A. C., Pharoah, P. D. P., McMullan, G., Day, N. E., Stratton, M. R., Peto, J., Ponder, B. J., & Easton, D. F. (2002). A comprehensive model for familial breast cancer incorporating BRCA1, BRCA2 and other genes. *Br J Cancer, 86*(1), 76-83.

Baldwin, J., Michnoff, C. H., Malmquist, N. A., White, J., Roth, M. G., Rathod, P. K., & Phillips, M. A. (2005). High-throughput screening for potent and selective inhibitors of Plasmodium falciparum dihydroorotate dehydrogenase. *J Biol Chem, 280*(23), 21847-21853.

Baliharová, V., Skálová, L., Maas, R. F. M., De Vrieze, G., Bull, S., & Fink-Gremmels, J. (2003). The effects of benzimidazole anthelmintics on P4501A in rat hepatocytes and HepG2 cells. *Research in Veterinary Science, 75*(1), 61-69.

Banasik, M., & Ueda, K. (1994). Inhibitors and activators of ADP-ribosylation reactions. *Molecular and Cellular Biochemistry, 138*(1-2), 185-197.

Barkalow, J. H., Breting, J., Gaede, B. J., Haight, A. R., Henry, R., Kotecki, B., Mei, J., Pearl, K. B., Tedrow, J. S., & Viswanath, S. K. (2007). Process Development for ABT-472, a Benzimidazole PARP Inhibitor. *Organic Process Research & Development, 11*(4), 693-698.

Batt, D. G., Copeland, R. A., Dowling, R. L., Gardner, T. L., Jones, E. A., Orwat, M. J., Pinto, D. J., Pitts, W. J., Magolda, R. L., & Jaffee, B. D. (1995). Immunosuppressive structure-activity relationships of Brequinar and related cinchoninic acid derivatives. *Bioorg Med Chem Lett, 5*(14), 1549-1554.

Batt, D. G., Petraitis, J. J., Sherk, S. R., Copeland, R. A., Dowling, R. L., Taylor, T. L., Jones, E. A., Magolda, R. L., & Jaffee, B. D. (1998). Heteroatom- and carbon-linked biphenyl analogs of Brequinar as immunosuppressive agents. *Bioorg Med Chem Lett, 8*(13), 1745-1750.

Baumgartner, R., Walloschek, M., Kralik, M., Gotschlich, A., Tasler, S., Mies, J., & Leban, J. (2006). Dual binding mode of a novel series of DHODH inhibitors. *J Med Chem, 49*(4), 1239-1247.

Breedveld, F. C., & Dayer, J-M. (2000). Leflunomide: mode of action in the treatment of rheumatoid arthritis. *Annals of the Rheumatic Diseases, 59*(11), 841-849.

Campeau, P. M., Foulkes, W. D., & Tischkowitz, M. D. (2008). Hereditary breast cancer: new genetic developments, new therapeutic avenues. *Hum Genet, 124*(1), 31-42.

Carpino, L. A. (1993). 1-Hydroxy-7-azabenzotriazole. An efficient peptide coupling additive. *Journal of the American Chemical Society, 115*(10), 4397-4398.

Castro, E., Goh, C., Olmos, D., Saunders, E., Leongamornlert, D., Tymrakiewicz, M., Mahmud, N., Dadaev, T., Govindasami, K., Guy, M., Sawyer, E., Wilkinson, R., Ardern-Jones, A., Ellis, S., Frost, D., Peock, S., Evans, D. G., Tischkowitz, M., Cole, T., Davidson, Ro., Eccles, D., Brewer, C., Douglas, F., Porteous, M. E., Donaldson, A., Dorkins, H., Izatt, L., Cook, J., Hodgson, S., Kennedy, M. J., Side, L. E., Eason, J., Murray, A., Antoniou, A. C., Easton, D. F., Kote-Jarai, Z., & Eeles, R. (2013). Germline BRCA Mutations Are Associated With Higher Risk of Nodal Involvement, Distant Metastasis, and Poor Survival Outcomes in Prostate Cancer. *Journal of Clinical Oncology, 31*(14), 1748-1757.

Chambon, P., Weill, J. D., & Mandel, P. (1963). Nicotinamide mononucleotide activation of a new DNA-dependent polyadenylic acid synthesizing nuclear enzyme. *Biochemical and Biophysical Research Communications, 11*(1), 39-43.

Chen, Z.-Z., Zhang, J., Tang, D-Y., & Xu, Z-G. (2014). Synthesis of fused benzimidazole–quinoxalinones via UDC strategy and following the intermolecular nucleophilic substitution reaction. *Tetrahedron Letters, 55*(16), 2742-2744.

Chung, L. W. (1996). Commentary on tumor suppressor gene, distal to BRCA-1, in prostate cancer. *J Urol, 155*(2), 430-431.

Clark, J. B., Ferris, G. M., & Pinder, S. (1971). Inhibition of nuclear NAD nucleosidase and poly ADP-ribose polymerase activity from rat liver by nicotinamide and 5'-methyl nicotinamide. *Biochim Biophys Acta, 238*(1), 82-85.

Cosi, C. (2002). New inhibitors of poly(ADP-ribose) polymerase and their potential therapeutic targets. *Expert Opinion on Therapeutic Patents, 12*(7), 1047-1071.

Costantino, G., Macchiarulo, A., Camaioni, E., & Pellicciari, R. (2001). Modeling of poly(ADP-ribose)polymerase (PARP) inhibitors. Docking of ligands and quantitative structure-activity relationship analysis. *J Med Chem, 44*(23), 3786-3794.

Cowen, D., Bedingfield, P., McConkey, G. A., Fishwick, C. W., & Johnson, A. P. (2010). A study of the effects of substituents on the selectivity of the binding of N-arylaminomethylene malonate inhibitors to DHODH. *Bioorg Med Chem Lett, 20*(3), 1284-1287.

Curtin, N. J., & Szabo, C. (2013). Therapeutic applications of PARP inhibitors: anticancer therapy and beyond. *Mol Aspects Med, 34*(6), 1217-1256.

Das, P., Deng, X., Zhang, L., Roth, M. G., Fontoura, B. M. A., Phillips, M. A., & De Brabander, J. K. (2013). SAR-Based Optimization of a 4-Quinoline Carboxylic Acid Analogue with Potent Antiviral Activity. *ACS Medicinal Chemistry Letters, 4*(6), 517-521.

Davies, M., Heikkila, T., McConkey, G. A., Fishwick, C. W., Parsons, M. R., & Johnson, A. P. (2009). Structure-based design, synthesis, and characterization of inhibitors of human and Plasmodium falciparum dihydroorotate dehydrogenases. *J Med Chem, 52*(9), 2683-2693.

Donawho, C. K., Luo, Y., Luo, Y., Penning, T. D., Bauch, J. L., Bouska, J. J., Bontcheva-Diaz, V. D., Cox, B. F., DeWeese, T. L., Dillehay, L. E., Ferguson, D. C., Ghoreishi-Haack, N. S., Grimm, D. R., Guan, R., Han, E. K., Holley-Shanks, R. R., Hristov, B., Idler, K. B., Jarvis, K., Johnson, E. F., Kleinberg, L. R., Klinghofer, V., Lasko, L. M., Liu, X., Marsh, K. C., McGonigal, T. P., Meulbroek, J. A., Olson, A. M., Palma, J. P., Rodriguez, L. E., Shi, Y., Stavropoulos, J. A., Tsurutani, A. C., Zhu, G. D., Rosenberg, S. H., Giranda, V. L., & Frost, D. J. (2007). ABT-888, an orally active poly(ADP-ribose) polymerase inhibitor that potentiates DNA-damaging agents in preclinical tumor models. *Clin Cancer Res, 13*(9), 2728-2737.

El-Khamisy, S. F., Masutani, M., Suzuki, H., & Caldecott, K. W. (2003). A requirement for PARP-1 for the assembly or stability of XRCC1 nuclear foci at sites of oxidative DNA damage. *Nucleic Acids Res, 31*(19), 5526-5533.

Erra, M., Moreno, I., Sanahuja, J., Andres, M., Reinoso, R. F., Lozoya, E., Pizcueta, P., Godessart, N., & Castro-Palomino, J. C. (2011). Biaryl analogues of teriflunomide as potent DHODH inhibitors. *Bioorg Med Chem Lett, 21*(24), 7268-7272.

Evans, D. R., & Guy, H. I. (2004). Mammalian Pyrimidine Biosynthesis: Fresh Insights into an Ancient Pathway. *Journal of Biological Chemistry, 279*(32), 33035-33038.

Ferraris, D., Ficco, R. P., Dain, D., Ginski, M., Lautar, S., Lee-Wisdom, K., Liang, S., Lin, Q., Lu, M. X. C., Morgan, L., Thomas, B., Williams, L. R., Zhang, J., Zhou, Y., & Kalish, V. J. (2003). Design and synthesis of poly(ADP-ribose) polymerase-1 (PARP-1) inhibitors. part 4: Biological evaluation of imidazobenzodiazepines as potent PARP-1 inhibitors for treatment of ischemic injuries. *Bioorganic & Medicinal Chemistry, 11*(17), 3695-3707.

Ferraris, D. V. (2010). Evolution of Poly(ADP-ribose) Polymerase-1 (PARP-1) Inhibitors. From Concept to Clinic. *J Med Chem, 53*(12), 4561-4584.

Försti, A., Luo, L., Vorechovsky, I., Söderberg, M., Lichtenstein, P., & Hemminki, K. (2001). Allelic imbalance on chromosomes 13 and 17 and mutation analysis of BRCA1 and BRCA2 genes in monozygotic twins concordant for breast cancer. *Carcinogenesis, 22*(1), 27-33.

Fraser, M., Berlin, A., Ouellet, V., Saad, F., & Bristow, R. G. (2014). Prostate Cancer Genomics as a Driver of Personalized Medicine. 233-245.

Fritzson, I., Svensson, B., Al-Karadaghi, S., Walse, B., Wellmar, U., Nilsson, U. J., da Graca Thrige, D., & Jonsson, S. (2010). Inhibition of human DHODH by 4-hydroxycoumarins, fenamic acids, and N-(alkylcarbonyl)anthranilic acids identified by structure-guided fragment selection. *ChemMedChem, 5*(4), 608-617.

Gaba, M., Singh, S., & Mohan, C. (2014). Benzimidazole: An emerging scaffold for analgesic and anti-inflammatory agents. *Eur J Med Chem, 76*, 494-505.

Gagne, J. P., Rouleau, M., & Poirier, G. G. (2012). Structural biology. PARP-1 activation--bringing the pieces together. *Science, 336*(6082), 678-679.

Gamble, A. B., Garner, J., Gordon, C. P., O'Conner, S. M. J., & Keller, P. A. (2007). Aryl Nitro Reduction with Iron Powder or Stannous Chloride under Ultrasonic Irradiation. *Synthetic Communications, 37*(16), 2777-2786.

Gandhi, V. B., Luo, Y., Liu, X., Shi, Y., Klinghofer, V., Johnson, E. F., Park, C., Giranda, V. L., Penning, T. D., & Zhu, G. D. (2010). Discovery and SAR of substituted 3-oxoisoindoline-4-carboxamides as potent inhibitors of poly(ADP-ribose) polymerase (PARP) for the treatment of cancer. *Bioorg Med Chem Lett, 20*(3), 1023-1026.

Giannini, G., Battistuzzi, G., Vesci, L., Milazzo, F. M., De Paolis, F., Barbarino, M., Guglielmi, M. B., Carollo, V., Gallo, G., Artali, R., & Dallavalle, S. (2014). Novel PARP-1 inhibitors based on a 2-propanoyl-3H-quinazolin-4-one scaffold. *Bioorg Med Chem Lett, 24*(2), 462-466.

Glendenning, J., & Tutt, A. (2011). PARP inhibitors – current status and the walk towards early breast cancer. *The Breast, 20*, S12-S19.

Gong, Y., Somersan Karakaya, S., Guo, X., Zheng, P., Gold, B., Ma, Y., Little, D., Roberts, J., Warrier, T., Jiang, X., Pingle, M., Nathan, C. F., & Liu, G. (2014). Benzimidazole-based compounds kill Mycobacterium tuberculosis. *Eur J Med Chem, 75*, 336-353.

Graziani, G., & Szabo, C. (2005). Clinical perspectives of PARP inhibitors. *Pharmacol Res, 52*(1), 109-118.

Griffin, R. J., Curtin, N. J., Newell, D. R., Golding, B. T., Durkacz, B. W., & Calvert, A. H. (1995). The role of inhibitors of poly(ADP-ribose) polymerase as resistance-modifying agents in cancer therapy. *Biochimie, 77*(6), 408-422.

Gruver, J. M., West, S. P., Collum, D. B., & Sarpong, R. (2010). Experimental Characterization and Computational Study of Unique C,N-Chelated Lithium Dianions. *Journal of the American Chemical Society, 132*(38), 13212-13213.

H. Boubaker, B. S., Boudyach, E.H., & Ait Benaoumar, A., (2008). Resistance of Verticillium theobromae to Benzimidazole Fungicides in Morocco. *Journal of Applied Sciences, 8*(21), 3903-3909.

Hall, J. M., Lee, M. K., Newman, B., Morrow, J. E., Anderson, L. A., Huey, B., & King, M. C. (1990). Linkage of early-onset familial breast cancer to chromosome 17q21. *Science, 250*(4988), 1684-1689.

Han, S-Y., & Kim, Y-A. (2004). Recent development of peptide coupling reagents in organic synthesis. *Tetrahedron, 60*(11), 2447-2467.

Hanan, E. J., Chan, B. K., Estrada, A. A., Shore, D. G., & Lyssikatos, J. P. (2010). Mild and General One-Pot Reduction and Cyclization of Aromatic and Heteroaromatic 2-Nitroamines to Bicyclic 2H-Imidazoles. *Synlett, 2010*(18), 2759-2764.

Hansen, M., Le Nours, J., Johansson, E., Antal, T., Ullrich, A., Loffler, M., & Larsen, S. (2004). Inhibitor binding in a class 2 dihydroorotate dehydrogenase causes variations in the membrane-associated N-terminal domain. *Protein Sci, 13*(4), 1031-1042.

Hartwig, J. F. (2011). Borylation and Silylation of C–H Bonds: A Platform for Diverse C–H Bond Functionalizations. *Accounts of Chemical Research, 45*(6), 864-873.

Herrmann, M. L., Schleyerbach, R., & Kirschbaum, B. J. (2000). Leflunomide: an immunomodulatory drug for the treatment of rheumatoid arthritis and other autoimmune diseases. *Immunopharmacology, 47*(2-3), 273-289.

Hobrecker, F. (1872). Ueber Reductionsprodukte der Nitracetamidverbindungen. *Berichte der deutschen chemischen Gesellschaft, 5*(2), 920-924.

Hurt, D. E., Sutton, A. E., & Clardy, J. (2006). Brequinar derivatives and species-specific drug design for dihydroorotate dehydrogenase. *Bioorg Med Chem Lett, 16*(6), 1610-1615.

Ingle, R. G., & Magar, D. D. (2011). Heterocyclic Chemistry Of Benzimidazoles And Potential Activities Of Derivatives. *Int. J. Drug Res. Tech., 1*(1), 26-32.

Ishida, J., Yamamoto, H., Kido, Y., Kamijo, K., Murano, K., Miyake, H., Ohkubo, M., Kinoshita, T., Warizaya, M., Iwashita, A., Mihara, K., Matsuoka, N., & Hattori, K. (2006). Discovery of potent and selective PARP-1 and PARP-2 inhibitors: SBDD analysis via a combination of X-ray structural study and homology modeling. *Bioorg Med Chem, 14*(5), 1378-1390.

Iwashita, A., Hattori, K., Yamamoto, H., Ishida, J., Kido, Y., Kamijo, K., Murano, K., Miyake, H., Kinoshita, T., Warizaya, M., Ohkubo, M., Matsuoka, N., & Mutoh, S. (2005). Discovery of quinazolinone and quinoxaline derivatives as potent and selective poly(ADP-ribose) polymerase-1/2 inhibitors. *FEBS Letters, 579*(6), 1389-1393.

Jagtap, P., & Szabo, C. (2005). Poly(ADP-ribose) polymerase and the therapeutic effects of its inhibitors. *Nature Reviews Drug Discovery, 4*(5), 421-440.

Judson Md, P. L., & Van Le Md, L. (1998). Familial Breast and Ovarian Cancer: The Role of The BRCA Genes. *Primary Care Update for OB/GYNS, 5*(3), 140-143.

Kalgutkar, A. S., Crews, B. C., Saleh, S., Prudhomme, D., & Marnett, L. J. (2005). Indolyl esters and amides related to indomethacin are selective COX-2 inhibitors. *Bioorg Med Chem, 13*(24), 6810-6822.

Kim, M. Y., Zhang, T., & Kraus, W. L. (2005). Poly(ADP-ribosyl)ation by PARP-1: 'PAR-laying' NAD+ into a nuclear signal. *Genes Dev, 19*(17), 1951-1967.

Kim, T., Na, H-S., & Löffler, M. (2003). Synthesis of β-hydroxy-propenamide derivatives and the inhibition of human dihydroorotate dehydrogenase. *Arch Pharm Res, 26*(3), 197-201.

Kim, Y., Kumar, M. R., Park, N., Heo, Y., & Lee, S. (2011). Copper-Catalyzed, One-Pot, Three-Component Synthesis of Benzimidazoles by Condensation and C–N Bond Formation. *J Org Chem, 76*(23), 9577-9583.

Kinoshita, T., Nakanishi, I., Warizaya, M., Iwashita, A., Kido, Y., Hattori, K., & Fujii, T. (2004). Inhibitor-induced structural change of the active site of human poly(ADP-ribose) polymerase. *FEBS Letters, 556*(1–3), 43-46.

Kroemer, J., Kirkpatrick, C., Maricle, B., Gawrych, R., Mosher, M. D., & Kaufman, D. (2006). Rieke zinc as a reducing agent for common organic functional groups. *Tetrahedron Letters, 47*(36), 6339-6341.

Langelier, M. F., & Pascal, J. M. (2013). PARP-1 mechanism for coupling DNA damage detection to poly(ADP-ribose) synthesis. *Curr Opin Struct Biol, 23*(1), 134-143.

Leban, J., Kralik, M., Mies, J., Baumgartner, R., Gassen, M., & Tasler, S. (2006). Biphenyl-4-ylcarbamoyl thiophene carboxylic acids as potent DHODH inhibitors. *Bioorg Med Chem Lett, 16*(2), 267-270.

Leban, J., Kralik, M., Mies, J., Gassen, M., Tentschert, K., & Baumgartner, R. (2005). SAR, species specificity, and cellular activity of cyclopentene dicarboxylic acid amides as DHODH inhibitors. *Bioorg Med Chem Lett, 15*(21), 4854-4857.

Leban, J., Saeb, W., Garcia, G., Baumgartner, R., & Kramer, B. (2004). Discovery of a novel series of DHODH inhibitors by a docking procedure and QSAR refinement. *Bioorg Med Chem Lett, 14*(1), 55-58.

Levy-Lahad, E., & Friedman, E. (2007). Cancer risks among BRCA1 and BRCA2 mutation carriers. *Br J Cancer, 96*(1), 11-15.

Liu, J. F., Konstantinopoulos, P. A., & Matulonis, U. A. (2014). PARP inhibitors in ovarian cancer: Current status and future promise. *Gynecol Oncol*.

Liu, S., Neidhardt, E. A., Grossman, T. H., Ocain, T., & Clardy, J. (2000). Structures of human dihydroorotate dehydrogenase in complex with antiproliferative agents. *Structure, 8*(1), 25-33.

Lolli, M. L., Giorgis, M., Tosco, P., Foti, A., Fruttero, R., & Gasco, A. (2012). New inhibitors of dihydroorotate dehydrogenase (DHODH) based on the 4-hydroxy-1,2,5-oxadiazol-3-yl (hydroxyfurazanyl) scaffold. *Eur J Med Chem, 49*, 102-109.

Lord, A., Mahon, F. M., & Threadgill, M. D. (2009). Design, Synthesis, and Evaluation in Vitro of Quinoline-8-carboxamides, a New Class of Poly(adenosine-diphosphate-ribose)polymerase-1 (PARP-1) Inhibitor. *J Med Chem, 52*(3), 868-877.

Ma, Z., Yoshimura, M. A., & Michailides, T. J. (2003). Identification and Characterization of Benzimidazole Resistance in Monilinia fructicola from Stone Fruit Orchards in California. *Appl Environ Microbiol, 69*(12), 7145-7152.

Malandrakis, A., Markoglou, A., & Ziogas, B. (2011). Molecular characterization of benzimidazole-resistant B. cinerea field isolates with reduced or enhanced sensitivity to zoxamide and diethofencarb. *Pesticide Biochemistry and Physiology, 99*(1), 118-124.

McLean, L. R., Zhang, Y., Degnen, W., Peppard, J., Cabel, D., Zou, C., Tsay, J. T., Subramaniam, A., Vaz, R. J., & Li, Y. (2010). Discovery of novel inhibitors for DHODH via virtual screening and X-ray crystallographic structures. *Bioorg Med Chem Lett, 20*(6), 1981-1984.

Miki, Y., Swensen, J., Shattuck-Eidens, D., Futreal, P., Harshman, K., Tavtigian, S., Liu, Q., Cochran, C., Bennett, LM., Ding, W., & Skolnick M. H. (1994). A strong candidate for the breast and ovarian cancer susceptibility gene BRCA1. *Science, 266*(5182), 66-71.

Miyashiro, J., Woods, K. W., Park, C. H., Liu, X., Shi, Y., Johnson, E. F., Bouska, J. J., Olson, A. M., Luo, Y., Fry, E. H., Giranda, V. L., & Penning, T. D. (2009). Synthesis and SAR of novel tricyclic quinoxalinone inhibitors of poly(ADP-ribose)polymerase-1 (PARP-1). *Bioorg Med Chem Lett, 19*(15), 4050-4054.

Miyaura, N., & Suzuki, A. (1979). Stereoselective synthesis of arylated (E)-alkenes by the reaction of alk-1-enylboranes with aryl halides in the presence of palladium catalyst. *Journal of the Chemical Society, Chemical Communications*(19), 866-867.

Miyaura, N., & Suzuki, A. (1995). Palladium-Catalyzed Cross-Coupling Reactions of Organoboron Compounds. *Chemical Reviews, 95*(7), 2457-2483.

Miyaura, N., Yamada, K., & Suzuki, A. (1979). A new stereospecific cross-coupling by the palladium-catalyzed reaction of 1-alkenylboranes with 1-alkenyl or 1-alkynyl halides. *Tetrahedron Letters, 20*(36), 3437-3440.

Montalbetti, C. A. G. N., & Falque, V. (2005). Amide bond formation and peptide coupling. *Tetrahedron, 61*(46), 10827-10852.

Morales, J., Li, L., Fattah, F. J., Dong, Y., Bey, E. A., Patel, M., Gao, J., & Boothman, D. A. (2014). Review of poly (ADP-ribose) polymerase (PARP) mechanisms of action and rationale for targeting in cancer and other diseases. *Crit Rev Eukaryot Gene Expr, 24*(1), 15-28.

Munier-Lehmann, H., Vidalain, P.-O., Tangy, F., & Janin, Y. L. (2013). On Dihydroorotate Dehydrogenases and Their Inhibitors and Uses. *J Med Chem, 56*(8), 3148-3167

Murai, J., Huang, S. Y., Das, B. B., Renaud, A., Zhang, Y., Doroshow, J. H., Ji, J., Takeda, S., & Pommier, Y. (2012). Trapping of PARP1 and PARP2 by Clinical PARP Inhibitors. *Cancer Res, 72*(21), 5588-5599.

Nakajima, N., & Ikada, Y. (1995). Mechanism of Amide Formation by Carbodiimide for Bioconjugation in Aqueous Media. *Bioconjugate Chemistry, 6*(1), 123-130.

Nannapaneni, D., Gupta, A. V., Reddy, M., & Sarva, R. (2010). Synthesis, characterization, and biological evaluation of benzimidazole derivatives as potential anxiolytics. *J Young Pharm, 2*(3), 273-279.

Ng, S. B., Buckingham, K. J., Lee, C., Bigham, A. W., Tabor, H. K., Dent, K. M., Huff, C. D., Shannon, P. T., Jabs, E. W., Nickerson, D. A., Shendure, J., & Bamshad, M. J. (2010). Exome sequencing identifies the cause of a mendelian disorder. *Nat Genet, 42*(1), 30-35.

Nguyen, T. B., Ermolenko, L., Dean, W. A., & Al-Mourabit, A. (2012). Benzazoles from Aliphatic Amines and o-Amino/Mercaptan/Hydroxyanilines: Elemental Sulfur as a Highly Efficient and Traceless Oxidizing Agent. *Organic Letters, 14*(23), 5948-5951.

Palma, J. P., Rodriguez, L. E., Bontcheva-Diaz, V. D., Bouska, J. J., Bukofzer, G., Colon-Lopez, M., Guan, R., Jarvis, K., Johnson, E. F., Klinghofer, V., Liu, X., Olson, A., Saltarelli, M. J., Shi, Y., Stavropoulos, J. A., Zhu, G. D., Penning, T. D., Luo, Y., Giranda, V. L., Rosenberg, S. H., Frost, D. J., & Donawho, C. K. (2008). The PARP inhibitor, ABT-888 potentiates temozolomide: correlation with drug levels and reduction in PARP activity in vivo. *Anticancer Res, 28*(5a), 2625-2635.

Park, J., Feng, J., Li, Y., Hammarsten, O., Brazil, D. P., & Hemmings, B. A. (2009). DNA-dependent protein kinase-mediated phosphorylation of protein kinase B requires a specific recognition sequence in the C-terminal hydrophobic motif. *J Biol Chem, 284*(10), 6169-6174.

Passaperuma, K., Warner, E., Hill, K. A., Gunasekara, A., & Yaffe, M. J. (2010). Is mammographic breast density a breast cancer risk factor in women with BRCA mutations? *J Clin Oncol, 28*(23), 3779-3783.

Peng, G., Chun-Jen Lin, C., Mo, W., Dai, H., Park, Y.-Y., Kim, S. M., Peng, Y., Mo, Q., Siwko, S., Hu, R., Lee, J-S., Hennessy, B., Hanash, S., Mills, G. B., & Lin, S-Y. (2014). Genome-wide transcriptome profiling of homologous recombination DNA repair. *Nat Commun, 5*.

Peng, J., Ye, M., Zong, C., Hu, F., Feng, L., Wang, X., Wang, Y., & Chen, C. (2011). Copper-catalyzed intramolecular C-N bond formation: a straightforward synthesis of benzimidazole derivatives in water. *J Org Chem, 76*(2), 716-719.

Penning, T. D., Zhu, G. D., Gandhi, V. B., Gong, J., Liu, X., Shi, Y., Klinghofer, V., Johnson, E. F., Donawho, C. K., Frost, D. J., Bontcheva-Diaz, V., Bouska, J. J., Osterling, D. J., Olson, A. M., Marsh, K. C., Luo, Y., Giranda, V. L. (2009). Discovery of the Poly(ADP-ribose) polymerase (PARP) inhibitor 2-[(R)-2-methylpyrrolidin-2-yl]-1H-benzimidazole-4-carboxamide (ABT-888) for the treatment of cancer. *J Med Chem, 52*(2), 514-523.

Penning, T. D., Zhu, G. D., Gandhi, V. B., Gong, J., Thomas, S., Lubisch, W., Grandel, R., Wernet, W., Park, C. H., Fry, E. H., Liu, X., Shi, Y., Klinghofer, V., Johnson, E. F., Donawho, C. K., Frost, D. J., Bontcheva-Diaz, V., Bouska, J. J., Olson, A. M., Marsh, K. C., Luo, Y., Rosenberg, S. H., & Giranda, V. L. (2008). Discovery and SAR of 2-(1-propylpiperidin-4-yl)-1H-benzimidazole-4-carboxamide: A potent inhibitor of poly(ADP-ribose) polymerase (PARP) for the treatment of cancer. *Bioorg Med Chem, 16*(14), 6965-6975.

Penning, T. D., Zhu, G. D., Gong, J., Thomas, S., Gandhi, V. B., Liu, X., Shi, Y., Klinghofer, V., Johnson, E. F., Park, C. H., Fry, E. H., Donawho, C. K., Frost, D. J., Buchanan, F. G., Bukofzer, G. T., Rodriguez, L. E., Bontcheva-Diaz, V., Bouska, J. J., Osterling, D. J., Olson, A. M., Marsh, K. C., Luo, Y., & Giranda, V. L. (2010). Optimization of phenyl-substituted benzimidazole carboxamide poly(ADP-ribose) polymerase inhibitors: identification of (S)-2-(2-fluoro-4-(pyrrolidin-2-yl)phenyl)-1H-benzimidazole-4-carboxamide (A-966492), a highly potent and efficacious inhibitor. *J Med Chem, 53*(8), 3142-3153.

Powell, C., Mikropoulos, C., Kaye, S. B., Nutting, C. M., Bhide, S. A., Newbold, K., & Harrington, K. J. (2010). Pre-clinical and clinical evaluation of PARP inhibitors as tumour-specific radiosensitisers. *Cancer Treat Rev, 36*(7), 566-575.

Purnell, M. R., & Whish, W. J. (1980). Novel inhibitors of poly(ADP-ribose) synthetase. *Biochem J, 185*(3), 775-777.

Ramanpreet, W., Hedaitullah, M., Syeda, F. N., & Khalid, I. (2011). Benzimidazole Derivatives - An Overview. *IJRPC, 1*(3), 565-574

Refaat, H. M. (2010). Synthesis and anticancer activity of some novel 2-substituted benzimidazole derivatives. *Eur J Med Chem, 45*(7), 2949-2956.

Rehman, F. L., Lord, C. J., & Ashworth, A. (2010). Synthetic lethal approaches to breast cancer therapy. *Nat Rev Clin Oncol, 7*(12), 718-724.

Romero-Castro, A., Leon-Rivera, I., Avila-Rojas, L. C., Navarrete-Vazquez, G., & Nieto-Rodriguez, A. (2011). Synthesis and preliminary evaluation of selected 2-aryl-5(6)-nitro- 1H-benzimidazole derivatives as potential anticancer agents. *Arch Pharm Res, 34*(2), 181-189.

Scarpelli, R., Boueres, J. K., Cerretani, M., Ferrigno, F., Ontoria, J. M., Rowley, M., Schultz-Fademrecht, C., Toniatti, C., & Jones, P. (2010). Synthesis and biological evaluation of substituted 2-phenyl-2H-indazole-7-carboxamides as potent poly(ADP-ribose) polymerase (PARP) inhibitors. *Bioorg Med Chem Lett, 20*(2), 488-492.

Schreiber, V., Dantzer, F., Ame, J.-C., & de Murcia, G. (2006). Poly(ADP-ribose): novel functions for an old molecule. *Nat Rev Mol Cell Biol, 7*(7), 517-528.

Seenaiah, D., Reddy, P. R., Reddy, G. M., Padmaja, A., Padmavathi, V., & Siva Krishna, N. (2014). Synthesis, antimicrobial and cytotoxic activities of pyrimidinyl benzoxazole, benzothiazole and benzimidazole. *Eur J Med Chem, 77*, 1-7.

Sloots, K., Ausems, M. G., & de Haan, H. H. (2002). Ovarian cancer in BRCA-positive women: vigilance is mandatory despite screening programs. *Eur J Obstet Gynecol Reprod Biol, 101*(2), 196-198.

Sodhi, R. K., Singh, N., & Jaggi, A. S. (2010). Poly(ADP-ribose) polymerase-1 (PARP-1) and its therapeutic implications. *Vascul Pharmacol, 53*(3-4), 77-87.

Steffen, J. D., Brody, J. R., Armen, R. S., & Pascal, J. M. (2013). Structural implications for selective targeting of PARPs. *Front Oncol, 3*.

Suzuki, A. (1999). Recent advances in the cross-coupling reactions of organoboron derivatives with organic electrophiles, 1995–1998. *Journal of Organometallic Chemistry, 576*(1–2), 147-168.

Suzuki, A. (2002). Cross-coupling reactions via organoboranes. *Journal of Organometallic Chemistry, 653*(1–2), 83-90.

Thunuguntla, S. S. R., Subramanya, H., Kunnam, S. R., Sanivaru, V. S. R., Bingi, C., Kusanur, R., Schwarz, M., & Arlt, M. (2010). Dihydroorotate dehydrogenase inhibitors: Google Patents.

Tonelli, M., Simone, M., Tasso, B., Novelli, F., Boido, V., Sparatore, F., Paglietti, G., Pricl, S., Giliberti, G., Blois, S., Ibba, C., Sanna, G., Loddo, R., & La Colla, P. (2010). Antiviral activity of benzimidazole derivatives. II. Antiviral activity of 2-phenylbenzimidazole derivatives. *Bioorg Med Chem, 18*(8), 2937-2953.

Tong, Y., Bouska, J. J., Ellis, P. A., Johnson, E. F., Leverson, J., Liu, X., Marcotte, P. A., Olson, A. M., Osterling, D. J., Przytulinska, M., Rodriguez, L. E., Shi, Y., Soni, N., Stavropoulos, J., Thomas, S., Donawho, C. K., Frost, D. J., Luo, Y., Giranda, V. L., & Penning, T. D. (2009). Synthesis and evaluation of a new generation of orally efficacious benzimidazole-based poly(ADP-ribose) polymerase-1 (PARP-1) inhibitors as anticancer agents. *J Med Chem, 52*(21), 6803-6813.

Valeur, E., & Bradley, M. (2009). Amide bond formation: beyond the myth of coupling reagents. *Chemical Society Reviews, 38*(2), 606-631.

Velez, J., Hail, N., Jr., Konopleva, M., Zeng, Z., Kojima, K., Samudio, I., & Andreeff, M. (2013). Mitochondrial uncoupling and the reprograming of intermediary metabolism in leukemia cells. *Front Oncol, 3*, 67.

Wang, W., & McMurray, J. S. (1999). A selective method for the preparation of primary amides: Synthesis of Fmoc-l-4-carboxamidophenylalanine and other compounds. *Tetrahedron Letters, 40*(13), 2501-2504.

Wang, X.-J., Yang, M.-L., Zhang, L.-P., Yao, T., Chen, C., Mao, L.-G., Wang, Y., & Wu, J. (2014). Design of novel bis-benzimidazole derivatives as DNA minor groove binding agents. *Chinese Chemical Letters, 25*(4), 589-592.

Weil, M. K., & Chen, A. P. (2011). PARP Inhibitor Treatment in Ovarian and Breast Cancer. *Curr Probl Cancer, 35*(1), 7-50.

Wesierska-Gadek, J., Zulehner, N., Ferk, F., Skladanowski, A., Komina, O., & Maurer, M. (2012). PARP inhibition potentiates the cytotoxic activity of C-1305, a selective inhibitor of topoisomerase II, in human BRCA1-positive breast cancer cells. *Biochem Pharmacol, 84*(10), 1318-1331.

White, A. W., Almassy, R., Calvert, A. H., Curtin, N. J., Griffin, R. J., Hostomsky, Z., Maegley, K., Newell, D. R., Srinivasan, S., & Golding, B. T. (2000). Resistance-modifying agents. 9. Synthesis and biological properties of benzimidazole inhibitors of the DNA repair enzyme poly(ADP-ribose) polymerase. *J Med Chem, 43*(22), 4084-4097.

White, A. W., Curtin, N. J., Eastman, B. W., Golding, B. T., Hostomsky, Z., Kyle, S., Li, J., Maegley, K. A., Skalitzky, D. J., Webber, S. E., Yu, X. H., & Griffin, R. J. (2004). Potentiation of cytotoxic drug activity in human tumour cell lines, by amine-substituted 2-arylbenzimidazole-4-carboxamide PARP-1 inhibitors. *Bioorg Med Chem Lett, 14*(10), 2433-2437.

Wooster, R., Bignell, G., Lancaster, J., Swift, S., Seal, S., Mangion, J., Collins, N., Gregory, S., Gumbs, C., Micklem, G., Barfoot, R., Hamoudi, R., Patel, S., Rices, C., Biggs, P., Hashim, Y., Smith, A., Connor, F., Arason, A., Gudmundsson, J., Ficenec, D., Kelsell, D., Ford, T. D. P., Timothy Bishop, D., Spurr, N. K., Ponder, B. A. J., Eeles, R., Peto, J., Devilee, P., Cornelisse, C., Lynch, H., Narod, S., Lenoir, G., Egilsson, V., Bjork Barkadottir, Rosa., Easton, D. F., Bentley, D. R., Futreal, P. A., Ashworth, A., & Stratton, M. R. (1995). Identification of the breast cancer susceptibility gene BRCA2. *Nature, 378*(6559), 789-792.

Wooster, R., Neuhausen, S., Mangion, J., Quirk, Y., Ford, D., Collins, N., Nguyen, K., Seal, S., Tran, T., Averil, D., Fields, P., Marshall, G., Narod, S., Lenoir, G. M., Lynch, H., Feunteun, J., Devilee, P., Cornelisse, C. J., Menko, F. H., Daly, P. A., Ormiston, W., McManus, R., Pye, C., Lewis, C. M., Cannon-Albright, L. A., Peto, J., Ponder, B. A. J., Skolnick, M. H., Easton, D. F., Goldgar, D. E., & Stratton, M. R. (1994). Localization of a breast cancer susceptibility gene, BRCA2, to chromosome 13q12-13. *Science, 265*(5181), 2088-2090.

Wright, J. B. (1951). The Chemistry of the Benzimidazoles. *Chemical Reviews, 48*(3), 397-541.

Wu, X.-F., Neumann, H., & Beller, M. (2010). Palladium-catalyzed carbonylative coupling of benzyl chlorides with aryl boronic acids in aqueous media. *Tetrahedron Letters, 51*(47), 6146-6149.

Xue, F., Luo, X., Ye, C., Ye, W., & Wang, Y. (2011). Inhibitory properties of 2-substituent-1H-benzimidazole-4-carboxamide derivatives against enteroviruses. *Bioorg Med Chem, 19*(8), 2641-2649.

Yang, Y., Li, B., Zhang, L., & Guan, Y. (2014). Triphenylamine based benzimidazole and benzothiazole: Synthesis and applications in fluorescent chemosensors and laser dyes. *Journal of Luminescence, 145*, 895-898.

Zameitat, E., Freymark, G., Dietz, C. D., Loffler, M., & Bolker, M. (2007). Functional expression of human dihydroorotate dehydrogenase (DHODH) in pyr4 mutants of ustilago maydis allows target validation of DHODH inhibitors in vivo. *Appl*

Environ Microbiol, 73(10), 3371-3379.

Zhu, G. D., Gandhi, V. B., Gong, J., Thomas, S., Luo, Y., Liu, X., Shi, Y.,Klinghofer, V., Johnson, E. F., Frost, D., Donawho, C., Jarvis, K., Bouska, J., Marsh, K. C., Rosenberg, S. H., Giranda, V. L., & Penning, T. D. (2008). Synthesis and SAR of novel, potent and orally bioavailable benzimidazole inhibitors of poly(ADP-ribose) polymerase (PARP) with a quaternary methylene-amino substituent. *Bioorg Med Chem Lett, 18*(14), 3955-3958.

Zhu, G. D., Gong, J., Gandhi, V., Penning, T., & Giranda, V. (2006). 2-(2-Methylpyrrolidin-2-yl)-1H-benzimidazole-4-carboxamide, aka veliparib, for example; poly(ADP-ribose)polymerase inhibitors; antiinflammatory, antitumor agents; Parkinson's disease: Google Patents.

Zhu, G. D., Gong, J., Gandhi, V. B., Liu, X., Shi, Y., Johnson, E. F., Donawho, C. K., Ellis, P. A., Bouska, J. J., Osterling, D. J., Olson, A. M., Park, C., Luo, Y., Shoemaker, A., Giranda, V. L., & Penning, T. D. (2012). Discovery and SAR of orally efficacious tetrahydropyridopyridazinone PARP inhibitors for the treatment of cancer. *Bioorg Med Chem, 20*(15), 4635-4645.

Zhu, Q., Wang, X., Chu, Z., He, G., Dong, G., & Xu, Y. (2013). Design, synthesis and biological evaluation of novel imidazo[4,5-c]pyridinecarboxamide derivatives as PARP-1 inhibitors. *Bioorg Med Chem Lett, 23*(7), 1993-1996.

LIST OF PUBLICATIONS

Tetrahedron Letters 51 (2010) 495–498

Contents lists available at ScienceDirect

Tetrahedron Letters

journal homepage: www.elsevier.com/locate/tetlet

An efficient synthesis of (±)-panduratin A and (±)-isopanduratin A, inhibitors of dengue-2 viral activity

Chin Fei Chee [a], Iskandar Abdullah [a], Michael J. C. Buckle [b], Noorsaadah Abd Rahman [a,*]

[a] Department of Chemistry, University of Malaya, 50603 Kuala Lumpur, Malaysia
[b] Department of Pharmacy, University of Malaya, 50603 Kuala Lumpur, Malaysia

ARTICLE INFO

Article history:
Received 3 September 2009
Revised 2 November 2009
Accepted 9 November 2009
Available online 12 November 2009

ABSTRACT

Panduratin A and its regioisomer isopanduratin A are synthesized in four steps from (*E*)-ocimene, [(*E*)-3,7-dimethyl-1,3,6-octatriene] via a Diels–Alder cycloaddition reaction.

Panduratin A and its regioisomer isopanduratin A are cyclohexenyl chalcone natural products that show a wide spectrum of biological activity.[1] It has recently been reported that panduratin A and hydroxypanduratin A (Fig. 1), isolated from *Boesenbergia rotunda* (L.) showed good inhibitory activities towards dengue-2 virus NS3 protease with K_i values of 25 and 21 μM, respectively.[2] While a number of syntheses of cyclohexenyl chalcones have been described,[3] surprisingly the synthesis of panduratin A has never been reported. Herein, we report an efficient method for the synthesis of (±)-panduratin A and (±)-isopanduratin A through Diels–Alder cyclization of 2′-hydroxy-4′-methoxy-6′-ethoxymethoxychalcone and (*E*)-ocimene.

Our studies began with model reactions between 2′,4′,6′-trihydroxychalcone **1** and 2,3-dimethyl-1,3-butadiene, carried out in various solvents as well as without solvent. Heating the two compounds for an extended period of time at 110 °C resulted in the formation of 5,7-dihydroxyflavanone (Table 1). The use of Lewis acid catalysts such as $BF_3{\cdot}Et_2O$, $AlCl_3$ and $ZnCl_2$, however, resulted in extensive polymerization of the diene.

The reaction was also carried out with 2′,4′,6′-trimethoxychalcone **2** (as the dienophile) and 2,3-dimethyl-1,3-butadiene. Initial reaction (Table 1, entry 5) performed at room temperature with 1 equiv of diene in dry toluene gave no product even after 30 h of stirring. Increasing the equivalence of diene also resulted in a similar observation. When the reactants were placed in a pressure tube and heated at 50 °C for 18 h, a small amount of the expected product was obtained (Table 1, entry 6). However, increasing the temperature to 120 °C and stirring overnight in a pressure tube resulted in the Diels–Alder adduct **5** being isolated in 93% yield (Table 1, entry 7).

Following the conditions described in Table 1, entry 7, compounds **4**, **6–8** and their regioisomers **4a**, **6a**, **7a** and **8a** were prepared in excellent yields and no polymerization of the diene (described as a complex mixture in Table 1) was observed. The products were isolated in a 3:2 *para*/*meta* ratio and the structure of the major product (the *para* isomer) for each reaction is given in Table 2.

The Diels–Alder reaction (Table 2, entry c) was first carried out under the same reaction conditions as those of entry 7 (Table 1) where excess ocimene was used and the reaction mixture was heated at 120 °C in a pressure tube. However, no Diels–Alder adduct was isolated even after the reaction was left for 24 h. The isolated product indicated polymerization of ocimene instead. The use of various Lewis acids to catalyze the reaction also resulted in polymerization of the acid-sensitive terminal conjugated double bond in ocimene.

Ocimene can exist in the *E*- or *Z*-configuration in nature (Scheme 1). When pure (*Z*)-ocimene was reacted with chalcone **2**, no Diels–Alder adduct was isolated. Instead, polymerization of the ocimene was observed. However, when a mixture of (*E*)- and

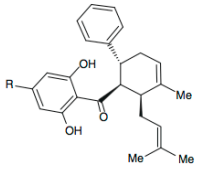

R = OMe : panduratin A
R = OH : hydroxypanduratin A

Figure 1. Panduratin A and hydroxypanduratin A.

* Corresponding author. Tel.: +60 3 79674643; fax: +60 3 79674193.
E-mail address: noorsaadah@um.edu.my (N.A. Rahman).

0040-4039/$ - see front matter © 2009 Elsevier Ltd. All rights reserved.
doi:10.1016/j.tetlet.2009.11.030

Table 1
Screening of the reaction conditions[a]

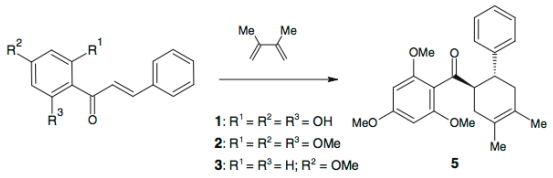

Entry	Dienophile	Temp (°C)	Time (h)	Catalyst (equiv)	Solvent	Product; yield[b] (%)
1	**1**	110	2	—	—	[c]
2	**1–3**	−78 (1 h)–rt	24	$ZnCl_2$ (1)	Et_2O	[d]
3	**1, 2**	0 (1 h)–rt	24	$AlCl_3$ (1)	Toluene	[d]
4	**1, 2**	0 (1 h)–rt	24	BF_3-Et_2O (1)	Et_2O	[d]
5	**2**	rt	30	—	Toluene	—
6	**2**	50	18	—	Toluene	**5** (30)[e]
7	**2**	120	24	—	—	**5** (93)[e]

[a] Reaction conditions: dienophile (1 mmol), N_2 atmosphere.
[b] Isolated yield.
[c] Formation of 5,7-dihydroflavanone.
[d] Complex mixture obtained but no adduct was formed.
[e] Reaction performed in a pressure tube.

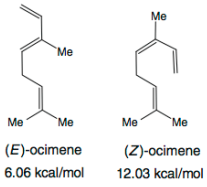

Scheme 1. *s-cis* Conformations of (*E*)-and (*Z*)-ocimene.

(*Z*)-ocimene was used in the Diels–Alder reaction with chalcone **2**, the adducts **6** and **6a** were isolated (Table 2).[4] Presumably, only (*E*)-ocimene underwent the Diels–Alder reaction. Examination of (*Z*)-ocimene indicated that the presence of a *Z*-prenyl substituent as part of the 1,3-butadiene moiety reduces its reactivity by hindering the approach of the dienophile. This limitation is not observed with (*E*)-ocimene. Molecular Mechanics calculations (MM+) revealed (*E*)-ocimene to be more stable than the *Z* isomer by about 6 kcal/mol. This observation could provide some rationale for our findings, where the reaction between trimethoxychalcone and a mixture of (*E*)- and (*Z*)-ocimene resulted in the formation of adducts **6** and **6a** while no product was observed when the reaction was conducted with (*Z*)-ocimene only.[5]

The synthesis of panduratin A and its regioisomer is illustrated in Scheme 2. Protection of the hydroxy group of commercially available 2′,6′-dihydroxy-4′-methoxyacetophenone **9** with 1-chloro-2-methoxyethane (MEM-Cl) followed by Claisen condensation with benzaldehyde in the presence of aqueous KOH in ethanol gave chalcone **10** in 85% yield. Reaction of chalcone **10** with 5 equiv of (*E*)-ocimene[4] at 150 °C led to the formation of a mixture of cycloadduct **11** and **11a** in quantitative yield. Deprotection of the MEM group gave panduratin A **12** and isopanduratin **12a** as a mixture in 89% yield.

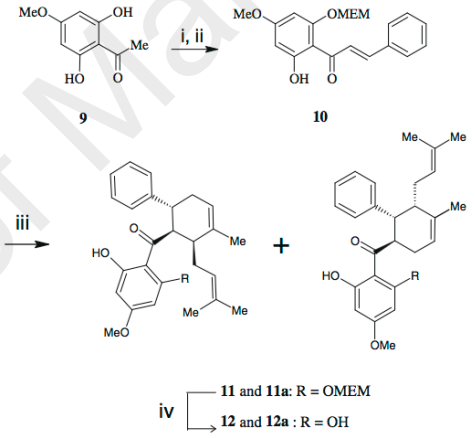

Scheme 2. Reagents and conditions: (i) MEM-Cl, dry acetone, K_2CO_3, rt, 8 h; (ii) benzaldehyde, 50% aq KOH, EtOH, 24 h, 85% over two steps; (iii) (*E*)-ocimene, 150 °C, pressure tube, 24 h; (iv) 3 M HCl, MeOH, 80 °C, 10 min, 89% over two steps.

In conclusion, we have reported a four-step synthesis of panduratin and isopanduratin A in 75% overall yield. Excellent yields are achieved for panduratin derivatives with various dienes. The syntheses involved a Diels–Alder reaction with a variety of dienes under moderate conditions (100–150 °C, neutral environment and no catalyst).

Table 2
Syntheses of panduratin A derivatives[a]

Entry	Dienophile; diene	Conditions	Product[b] (yield, %)
a	Dienophile = **2**; diene = 	120 °C, Pressure tube, 24 h	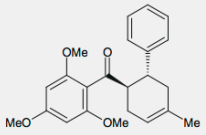 **4a** *para*/*meta*: 3:2 (86)
b	Dienophile = **2**; Diene = 	120 °C, Pressure tube, 18 h	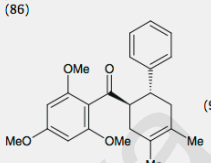 (93) **5**
c	Dienophile = **2**; Diene = 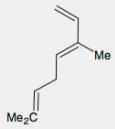 (*E*)-Ocimene	150 °C, Pressure tube, 15 h	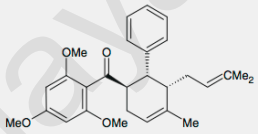 **6a** *para*/*meta*: 3:2 (99)
d	Dienophile = **3**; Diene = 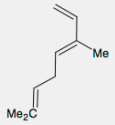 (*E*)-Ocimene	150 °C, Pressure tube, 14 h	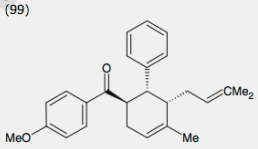 **7a** *para*/*meta*: 3:2 (96)
e	Dienophile = **2**; Diene = 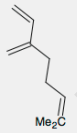 Myrcene	120 °C, Pressure tube, 24 h	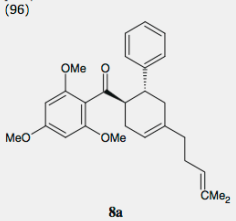 **8a** *para*/*meta*: 3:2 (89)

[a] All products were identified by ^{1}H, ^{13}C, DEPT, COSY, HMQC, HMBC and H2BC NMR spectroscopy.
[b] Isolated yields (mixture of regioisomers), based on chalcone.

Acknowledgements

This work was supported by grants from the Ministry of Science, Technology and Innovation (Science Fund) and the Ministry of Higher Education under the Fundamental Research Grant Scheme.

Supplementary data

Supplementary data (general procedures and spectral data of all new compounds) associated with this article can be found, in the online version, at doi:10.1016/j.tetlet.2009.11.030.

References and notes

1. Win, N. N.; Awale, S.; Esumi, H.; Tezuka, Y.; Kadota, S. *J. Nat. Prod.* **2007**, *70*, 1582–1587; Pandji, C.; Grimm, C.; Wray, V.; Witte, L.; Proksch, P. *Phytochemistry* **1993**, *34*, 415–419; Tuntiwachwuttikul, P.; Pancharoen, O.; Reutrakul, V.; Byrne, L. T. *Aust. J. Chem.* **1984**, *37*, 449–453; Morikawa, T.; Funakoshi, K.; Ninomiya, K.; Yasuda, D.; Miyagawa, K.; Matsuda, H.; Yoshikawa, M. *Chem. Pharm. Bull.* **2008**, *56*, 956–962; Gu, J. Q.; Park, E. J.; Vigo, J. S.; Graham, J. G.; Fong, H. H. S.; Pezzuto, J. M.; Kinghorn, A. D. *J. Nat. Prod.* **2002**, *65*, 1616–1620.
2. Tan, S. K.; Pippen, R.; Yusof, R.; Ibrahim, H.; Khalid, N.; Rahman, N. A. *Bioorg. Med. Chem. Lett.* **2006**, *16*, 3337–3340.
3. Cong, H.; Ledbetter, D.; Rowe, G. T.; Caradonna, J. P.; Porco, J. A., Jr. *J. Am. Chem. Soc.* **2008**, *130*, 9424–9425; Shibata, K.; Tatsukawa, A.; Umeoka, K.; Lee, H. S.; Ochi, M. *Tetrahedron* **2000**, *56*, 8821–8824; Jung, E. M.; Lee, Y. R. *Bull. Korean Chem. Soc.* **2008**, *29*, 1199–1204; Corbett, J. L.; Weavers, R. T. *Synth. Commun.* **2008**, *38*, 489–498.
4. Ocimene is sold by International Flavors and Fragrances as a mixture of *E* and *Z* isomers. For the total synthesis of (*E*)-ocimene from isoprene see Chou, T. S.; Tso, H. H.; Chang, L. J. *Chem. Commun.* **1984**, 1323–1324.
5. (*Z*)-Ocimene can be purchased from Sigma–Aldrich. (*E*)-Ocimene is thermally more stable than (*Z*)-ocimene. See Wolinsky, J.; Chollar, B.; Baird, M. D. *J. Am. Chem. Soc.* **1962**, *84*, 2775–2779.

European Journal of Medicinal Chemistry 84 (2014) 382–394

Contents lists available at ScienceDirect

European Journal of Medicinal Chemistry

journal homepage: http://www.elsevier.com/locate/ejmech

Original article

Discovery of azetidine based ene-amides as potent bacterial enoyl ACP reductase (FabI) inhibitors☆

Mohamed Takhi [a], Kandepu Sreenivas [a], Chandrashekar K. Reddy [a], Mahadari Munikumar [a], Kolakota Praveena [a], Pabolu Sudheer [a], Bandaru N.V.M. Rao [a], Gollamudi Ramakanth [a], Jampala Sivaranjani [a], Shardaprasad Mulik [a], Yeruva R. Reddy [a], Krishnamurthy Narasimha Rao [b], Rentala Pallavi [b], Anirudha Lakshminarasimhan [b], Sunil K. Panigrahi [b], Thomas Antony [b], Iskandar Abdullah [c], Yean K. Lee [c], Murali Ramachandra [b], Rohana Yusof [d], Noorsaadah A. Rahman [c], Hosahalli Subramanya [b, *]

[a] Aurigene Discovery Technologies Ltd, Bollaram Road, Miyapur, Hyderabad 500 049, India
[b] Aurigene Discovery Technologies Ltd, 39-40, KIADB Industrial Area, Phase II, Electronic City, Hosur Road, Bangalore 560 100, India
[c] Department of Chemistry, Faculty of Science, University of Malaya, 50603 Kuala Lumpur, Malaysia
[d] Department of Molecular Medicine, Faculty of Medicine, University of Malaya, 50603 Kuala Lumpur, Malaysia

ARTICLE INFO

Article history:
Received 31 January 2014
Received in revised form
9 July 2014
Accepted 10 July 2014
Available online 11 July 2014

Keywords:
FabI inhibitor
Enoyl ACP reductase
Antibacterial
Azetidine
Ene-amide

ABSTRACT

A novel and potent series of ene-amides featuring azetidines has been developed as FabI inhibitors active against drug resistant Gram-positive pathogens particularly staphylococcal organisms. Most of the compounds from the series possessed excellent biochemical inhibition of *Staphylococcus aureus* FabI enzyme and whole cell activity against clinically relevant MRSA, MSSA and MRSE organisms which are responsible for significant morbidity and mortality in community as well as hospital settings. The binding mode of one of the leads, **AEA16**, in *Escherichia coli* FabI enzyme was determined unambiguously using X-ray crystallography. The lead compounds displayed good metabolic stability in mice liver microsomes and pharmacokinetic profile in mice. The in vivo efficacy of lead **AEA16** has been demonstrated in a lethal murine systemic infection model.

1. Introduction

The emergence of bacterial resistance continues to hamper the effectiveness of existing antibacterial therapies and poses serious threat worldwide in community and nosocomial settings. Multidrug-resistant Gram-positive bacteria such as methicillin-resistant *Staphylococcus aureus* (MRSA), *Staphylococcus epidermidis* (MRSE) and vancomycin-resistant *S. aureus* (VRSA) are of major concern [1]. This challenge is further exacerbated by the reduced interest of major pharmaceutical companies in antibacterial drug discovery leading to paucity in new antibiotics pipeline [2]. Hence, there is a pressing need for increased and accelerated efforts to identify new therapeutics based on novel mechanism of action to combat bacterial resistance. In recent times, there has been a great deal of interest in targeting bacterial fatty acid biosynthesis (FAB) as a viable strategy to develop novel antibacterial agents.

The bacterial fatty acid synthase system (FASII) utilizes discrete monofunctional enzymes that operate in conjunction with acyl carrier protein (ACP)-associated substrates. In mammalian fatty acid synthase (FASI) pathway, lipid biosynthesis is mediated by a single multifunctional enzyme-ACP complex. The differences in prokaryote and eukaryote fatty acid biosynthesis provide an opportunity for selective FASII inhibition [3,4]. The inhibition of FASII pathway causes the breakdown of cell wall and disruption of cell membrane demonstrating its importance for bacterial survival [5].

FabI is an enoyl-ACP reductase that catalyses the ultimate and rate limiting step of chain elongation in each cycle in FASII pathway. The reaction involves the conjugate reduction of an enoyl-ACP to the corresponding acyl-ACP using the cofactor NADH or NADPH as a hydride source as shown in Scheme 1 [3–6]. FabI is an essential

☆ Aurigene Publication No H-05-0201-2012.
* Corresponding author.
E-mail address: hosahalli_s@aurigene.com (H. Subramanya).

http://dx.doi.org/10.1016/j.ejmech.2014.07.036
0223-5234/

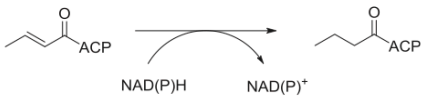

Scheme 1. FabI biosynthetic reaction.

enzyme for the viability of several bacteria and shows low degree of sequence homology with mammalian enzymes [3]. Several isoforms (FabI, FabK, FabL and FabV) of enoyl-ACP reductases (FabI isozymes) have been reported in literature [3,7,8]. Different bacteria have been reported to have one or more of these isoforms. For example, single isoform, FabI is found in *S. aureus* and *Escherichia coli*, and FabK is present in *Staphylococcus pneumoniae*. However, two isoforms FabI and FabV are present in *Pseudomonas aeruginosa* and FabI and FabL are present in *Bacillus subtilis*. These isoforms of enoyl ACP-reductases have high sequence and structural similarities. However, there are differences in the active site of these enzymes. Therefore, development of inhibitors that act on all the isoforms leading to broad spectrum activity could be challenging.

The novel mechanism of action with a potential for activity against drug resistant staphylococcal bacteria has led to the discovery of several FabI inhibitors based on different chemotypes. These include indole naphthyridinones [9], 2,34,5-tetrahydro-1H-pyrido[2,4-b and e] [1,4] diazepines [10], spiro-naphthyridinone piperidines [11], 1,2,3,4-tetrahydropyrido-indoles [12], 4-pyridones [13,14], biphenyl ethers [15] and aminopyridines [16]. Representative FabI inhibitors are shown in Fig. 1. **AFN-1252** [17], **MUT-056399** (FAB-001) [18] and **CG-400549** [19] have advanced to clinical trials for the treatment of Gram-positive bacterial infections caused by MSSA, MRSA and MRSE pathogens. Triclosan, a widely used biocide in a variety of consumer products, is known to act via FabI inhibition [20].

In pursuit of our antibacterial drug discovery programs [21,22], we were interested in developing novel and potent FabI inhibitors for the treatment of drug resistant staphylococcal infections. The efforts in this direction led to the development of a novel series of FabI inhibitors featuring azetidine ene-amides (AEAs) showing excellent in vitro and in vivo profile. This paper outlines the design, synthesis, SAR, metabolic stability, in vivo pharmacokinetic profile and in vivo antibacterial activity of a series of azetidine ene-amides (AEAs).

2. Results and discussion

2.1. Initial design of FabI inhibitors

We used structure-guided approach based on X-ray structure of **AFN-1252** bound to *E. coli* FabI determined in-house [23]. Critical interactions observed between **AFN-1252** and *E. coli* FabI are shown in Fig. 2. The pyridine nitrogen and amidic NH makes two H-bonds with residue Ala-95 while the carbonyl oxygen in the ene-amide moiety is engaged in H-bond interaction with NADH and side chain of Tyr-156 residue. The benzofuran ring occupies a hydrophobic pocket formed by the residues Tyr-146, Met-159 and Phe-203 and makes a favourable π-stacking interaction with residue Tyr-146. The methyl substitution on benzofuran moiety at 3-position further enhances this stacking interaction.

The crystal structure of **AFN-1252** bound to *E. coli* FabI revealed that ample space is available around the ene-amidic nitrogen for the design of novel FabI inhibitors. Keeping these observations in view, we designed novel FabI inhibitors by introducing azetidine ring which is capable of producing conformationally rigid amides that are relatively resistant to enzymatic hydrolysis compared to

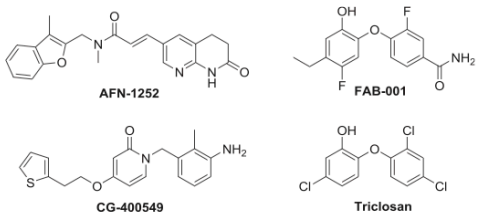

Fig. 1. FabI inhibitors.

open chain amides (Fig. 3) [24,25]. We envisaged that such modification could engender compounds with good metabolic stability and pharmacokinetic profile while retaining the potency. Indeed, the initial compounds **AEA2** and **AEA3** did show *S. aureus* FabI enzyme inhibition when tested at 1 μM concentration as shown in Fig. 3.

2.2. Design, synthesis and SAR of substituted azetidine ene amides (AEAs) with naphthyridinon-one on right hand side

Encouraged by the biochemical data of initial compounds **AEA2** and **AEA3** we set out to investigate further the effect of azetidines on SAR paradigm of ene-amide scaffold through iterative medicinal chemistry approach. We initiated our efforts by varying different substitutions on azetidine moiety on the left hand side (LHS) followed by the modification of cyclic amide ring on right hand side (RHS) as shown in Fig. 3.

The first iteration of SAR was focussed on the left hand side, exploring the hydrophobic pocket in the FabI active site. Accordingly, several analogues with structurally diverse and lipophilic substitutions at the 3-position of azetidine as exemplified by azetidine ene-amides **AEA4-21** were designed and synthesized. We hypothesized that these LHS substitutions on azetidine could optimize interactions in the hydrophobic pocket and thereby enhance biochemical and in vitro antibacterial activity.

The synthesis of azetidine ene-amides **AEA1-12** is delineated in Scheme 2. The key carboxylic acid intermediate **1** has been conveniently prepared according to the literature procedure [9]. The compound **AEA1** [25] was made by coupling acid **1** and

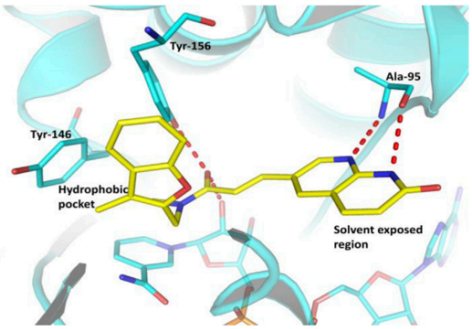

Fig. 2. X-ray structure of **AFN-1252** (shown in yellow) in complex with *E. coli* FabI. NADH is shown in cyan colour. Hydrogen bond interactions are shown in dotted lines.

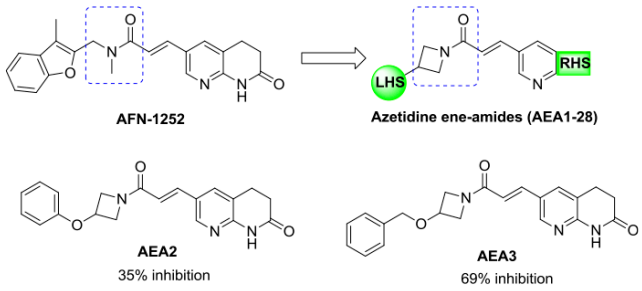

Fig. 3. Design of azetidine ene-amide series and initial hits.

commercially available azetidine **2** under **EDC·HCl** and **HOBt** conditions in the presence of Hunig's base. The substituted azetidine counterparts have been accessed by different routes following reported procedures and coupled with the carboxylic acid **1** to produce final molecules. Compounds **AEA2** and **AEA3** have been made starting from readily available amines **3** and **4** respectively [25]. The azetidine amides **AEA4-11** were obtained by coupling acid **1** and the amines **5**–**12** made following literature procedures [26]. The base promoted *O*-arylation of alcohol **13** with 2-chloro benzothiazole in the presence of sodium hydride furnished **14** which in turn was treated with trifluoroacetic acid followed by coupling with acid **1** to yield **AEA12**.

The synthesis of carbon linked azetidines (**AEA13**–**21**) was executed as represented in Scheme 3. Benzothiazole nucleus was introduced to the azetdine **15** [27] employing the Minisci reaction conditions [28]. The radical mediated oxidative coupling of benzothiazole and **15** in the presence of hydrogen peroxide and ferrous sulphate produced the azetidine derivative **16** which subsequently furnished **AEA13**. Similarly, azetidine intermediates **18**–**24** were synthesized by reacting iodide **17** [28] with corresponding heteroaryls under the Minisci reaction conditions. The transformation of these intermediates to final compounds **AEA14**–**20** followed routine procedures. The compound **AEA21** was smoothly obtained by coupling commercially available phenyl-3-azetidine with acid **1** under standard amide coupling conditions.

The final compounds were screened in a *S. aureus* FabI biochemical assay followed by whole cell assay comprising a panel of MSSA, MRSA and MRSE organisms. As shown in Table 1, introduction of azetidine resulted in potent FabI inhibitors illustrating a range of tolerable substitutions on azetidine ring.

Unsubstituted analogue **AEA1** is inactive probably because of the lack of a group occupying the hydrophobic pocket. However, substituted azetidines that have moieties interacting with hydrophobic pocket demonstrated good biochemical and cell based activities. Among the azetidinyl ethers **AEA3** and **AEA4**, a noticeable increase in FabI potency and whole cell activity was observed when oxygen is in conjugation with phenyl moiety with a methylene spacer as exemplified by **AEA4** (IC_{50} = 0.265 μM, MIC = 0.25–1 μg/mL). The fluoro phenyl derivatives **AEA5-7**, in general, showed good FabI enzyme activity and the p-fluoro phenyl analogue **AEA7** showed superior antibacterial activity with MICs in the range of 0.25–1 μg/mL compared to other fluoro phenyl analogues. In the case of methyl substituted phenyl analogues **AEA8-10**, ortho derivative **AEA8** possessed potent enzyme activity (IC_{50} = 0.177 μM) which translated into good whole cell activity (MIC = 0.25–1 μg/mL) compared to other isomers. Introduction of biaryl moieties on azetidine through oxymethylene (**AEA11**), oxygen (**AEA12**) and methylene (**AEA13**) spacers yielded compounds with poor to moderate potency which could be due to unfavourable geometry leading to the loss of π-stacking interaction with Tyr-146. In contrast, direct linkage of biaryl moiety to azetidine exemplified by **AEA14** led to dramatic improvement in FabI inhibition (IC_{50} = 0.373 μM) as well as cell based activity against staphylococcal strains (MIC = 0.25–1 μg/mL). Encouraged by this SAR finding, a few more analogues (**AEA15**–**21**) were made wherein an aryl or a biaryl moiety is directly attached to azetidine at the 3-position through carbon–carbon linkage as mentioned in Scheme 3.

In a gratifying result, installation of 3-methyl benzoxazole on azetidine afforded the compound **AEA16** with improved FabI enzyme inhibition (IC_{50} = 0.141 μM) and the best antibacterial activity against various staphylococcal organisms (MIC = 0.06–0.5 μg/mL). The 5-methoxy-benzoxazole **AEA17** and 5-chloro benzoxazole

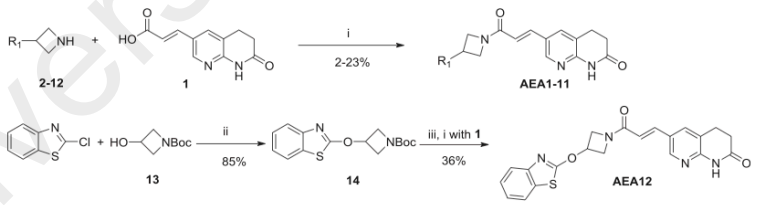

Scheme 2. Reagents and conditions: (i) **EDC·HCl**, **HOBt**, DIPEA, r.t, overnight; (ii) NaH, DMF, 100 °C, overnight; (iii) TFA, CH_2Cl_2, r.t, 2 h. R_1 = H, **2**, **AEA1**; R_1 = PhO, **3**, **AEA2**; R_1 = $PhCH_2O$, **4**, **AEA3**; R_1 = $PhOCH_2$, **5**, **AEA4**; R_1 = o-fluoro-C_6H_4-OCH_2, **6**, **AEA5**; R_1 = m-fluoro-C_6H_4-OCH_2, **7**, **AEA6**; R_1 = p-fluoro-C_6H_4-OCH_2, **8**, **AEA7**; R_1 = o-methyl-C_6H_4-OCH_2, **9**, **AEA8**; R_1 = m-methyl-C_6H_4-OCH_2, **10**, **AEA9**; R_1 = p-methyl-C_6H_4-OCH_2, **11**, **AEA10**; R_1 = 2-napthyl-OCH_2, **12**, **AEA11**.

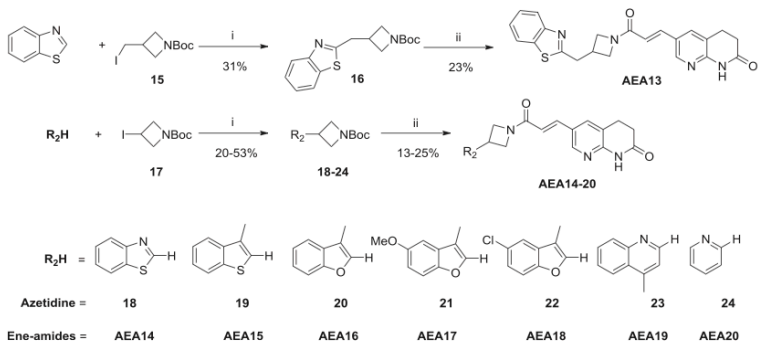

Scheme 3. Reagents and conditions: (i) $FeSO_4{\cdot}7H_2O$, H_2SO_4, H_2O_2, DMSO, r.t, 16 h; (ii) (a) TFA, CH_2Cl_2, r.t, 2 h (b) 1, EDC·HCl, HOBt, DIPEA, r.t, overnight.

AEA18 exhibited good in vitro antibacterial profile. However, quinoline **AEA19** and pyridine **AEA20** exhibited poor to moderate whole cell activity, presumably due to poor cell permeability of molecule and/or efflux barriers present in bacterial membrane.

2.3. Design, synthesis and SAR of benzofuranyl-azetidine ene amides with variation on right hand side

Having established SAR on left hand side, we turned our attention to the right hand side (RHS) part of the ene-amide scaffold. In this iteration, modifications were carried out on the potent compound **AEA16** keeping the 2-benzfuranyl azetidine moiety constant. Substitutions on RHS occupy a hydrophilic pocket and compounds with basic functionalities in this region have been previously reported [10,11]. Accordingly, a cross section of analogues with variations (**AEA22–28**) on pyridine ring have been made and screened.

Compounds**AEA22–24** have been prepared by coupling amine **25**, obtained from **20**, with corresponding acids **26** [9], **27** [29] and **28** [30] as shown in Scheme 4. The azetidine ene-amides **AEA25–28** were synthesized in a convergent manner as delineated in Scheme 5. The bromo-diazepinone intermediates **30** [10], **31** [10], **32** [31], **33** [10] have been obtained according to literature procedures and coupled to acrylamide **29** under Heck reaction conditions to furnish corresponding products **AEA25–28**.

These analogues were also tested in biochemical and whole cell assays. The results are summarized in Table 2. Although its enzyme activity is retained, the acetamide **AEA22** showed inferior cell based activity compared to its cyclic congener **AEA16**. Surprisingly, 1,2,3-triazole substituted acetamide **AEA23** showed poor biochemical and antibacterial activities which could be due to the disturbance in a hydrogen bonding network between the backbone carbonyl and amide hydrogen of Ala-95 from *S. aureus* FabI enzyme. The substitution of N-alkyl morpholine onto cyclic urea yielded highly potent FabI inhibitor **AEA24** with IC_{50} of 58 nM. This observation is reminiscent to the results reported by the Affinium group wherein the basic appendage can occupy the solvent pocket away from the target site [11]. The N-methyl diazepinone **AEA26** was found to be equipotent to its corresponding N–H diazepinone **AEA25** and showed MICs in the range of 0.25–0.5 μg/mL. Extended substitutions on diazepinone yielded less potent **AEA27** compared to **AEA24** which could be due to inability of this morpholine group to access the solvent pocket. The compound **AEA28** showed almost equal biochemical potency and cell based activity to its positional isomer **AEA25**.

Above SAR results indicate that right combination of groups on both sides of ene-amide scaffold is essential for achieving good FabI potency as well as in vitro antibacterial activity. Further, in addition to biochemical potency, appropriate balance of physicochemical properties such as clogP, molecular weight and polarity are critical to overcome bacterial cell membrane permeability barriers [32]. Therefore, the variation in MIC values of these compounds can be a consequence of differences in their aforementioned properties. Among these compounds, best in vitro antibacterial activity (MIC = 0.06 μg/mL) is obtained against MRSA and MSSA organisms for **AEA16** which possess a naphthyridinone ring on the right hand side and benzofuranyl moiety on left hand side. These structural features are similar to **AFN-1252** as shown in Fig. 4.

An X-ray crystal structure of one of the leads **AEA16** bound to *E. coli* FabI enzyme (Fig. 5) in the presence of NADH was determined to a resolution of 3.2 Å [33] and it was found to be similar to other crystal structures reported from the ene-amide series [9].

A superposition of **AEA16**, **AFN-1252** and triclosan X-ray structures (PDB ID: 1C14) is shown in Fig. 6. It is evident that critical interactions observed in **AFN-1252** are conserved in **AEA16** bound *E. coli* FabI complex. Benzofuran moieties in the **AEA16** and **AFN-1252**, and chlorine atom in triclosan occupy the same hydrophobic pocket. Hydroxyl moiety of triclosan is hydrogen bonded to Tyr-156 and NADH whereas oxygen atoms of carbonyls of **AFN-1252** and **AEA16** in the ene-amide moiety are engaged in hydrogen boding with the same residues. This key hydrogen bond interaction with Tyr-156 residue is also reported in several known FabI inhibitors [9,17,34,35].

2.4. Metabolic stability and in vivo pharmacokinetic profile of selected compounds

Selected compounds possessing good cell based activity were tested for metabolic stability in mice liver microsomes. The compounds showing good metabolic stability were further evaluated for in vivo pharmacokinetic properties in mice by oral route. The results are summarized in Table 3. Most of these azetidine ene-amides, except **AEA26**, were found to have high metabolic stability. The good metabolic stability of these analogues could be due to enzymatic stability of cyclic and conformationally restricted azetidine amide. The compound **AEA26** appears to be metabolically less stable likely because of demethylation of diazepinone ring by liver enzymes [36]. **AFN-1252** was found to be less stable compared to azetidine ene-amide analogues presumably due to the presence of open chain amide as discussed. Most of these compounds

Table 1
SAR on LHS part of ene-amide.

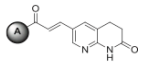

Compound no	A	*S. aureus* FabI inhibition		MIC (μg/mL)[a]		
		%@1 μM	IC_{50}(μM)	MSSA[b]	MRSA[c]	MRSE[d]
AEA1		15%	ND[e]	>32	>32	>32
AEA2	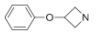	35%	ND[e]	4	4	16
AEA3	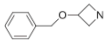	69%	0.376	1	2	2
AEA4		81%	0.265	0.25	0.25	1
AEA5	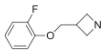	99%	0.378	1	1	2
AEA6	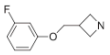	89%	0.438	1	2	2
AEA7	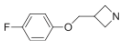	92%	0.316	0.25	0.5	1
AEA8	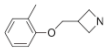	80%	0.177	0.25	0.5	1
AEA9	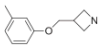	47%	ND	2	2	2
AEA10	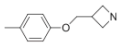	67%	0.921	1	1	2
AEA11	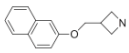	68%	1.41	4	4	>32
AEA12	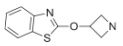	16%	ND[e]	>32	>32	>32
AEA13	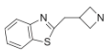	41%	ND[e]	2	4	2
AEA14	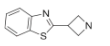	83%	0.373	0.25	0.25	1
AEA15	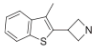	89%	0.709	0.125	0.25	2
AEA16	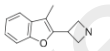	96%	0.141	0.06	0.06	0.5
AEA17	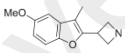	ND[e]	ND[e]	0.5	1	2
AEA18	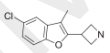	82%	0.204	0.25	0.25	0.5
AEA19	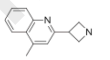	84%	0.242	32	>32	>32
AEA20		87%	0.242	4	8	16
AEA21		80%	0.488	1	2	2

[a] MIC = Minimum inhibitory concentration.
[b] MSSA – methicillin-sensitive *Staphylococcus aureus* ATCC 29213.
[c] MRSA – methicillin-resistant *Staphylococcus aureus* ATCC 33591.
[d] MRSE – methicillin-resistant *Staphylococcus epidermidis* AUCC 704.
[e] ND = Not determined.

possessed excellent pharmacokinetic profile with good systemic exposures as exemplified by **AEA7**, **AEA14**, **AEA16** and **AEA18.** Among these compounds **AEA8**, **AEA15** and **AEA25** showed relatively lower AUC and C_{max} values compared to the rest of the molecules. Higher rate of clearance due to lower metabolic stability of **AEA8** and **AEA15** could be contributing to lower AUC and C_{max} values compared to other compounds. Despite the good metabolic stability, **AEA25** showed suboptimal pharmacokinetics which could be a consequence of poor absorption. **AFN-1252** displayed a poor pharmacokinetic profile compared to these azetidine-ene amides presumably due to its poor metabolic stability in mice liver microsomes.

2.5. In vivo efficacy of compound *AEA16*

Based on potent cell based activity (MIC = 0.06 μg/mL) and favourable pharmacokinetic profile, compound **AEA16** was advanced to in vivo efficacy studies in a lethal murine systemic infection model by oral route, employing MRSA as the infectious organism. The results are presented in Table 4. **AEA16** protected the mice from infection at the ED_{50} dose of 0.90 mg/kg/day which was superior to that of Linezolid (ED_{50} = 2.8 mg/kg/day), a current standard of care for the treatment of MRSA infections. The potent in vitro antibacterial activity of lead **AEA16** coupled with good pharmacokinetic profile led to impressive in vivo efficacy.

3. Conclusions

In summary, we have developed a potent and promising series of ene-amides bearing azetidines as FabI inhibitors active against a panel of resistant staphylococcal organisms. Structure-guided SAR in iterative approach through the introduction of structurally diverse azetidines followed by right hand side modifications afforded potent compounds with excellent FabI inhibition ($IC_{50} \geq 0.058$ μM) and antibacterial activity (MICs ≥0.06 μg/mL) against MSSA, MRSA and MRSE pathogens. Excellent metabolic stability and pharmacokinetic properties have been observed for the compounds from this series. The lead **AEA16** demonstrated very good in vivo efficacy in a murine systemic infection model. The key SAR insights in this program will be utilized for further optimization of ene-amide series to identify a clinical candidate.

4. Experimental

4.1. General

All chemicals were purchased from Sigma–Aldrich, Lancaster and Combiblock and were used without further purification. Reactions were monitored by TLC performed on silica gel aluminium

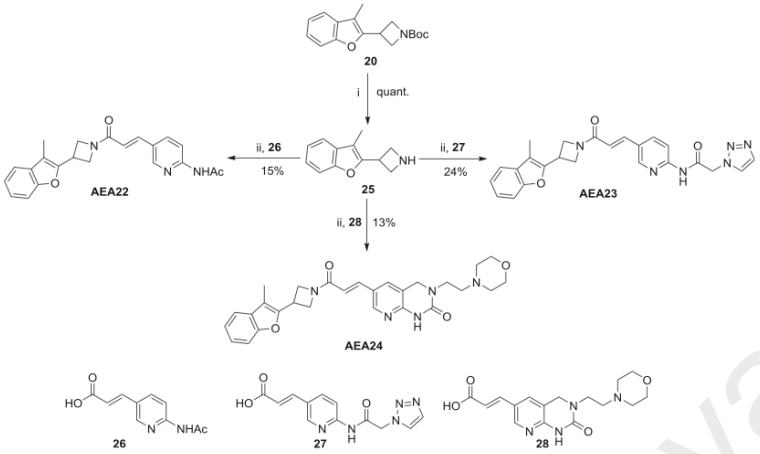

Scheme 4. Reagents and conditions: (i) TFA, CH_2Cl_2, r.t, 2 h; (ii) EDC·HCl, HOBt, DIPEA, r.t, overnight.

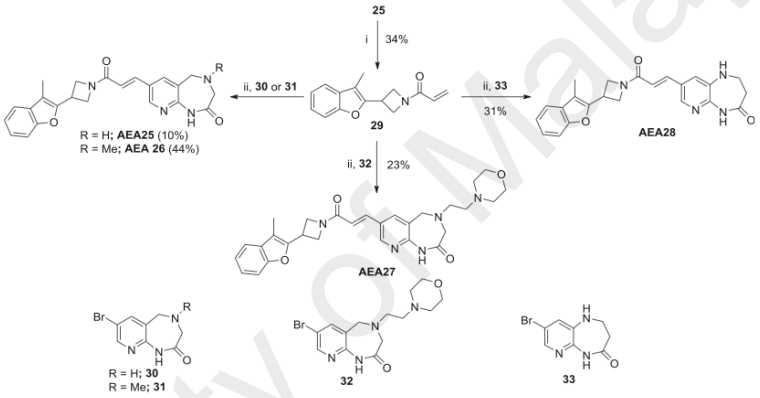

Scheme 5. Reagents and conditions: (i) Acryloyl chloride, Et_3N, CH_2Cl_2, r.t, 16 h; (ii) $Pd(OAc)_2$, P(o-tolyl)$_3$, DIPEA, Propionitrile, reflux, 6 h.

plates containing 60 F254. Column chromatography was performed with Merck 100–200 mesh silica gel. ^{1}H NMR and ^{13}C NMR were recorded on Varian Mercury Plus (400 MHz) or Varian Unity Inova (500 MHz) instruments. Chemical shifts are reported in parts per million (δ in ppm) relative to the peak for tetramethylsilane (TMS) as internal standard and the coupling constants are reported in Hertz (Hz). High resolution mass spectra (HRMS) were recorded on a Waters LCT-Premier mass spectrometer. IR spectra were recorded on a FT-IR spectrometer and only major peaks are reported in cm^{-1}.

4.2. General procedure for the synthesis of ***AEA1-24***

Diisopropyl ethyl amine (3 equiv) was added to a stirred solution of **azetidine or substituted** azetidine-TFA salt (1.1 equiv), carboxylic acid **1** (1 equiv), **HOBt** (2 equiv) and **EDC·HCl** (2 equiv) in DMF (10 volumes) at room temperature. The reaction mixture was stirred at the same temperature for 16 h, then diluted with H_2O (50 volumes) and extracted with ethyl acetate (3 × 50 volumes). The combined organic layers were washed with brine (50 volumes), dried over Na_2SO_4, filtered and volatiles were removed under vacuum. The crude residue was purified by column chromatography to furnish the desired products **AEA1-24**.

4.2.1. *(E)-6-(3-(azetidin-1-yl)-3-oxoprop-1-en-1-yl)-3,4-dihydro-1,8-naphthyridin-2(1H)-one (**AEA1**)*

Yield: 9%; White solid; mp: 278–279 °C; IR (KBr, cm^{-1}): 3535, 2883, 1654, 1598, 1462, 1300, 1197, 983, 852, 530; ^{1}H NMR (400 MHz, DMSO-d$_6$): δ_H 10.64 (s, 1H), 8.33 (d, J = 1.5 Hz, 1H), 8.00 (s, 1H), 7.38 (d, J = 15.9 Hz, 1H), 6.69 (d, J = 15.9 Hz, 1H) 4.28 (t, J = 7.6 Hz, 2H), 3.94 (t, J = 7.6 Hz, 2H), 2.91 (t, J = 7.6 Hz, 2H), 2.58–2.52 (m, 2H), 2.28–2.20 (m, 2H); ^{13}C NMR (500 MHz, DMSO-d$_6$): δ_C 14.8, 23.2, 30.0, 47.6, 49.8, 116.1, 119.0, 125.3, 133.5, 136.3,

Table 2
SAR on RHS part of ene-amide.

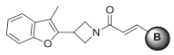

Compound no	B	*S. aureus* FabI inhibition		MIC μg/mL[a]		
		%@1 μM	IC_{50}(μM)	MSSA[b]	MRSA[c]	MRSE[d]
AEA22		97%	0.161	1	1	8
AEA23	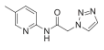	66%	0.843	>32	>32	>32
AEA24	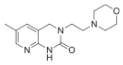	105%	0.058	1	1	2
AEA25		83%	0.384	0.25	0.25	1
AEA26		99%	0.112	0.25	0.25	0.5
AEA27	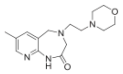	100%	0.289	1	1	2
AEA28		92%	0.316	0.25	0.5	1
AFN-1252		100%	0.029	0.008	0.008	0.008

[a] MIC = Minimum inhibitory concentration.
[b] MSSA – methicillin-sensitive *Staphylococcus aureus* ATCC 29213.
[c] MRSA- methicillin-resistant *Staphylococcus aureus* ATCC 33591.
[d] MRSE – methicillin-resistant *Staphylococcus epidermidis* AUCC 704.

147.1, 152.3, 164.8, 170.9; HRMS *m/z* Calcd for $C_{14}H_{15}N_3O_2$ $[M+H]^+$: 258.1243, Found: 258.1246.

*4.2.2. (E)-6-(3-oxo-3-(3-phenoxyazetidin-1-yl)prop-1-en-1-yl)-3,4-dihydro-1,8-naphthyridin-2(1H)-one (**AEA2**)*

Yield = 17%; White solid; mp: 244–245 °C; IR (KBr, cm^{-1}): 3061, 2873, 1658, 1600, 1489, 1354, 1236, 1192, 1024, 842, 754, 692; ^1H NMR (400 MHz, DMSO-d_6): δ_H 10.65 (brs, 1H), 8.35 (d, J = 1.9 Hz, 1H), 8.02 (s, 1H), 7.42 (d, J = 15.6 Hz, 1H), 7.35–7.31 (m, 2H), 7.00 (t, J = 7.3 Hz, 1H), 6.88 (d, J = 7.8 Hz, 2H), 6.76 (d, J = 15.6 Hz, 1H), 5.11–5.08 (m, 1H), 4.77–4.73 (m, 1H), 4.42 (dd, J = 7.0 Hz, 10.5 Hz, 1H), 4.22 (dd, J = 3.1 Hz, 9.5 Hz, 1H), 3.90 (dd, J = 3.1 Hz, 10.9 Hz, 1H), 2.90 (t, J = 7.8 Hz, 2H), 2.53 (d, J = 7.8 Hz, 2H); ^{13}C NMR (400 MHz, DMSO-d_6): δ_C 23.3, 29.9, 54.6, 57.0, 65.3, 114.6, 116.2, 119.0, 121.3, 125.2, 129.7, 133.6, 136.9, 141.2, 152.4, 156.2, 165.1, 170.9; HRMS *m/z* Calcd for $C_{20}H_{19}N_3O_3$ $[M+H]^+$: 350.1505, Found: 350.1489.

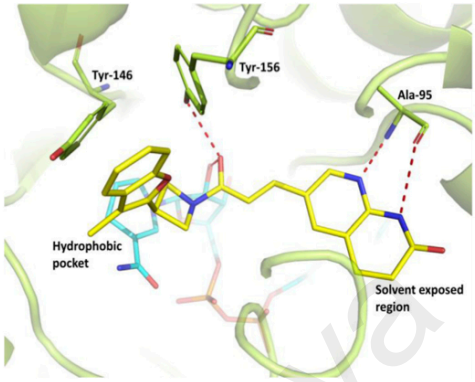

Fig. 5. X-ray structure of **AEA16** (shown in yellow) in complex with *E. coli* FabI. NADH is shown in cyan colour. Hydrogen bonded interaction is shown in dotted line.

*4.2.3. (E)-6-(3-(3-(benzyloxy)azetidin-1-yl)-3-oxoprop-1-en-1-yl)-3,4-dihydro-1,8-naphthyridin-2(1H)-one (**AEA3**)*

Yield = 22%; Off-white solid; mp: 205–206 °C; IR (KBr, cm^{-1}): 3485, 2924, 1687, 1591, 1452, 1357, 1296, 1192, 974, 846, 698, 530; ^1H NMR (400 MHz, DMSO-d_6) δ_H 10.65 (brs, 1H), 8.30 (s, 1H), 8.00 (s, 1H), 7.39 (d, J = 15.2 Hz, 1H), 7.37–7.31 (m, 5H), 6.70 (d, J = 15.6 Hz, 1H), 4.47–4.44 (m, 4H), 4.14–4.10 (m, 2H), 3.73 (d, J = 7.8 Hz, 1H), 2.91 (t, J = 7.6 Hz, 2H), 2.58–2.52 (m, 2H); ^{13}C NMR (400 MHz, DMSO-d_6): δ_C 23.3, 30.0, 54.9, 57.0, 66.9, 70.0, 116.3, 119.0, 125.2, 127.7, 127.9, 128.3, 133.5, 136.6, 137.5, 147.2, 152.4, 165.1, 170.9; HRMS *m/z* Calcd for $C_{21}H_{21}N_3O_3$ $[M+H]^+$: 364.1661, Found: 364.1666.

*4.2.4. (E)-6-(3-oxo-3-(3-(phenoxymethyl)azetidin-1-yl)prop-1-en-1-yl)-3,4-dihydro-1,8-naphthyridin-2(1H)-one (**AEA4**)*

Yield = 17%; Pale yellow solid; mp: 207–208 °C; IR (KBr, cm^{-1}): 3199, 2875, 1701, 1492, 1236, 989, 761, 528 ^1H NMR (400 MHz, DMSO-d_6): δ_H 8.58 (brs, 1H), 8.33 (d, J = 1.5 Hz, 1H), 7.64 (s, 1H), 7.60 (d, J = 15.6 Hz, 1H), 7.31 (d, J = 7.6 Hz, 1H), 7.29 (d, J = 7.3 Hz, 1H), 6.98 (t, J = 7.3 Hz, 1H), 6.91 (d, J = 8.0 Hz, 2H), 6.45 (d, J = 15.6 Hz, 1H), 4.45 (t, J = 8.4 Hz, 1H), 4.26 (dd, J = 8.6 Hz, 17.3 Hz, 1H), 4.23–4.18 (m, 1H), 4.17–4.12 (m, 2H), 4.10–3.99 (m, 1H), 3.64 (t, J = 6.1 Hz, 1H), 2.99 (t, J = 7.3 Hz, 2H), 2.69 (t, J = 7.3 Hz, 2H); ^{13}C NMR (500 MHz, DMSO-d_6): δ_C 23.3, 27.6, 30.0, 49.9, 52.5, 69.0, 114.5, 116.2, 119.0, 120.7, 125.3, 129.4, 133.5, 136.4, 147.1, 152.3, 158.3, 165.1, 170.9; HRMS *m/z* Calcd for $C_{21}H_{21}N_3O_3$ $[M+H]^+$: 364.1661, Found: 364.1660.

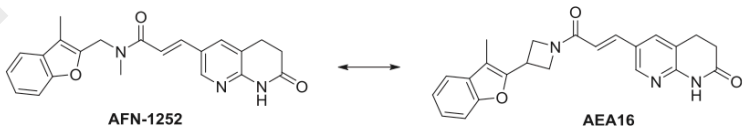

Fig. 4. Structural similarities between **AFN-1252** and **AEA16**.

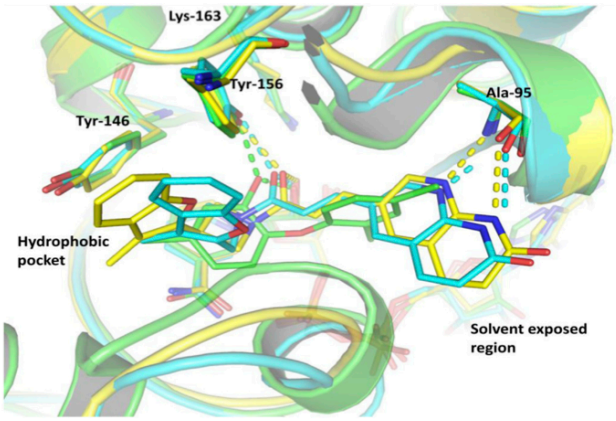

Fig. 6. Superposition of X-ray structure of **AEA16** (yellow), **AFN-1252** (cyan) and triclosan (green) in complex with *E. coli* FabI. Hydrogen bonding interaction is shown in dotted line.

Table 3
Metabolic stability and in vivo pharmacokinetic parameters of selected compounds.

Compound	Metabolic stability[a]		In vivo pharmacokinetics[b]			
	15 min	60 min	AUC (μg/mL*h)	C_{max} (μg/mL)	$t_{1/2}$ (h)	T_{max} (h)
AEA7	91.7%	83.4%	95.2	15.1	3.23	2.0
AEA8	82.1%	44.4%	38.5	7.60	4.74	2.0
AEA14	84.0%	59.9%	75.9	14.4	2.17	2.0
AEA15	65.5%	36.1%	35.5	2.79	4.11	4.0
AEA16	79.4%	55.7%	63.5	8.95	3.20	2.0
AEA18	81.0%	80.2%	86.8	8.10	2.00	1.0
AEA25	96.2%	76.4%	9.0	2.25	8.5	0.5
AEA26	25.6%	6.6%	ND[c]	ND[c]	ND[c]	ND[c]
AFN-1252	55.4%	17.5%	2.20	0.44	1.84	1.00

[a] Metabolic stability study was carried in the presence of mice liver microsomes and measured percentage of compound remaining after 15 min and 60 min.
[b] Pharmacokinetic experiments were performed in mice using single dose (10 mg/kg) through oral route of administration.
[c] ND = not determined.

*4.2.5. (E)-6-(3-(3-((2-fluorophenoxy)methyl)azetidin-1-yl)-3-oxoprop-1-en-1-yl)-3,4-dihydro-1,8-naphthyridin-2(1H)-one (**AEA5**)*

Yield = 13%; Pale yellow solid; mp: 186–187 °C; IR (KBr, cm^{-1}): 3041, 1649, 1589, 1504, 1282, 1193, 1109,842, 748; ^{1}H NMR (400 MHz, DMSO-d_6): δ_H 10.65 (s, 1H), 8.34 (s, 1H), 8.03 (s, 1H), 7.40 (d, J = 15.7 Hz, 1H), 7.22–7.12 (m, 3H), 6.98–6.94 (m, 1H), 6.74 (d, J = 15.6 Hz, 1H), 4.43 (t, J = 8.8 Hz, 1H), 4.26–4.06 (m, 4H), 3.82–3.76 (m, 1H), 3.16–3.06 (m, 1H), 2.92–2.88 (m, 2H), 2.55–2.53 (m, 2H); ^{13}C NMR (500 MHz, DMSO-d_6): δ_C 23.2, 27.6, 30.0, 49.8, 52.4, 70.3, 115.4, 116.0, 116.2, 119.0, 121.3, 124.8, 125.3, 133.5, 136.5, 146.3, 147.1, 150.8, 152.3, 165.1, 170.9; HRMS *m/z* Calcd for $C_{21}H_{20}FN_3O_3$ $[M+H]^+$: 382.1567, Found: 382.1569.

Table 4
In vivo efficacy of **AEA16** in murine systemic infection model.

Compound	ED_{50} (mg/kg)
AEA16	0.90 (0.5–1.9)[a]
Linezolid	2.30 (1.2–4.6)[a]

[a] Values in brackets denote confidence range.

*4.2.6. (E)-6-(3-(3-((3-fluorophenoxy)methyl)azetidin-1-yl)-3-oxoprop-1-en-1-yl)-3,4-dihydro-1,8-naphthyridin-2(1H)-one (**AEA6**)*

Yield = 22%; Cream colour solid; mp: 228–229 °C; IR (KBr, cm^{-1}): 2877, 1591, 1489, 1136, 950, 842,528; ^{1}H NMR (400 MHz, DMSO-d_6): δ_H 10.65 (s, 1H), 8.34 (d, J = 1.5 Hz, 1H), 8.03 (s, 1H), 7.40 (d, J = 15.7 Hz, 1H), 7.32 (q, J = 8.3 Hz, 1H), 6.87–6.78 (m, 3H), 6.74 (d, J = 15.6 Hz, 1H), 4.43 (t, J = 8.8 Hz, 1H), 4.20–4.06 (m, 4H), 3.78–3.74 (m, 1H), 3.12–3.06 (m, 1H), 2.91 (t, J = 7.8 Hz, 2H), 2.55–2.51 (m, 2H); ^{13}C NMR (500 MHz, DMSO-d_6): δ_C 23.3, 27.5, 30.0, 49.9, 52.4, 69.5, 102.0, 107.4, 110.9, 116.2, 119.0, 125.2, 130.6, 130.7, 133.5, 136.5, 147.1, 152.3, 159.9, 165.1, 170.9; HRMS *m/z* Calcd for $C_{21}H_{20}FN_3O_3$ $[M+H]^+$: 382.1567, Found: 382.1602.

*4.2.7. (E)-6-(3-(3-((4-fluorophenoxy)methyl)azetidin-1-yl)-3-oxoprop-1-en-1-yl)-3,4-dihydro-1,8-naphthyridin-2(1H)-one (**AEA7**)*

Yield = 21%; White solid; mp: 98–99 °C; IR (KBr, cm^{-1}): 2879, 1687, 1604, 1506, 1203, 829, 750; ^{1}H NMR (400 MHz, DMSO-d_6): δ_H 8.55 (brs, 1H), 8.34 (d, J = 1.9 Hz, 1H), 7.64 (d, J = 1.6 Hz, 1H), 7.58 (d, J = 15.6 Hz, 1H), 7.01–6.97 (m, 2H), 6.87–6.84 (m, 2H), 6.45 (d, J = 15.6 Hz, 1H), 4.47–4.43 (m, 1H), 4.27–4.20 (m, 2H), 4.19–4.10 (m, 2H), 4.08–3.98 (m, 1H), 3.14–3.11 (m, 1H), 2.99 (t, J = 7.6 Hz, 2H), 2.72–2.68 (m, 2H); ^{13}C NMR (400 MHz, DMSO-d_6): δ_C 23.3, 27.6, 30.0, 49.9, 52.4, 69.7, 115.7, 115.8, 115.8, 115.9, 116.2, 119.0, 125.3, 133.5, 136.4, 147.1, 152.3, 154.8, 157.7, 165.0, 170.9; HRMS *m/z* Calcd for $C_{21}H_{20}FN_3O_3$ $[M+H]^+$: 382.1567, Found: 382.1581.

*4.2.8. (E)-6-(3-oxo-3-(3-((o-tolyloxy)methyl)azetidin-1-yl)prop-1-en-1-yl)-3,4-dihydro-1,8-naphthyridin-2(1H)-one (**AEA8**)*

Yield = 27%; Yellow solid; mp: 220–221 °C; IR (KBr, cm^{-1}): 2877, 1654, 1591, 1494, 1365, 1246, 1192, 989, 750, 528; ^{1}H NMR (400 MHz, DMSO-d_6): δ_H 10.64 (brs, 1H), 8.34 (s, 1H), 8.03 (s, 1H), 7.40 (d, J = 15.7 Hz, 1H), 7.15–7.12 (m, 2H), 6.96 (d, J = 8.3 Hz, 2H), 6.85 (d, J = 7.3 Hz, 1H), 6.75 (d, J = 15.7 Hz, 1H), 4.44–4.40 (m, 1H), 4.22–4.12 (m, 2H), 4.10–4.06 (m, 1H), 3.88–3.83 (m, 1H), 3.14–3.04 (m, 1H), 2.90 (t, J = 7.8 Hz, 2H), 2.54–2.52 (m, 2H), 2.13 (s, 3H); ^{13}C NMR (500 MHz, DMSO-d_6): δ_C 15.7, 23.2, 27.8, 30.0, 49.8, 52.3, 68.7, 111.5, 116.2, 119.0, 120.4, 125.3, 125.7, 126.9, 130.3, 133.5, 136.4, 147.1,

152.3, 156.4, 165.1, 170.9; HRMS *m/z* Calcd for $C_{22}H_{23}N_3O_3$ $[M+H]^+$: 378.1818, Found: 378.1843.

*4.2.9. (E)-6-(3-oxo-3-(3-((m-tolyloxy)methyl)azetidin-1-yl)prop-1-en-1-yl)-3,4-dihydro-1,8-naphthyridin-2(1H)-one (**AEA9**)*

Yield = 27%; Yellow Solid; mp: 208–209 °C; IR (KBr, cm^{-1}): 3537, 2877, 1687, 1602, 1454, 1292, 1159, 977, 771, 688; ^1H NMR (400 MHz, DMSO-d_6): δ_H 10.64 (s, 1H), 8.34 (d, J = 2.0 Hz, 1H), 8.03 (s, 1H), 7.40 (d, J = 16.2 Hz, 1H), 7.16 (t, J = 7.8 Hz, 1H), 6.79–6.72 (m, 4H), 4.43–4.38 (m, 1H), 4.15–4.04 (m, 4H), 3.78–3.73 (m, 1H), 3.07–3.04 (m, 1H), 2.92–2.87 (m, 2H), 2.54–2.50 (m, 2H), 2.27 (s, 3H); ^{13}C NMR (500 MHz, DMSO-d_6): δ_C 21.0, 23.3, 27.6, 30.0, 49.9, 52.4, 68.9, 111.5, 115.1, 116.2, 119.0, 121.4, 125.3, 129.2, 133.5, 136.4, 138.9, 147.1, 152.3, 158.4, 165.0, 170.9; HRMS *m/z* Calcd for $C_{22}H_{23}N_3O_3$ $[M+H]^+$: 378.1818, Found: 378.1774.

*4.2.10. (E)-6-(3-oxo-3-(3-((p-tolyloxy)methyl)azetidin-1-yl)prop-1-en-1-yl)-3,4-dihydro-1,8-naphthyridin-2(1H)-one (**AEA10**)*

Yield = 32%; Pale brown solid; 210–211 °C; IR (KBr, cm^{-1}): 2875, 1689, 1602, 1510, 1359, 1292, 1242, 1193, 977, 815, 526; ^1H NMR (400 MHz, DMSO-d_6): δ_H 10.65 (s, 1H), 8.34 (d, J = 1.9 Hz, 1H), 8.02 (s, 1H), 7.39 (d, J = 15.6 Hz, 1H), 7.09 (t, J = 8.4 Hz, 2H), 6.85 (d, J = 8.8 Hz, 2H), 6.74 (d, J = 15.6 Hz, 1H), 4.40 (t, J = 8.8 Hz, 1H), 4.13–4.09 (m, 4H), 3.77–3.74 (m, 1H), 3.10–3.02 (m, 1H), 2.92–2.88 (m, 2H), 2.55–2.53 (m, 2H), 2.23 (s, 3H); ^{13}C NMR (500 MHz, DMSO-d_6): δ_C 20.0, 23.3, 27.6, 30.0, 40.9, 52.5, 69.1, 114.3, 116.2, 119.0, 125.3, 129.4, 129.8, 133.5, 136.4, 147.1, 152.3, 156.3, 165.0, 170.9; HRMS m/z Calcd for $C_{22}H_{23}N_3O_3$ $[M+H]^+$: 378.1818, Found: 378.1855.

*4.2.11. (E)-6-(3-(3-(naphthalen-2-yloxy)azetidin-1-yl)-3-oxoprop-1-en-1-yl)-3,4-dihydro-1,8-naphthyridin-2(1H)-one (**AEA11**)*

Yield = 23%; Brown solid; 250–251 °C; IR (KBr, cm^{-1}): 3197, 3059, 2875, 1681, 1598, 1442, 1215, 844, 756, 528; ^1H NMR (400 MHz, DMSO-d_6): δ_H 10.64 (brs, 1H), 8.35 (d, J = 1.0 Hz, 1H), 8.03 (s, 1H), 7.83 (d, J = 8.8 Hz, 1H), 7.80 (d, J = 8.3 Hz, 2H), 7.45 (d, J = 7.8 Hz, 1H), 7.41 (d, J = 15.6 Hz, 1H), 7.39–7.37 (m, 2H), 7.18 (dd, J = 2.4 Hz, 8.8 Hz, 1H), 6.76 (d, J = 15.6 Hz, 1H), 4.50–4.42 (m, 1H), 4.31 (d, J = 6.3 Hz, 2H), 4.22–4.10 (m, 2H), 3.88–3.80 (m, 1H), 3.20–3.10 (m, 1H), 2.91 (t, J = 7.9 Hz, 2H), 2.56–2.53 (m, 2H); ^{13}C NMR (500 MHz, DMSO-d_6): δ_C 23.3, 27.6, 30.0, 50.0, 52.5, 69.1, 106.9, 116.2, 118.5, 119.0, 123.6, 125.3, 126.4, 126.6, 127.4, 128.5, 129.3, 133.5, 134.2, 136.5, 147.1, 152.3, 156.3, 165.1, 170.9; HRMS *m/z* Calcd for $C_{25}H_{23}N_3O_3$ $[M+H]^+$: 414.1818; Found: 414.1840.

*4.2.12. (E)-6-(3-(3-(benzo[d]thiazol-2-yloxy)azetidin-1-yl)-3-oxoprop-1-en-1-yl)-3,4-dihydro-1,8-naphthyridin-2(1H)-one (**AEA12**)*

Yield = 36%; White solid; mp: 275–276 °C; IR (KBr, cm^{-1}): 3460, 2922, 1656, 1527, 1442, 1253, 1043, 761; ^1H NMR (400 MHz, DMSO-d_6): δ_H 10.65 (brs, 1H), 8.35 (s, 1H), 8.04 (s, 1H), 7.94 (d, J = 7.9 Hz, 1H), 7.69 (d, J = 7.9 Hz, 1H), 7.43 (d, J = 15.6 Hz, 1H), 7.43 (s, 1H), 7.32 (d, J = 7.6 Hz, 1H), 6.78 (d, J = 15.6 Hz, 1H), 5.63 (t, J = 3.2 Hz, 1H), 4.83–4.79 (m, 1H), 4.45–4.16 (m, 2H), 4.10–4.08 (m, 1H), 2.90 (t, J = 7.6 Hz, 2H), 2.54–2.50 (m, 2H); ^{13}C NMR (500 MHz, DMSO-d_6): δ_C 23.3, 29.9, 54.4, 57.2, 70.1, 116.2, 119.0, 120.7, 122.2, 124.0, 125.2, 126.3, 131.5, 133.6, 136.9, 147.3, 148.6, 152.4, 165.2, 170.6, 170.9; HRMS *m/z* Calcd for $C_{21}H_{18}N_4O_3S$ $[M+H]^+$: 407.1178, Found: 407.1165.

*4.2.13. (E)-6-(3-(3-(benzo[d]thiazol-2-ylmethyl)azetidin-1-yl)-3-oxoprop-1-en-1-yl)-3,4-dihydro-1,8-naphthyridin-2(1H)-one (**AEA13**)*

Yield = 23%; Pale brown solid; mp: 78–79 °C; IR (KBr, cm^{-1}): 3537, 3118, 2870, 1691, 1656, 1444, 1284, 1182, 773, 524; ^1H NMR (400 MHz, DMSO-d_6): δ_H 10.64 (brs, 1H), 8.33 (d, J = 1.5 Hz, 1H), 8.07 (d, J = 7.9 Hz, 1H), 8.03 (s, 1H), 7.95 (d, J = 7.9 Hz, 1H), 7.52–7.48 (m, 1H), 7.43 (d, J = 7.3 Hz, 1H), 7.39 (d, J = 15.8 Hz, 1H), 6.74 (d, J = 15.8 Hz, 1H), 4.46 (t, J = 8.5 Hz, 1H), 4.13 (t, J = 8.7 Hz, 2H), 3.79 (dd, J = 5.5 Hz, 10.1 Hz, 1H), 3.49 (d, J = 7.9 Hz, 2H), 3.22–3.16 (m, 1H), 2.89 (t, J = 7.6 Hz, 2H), 2.64–2.52 (m, 2H); ^{13}C NMR (500 MHz, DMSO-d_6): δ_C 23.2, 27.8, 30.0, 37.1, 52.5, 54.8, 116.3, 119.0, 122.0, 122.2, 124.9, 125.3, 126.1, 133.5, 134.6, 136.4, 147.2, 152.3, 152.7, 165.09, 169.0, 170.9; HRMS *m/z* Calcd for $C_{22}H_{20}N_4O_2S$ $[M+H]^+$: 405.1385, Found: 405.1386.

*4.2.14. (E)-6-(3-(3-(benzo[d]thiazol-2-yl)azetidin-1-yl)-3-oxoprop-1-en-1-yl)-3,4-dihydro-1,8-naphthyridin-2(1H)-one (**AEA14**)*

Yield = 25%; Brown solid; mp: 258–259 °C; IR (KBr, cm^{-1}): 3061, 2879, 1602, 1452, 1359, 1294, 1192, 1120, 979, 844, 761, 530; ^1H NMR (400 MHz, DMSO-d_6): δ_H 10.66 (brs, 1H), 8.37 (s, 1H), 8.12 (d, J = 7.6 Hz, 1H), 8.05 (s, 1H), 8.02 (d, J = 7.9 Hz, 1H), 7.55–7.52 (m, 1H), 7.46 (s, 1H), 7.45 (d, J = 15.9 Hz, 1H), 6.80 (d, J = 15.9 Hz, 1H), 4.85–4.75 (m, 1H), 4.75–4.55 (m, 1H), 4.50–4.35 (m, 2H), 4.25–4.15 (m, 1H), 2.91 (t, J = 7.4 Hz, 2H), 2.55–2.49 (m, 2H); ^{13}C NMR (400 MHz, DMSO-d_6): δ_C 23.3, 30.0, 31.6, 53.6, 55.6, 116.0, 119.0, 122.3, 122.5, 125.2, 126.3, 133.6, 134.7, 136.9, 137.8, 147.3, 152.4, 152.5, 165.3, 170.9, 171.5; HRMS *m/z* Calcd for $C_{21}H_{18}N_4O_2S$ $[M+H]^+$: 391.1229, Found: 391.1173.

*4.2.15. (E)-6-(3-(3-(3-methylbenzo[b]thiophen-2-yl)azetidin-1-yl)-3-oxoprop-1-en-1-yl)-3,4-dihydro-1,8-naphthyridin-2(1H)-one (**AEA15**)*

Yield = 23%; White solid; mp: 255–256 °C; IR (KBr, cm^{-1}): 3018, 1656, 1462, 1215, 1190, 756, 669; ^1H NMR (400 MHz, DMSO-d_6): δ_H 10.66 (brs, 1H), 8.37 (s, 1H), 8.04 (s, 1H), 7.94 (d, J = 7.8 Hz, 1H), 7.72 (d, J = 7.8 Hz, 1H), 7.46 (d, J = 15.6 Hz, 1H), 7.41–7.33 (m, 2H), 6.80 (d, J = 15.6 Hz, 1H), 4.82 (d, J = 7.8 Hz, 1H), 4.51–4.41 (m, 2H), 4.35 (d, J = 8.3 Hz, 1H), 4.00–3.99 (m, 1H), 2.94–2.89 (m, 2H), 2.66–2.53 (m, 2H), 2.32 (s, 3H); ^{13}C NMR (400 MHz, DMSO-d_6): δ_C 11.4, 23.3, 27.4, 30.0, 55.4, 57.5, 113.8, 116.1, 116.6, 119.1, 121.7, 122.5, 124.3, 125.3, 128.1, 133.79, 137.0, 147.2, 152.4, 158.2, 158.6, 165.2, 171.0; HRMS *m/z* Calcd for $C_{23}H_{21}N_3O_2S$ $[M+H]^+$: 404.1433, Found: 404.1394.

*4.2.16. (E)-6-(3-(3-(3-methylbenzofuran-2-yl)azetidin-1-yl)-3-oxoprop-1-en-1-yl)-3,4-dihydro-1,8-naphthyridin-2(1H)-one (**AEA16**)*

Yield = 20%; White solid; mp: 236–237 °C; IR (KBr, cm^{-1}): 3128, 2881, 1691, 1651, 1454, 1192, 979, 748, 675, 526; ^1H NMR (400 MHz, DMSO-d_6): δ_H 10.66 (brs, 1H), 8.37 (s, 1H), 8.03 (s, 1H), 7.56–7.53 (m, 2H), 7.47 (d, J = 15.6 Hz, 1H), 7.28–7.24 (m, 2H), 6.80 (d, J = 15.6 Hz, 1H), 4.75–4.62 (m, 1H), 4.54–4.48 (m, 1H), 4.40–4.32 (m, 1H), 4.31–4.21 (m, 1H), 4.18–4.10 (m, 1H), 2.91 (t, J = 7.9 Hz, 2H), 2.56–2.52 (m, 2H), 2.19 (s, 3H); ^{13}C NMR (400 MHz, DMSO-d_6): δ_C 7.5, 23.3, 24.6, 30.0, 52.4, 54.4, 110.8, 111.4, 116.1, 119.1, 119.3, 122.5, 124.1, 125.3, 129.6, 133.7, 136.9, 147.3, 151.6, 152.5, 153.4, 165.2, 171.0; HRMS *m/z* Calcd for $C_{23}H_{21}N_3O_3$ $[M+H]^+$: 388.1661, Found: 388.1685.

*4.2.17. (E)-6-(3-(3-(5-methoxy-3-methylbenzofuran-2-yl)azetidin-1-yl)-3-oxoprop-1-en-1-yl)-3,4-dihydro-1,8-naphthyridin-2(1H)-one (**AEA17**)*

Yield = 16%; White solid; mp: 238–239 °C; IR (KBr, cm^{-1}): 3745, 2924, 1656, 1462, 1192, 833, 723; ^1H NMR (400 MHz, DMSO-d_6): δ_H 10.66 (brs, 1H), 8.37 (s, 1H), 8.03 (s, 1H), 7.46 (d, J = 15.6 Hz, 1H), 7.44 (d, J = 8.8 Hz, 1H), 7.04 (d, J = 2.4 Hz, 1H), 6.85 (dd, J = 2.5 Hz, 8.8 Hz, 1H), 6.79 (d, J = 15.6 Hz, 1H), 4.67 (t, J = 8.6 Hz, 1H), 4.49–4.45 (m, 1H), 4.33 (t, J = 9.2 Hz, 1H), 4.26–4.19 (m, 1H), 4.12–4.08 (m, 1H), 3.79 (s, 3H), 2.91 (t, J = 7.6 Hz, 2H), 2.55–2.50 (m, 2H), 2.16 (s, 3H); ^{13}C NMR (400 MHz, DMSO-d_6): δ_C 7.5, 23.3, 24.7, 30.0, 52.4, 54.4, 55.6, 111.3, 111.6, 112.3, 113.7, 116.2, 116.6, 119.1, 125.3, 130.3, 133.8,

136.9, 147.1, 152.4, 155.5, 158.6, 165.22, 171.0; HRMS *m/z* Calcd for $C_{24}H_{23}N_3O_4$ $[M+H]^+$: 418.1767, Found: 418.1731.

*4.2.18. (E)-6-(3-(3-(5-chloro-3-methylbenzofuran-2-yl)azetidin-1-yl)-3-oxoprop-1-en-1-yl)-3,4-dihydro-1,8-naphthyridin-2(1H)-one (**AEA18**)*

Yield = 14%; White solid; mp: 261–262 °C; IR (KBr, cm^{-1}): 2949, 1689, 1602, 1444, 1190, 977, 750, 526; ^1H NMR (400 MHz, DMSO-d_6): δ_H 10.66 (brs, 1H), 8.37 (s, 1H), 8.03 (s, 1H), 7.63 (s, 1H), 7.59 (d, J = 8.8 Hz, 1H), 7.46 (d, J = 15.8 Hz, 1H), 7.30 (dd, J = 1.6 Hz, 8.5 Hz, 1H), 6.78 (d, J = 15.8 Hz, 1H), 4.68 (t, J = 8.5 Hz, 1H), 4.51–4.46 (m, 1H), 4.37–4.25 (m, 2H), 4.14–4.10 (m, 1H), 2.91 (t, J = 7.5 Hz, 2H), 2.54–2.51 (m, 2H), 2.17 (s, 3H); ^{13}C NMR (500 MHz, DMSO-d_6): δ_C 7.3, 23.3, 24.6, 30.0, 52.3, 54.3, 111.4, 112.4, 116.1, 118.9119.0, 123.9, 125.2, 127.0, 131.3, 133.6, 136.9, 147.2, 151.9, 152.4, 153.5, 165.1, 170.9; HRMS *m/z* Calcd for $C_{23}H_{20}ClN_3O_3$ $[M+H]^+$: 422.1271, Found: 422.1289.

*4.2.19. (E)-6-(3-(3-(4-methylquinolin-2-yl)azetidin-1-yl)-3-oxoprop-1-en-1-yl)-3,4-dihydro-1,8-naphthyridin-2(1H)-one (**AEA19**)*

Yield = 18%; Brown solid; mp: 223–224 °C; IR (KBr, cm^{-1}): 3061, 1651, 1598, 1489, 1290, 1190, 972, 848, 769, 526; ^1H NMR (400 MHz, DMSO-d_6): δ_H 10.65 (brs, 1H), 8.36 (d, J = 1.5 Hz, 1H), 8.08 (d, J = 7.8 Hz, 1H), 8.05 (s, 1H), 8.00 (d, J = 8.3 Hz, 1H), 7.82–7.73 (m, 1H), 7.63–7.59 (m, 1H), 7.46–7.41 (m, 2H), 6.81 (d, J = 15.6 Hz, 1H), 4.73–4.63 (m, 2H), 4.41–4.37 (m, 1H), 4.24–4.15 (m, 2H), 2.91 (t, J = 7.6 Hz, 2H), 2.69 (s, 3H), 2.55–2.53 (m, 2H); ^{13}C NMR (500 MHz, DMSO-d_6): δ_C 18.1, 23.3, 30.0, 34.4, 52.9, 54.7, 116.3, 119.0, 121.0, 124.1, 125.3, 126.0, 126.7, 129.0, 129.4, 133.6, 136.6, 145.0, 147.0, 147.2, 152.4, 160.5, 165.2, 170.9; HRMS *m/z* Calcd for $C_{24}H_{22}N_4O_2$ $[M+H]^+$: 399.1821, Found: 399.1833.

*4.2.20. (E)-6-(3-oxo-3-(3-(pyridin-2-yl)azetidin-1-yl)prop-1-en-1-yl)-3,4-dihydro-1,8-naphthyridin-2(1H)-one (**AEA20**)*

Yield = 23%; Brown solid; mp: 222–223 °C; IR (KBr, cm^{-1}): 3007, 2877, 2677, 1687, 1597, 1433, 1357, 1188, 779, 530; ^1H NMR (400 MHz, DMSO-d_6): δ_H 10.67 (brs, 1H), 8.61 (d, J = 4.4 Hz, 1H), 8.36 (s, 1H), 8.03 (s, 1H), 7.80–7.76 (m, 1H), 7.42 (d, J = 15.6 Hz, 1H), 7.37 (d, J = 7.8 Hz, 1H), 7.30 (dd, J = 5.1 Hz, 7.1 Hz, 1H), 6.77 (d, J = 15.6 Hz, 1H), 4.65 (t, J = 8.0 Hz, 1H), 4.48–4.45 (m, 1H), 4.46 (t, J = 8.8 Hz, 1H), 4.10–3.99 (m, 2H), 3.09 (dt, J = 7.3 Hz, 12.2 Hz, 2H), 2.90 (t, J = 7.6 Hz, 2H); ^{13}C NMR (400 MHz, DMSO-d_6): δ_C 23.3, 30.0, 33.9, 53.4, 55.4, 116.2, 119.0, 122.2, 122.4, 125.3, 133.6, 136.5, 136.8, 147.1, 149.4, 152.4, 160.3, 165.1, 170.9; HRMS *m/z* Calcd for $C_{19}H_{18}N_4O_2$ $[M+H]^+$: 335.1508, Found: 335.1515.

*4.2.21. (E)-6-(3-oxo-3-(3-phenylazetidin-1-yl)prop-1-en-1-yl)-3,4-dihydro-1,8-naphthyridin-2(1H)-one (**AEA21**)*

Yield = 50%; Off-white Solid; mp: 268–269 °C; IR (KBr, cm^{-1}): 3034, 2875, 1656, 1591, 1365, 1290, 1193, 758, 700; ^1H NMR (400 MHz, DMSO-d_6): δ_H 10.65 (s, 1H), 8.35 (d, J = 2.0 Hz, 1H), 8.02 (d, J = 0.9 Hz, 1H), 7.43 (d, J = 15.7 Hz, 1H), 7.38–7.36 (m, 4H), 7.35–7.25 (m, 1H), 6.77 (d, J = 15.6 Hz, 1H), 4.71 (t, J = 8.3 Hz, 1H), 4.39–4.27 (m, 2H), 3.95–3.89 (m, 2H), 2.93–2.89 (m, 2H), 2.56–2.51 (m, 2H); ^{13}C NMR (400 MHz, DMSO-d_6): δ_C 23.3, 30.0, 32.6, 54.8, 56.9, 116.3, 119.0, 125.3, 126.7, 128.6, 133.5, 136.5, 136.8, 142.1147.1, 147.7, 165.1, 170.9; HRMS *m/z* Calcd for $C_{20}H_{19}N_3O_2$ $[M+H]^+$: 334.1556, Found: 334.1557.

*4.2.22. (E)-N-(5-(3-(3-(3-methylbenzofuran-2-yl)azetidin-1-yl)-3-oxoprop-1-en-1-yl)pyridin-2-yl)acetamide (**AEA22**)*

Yield = 15%; White solid; mp: 226–227 °C; IR (KBr, cm^{-1}): 3255, 2949, 2883, 1651, 1519, 1444, 1301, 975, 837, 744, 624; ^1H NMR (400 MHz, DMSO-d_6): δ_H 10.67 (s, 1H), 8.61 (d, J = 1.9 Hz, 1H), 8.14–8.08 (m, 1H), 8.11 (m, 1H), 7.56–7.53 (m, 2H), 7.49 (d, J = 15.7 Hz, 1H), 7.28–7.24 (m, 2H), 6.84 (d, J = 15.7 Hz, 1H), 4.71–4.67 (m, 1H), 4.52–4.48 (m, 1H), 4.37–4.33 (m, 1H), 4.30–4.23 (m, 1H), 4.15–4.11 (m, 1H), 2.18 (s, 3H), 2.10 (s, 3H); ^{13}C NMR (400 MHz, DMSO-d_6): δ_C 7.4, 23.9, 24.6, 52.4, 54.4, 110.8, 111.3, 112.8, 116.7, 119.2, 122.4, 124.1, 126.1, 129.6, 136.5, 136.6, 148.5, 151.5, 152.7, 153.4, 165.0, 169.4; HRMS *m/z* Calcd for $C_{22}H_{21}N_3O_3$ $[M+H]^+$:376.1661, Found: 376.1678.

*4.2.23. (E)-N-(5-(3-(3-(3-methylbenzofuran-2-yl)azetidin-1-yl)-3-oxoprop-1-en-1-yl)pyridin-2-yl)-2-(1H-1,2,3-triazol-1-yl) acetamide (**AEA23**)*

Yield = 24%; Pale yellow solid; mp: 227–228 °C; IR (KBr, cm^{-1}): 3321, 2951, 1697, 1537, 1390, 1305, 744; ^1H NMR (400 MHz, DMSO-d_6): δ_H 11.21 (s, 1H), 8.68 (d, J = 1.9 Hz, 1H), 8.20 (dd, J = 2.5 Hz, 8.8 Hz, 1H), 8.16 (s, 1H), 8.03 (d, J = 8.3 Hz, 1H), 7.77 (s, 1H), 7.56–7.54 (m, 2H), 7.51 (d, J = 15.6 Hz, 1H), 7.30–7.22 (m, 2H), 6.89 (d, J = 15.6 Hz, 1H), 5.46 (s, 2H), 4.72–4.67 (m, 1H), 4.52–4.48 (m, 1H), 4.38–4.33 (m, 1H), 4.29–4.23 (m, 1H), 4.16–4.12 (m, 1H), 2.19 (s, 3H); ^{13}C NMR (500 MHz, DMSO-d_6): δ_C 7.4, 24.6, 51.9, 52.4, 54.4, 110.8, 111.3, 113.1, 117.2, 119.2, 122.4, 124.1, 126.5, 126.8, 129.6, 133.1, 136.4, 136.8, 148.7, 151.5, 152.0, 153.4, 164.9, 165.4; HRMS *m/z* Calcd for $C_{24}H_{22}N_6O_3$ $[M+H]^+$:443.1832, Found: 443.1816.

*4.2.24. (E)-6-(3-(3-(3-methylbenzofuran-2-yl)azetidin-1-yl)-3-oxoprop-1-en-1-yl)-3-(2-morpholinoethyl)-3,4-dihydropyrido[2,3-d]pyrimidin-2(1H)-one (**AEA24**)*

Yield = 13%; Off-white solid; mp: 218–219 °C; (KBr, cm^{-1}): 2949, 2818, 1672, 1593, 1492, 1450, 1408, 1296, 1114, 746; ^1H NMR (400 MHz, DMSO-d_6): δ_H 9.88 (brs, 1H), 8.35 (s, 1H), 7.93 (s, 1H), 7.56–7.53 (m, 2H), 7.45 (d, J = 15.8 Hz, 1H), 7.30–7.23 (m, 2H), 6.74 (d, J = 15.5 Hz, 1H), 4.67 (t, J = 8.5 Hz, 1H), 4.54 (s, 2H), 4.50–4.47 (m, 1H), 4.36–4.33 (m, 1H), 4.29–4.25 (m, 1H), 4.14–4.11 (m, 1H), 3.60–3.50 (m, 4H), 3.45 (t, J = 6.1 Hz, 2H), 2.41–2.35 (m, 6H), 2.19 (s, 3H); ^{13}C NMR (500 MHz, DMSO-d_6): δ_C 7.4, 24.6, 40.0, 46.9, 52.4, 53.2, 54.3, 55.4, 65.9, 110.8, 111.3, 113.4, 115.5, 119.2, 122.4, 124.1, 124.5, 129.6, 131.7, 136.9, 148.2, 151.2, 151.5, 152.8, 153.4, 165.1; HRMS *m/z* Calcd for $C_{28}H_{31}N_5O_4$ $[M+H]^+$: 502.2454, Found: 502.2432.

*4.3. General procedure for the synthesis of **AEA25–28***

To a stirred suspension of bromo derivative **30** or **31** or **32** or **33** (1 equiv), acrylamide **29** (1.3 equiv) in propionitrile:DMF (4:1 volumes) was added diisopropyl ethyl amine (3 equiv) and the reaction mixture was degassed with nitrogen for 10 min. Then $Pd(OAc)_2$ (0.2 equiv), P(o-tolyl)$_3$ (0.4 equiv) were added, again degassed with nitrogen for another 10 min and the reaction mixture was allowed to stir at 110 °C for 16 h. The reaction mixture was cooled to room temperature, filtered through celite and filtrate was evaporated under vacuum. The resulting residue was diluted with H_2O (50 volumes) and extracted with ethyl acetate (3 × 50 volumes). The combined organic layers were washed with brine (50 volumes), dried over Na_2SO_4, filtered and volatiles were removed under vacuum. The crude residue was purified by column chromatography to furnish the desired products **AEA25–28**.

*4.3.1. (E)-7-(3-(3-(3-methylbenzofuran-2-yl)azetidin-1-yl)-3-oxoprop-1-en-1-yl)-4,5-dihydro-1H-pyrido[2,3-e][1,4]diazepin-2(3H)-one (**AEA25**)*

Yield = 10%; Pale yellow solid; mp: 204–205 °C; IR (KBr, cm^{-1}): 3280, 3062, 2912, 2883, 1651, 1454, 1328, 977, 856, 748; ^1H NMR (400 MHz, DMSO-d_6): δ_H 10.07 (brs, 1H), 8.45 (d, J = 2.0 Hz, 1H), 7.98 (s, 1H), 7.56–7.53 (m, 2H), 7.47 (d, J = 15.7 Hz, 1H), 7.30–7.22 (m, 2H), 6.83 (d, J = 16.2 Hz, 1H), 4.69 (t, J = 8.5 Hz, 1H), 4.52–4.48

(m, 1H), 4.35 (t, J = 9.3 Hz, 1H), 4.30–4.23 (m, 1H), 4.15–4.11 (m, 1H), 3.90 (s, 2H), 3.63 (s, 2H), 3.06 (brs, 1H), 2.19 (s, 3H); ^{13}C NMR (400 MHz, DMSO-d_6): δ_C 7.4, 24.6, 50.3, 52.4, 54.4, 55.1, 110.8, 111.3, 116.7, 119.3, 122.4, 124.1, 125.2, 126.5, 129.6, 135.4, 136.4, 147.1, 151.0, 151.5, 153.4, 165.1, 174.5; HRMS m/z Calcd for $C_{23}H_{22}N_4O_3$ $[M+H]^+$: 403.1770, Found: 403.1757.

*4.3.2. (E)-4-methyl-7-(3-(3-(3-methylbenzofuran-2-yl)azetidin-1-yl)-3-oxoprop-1-en-1-yl)-4,5-dihydro-1H-pyrido[2,3-e][1,4] diazepin-2(3H)-one (**AEA26**)*

Yield = 44%; Pale green solid; mp: 218–219 °C; IR (KBr, cm^{-1}): 3062, 2945, 2879, 1651, 1454, 1344, 850, 742, 663; ^{1}H NMR (400 MHz, DMSO-d_6): δ_H 10.38 (brs, 1H), 8.54 (s, 1H), 8.11 (s, 1H), 7.56–7.54 (m, 2H), 7.50 (d, J = 15.6 Hz, 1H), 7.30–7.22 (m, 2H), 6.86 (d, J = 15.6 Hz, 1H), 4.70 (t, J = 8.6 Hz, 1H), 4.53–4.49 (m, 1H), 4.36 (t, J = 9.0 Hz, 1H), 4.29–4.26 (m, 1H), 4.15–4.12 (m, 1H), 3.80 (s, 2H), 3.44 (s, 2H), 2.37 (s, 3H), 2.19 (s, 3H); ^{13}C NMR (400 MHz, DMSO-d_6): δ_C 7.4, 24.6, 42.3, 52.4, 54.4, 56.8, 60.3, 110.8, 111.3, 117.2, 119.2, 122.4, 123.0, 124.1, 126.1, 129.6, 136.2, 137.0, 148.0, 151.5, 151.8, 153.4, 165.0, 171.4; HRMS m/z Calcd for $C_{24}H_{24}N_4O_3$ $[M+H]^+$:417.1927, Found: 417.1877.

*4.3.3. (E)-7-(3-(3-(3-methylbenzofuran-2-yl)azetidin-1-yl)-3-oxoprop-1-en-1-yl)-4-(2-morpholinoethyl)-4,5-dihydro-1H-pyrido [2,3-e][1,4]diazepin-2(3H)-one (**AEA27**)*

Yield = 23%; Pale yellow solid; mp: 240–241 °C; IR (KBr, cm^{-1}): 3059, 2947, 2812, 1658, 1454, 1114, 854, 746; ^{1}H NMR (400 MHz, DMSO-d_6): δ_H 10.32 (s, 1H), 8.52 (d, J = 2.0 Hz, 1H), 8.10 (d, J = 2.0 Hz, 1H), 7.56–7.53 (m, 1H), 7.49 (d, J = 15.9 Hz, 1H), 7.26–7.24 (m, 2H), 6.86 (d, J = 15.9 Hz, 1H), 4.68–4.64 (m, 1H), 4.52–4.48 (m, 1H), 4.39–4.36 (m, 2H), 4.28–4.20 (m, 1H), 4.18–4.16 (m, 2H), 3.91 (s, 2H), 3.53 (s, 2H), 3.52–3.51 (m, 3H), 3.29 (s, 2H), 2.67–2.65 (m, 2H), 2.42–2.40 (m, 2H), 2.33–2.31 (m, 2H), 2.19 (s, 3H); ^{13}C NMR (400 MHz, DMSO-d_6): δ_C 7.4, 24.6, 50.2, 52.4, 53.4, 54.4, 55.2, 56.3, 59.1, 66.0, 110.8, 111.3, 117.1, 119.2, 122.4, 123.1, 124.1, 125.9, 129.6, 136.3, 137.1, 147.9, 151.5, 151.7, 153.4, 165.0, 172.1; HRMS m/z Calcd for $C_{29}H_{33}N_5O_4$ $[M+H]^+$: 516.2611, Found: 516.2665.

*4.3.4. (E)-8-(3-(3-(3-methylbenzofuran-2-yl)azetidin-1-yl)-3-oxoprop-1-en-1-yl)-2,3-dihydro-1H-pyrido[2,3-b][1,4]diazepin-4(5H)-one (**AEA28**)*

Yield = 31%; Pale brown solid; mp: 301–302 °C; IR (KBr, cm^{-1}): 3302, 3066, 2947, 2881, 1656, 1585, 1452, 1382, 850, 744; ^{1}H NMR (400 MHz, DMSO-d_6): δ_H 9.75 (s, 1H), 7.99 (d, J = 1.5 Hz, 1H), 7.56–7.52 (m, 2H), 7.39 (d, J = 15.6 Hz, 1H), 7.36 (d, J = 1.9 Hz, 1H), 7.30–7.22 (m, 2H), 6.65 (d, J = 15.6 Hz, 1H), 6.07 (t, J = 3.6 Hz, 1H), 4.68 (t, J = 8.5 Hz, 1H), 4.51–4.46 (m, 1H), 4.35 (t, J = 9.3 Hz, 1H), 4.30–4.24 (m, 1H), 4.13 (dd, J = 5.9 Hz, 9.3 Hz, 1H), 3.44–3.40 (m, 2H), 2.61 (t, J = 5.4 Hz, 2H), 2.19 (s, 3H); ^{13}C NMR (500 MHz, DMSO-d_6): δ_C 7.4, 24.6, 37.7, 42.2, 52.4, 54.3, 110.8, 111.3, 116.3, 119.2, 122.4, 122.7, 124.1, 126.5, 129.6, 135.0, 136.9, 137.4, 140.0, 151.4, 153.3, 164.9, 172.1; HRMS m/z Calcd for $C_{23}H_{22}N_4O_3$ $[M+H]^+$: 403.1770, Found: 403.1803.

4.4. S. aureus FabI biochemical assay

The enzymatic assay [17] is based on the decrease in absorbance at 340 nm resulting from the oxidation of NADPH accompanying the reduction of enoyl – ACP, catalysed by FabI enzyme. The assay was carried out in 100 mM Sodium ADA (N-[2-Acetamido] iminodiacetic acid) buffer, pH 6.5. FabI enzyme (2400 ng/assay) was pre-incubated with NADH (375 μM) and test compounds for 30 min and the reaction was started by adding Crotonoyl CoA (250 μM). The total reaction volume was 100 μL. After 2 h incubation at room temperature, the absorbance at 340 nm was measured and the enzyme activity was determined. Test compounds were initially screened at 1 μM, in duplicate. Dose–response studies were subsequently carried out for active compounds. IC_{50} values were determined by fitting the activity data at different concentrations of the compound to sigmoidal dose response (variable slope) curve fitting program using GraphPad Prism software V5. The standard error in IC_{50} values estimated from the curve fitting was <15%.

4.5. In vitro antibacterial screen

Minimum Inhibitory Concentration (MIC) was determined by broth microdilution method as per CLSI guidelines. Serial two-fold dilution of the compounds was made using MHB in 96 well microtitre plates at twice the desired final concentration. 50 μL of the adjusted inoculum suspension was dispensed into each well to give a final inoculum density of 5×10^5 CFU/mL. Broth, compound and organism controls were set up in duplicate. *S. aureus* ATCC 29213 was incorporated as a quality control strain in the study. Plates were incubated at 35 ± 2 °C for 16–20 h in an ambient air incubator. After the incubation period, growth of organism in the wells was detected by unaided eye facilitated by a viewing device. The amount of growth in the wells containing the antibiotic was compared with the amount of growth in organism control wells (no antibiotic) to help in determining the end point. MIC was the lowest concentration of the antibiotic/compound which inhibits bacterial growth as detected by unaided eye and expressed as μg/mL.

4.6. Protein expression, purification and co-crystallization of E. coli FabI [37]

Gene sequence corresponding to full length *E. coli* FabI was cloned into pET28a vector. Transformants of *E. coli* BL21DE3 containing pET28a-Ec FabI were grown to an optical density (595 nm) of 0.8 and induced with 0.5 mM IPTG at 18 °C for 18 h. Cell pellet was resuspended in lysis buffer containing 50 mM Tris pH 7.5, 500 mM NaCl, 1 mM DTT, 50 μg/μL Lysozyme, cells lysed with sonication and clarified lysate passed through Ni-NTA column. Protein was eluted with buffer containing 50 mM Tris pH 7.5, 500 mM NaCl, 1 mM DTT and 250 mM imidazole. Fractions containing *E. coli* FabI were pooled and passed through Superdex-75 gel filtration column. Fractions containing pure FabI protein were incubated with 5 M excess of inhibitor and 2 M excess of NADH for 1 h at 4 °C. After, incubation protein was concentrated to 16 mg/mL for crystallization experiments. Crystals were grown at 20 °C using hanging drop vapour diffusion method. Crystallization well buffer contained 0.1 M sodium acetate pH 4.6, 12% PEG 4000 and 200 mM ammonium acetate. One microlitre protein solution was mixed with one microlitre of crystallization well buffer containing 0.1 M sodium acetate pH 4.6, 12% PEG 4000 and 200 mM ammonium acetate. Crystals with the dimensions of 0.1 × 0.05 × 0.05 mm were obtained overnight.

4.7. X-ray crystallography

The co-crystals were flash frozen at 100 K using 20% glycerol as cryo-protectant. The diffraction data sets were collected using in-house Rigaku RU300 X-ray generator with R-AXIS IV++ detector to a maximum resolution of 3.2 Å. Data indexing, integration and scaling were performed using DENZO and SCALEBPCK [38]. The structure was solved by molecular replacement (MR) method using the PDB code 1C14 as the template search model. Alternate cycles of restrained refinement and manual rebuilding were performed with the programs REFMAC 5.2.0001 [39,40] and Coot [41] respectively. 5% of the reflections were randomly excluded from the refinement to monitor the free residual-factor (R_{free}). A summary of the data reduction and

structure refinement statistics is provided in supplementary material. Coordinates of the X-ray structure have been deposited in the Protein Data Bank with accession codes 4JQC (AFN-1252) and 4JX8 (AEA16). Figures showing structural models were rendered using PyMOL [42]. Inhibitors could be modelled into the electron density unambiguously near the active site. Figure depicting the electron density map is shown in the supplementary information.

4.8. Metabolic stability study in mice liver microsomes

In vitro metabolism of compounds was studied in mouse liver microsomes to assess the metabolic stability at 1 μM concentration. The typical reaction mixture consists of incubation buffer (KH_2PO_4, pH 7.4), protein (liver microsomes, assay concentration: 0.3 mg/mL), NADPH (assay concentration: 1 mM) and test compound. Reaction was initiated by the addition of 20 μL of NADPH. Reaction mixture was incubated at 37 °C in a water bath. Reactions were terminated at designated time points (0, 15 and 60 min) by adding 100 μL of acetonitrile containing internal standard (carbamazapine – 0.5 μg/mL) and contents were extracted by cyclo-mixing for 2 min. This mixture was centrifuged for 5 min at 13,000 rpm and 180 μL of the clear supernatant was separated. An aliquot of 20 μL of the sample was injected onto LC-MS/MS for analysis. The percentage of parent remaining at the termination of reaction was quantified.

4.9. In vivo pharmacokinetic study protocol

The male Swiss albino mice (CD-1) (n = 8–9), weighing between 25 and 35 g were used to determine the pharmacokinetic parameters of test compounds. The oral pharmacokinetics study was conducted under fasted condition (~4 h) and animals had free access to water. Test compound was administered by oral gavage at dose of 10 mg/kg as a suspension. The excipients used for the formulation was 0.25% Tween 80 and 0.225% of sodium carboxy methyl cellulose. Blood samples (0.25 mL) were collected from retro-orbital plexus at designated time points (sparse sampling, n = 3 per time point) into micro centrifuge tubes containing 10 μL of EDTA and centrifuged at 13,000 rpm for 4 min. The supernatant plasma was stored at −20 °C until analysis. The samples were analysed for test compound concentration using a suitable LC-MS/MS method. The pharmacokinetic parameters of test compound were calculated by non-compartmental analysis using WinNonlin® Professional Version 5.2.

4.10. In vivo efficacy study protocol

All in vivo experiments were approved by the institutional animal ethics committee (IAEC). Female and male CD1 mice, 4–6 weeks old, weighing 20 ± 2 g were used in the study. Organisms were sub-cultured on Columbia blood agar (CBA) media and incubated at 35 ± 2 °C for 18–24 h. Inoculum was prepared in normal saline and further diluted with mucin to achieve final concentration of 5% (w/v). Three doses were tested per compound and/or standard drug using 6 animals per dose group (3 males, 3 females). Each mice was administered 0.5 mL of inoculum (cfu $2–3 \times 10^8$ cfu/animal) by intra-peritoneal route. One group of mice was not treated and served as untreated control (UTC). Respective vehicle control groups were also included. Test compounds and standard antibiotics were formulated in Tween 80 + 0.25% CMC for oral administration and were administered as *b.i.d.* at 1 h and 4 h post infection. Animals were monitored for 5 days and end point was determined by survival/death in each treated and untreated groups. The ED_{50} was calculated by non-linear regression analysis using GraphPad Prism software V5.

Acknowledgements

We appreciate the services extended by the Analytical Research department of Aurigene Discovery Technologies for having carried out all the analytical work. NAR, RY, IA and YKL acknowledge the support from the University of Malaya, Malaysia.

Appendix A. Supplementary data

Supplementary data related to this article can be found at http://dx.doi.org/10.1016/j.ejmech.2014.07.036.

References

[1] C.A. Loffler, C. MacDougall, Update on prevalence and treatment of methicillin-resistant *Staphylococcus aureus* infections, Expert Rev. Anti-infect. Ther. 5 (2007) 961–981.
[2] S.J. Projan, Why is big pharma getting out of antibacterial drug discovery? Curr. Opin. Microbiol. 6 (2003) 427–430.
[3] S.W. White, J. Zheng, Y. Zhang, C.O. Rock, The structural biology of type II fatty acid biosynthesis, Annu. Rev. Biochem. 74 (2005) 791–831.
[4] H. Lu, P. Tonge, Inhibitors of FabI, an enzyme drug target in the bacterial fatty acid biosynthesis pathway, J. Acc. Chem. Res. 41 (2008) 11–20.
[5] H. Xu, T.J. Sullivan, J. Sekiguchi, T. Kirikae, I. Ojima, C.F. Stratton, W. Mao, F.L. Rock, M.R.K. Alley, F. Johnson, S.G. Walker, P.J. Tonge, Mechanism and inhibition of *S. a* FabI, the enoyl reductase from *Staphylococcus aureus*, Biochemistry 47 (2008) 4228–4236.
[6] J. Schiebel, A. Chang, H. Lu, M.V. Baxter, P.J. Tonge, C. Kisker, *Staphylococcus aureus* FabI: inhibition, substrate recognition and potential implications for in vivo essentiality, Structure 20 (2012) 802–813.
[7] K.H. Kim, B.H. Ha, S.J. Kim, S.K. Hong, K.Y. Hwang, E.E. Kim, Crystal structures of enoyl-ACP reductases I (FabI) and III (FabL) from *B. subtilis*, J. Mol. Biol. 406 (2011) 403–415.
[8] L. Zhu, J. Lin, J. Ma, J.E. Cronan, H. Wang, Triclosan resistance of *Pseudomonas aeruginosa* PAO1is due to FabV, a triclosan resistant enoyl-acyl carrier protein reductase, Antimicrob. Agents Chemother. 54 (2010) 689–698.
[9] M.A. Seefeld, W.H. Miller, K.A. Newlander, W.J. Burgess, W.E. DeWolf, P.A. Elkins, M.S. Head, D.R. Jakas, C.A. Janson, P.M. Keller, P.J. Manley, D.A. Heerding, G. Chan, A.P. Fosberry, D.D. Jaworski, T.D. Moore, D.J. Payne, S. Pearson, B.J. Polozzi, X. Qiu, S.F. Rittenhouse, I.N. Uzinkas, N.G. Wallis, W.F. Huffman, Indole-naphthyridinone as inhibitors of bacterial enoyl-ACP reductases FabI and FabK, J. Med. Chem. 46 (2003) 1627–1635.
[10] J. Ramnauth, M.D. Surman, P.B. Sampson, B. Forrest, J. Wilson, E. Freeman, D.D. Manning, F. Martin, A. Toro, M. Domagala, D.E. Awrey, E. Bardouniotis, N. Kaplan, J. Berman, H.W. Pauls, 2,34,5-Tetrahydro-1H-pyrido[2,4-b and e][1,4] diazepines as inhibitors of the bacterial enoyl ACP reductase FabI, Bioorg. Med. Chem. Lett. 19 (2009) 5359–5362.
[11] P.B. Sampson, C. Picard, S. Handerson, T.E. McGrath, M. Domagala, A. Leeson, V. Romanov, D.E. Awrey, D. Thambipillai, E. Bardouniotis, N. Kaplan, J.M. Berman, H.W. Pauls, Spiro-naphthyridinone piperidines as inhibitors of *S. aureus* and *E. coli* enoyl-ACP reductase (FabI), Bioorg. Med. Chem. Lett. 19 (2009) 5355–5358.
[12] M.A. Seefeld, W.H. Miller, K.A. Newlander, W.J. Burgess, D.J. Payne, S.F. Rittenhouse, T.D. Moore, W.E. DeWolf Jr., P.M. Keller, X. Qiu, C.A. Janson, K. Vaidya, A.P. Fosberry, M.G. Smyth, D.D. Jawroski, C. Slater-Radosti, W.F. Huffman, Inhibitors of bacterial enoyl acyl carrier protein reductase (FabI): 2,9-disubstituted 1,2,3,4-tetrahydropyrido[3,4]indoles as potential antibacterial agents, Bioorg. Med. Chem. Lett. 11 (2001) 2241–2244.
[13] H. Kitagawa, T. Ozava, S. Takahata, M. Iida, M. Yamada, Phenylimidazole derivatives of 4-pyridone as dual inhibitors of bacterial enoyl-acyl carrier protein reductases FabI and FabK, J. Med. Chem. 50 (2007) 4710–4720.
[14] H. Kitagawa, K. Kumura, S. Takahata, M. Iida, K. Atsumi, 4-Pyridone derivatives as new inhibitors of bacterial enoyl-ACP reductase FabI, Bioorg. Med. Chem. Lett. 15 (2007) 1106–1116.
[15] M. Chhibber, G. Kumar, P. Parasuraman, T.N. Ramya, N. Surolia, A. Surolia, Novel diphenyl ethers: design, docking studies, synthesis and inhibition of enoyl ACP reductase of *Plasmodium falciparum* and *Escherichia coli*, Bioorg. Med. Chem. 14 (2006) 8086–8098.
[16] W.H. Miller, M.A. Seefeld, K.A. Newlander, I.N. Uzinskas, W.J. Burgess, D.A. Heerding, C.C.K. Yuan, M.S. Head, D.J. Payne, S.F. Rittenhouse, T.D. Moore, S.C. Pearson, V. Berry, W.E. DeWolf, B.J. Poloizzi, X. Qiu, C.A. Janson, Discovery of aminopyridine-based inhibitors of bacterial enoyl-ACP reductase (FabI), J. Med. Chem. 45 (2002) 3246–3256.
[17] N. Kaplan, M. Albert, D. Awrey, E. Bardouniotis, J. Berman, T. Clarke, M. Dorsey, B. Hafkin, J. Ramnauth, V. Romanov, M.B. Schmid, R. Thalakada, J. Yethon, H.W. Pauls, Mode of action, *in vitro* activity and *in vivo* efficacy of AFN-1252, a selective antistaphylococcal FabI inhibitor, Antimicrob. Agents Chemother. 56 (2012) 5865–5874.
[18] S. Escaich, L. Prouvensier, M. Saccomani, L. Durant, M. Oxoby, V. Gerusz, F. Moreau, V. Vongsothi, C. Maher, I. Morrisey, C. Soulama-Mouze, The

MUT056399 inhibitor of FabI is a new antistaphylococcal compound, Antimicrob. Agents Chemother. 55 (2011) 4692–4697.
[19] T. Bogdanovich, C. Clark, K. Kosowka-shick, B. Dewasse, P. McGhee, P.C. Applebaum, Antistaphylococcal activity of CG400549, a new experimental FabI inhibitor compared with that of other agents, Antimicrob. Agents Chemother. 51 (2007) 4191–4195.
[20] H. Schweiser, Triclosan: a widely used biocide and its link to antibiotics, FEMS Microbiol. Lett. 202 (2001) 1–7.
[21] M. Takhi, C. Murugan, M. Munikumar, K.M. Bhaskarreddy, G. Singh, K. Sreenivas, M. Sitaramkumar, N. Selvakumar, J. Das, S. Trehan, J. Iqbal, Synthesis and antibacterial activity of novel oxazolidinones bearing N-hydroxyacetamidine substituent, Bioorg. Med. Chem. Lett. 16 (2006) 2391–2395.
[22] M. Takhi, G. Singh, C. Murugan, N. Thaplyyal, S. Maitra, K.M. Bhaskarreddy, P.V.S. Amarnath, A. Mallik, T. Harisudan, R.K. Trivedi, K. Sreenivas, N. Selvakumar, J. Iqbal, Novel and potent oxazolidinones featuring 3-indolylglyoxamide, Bioorg. Med. Chem. Lett. 18 (2008) 5150–5155.
[23] PDB Reference 4JQC.
[24] While our work on azetidine ene-amide series was in progress, FAB pharma published a patent having close prior art,[25] where compounds **AEA1-3** and **AEA16** were disclosed.
[25] V. Gerusz, S. Escaich, M. Oxoby, A. Denis, Novel heterocyclic acrylamides and their use as pharmaceuticals, PCT Intl. Appl. (2011). WO 061214A1.
[26] H. Bregman, J.L. Buchanan, N. Chakka, E.F. Dimauro, B. Du, H.N. Nguyen, X.M. Zheng, Aryl carboxamide derivatives as sodium channel inhibitors for treatment of pain, PCT Intl. Appl. (2011). WO 103196.
[27] W.A. Slusarchyk, S.A. Bolton, K.S. Hartl, M.H. Huang, G. Jacobs, W. Meng, M.L. Ogletree, Z. Pi, W.A. Schumacher, S.M. Seiler, J.C. Sutton, U. Treuner, R. Zahler, G. Zhao, G. Bisacchi, Synthesis of potent and highly selective inhibitors of human tryptase, Bioorg. Med. Chem. Lett. 12 (2002) 3235–3238.
[28] M.A.J. Duncton, M.A. Estiarte, R.J. Johnson, M. Cox, D.J.R. O'Mahony, W.T. Edwards, M.G. Kelly, Preparation of heteroaryloxetanes and heteroarylazetidines by use of Minisci reaction, J. Org. Chem. 74 (2009) 6354–6357.
[29] M. Takhi, H. Subramanya, S.K. Panigrahi, M. Munikumar, K.C. Reddy, Substituted pyridine derivatives as FabI inhibitors, PCT Intl. Appl. (2013). WO 080222.
[30] J. Berman, P. Sampson, H.W. Pauls, J. Ramnauth, D. Manning, M.D. Surman, D. Xie, H.Y. Decornez, Heterocyclic compounds, methods of making them and their use in therapy, PCT Intl. Appl. (2004). WO 052890.
[31] J.M. Berman, M.D. Schmid, J.D. Medelin, N. Kaplan, Compositions Comprising Multiple Bioactive Agents, and Methods of Using the Same, US0142265A1 (2006).
[32] R. O'Shea, H.E. Moser, Physicochemical properties of antibacterial compounds: implications in drug discovery, J. Med. Chem. 51 (2008) 2871–2878.
[33] PDB Reference 4JX8.
[34] J. Schiebel, A. Chang, S. Shah, Y. Lu, L. Liu, P. Pan, M.W. Hirschbeck, M. Tareilus, S. Eltschkner, W. Yu, J.E. Cummings, S.E. Knudson, G.R. Bommineni, S.G. Walker, R.A. Slayden, C.A. Sotriffer, P.J. Tonge, C. Kisker, Rational design of broad spectrum antibacterial activity based on a clinically relevant enoyl-acyl carrier protein (ACP) reductase inhibitor, J. Biol. Chem. 289 (2014) 15987–16005.
[35] X. Qiu, C.A. Janson, R.I. Court, M.G. Smyth, D.J. Payne, S.S. Abdel-Meguid, Molecular basis for triclosan activity involves a flipping loop in the active site, Protein Sci. 8 (1999) 2529–2532.
[36] Y. Li, W. G Lai, A. Whitcher-Johnstone, C.A. Busacca, M.C. Eriksson, J.C. Lorenz, D.J. Tweedie, Metabolic switching of BILR 355 in the presence of ritonavir. I. Identifying an unexpected disproportionate human metabolite, Drug. Metab. Dispos. 40 (2012) 1122–1129.
[37] M.J. Stewart, S. Parikh, G. Xiao, P.J. Tonge, C. Kisker, Structural basis and mechanism of enoyl reductase inhibition by triclosan, J. Mol. Biol. 290 (1999) 859–865.
[38] Z. Otwinowski, W. Minor, Processing of X-ray diffraction data collected in oscillation mode, in: C.W. Carter Jr., R.M. Sweet (Eds.), Methods in Enzymology, Macromolecular Crystallography, Part A, vol. 276, Academic Press, New York, 1997, pp. 307–326.
[39] Collaborative Computational Project, Number 4, The CCP4 suite: programs for protein crystallography, Acta Crystallogr. D Biol. Crystallogr. 50 (1994) 760–763.
[40] A.A. Vagin, R.S. Steiner, A.A. Lebedev, L. Potterton, S. McNicholas, F. Long, G.N. Murshudov, REFMAC5 dictionary: organisation of prior chemical knowledge and guidelines for its use, Acta Crystallogr. D60 (2004) 2284–2295.
[41] P. Emsley, K. Cowtan, Coot: model-building tools for molecular graphics, Acta Crystallogr. D60 (2004) 2126–2132.
[42] W.L. DeLano, The PyMOL Molecular Graphics System, 2002 on World Wide Web, http://www.pymol.org.

Bioorganic & Medicinal Chemistry 23 (2015) 4669–4680

Contents lists available at ScienceDirect

Bioorganic & Medicinal Chemistry

journal homepage: www.elsevier.com/locate/bmc

Benzimidazole derivatives as potential dual inhibitors for PARP-1 and DHODH

Iskandar Abdullah [a,*], Chin Fei Chee [a,b,e], Yean-Kee Lee [a], Siva Sanjeeva Rao Thunuguntla [c], K. Satish Reddy [c], Kavitha Nellore [c], Thomas Antony [c,*], Jitender Verma [c], Kong Wai Mun [b], Shatrah Othman [a,d], Hosahalli Subramanya [c], Noorsaadah Abd. Rahman [a,*]

[a] Drug Design and Development Research Group, Department of Chemistry, Faculty of Science, University of Malaya, Malaysia
[b] Aurigene Discovery Technologies (Malaysia) Sdn. Bhd, Malaysia
[c] Aurigene Discovery Technologies (India) Ltd, India
[d] Department of Molecular Medicine, Faculty of Medicine, University of Malaya, Malaysia
[e] School of Pharmacy, International Medical University, 57000 Kuala Lumpur, Malaysia

ARTICLE INFO

Article history:
Received 8 April 2015
Revised 28 May 2015
Accepted 29 May 2015
Available online 5 June 2015

Keywords:
Poly (ADP-ribose) polymerase
PARP
PARP-1
Dihydroorotate dehydrogenase
DHODH
Benzimidazole

ABSTRACT

Poly (ADP-ribose) polymerases (PARPs) play diverse roles in various cellular processes that involve DNA repair and programmed cell death. Amongst these polymerases is PARP-1 which is the key DNA damage-sensing enzyme that acts as an initiator for the DNA repair mechanism. Dihydroorotate dehydrogenase (DHODH) is an enzyme in the pyrimidine biosynthetic pathway which is an important target for anti-hyperproliferative and anti-inflammatory drug design. Since these enzymes share a common role in the DNA replication and repair mechanisms, it may be beneficial to target both PARP-1 and DHODH in attempts to design new anti-cancer agents.

Benzimidazole derivatives have shown a wide variety of pharmacological activities including PARP and DHODH inhibition. We hereby report the design, synthesis and bioactivities of a series of benzimidazole derivatives as inhibitors of both the PARP-1 and DHODH enzymes.

1. Introduction

Poly (ADP-ribose) polymerases (PARPs) comprise 18 putative family members of the nuclear enzymes that have significant roles in multifunctional cellular processes, including detection and repair of damaged DNA and RNA.[1] PARP-1, PARP-2 and PARP-3 are the best studied members of this family of enzymes due to their role in DNA repair.[24] Other distinct biochemical activities of PARP-1 are epigenetic chromatic modifications, genomic stability regulations,[7,22] replication and transcription of DNA[18] and distinctive cell death formation known as parthanatos.[10,14] PARP-1 is known to be the trigger point in the DNA repair mechanism for single strand breaks where it acts as the DNA damage-sensing enzyme. In response to DNA damage that may have occurred due to radiation or chemotherapeutic agents, PARP-1 initiates its repair process by binding to the damaged site and catalyzing the synthesis of long, branched poly (ADP-ribose) chains using nicotinamide adenine dinucleotide (NAD+) as the substrate. These actions of PARP-1 result in the resistance that frequently develops after cancer therapy. Hence inhibition of the PARP-1 enzyme is believed to enhance sensitivity towards radiotherapy and certain kinds of DNA targeting cancer chemotherapies.[17]

To date, a significant number of potent PARP-1 inhibitors have been reported accentuating the role of PARP-1. Inhibition of PARP in homologous recombination (HR) deficient tumor cells have also exclusively explained the crucial role of PARP-1 in DNA repair.[11,28] These inhibitors generally bind to the nicotinamide binding site of the PARP-1 catalytic domain, thus inhibiting automodification and subsequent release of the enzyme from the site of DNA damage as well as preventing the access of other repair proteins to the site of DNA damage. The binding of these inhibitors mimics the binding mode of nicotinamide towards PARP-1 with key interactions to Ser243 (C=O to O—H Ser) and Gly202 (C=O to N—H Gly and N—H to C=O Gly) through hydrogen-bonding and π–π stacking with Tyr246, which is approximately coplanar with the benzimidazole moiety of the ligand.[29] In addition, Griffin and co-workers reported an intramolecular hydrogen bond between the carboxamide hydrogen on C2 of the indole ring to the nitrogen in the indole ring. This intramolecular H-bond resulted in a pseudo-6-membered ring, creating a rigid 6:6:5 tricyclic system which improved its potency.[15,25] A water molecule also plays a crucial role at the

* Corresponding authors. Tel.: +60 3 79674049; fax: +60 3 79674139.
E-mail address: Iskandar.a@um.edu.my (I. Abdullah).

http://dx.doi.org/10.1016/j.bmc.2015.05.051
0968-0896/

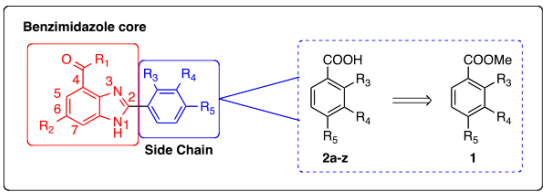

Scheme 1. Side chain preparation from phenyl ester **1**.

active site by interacting with the catalytically important carboxylate group of Glu327 which forms a hydrogen bond with the NH indole of benzimidazole of the ligand.[29,30]

Inhibition of pyrimidine biosynthesis has been shown to have an efficacious anti-proliferative effect on cells that are dividing rapidly.[13] Mitochondrial enzyme, dihydroorotate dehydrogenase (DHODH) catalyzes the fourth step in the de novo biosynthetic pathway of pyrimidines, converting dihydroorotate to orotate by oxidative reaction, with flavin mononucleotide (FMN) and ubiquinone (CoQ) acting as co-factors.[13] This enzyme has been identified as a therapeutic target for treatment of cancer,[9,12] as well as several autoimmune disorders such as rheumatoid arthritis and multiple sclerosis.[16] Inhibition of enzymatic activities has been reported on *h*DHODH and *Pf*DHODH by X-ray crystallographic studies with known inhibitors such as leflunomide, teriflunomide (the active metabolite of leflunomide) and brequinar. These inhibitors are positioned in the suggested ubiquinone binding site where polar and hydrophobic residues contribute to the binding. The carboxylic acid group from the inhibitors shows good hydrogen-bonding interactions with the guanidinyl moiety of Arg136 and an additional hydrogen bonding interaction to the side chain of Gln47.

Targeting both PARP-1 and DHODH for anti-cancer therapy would certainly be beneficial as these enzymes share a common role in the DNA replication and repair mechanisms which are involved in the hyper-proliferation of cancer cells. Since benzimidazole-containing compounds have been reported to show good

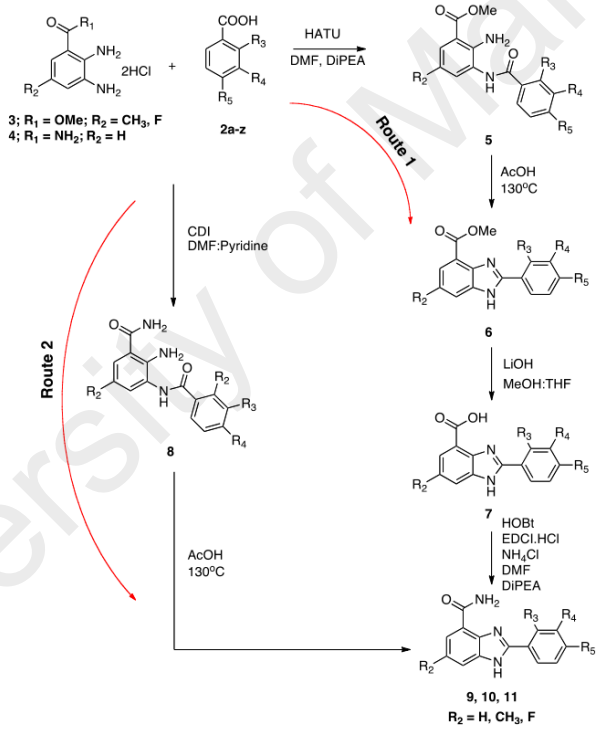

Scheme 2. General strategy for the synthesis of benzimidazole carboxamide and carboxylic acid derivatives.

pharmacological activity against these targets,[6,8,23] we have chosen them as lead structures in the search for dual PARP-1/DHODH inhibitors described in this study.

2. Results and discussion

2.1. Chemistry

Numerous reports on benzimidazole ring system construction have been published.[3,20,21]

We started off with the preparation of methyl ester **1** with different functional groups placed at the *ortho* (R_3), *meta* (R_4) and *para* (R_5) positions of the phenyl ring moiety to be connected at position 2 of the benzimidazole core as shown in Scheme 1. Saponification of **1** led to carboxylic acids **2a–z** (Supporting information). Two different routes were employed to prepare the benzimidazole compounds (Scheme 2). Route 1 involved coupling of diamine **3** using standard 1-[bis(dimethylamino)methylene]-1*H*-1,2,3-triazolo[4,5-*b*]pyridinium 3-oxide hexafluorophosphate (HATU) in dimethylformamide and the presence of *N*,*N*-diisopropylethylamine (DiPEA) as base[31] for the formation of **5**. Subsequent thermal cyclization of **5** in AcOH gave intermediate **6**. Saponification of ester **6** with LiOH provided carboxylic acid derivatives **7a–g** (Table 1), which were then converted to the corresponding carboxamide benzimidazole derivatives **9a–i**, **10a–i** and **11a–j** with hydroxybenzotriazole (HOBt) and 1-ethyl-3-(3-dimethylaminopropyl)carbodiimide (EDCI).

Alternatively, **9a–i**, **10a–i** and **11a–j** (Table 2) could be prepared via Route 2. Reacting 2,3-diaminobenzamide (**4**) with **2a–z** in the presence of 1,1′-carbonyldiimidazole (CDI) in pyridine and dimethylformamide (DMF) (1:1 v/v) gave amide **8** which could be cyclized to benzimidazole **9**, **10** and **11** by refluxing in AcOH as reported by Penning and co-workers.[20]

2.2. Pharmacological evaluation

2.2.1. Poly (ADP-ribose) polymerase (PARP) colorimetric assay

The inhibitory effect of compounds **7a–g**, **9a–i**, **10a–i** and **11a–j** on PARP-1 activity was measured using an HT Universal Colorimetric PARP assay kit (Trevigen, Gaithersburg, MD, USA). With slight modification, the assays were carried out by quantifying the incorporation of biotinylated poly (ADP-ribose) onto histone proteins in 96-well plate. In brief, the experiment began with pre-incubating 10 μl of PARP-1 enzyme (0.25 U) with 15 μl of tested compounds in rehydrated histone-coated wells followed by addition of 25 μl of PARP cocktail mixture containing 2 μl of 10× PARP Cocktail, 2 μl of 10× activated DNA and 21 μl of 1× PARP buffer into the wells. After 60 min of incubation, the wells were washed twice with 1× PBS + 0.1% Triton X-100 followed by 1× PBS. 50 μl of 1× Strep-HRP was then added and incubated for 60 min. The wells were washed again as in the previous step. 50 μl of pre-warmed TACS-Sapphire substrate was added and the mixture was incubated for 15 min in the dark. The reactions were terminated with 50 μl 0.2 M HCl. The absorbance reading at 450 nm was measured using a VICTOR X5 2030 Multilabel Reader (Perkin–Elmer, Waltham, MA, USA). IC_{50} values were determined by fitting the activity data at different concentrations of the compound to a sigmoidal dose–response curve using GraphPad Prism software version 6.00.

2.2.2. Dihydroorotate dehydrogenase (DHODH) enzymatic assay

Compounds **7a–g**, **9a–i**, **10a–i** and **11a–j** were evaluated for their potency to inhibit DHODH in a coupled enzymatic spectrophotometric assay. The assay is based on the decrease in absorbance at 610 nm resulting from the oxidation of L-dihydrooroticacid (L-DHO) facilitated by the reduction of 2,6-dichloroindophenol (DCIP) and decylubiquinone (DUQ).[2] The decrease in absorbance at 610 nm is proportional to the reduction of DCIP. The assay buffer was 50 mM TrisHCl, 150 mM KCl and 0.8% Triton, pH 8.0. A 100 μl reaction mixture was used in 96-well plates at room temperature. A mixture of 82 μl of enzyme (25 ng) in buffer and 5 μl of test compounds were pre-incubated for 30 min and the reaction was started by adding 13 μl of substrate mixture (20 mM of L-DHO, 2 mM of DUQ and 2 mM of DCIP). The final concentration of DMSO used was 1%. The absorbance of each well was measured after 20 min of the reaction at 610 nm using a VICTOR X5 Multilabel Reader (Perkin–Elmer) every 10 min for 1 h. IC_{50} values were determined from the dose response plot using GraphPad Prism software version 6.00.

The preliminary activity for both the PARP and DHODH assays was measured at 10 μM concentration of the synthesized compounds (**7a–g**, **9a–i**, **10a–i** and **11a–j**) along with veliparib and brequinar as reference inhibitors (Table 3).

Table 1
Chemical structure of benzimidazole carboxylic acid derivatives synthesized via Scheme 2

Entry	Compound
7a	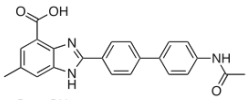
7b	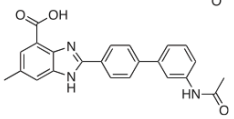
7c	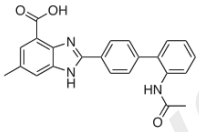
7d	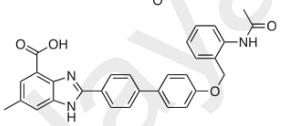
7e	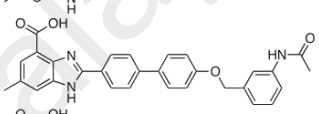
7f	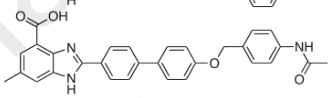
7g	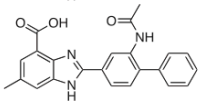

2.4. Structure–activity relationship (SAR) studies

In this work, we designed and synthesized diversified compounds (as shown in Table 3) by substituting various electron-

Table 2
Chemical structure of benzimidazole carboxamide derivatives synthesized via Scheme 2

Entry	Product	Entry	Product	Entry	Product
9a[a]	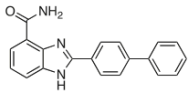	**10a**	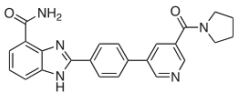	**11a**	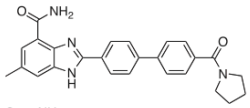
9b	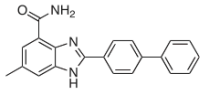	**10b**	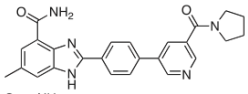	**11b**	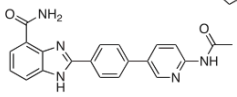
9c[b]	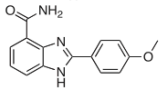	**10c**	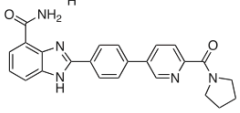	**11c**	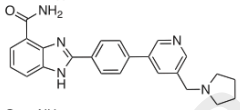
9d	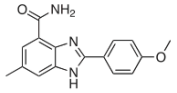	**10d**	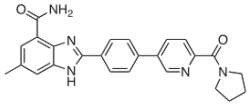	**11d**	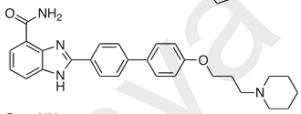
9e[b]	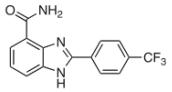	**10e**[a]	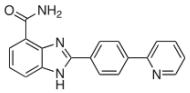	**11e**	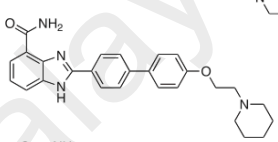
9f	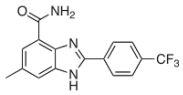	**10f**	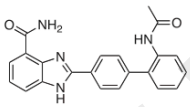	**11f**	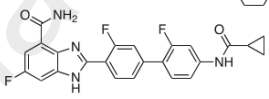
9g	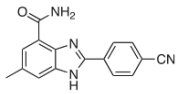	**10g**	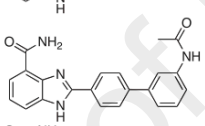	**11g**	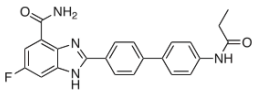
9h	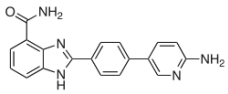	**10h**	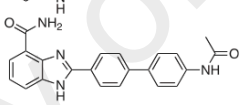	**11h**	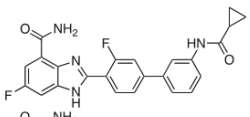
9i[a]	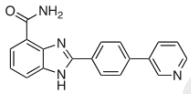	**10i**	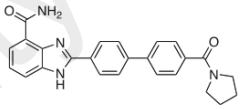	**11i**	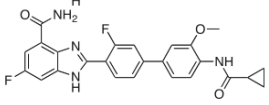
				11j	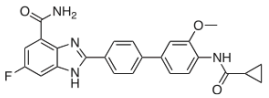

[a] Compounds reported by Tong and group.[27]
[b] Compounds reported by Alex and group.[29]

donating and electron-withdrawing groups into the benzimidazole scaffold and evaluated their biological activities for the two targets, PARP-1 and DHODH. The compounds were docked into PARP-1 and DHODH, and their interactions with the active site residues were analyzed in order to rationalize their potencies in the two targets. Compound **I1** (Fig. 1) has been reported by Thunuguntla's group to inhibit DHODH[26] with IC_{50} of 0.75 μM. Replacing the carboxylic acid substituent at the C4 position of the benzimidazole ring in this compound with an amide functionality (**9a**) gave improved activity against PARP-1 (IC_{50} = 0.71 μM), but at the same time the DHODH potency was reduced by several folds (IC_{50} = 9.80 μM). Introduction of the amide group probably would have reduced

Table 3
PARP-1 and DHODH inhibition by benzimidazole derivatives

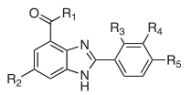

Entry	R_1	R_2	R_3	R_4	R_5	PARP-1 IC_{50} (μM)/% inhibition at 10 μM	DHODH IC_{50} (μM)/% inhibition at 10 μM
Veliparib (ABT-888)					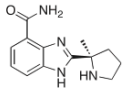	0.005	–
Brequinar					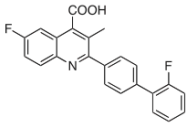	–	0.012
9a[a]	NH_2	H	H	H		0.71	9.80
9b	NH_2	CH_3	H	H		28%	7.80
9c[b]	NH_2	H	H	H	$-OCH_3$	NA	NA
9d	NH_2	CH_3	H	H		NA	NA
9e[b]	NH_2	H	H	H	$-CF_3$	NA	NA
9f	NH_2	CH_3	H	H		NA	NA
9g	NH_2	CH_3	H	H	–CN	NA	NA
9h	NH_2	H	H	H	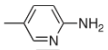	0.032	20
9i[a]	NH_2	H	H	H		0.022	19
10a	NH_2	H	H	H	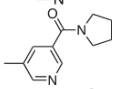	0.029	28
10b	NH_2	CH_3	H	H		NA	50
10c	NH_2	H	H	H	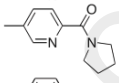	0.012	NA
10d	NH_2	CH_3	H	H		17	37
10e[a]	NH_2	H	H	H		0.083	28
10f	NH_2	H	H	H		0.14	51
10g	NH_2	H	H	H	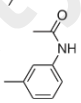	0.46	42
10h	NH_2	H	H	H	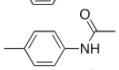	16	56
10i	NH_2	H	H	H	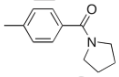	0.31	20
11a	NH_2	CH_3	H	H		NA	NA
11b	NH_2	H	H	H	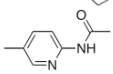	0.049	40

(*continued on next page*)

Table 3 (*continued*)

Entry	R_1	R_2	R_3	R_4	R_5	PARP-1 IC_{50} (μM)/% inhibition at 10 μM	DHODH IC_{50} (μM)/% inhibition at 10 μM
11c	NH_2	H	H	H	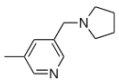	0.061	55
11d	NH_2	CH_3	H	H	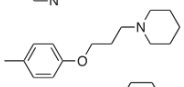	2.28	NA
11e	NH_2	H	H	H	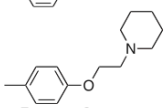	0.72	31
11f	NH_2	F	F	H	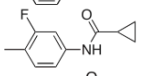	0.084	48
11g	NH_2	F	H	H	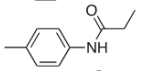	1.72	NA
11h	NH_2	F	F	H	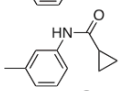	1.28	38
11i	NH_2	F	F	H	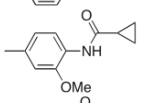	0.98	23
11j	NH_2	F	H	H		5.96	NA
7a	OH	CH_3	H	H	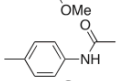	NA	0.21
7b	OH	CH_3	H	H	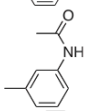	NA	1.38
7c	OH	CH_3	H	H		NA	32
7d	OH	CH_3	H	H	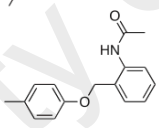	10.63	0.30
7e	OH	CH_3	H	H	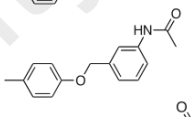	NA	0.028
7f	OH	CH_3	H	H	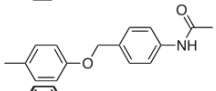	44	0.013
7g	OH	CH_3	H	NHAc		NA	47

The activity is expressed as percent inhibition at 10 μM or IC_{50} values.
*NA = not active (less than 15% inhibition @ 10 μM).
[a] Compounds reported by Tong and group.[27]
[b] Compounds reported by Alex and group.[29]

the strength of H-bonding in this crucial region of the DHODH active site, which appears to prefer a purely acceptor moiety (like the COOH group which gets deprotonated at pH 7.4) to form H-bonds with the donor groups of Arg136 and Gln47, and a

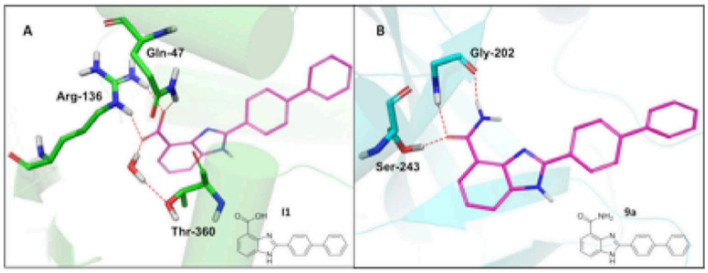

Figure 1. Docking modes showing the interactions of compounds **I1** (A) and **9a** (B) in DHODH (pdb ID: 4IGH) and PARP-1 (pdb ID: 4HHZ), respectively.

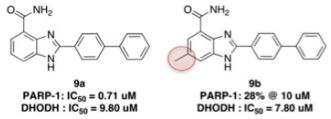

Figure 2. Structure and biochemical activity of compounds **9a** and **9b**.

water-mediated H-bond with Thr360 (Fig. 1A). This observation indicated that the COOH group at C4 position favors DHODH activity, while the $CONH_2$ substituent favors PARP-1 activity (by gaining polar contacts with the donor and acceptor groups of Ser243 and Gly202 as shown in Fig. 1B). Incorporating a CH_3 group at the R_2 position of the benzimidazole ring (**9b**) proved detrimental for PARP-1 activity, but it slightly improved the DHODH potency (Fig. 2). This might be due to the availability of enough space to accommodate a methyl group at this particular site of the DHODH pocket, in comparison to that in the PARP-1 active site where the same group could not be endured well.

Compounds **9c–g**, with functional groups other than a phenyl ring at the *para* position (R_5) were found to be completely inactive for both targets. Substituting a strongly electron-donating methoxy group at R_5 position (**9c** and **9d**), produced a devastating effect on the activity. Another approach was then carried out by substituting strong electron-withdrawing groups at this position such as $–CF_3$ (**9e** and **9f**) and –CN (**9g**), but these also proved to be inactive. These observations indicated that instead of small electron donating or withdrawing groups, a relatively bulkier system (e.g., in the form of a second phenyl ring) is required to sufficiently occupy the space available around this position in both PARP-1 and DHODH enzymes.

Further investigations were performed on the second phenyl ring in order to study the effect of substituting various functional groups at its *ortho*, *meta* and *para* positions. Incorporation of an acetamide group (NHAc) at the *ortho* (**10f**) and *meta* (**10g**) positions showed significant improvement especially in PARP-1 potency, but *para* substitution (**10h**) resulted in the loss of activity compared to the parent compound **9a**. These *o*- and *m*-acetamide substitutions showed H-bonding interactions with Arg217 (water-mediated) and Asp105, respectively, but the *p*-substitution failed to fetch any such interaction in PARP-1. In case of DHODH, the *o*-(**10f**) and *p*-(**10h**) acetamide substituted compounds did show H-bonding with Tyr38 and Leu67, respectively, but they only seemed to result in around 50% inhibition of the activity at 10 μM concentration (compound **10g** also demonstrated 45% inhibition of the DHODH activity at a relatively lower concentration of 1 μM). The interactions between compound **10g** and the active site residues of DHODH and PARP-1 is shown in Figure 3.

Substituting pyrrolidinyl methanone at the *para* position of the second phenyl ring as in the compounds **10c** and **10i** showed comparable potency in PARP-1 but poor activity in DHODH enzyme. As observed with compound **9b**, methyl substitution at the R_2 position for compounds **10d** and **11a** resulted in diminished activities, particularly for PARP-1 enzyme. When pyrrolidinyl methanone was substituted at position 3 of the pyridine ring as depicted by compounds **10a** and **10b**, a reduction in the activity was observed against both PARP-1 and DHODH as compared to the parent compound **9i**. Compound **10b** showed poor activity in PARP-1 probably due to the presence of the unfavorable $–CH_3$ group at the R_2 position. It is noteworthy that in all these analogs, the pyrrolidinyl methanone moiety could not gain any polar contact in the active site of both PARP-1 and DHODH. Increasing the chain length at *para* position of the second phenyl ring of the benzimidazole in compound **11d** did not result in good inhibitory activities. Compound **11e**, with one carbon atom less than **11d** however, exhibited reasonable activity. In both these compounds, the piperidinyl nitrogen got protonated at pH 7.4 and entered into H-bonding with Ile218 and Tyr38 in PARP-1 and DHODH, respectively.

Substituting the R_5 position of the benzimidazole scaffold with a hetero-aromatic moiety and removing the methyl substituent from the R_2 position dramatically improved the PARP-1 activity as exhibited by compound **9i** (IC_{50} = 0.022 μM). A slight decrease in activity was observed with electron donating groups attached to the hetero-aromatic moiety, for example, in compounds **9h** ($–NH_2$, IC_{50} = 0.032 μM) and **11b** ($–NHCOCH_3$, IC_{50} = 0.049 μM). Compound **10e** with a 2-pyrinyl moiety at R_5 position showed a drop in activity in PARP-1 with IC_{50} of 0.083 μM. The compounds **9h** and **11b** with polar groups (NH_2 and NHAc, respectively) towards the solvent exposed region could not fetch any polar interaction in PARP-1 active site. Though the pyridyl nitrogen (in most of the acetamide analogs) and the $–NHCOCH_3$ group in **11b** did form H-bond with Tyr38 and Leu67, respectively, in the DHODH pocket, but they failed to enhance the potency. In addition, a 3-fold drop in PARP-1 activity was observed with compound **11c** having a methyl-pyrrolidine moiety at position 3 of the pyridine ring (IC_{50} = 0.061 μM), but at the same time there is an increase in the DHODH activity to 55% at 10 μM concentration. However, the protonated nitrogen of the methyl-pyrrolidine group in this compound could not gain any polar contact in both the PARP-1 and DHODH enzymes.

The effects of fluoro and cyclopropane substitutions as bioisosteres were also investigated while maintaining the carboxamide group at the R_4 position of the benzimidazole scaffold. The only compound which demonstrated modest PARP-1 and DHODH dual activities was **11f** with fluorine substituted at R_3 and *meta* position of the second phenyl ring, in addition of the cyclopropanecarboxamide group at the *para* position. However, other compounds in

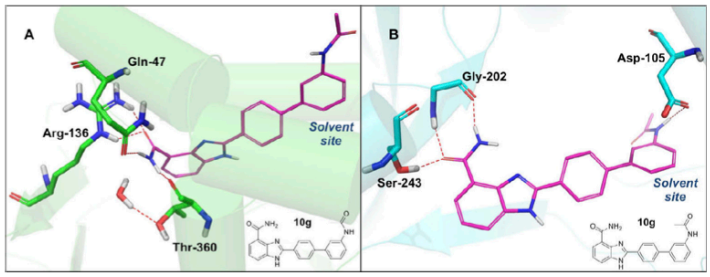

Figure 3. Docking modes showing the interactions of compound **10g** in DHODH (A, pdb ID: 4IGH) and PARP-1 (B, pdb ID: 4HHZ), respectively.

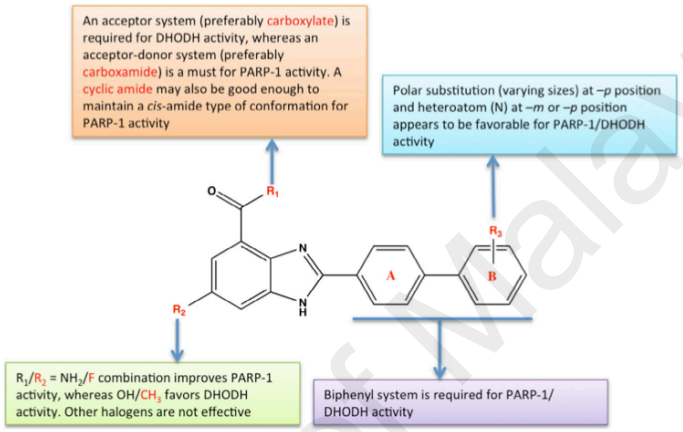

Figure 4. Summary of the SAR points for possible dual inhibition of DHODH and PARP-1 enzymes.

the same class, **11g**, **11h**, **11i** and **11j**, failed to exhibit any improvement in the dual activity. Compared to the methyl group, fluoro was well tolerated at R_2 position and resulted in improved PARP-1 activity. The cyclopropanecarboxamide group in most of these analogs formed H-bonding with Tyr49 and Leu67 in PARP-1 and DHODH, respectively.

Since it has been reported that the –COOH group at the R_4 position is favorable for DHODH activity,[4,5,19] we proceeded to synthesize seven benzimidazole carboxylic acid derivatives (Table 1). All these compounds have a methyl group at R_2 position, along with varied substitutions primarily on the second phenyl ring. Compound **7a** with an acetamide group at the *para* position of the second phenyl ring showed reasonably good DHODH activity (IC_{50} = 0.21 μM), compared to the *ortho* (**7c**) and *meta* (**7b**) substituted analogs. Similarly, compounds **7d**, **7e**, and **7f**, with a much bulkier substitution at the *para* position of the second phenyl ring displayed modest DHODH inhibitory activities (IC_{50} = 0.30 μM, 0.028 μM, and 0.013 μM, respectively). However, all the compounds shown in Table 1 had weak activity for PARP-1 except for compound **7f** which exhibited 44% inhibition at 10 μM concentration. The diminished PARP-1 activity of all these compounds may be attributed partly to the detrimental effect of methyl group at R_2 position, as well as to the absence of the favorable carboxamide moiety at R_4 position of the benzimidazole moiety. A summary of our SAR findings with respect to PARP-1 and DHODH dual inhibition is shown in Figure 4.

3. Conclusion

We have studied various benzimidazole derivatives as prospective inhibitors of both PARP-1 and DHODH enzymes. All the compounds have been synthesized in good yields. Several compounds, namely **7f**, **10g**, **11c** and **11f** showed dual potencies, albeit with relatively lower activity for both the targets. These compounds, however, can be considered for further study to understand the binding mechanisms and enhance their potential as dual inhibitors of PARP-1 and DHODH.

4. Experimental

4.1. Modeling

4.1.1. Ligand and protein preparation

The 2D structures of the ligands were sketched using ChemBioDraw Ultra 12.0 program and then converted into 3D format with the *LigPrep* utility of Schrödinger Software Suite 2014-1.

Similarly the protein–ligand complexes, obtained from the Protein Data Bank (PDB ID: 4IGH for DHODH and 4HHZ for PARP-1) were prepared using the *Protein Preparation Wizard* utility of the software. Hydrogen atoms were added, bond orders assigned, missing side-chains filled, and water molecules outside the active site deleted, followed by restrained minimization to relieve the strain and steric clashes in the protein–ligand complexes.

4.1.2. Receptor-grid generation

Using the *Glide* module of the Schrödinger Software Suite, the active site was defined by constructing a receptor grid spanning amino acid residues within a distance of around 10 Å from the co-crystallized ligand in the protein complexes. Some key hydrogen-bonding constraints (involving residues such as Gln47 and Arg136 in DHODH and Gly202 and Ser243 in PARP-1) were also defined while generating the receptor grid, to be employed in protein–ligand docking.

4.1.3. Protein–ligand docking

The prepared ligands (in sdf format) and protein structures (as receptor grids) were supplied as input files to the *Glide* module of the software for docking. During *Glide* docking, extra precision (XP) mode was employed. The protein was kept rigid, while ligands were given full flexibility in addition to sampling of nitrogen inversions and ring conformations. However the amide torsions were restricted to the *trans*-conformation only. Other parameters included adding *Epik* state penalties to docking scores, rewarding intramolecular hydrogen bonds, and enhancing planarity of the conjugated pi groups. The docking protocol was set to report at least 10 poses per ligand, which were viewed and analyzed within the protein active site for desired interactions using the *Maestro* viewer of the Schrodinger Software Suite.

4.2. Chemistry

Chemicals and reagents were either purchased from Merck, Sigma–Aldrich or provided by Aurigene Discovery Technologies Limited and used without further purification. NMR spectra were recorded on JEOL Lambda 400 and ECA 400. Thin layer chromatography (TLC) were carried out by using aluminum sheets TLC silica 60 F_{254} and flash column chromatography used were silica gel (40–60 μm) purchased from Merck. Anhydrous tetrahydrofuran (THF) used were purified from PureSolv solvent purification system and dichloromethane (CH_2Cl_2) were distilled from CaH_2 prior to use. Melting point were measured with Stuart Melting 30 (SMP 30) apparatus. Semi-preparative HPLC was performed on Waters HPLC Binary PUMP 1525, Waters Photodiode Array Detector 2998 with Merck Chromolith® Performance Reverse-phase C-18 column (100–4.6 mm). LC/MS was run on Agilent 1200 Series/Agilent Technologies 6530 Q-TOF (ESI) with Agilent Zorbax C-18 column.

4.2.1. General procedure for synthesis of 5

To a round bottom flask equipped with a magnetic stir bar was added diamine benzoate (**3**; $R_2 = CH_3$; F) (1 mmol), carboxylic acid **2a–z** (1 mmol), HATU (1.3 mmol) and dissolved in DMF (6 ml) stirred under N_2 gas. DiPEA (2 ml) was then added to the mixture and reaction mixture was left to stir for 3 h. Water (100 ml) was added to the reaction mixture, filtered and dried to afford **5** which was used without further purification.

4.2.2. General procedure for synthesis of 6

Compound **5** was dissolved in acetic acid (10 ml/mmol) and refluxed at 130 °C until reaction is fully completed under TLC analysis monitoring. Flash column chromatography with EtOAc/Hex (3:1 v/v) elution yielded purified compound **6**.

4.2.3. General procedure for synthesis of 7

Compound **6** was dissolved in mixture of MeOH/THF (1:1 v/v) followed by the addition of $LiOH{\cdot}H_2O$ (3–5 equiv) per mol and the reaction mixture was allowed to stir overnight. Upon reaction completion, solvents were removed in vacuo. The resulted aqueous mixture pH was adjusted to 2 with 10% HCl to obtain the desired product **7** which was filtered and dried and used without further purification.

4.2.3.1. 2-(4′-Acetamido-[1,1′-biphenyl]-4-yl)-6-methyl-1*H*-benzimidazole-4-carboxylic acid (7a). ^{1}H NMR (400 MHz, DMSO-d_6): δ 10.28 (s, NH), 8.33 (d, J = 8.3, 2H), 7.91 (d, J = 8.0, 2H), 7.83 (s, 1H), 7.81 (s, 1H), 7.75 (d, J = 9.0, 2H), 7.72 (d, J = 8.8, 2H), 2.50 (s, 3H), 2.06 (s, 3H). ^{13}C NMR (100 MHz, DMSO-d_6): δ 169.10, 166.12, 151.38, 143.58, 139.96, 135.99, 134.90, 133.14, 131.05, 129.69, 128.22, 127.49, 126.71, 123.07, 119.71, 119.44, 117.08, 24.23, 21.12. HRMS (ESI) calculated for $C_{23}H_{19}N_3O_3$ $(M+H)^+$: 386.1504, found 386.1499.

4.2.3.2. 2-(3′-Acetamido-[1,1′-biphenyl]-4-yl)-6-methyl-1*H*-benzimidazole-4-carboxylic acid (7b). ^{1}H NMR (270 MHz, DMSO-d_6): δ 10.08 (s, NH), 8.37 (d, J = 8.1, 2H), 7.97 (s, 1H), 7.76 (d, J = 8.4, 2H), 7.70 (s, 1H), 7.65 (s, 1H), 7.60 (br s, 1H), 7.41 (s, 1H), 7.39 (s, 1H), 2.46 (s, 3H), 2.07 (s, 3H). ^{13}C NMR (67 MHz, DMSO-d_6): δ 168.67, 166.83, 152.52, 141.74, 140.04, 139.82, 129.53, 128.60, 128.12, 126.91, 125.80, 121.57, 118.67, 117.32, 24.12, 21.02. HRMS (ESI) calculated for $C_{23}H_{19}N_3O_3$ $(M+H)^+$: 386.1504, found 386.1502.

4.2.3.3. 2-(2′-Acetamido-[1,1′-biphenyl]-4-yl)-6-methyl-1*H*-benzimidazole-4-carboxylic acid (7c). ^{1}H NMR (270 MHz, CD_3OD): δ 8.03 (d, J = 8.3, 2H), 7.84 (s, 1H), 7.53 (d, J = 8.3, 1H), 7.40 (d, J = 8.3, 2H), 7.38 (d, J = 5.9, 1H), 7.30–7.21 (m, 3H), 2.33 (s, 3H), 1.88 (s, 3H). ^{13}C NMR (67 MHz, CD_3OD): δ 172.44, 167.62, 154.55, 145.16, 142.97, 138.17, 135.47, 133.25, 131.39, 130.50, 129.48, 128.58, 128.52, 128.46, 127.96, 127.44, 124.14, 115.25, 22.92, 21.29. HRMS (ESI) calculated for $C_{23}H_{19}N_3O_3$ $(M+H)^+$: 386.1504, found 386.1510.

4.2.3.4. 2-(4′-((2-Acetamidobenzyl)oxy)-[1,1′-biphenyl]-4-yl)-6-methyl-1*H*-benzimidazole-4-carboxylic acid (7d). ^{1}H NMR (400 MHz, DMSO-d_6): δ 9.66 (s, NH), 8.40 (d, J = 8.5, 2H), 7.96 (d, J = 7.9, 2H), 7.89 (br s, 2H), 7.80 (d, J = 8.5, 2H), 7.47 (d, J = 7.3, 1H), 7.43 (d, J = 7.9, 1H), 7.30 (t, J = 7.9, 1H), 7.20 (t, J = 7.3, 1H), 7.12 (d, J = 8.5, 2H), 5.16 (s, 2H), 2.54 (s, 3H), 2.07 (s, 3H). ^{13}C NMR (100 MHz, DMSO-d_6): δ 168.71, 165.65, 158.94, 150.77, 144.10, 135.75, 130.88, 130.76, 130.04, 129.97, 129.49, 128.71, 128.33, 128.02, 126.44, 125.42, 125.30, 121.20, 118.51, 117.25, 115.50, 66.24, 23.31, 20.87. HRMS (ESI) calculated for $C_{30}H_{25}N_3O_4$ $(M+H)^+$: 492.1923, found 492.1929.

4.2.3.5. 2-(4′-((3-Acetamidobenzyl)oxy)-[1,1′-biphenyl]-4-yl)-6-methyl-1*H*-benzimidazole-4-carboxylic acid (7e). ^{1}H NMR (400 MHz, DMSO-d_6): δ 10.26 (s, NH), 8.40 (d, J = 8.3, 2H), 7.89 (d, J = 8.3, 2H), 7.84 (s, 1H), 7.83 (s, 1H), 7.78 (s, 1H), 7.73 (d, J = 8.5, 2H), 7.60 (d, J = 8.0, 1H), 7.31 (t, J = 7.8, 1H), 7.13 (d, J = 10.2, 1H), 7.10 (d, J = 8.8, 2H), 5.12 (s, 2H), 2.51 (s, CH_3), 2.09 (s, CH_3). ^{13}C NMR (100 MHz, DMSO-d_6): δ 168.66, 165.72, 158.89, 150.65, 143.78, 139.67, 137.47, 135.24, 134.37, 130.83, 129.99, 129.80, 128.86, 128.41, 128.23, 126.34, 122.19, 121.55, 118.62, 118.08, 117.09, 115.46, 115.42, 69.42, 24.12, 20.96. HRMS (ESI) calculated for $C_{30}H_{25}N_3O_4$ $(M+H)^+$: 492.1923, found 492.1922.

4.2.3.6. 2-(4′-((4-Acetamidobenzyl)oxy)-[1,1′-biphenyl]-4-yl)-6-methyl-1*H*-benzimidazole-4-carboxylic acid (7f). ^{1}H NMR (400 MHz, DMSO-d_6): δ 10.30 (s, NH), 8.34 (d, J = 8.5, 2H), 7.88 (d, J = 8.5, 2H), 7.78 (br s, 2H), 7.75 (d, J = 8.8, 2H), 7.60 (d, J = 8.5,

2H), 7.38 (d, J = 8.5, 2H), 7.12 (d, J = 8.8, 2H), 5.09 (s, 2H), 2.03 (s, CH_3). ^{13}C NMR (100 MHz, DMSO-d_6): δ 168.41, 166.14, 158.77, 151.65, 143.06, 139.09, 133.69, 131.29, 131.14, 129.11, 128.48, 128.14, 127.34, 126.37, 124.12, 120.01, 118.95, 116.60, 115.50, 69.18, 24.11, 20.91. HRMS (ESI) calculated for $C_{30}H_{25}N_3O_4$ $(M+H)^+$: 492.1923, found 492.1928.

4.2.3.7. 2-(2-Acetamido-[1,1′-biphenyl]-4-yl)-6-methyl-1*H*-benzimidazole-4-carboxylic acid (7g). ^{1}H NMR (400 MHz, DMSO-d_6): δ 9.52 (s, NH), 8.40 (s, 1H), 8.22 (d, J = 7.8, 1H), 7.74 (s, 1H), 7.71 (s, 1H), 7.52 (d, J = 8.1, 1H), 7.49–7.46 (m, 5H), 1.95 (s, 3H). ^{13}C NMR (100 MHz, DMSO-d_6): δ 169.06, 166.51, 151.76, 139.21, 138.29, 135.32, 132.22, 130.79, 128.66, 128.55, 127.73, 127.55, 127.05, 126.43, 125.49, 116.10, 22.97, 20.98. HRMS (ESI) calculated for $C_{23}H_{19}N_3O_3$ $(M+H)^+$: 386.1504, found 386.1505.

4.2.4. General procedure for synthesis of 8

To a solution of DMF/pyridine (1:1 v/v) was added compound **2a–z** (0.9 mmol) and 1,1′-carbonyldiimidazole (CDI) (0.9 mmol) stirred at 60 °C under N_2 gas atmosphere for 3 h. After the reaction mixture was cooled down to room temperature, 2,3-diaminobenzamide **4** (1 mmol) was added and left to stir overnight until the completion of the reaction as monitored by TLC analysis. Water (100 ml) was added and the resulting product **8** was filtered and dried without further purification.

4.2.5. General procedure for synthesis of 9, 10 and 11

4.2.5.1. From compound 7. To a solution of DMF (6 ml) was added EDCI·HCl (2 mmol), HOBt (2 mmol), NH_4Cl (5 mmol), compound **7** (1 mmol) followed by DiPEA (1 ml) and was left to stir overnight until reaction was completed judged by TLC analysis. Water (100 ml) was added to the reaction mixture which the resulting product was filtered and dried to afford compound **9**, **10** and **11**.

4.2.5.2. From compound 8. Compound **8** was dissolved in acetic acid (AcOH) (10 ml/mmol) and refluxed at 130 °C until reaction was fully completed under TLC analysis monitoring. Flash column chromatography with EtOAc/Hex (3:1 v/v) elution yielded purified compound **9**, **10** and **11**.

4.2.5.3. 2-([1,1′-Biphenyl]-4-yl)-1*H*-benzimidazole-4-carboxamide (9a). Compound reported by Tong et al.[27]

4.2.5.4. 2-([1,1′-Biphenyl]-4-yl)-6-methyl-1*H*-benzimidazole-4-carboxamide (9b). ^{1}H NMR (400 MHz, DMSO-d_6): δ 13.29 (s, $CONH_2$), 9.34 (s, NH), 8.31 (d, J = 7.1, 2H), 7.91 (d, J = 8.1, 1H), 7.79 (d, J = 7.8, 2H), 7.72 (s, 1H), 7.54 (s, 1H), 7.51 (t, J = 7.8, 2H), 7.43 (t, J = 7.3, 1H). ^{13}C NMR (100 MHz, DMSO-d_6): δ 166.33, 151.19, 141.89, 139.83, 139.18, 135.76, 132.02, 129.14, 128.23, 128.11, 127.37, 127.33, 126.80, 124.39, 121.87, 114.82, 21.34. HRMS (ESI) calculated for $C_{21}H_{17}N_3O$ $(M+H)^+$: 328.1449, found 328.1461.

4.2.5.5. 2-(4-Methoxyphenyl)-1*H*-benzimidazole-4-carboxamide (9c). Compound reported by White et al.[29]

4.2.5.6. 2-(4-Methoxyphenyl)-6-methyl-1*H*-benzimidazole-4-carboxamide (9d). ^{1}H NMR (270 MHz, DMSO-d_6): δ 12.99 (s, $CONH_2$), 9.28 (s, NH), 8.09 (d, J = 8.9, 2H), 7.61 (s, 1H), 7.41 (s, 1H), 7.07 (d, J = 8.9, 2H), 3.79 (s, 3H), 2.41 (s, 3H). ^{13}C NMR (67 MHz, DMSO-d_6): δ 166.33, 161.03, 151.59, 139.84, 135.63, 131.35, 128.39, 123.97, 121.72, 121.53, 114.52, 114.47, 55.41, 21.25. HRMS (ESI) calculated for $C_{16}H_{15}N_3O_2$ $(M+H)^+$: 282.1242, found 282.1239.

4.2.5.7. 2-(4-(Trifluoromethyl)phenyl)-1*H*-benzimidazole-4-carboxamide (9e). Compound reported by White et al.[29]

4.2.5.8. 6-Methyl-2-(4-(trifluoromethyl)phenyl)-1*H*-benzimidazole-4-carboxamide (9f). ^{1}H NMR (400 MHz, DMSO-d_6): δ 13.52 (br s, $CONH_2$), 9.24 (s, NH), 8.44 (d, J = 8.1, 2H), 7.96 (d, J = 8.1, 2H), 7.74 (s, 1H), 7.57 (s, 1H), 2.47 (s, 3H). ^{13}C NMR (100 MHz, DMSO-d_6): δ 166.09, 149.81, 139.51, 135.78, 133.10, 132.54, 130.16, 129.84, 128.14, 127.42, 126.00, 122.72, 122.19, 115.19, 21.25. HRMS (ESI) calculated for $C_{16}H_{12}N_3F_3O$ $(M+H)^+$: 320.1010, found 320.1009.

4.2.5.9. 2-(4-Cyanophenyl)-6-methyl-1*H*-benzimidazole-4-carboxamide (9g). ^{1}H NMR (400 MHz, DMSO-d_6): δ 13.45 (br s, $CONH_2$), 9.29 (s, NH), 8.31 (d, J = 9.7, 2H), 8.06 (d, J = 7.3, 2H), 7.72 (d, J = 1.8, 1H), 7.55 (d, J = 1.7, 1H). ^{13}C NMR (100 MHz, DMSO-d_6): δ 167.81, 166.67, 151.10, 140.12, 136.18, 135.99, 132.81, 132.15, 128.72, 127.03, 125.12, 122.48, 115.45, 21.77. HRMS (ESI) calculated for $C_{16}H_{12}N_4O$ $(M+H)^+$: 277.1089, found 277.1092.

4.2.5.10. 2-(4-(6-Aminopyridin-3-yl)phenyl)-1*H*-benzimidazole-4-carboxamide (9h). ^{1}H NMR (400 MHz, DMSO-d_6): δ 13.39 (s, $CONH_2$), 9.39 (s, NH), 8.39 (s, 1H), 8.27 (d, J = 8.3, 2H), 7.88–7.79 (m, 4H), 7.74 (d, J = 8.3, 1H), 7.35 (t, J = 7.6, 1H), 6.58 (d, J = 8.7, 1H), 6.28 (s, NH_2). ^{13}C NMR (100 MHz, DMSO-d_6): δ 166.21, 159.46, 151.83, 145.83, 141.58, 140.06, 135.48, 135.36, 127.46, 126.75, 125.65, 122.89, 122.70, 122.28, 114.90, 108.16. HRMS (ESI) calculated for $C_{19}H_{15}N_5O$ $(M+H)^+$: 330.1354, found 330.1348.

4.2.5.11. 2-(4-(Pyridin-3-yl)phenyl)-1*H*-benzimidazole-4-carboxamide (9i). Compound reported by Tong et al.[27]

4.2.5.12. 2-(4-(5-(Pyrrolidine-1-carbonyl)pyridin-3-yl)phenyl)-1*H*-benzimidazole-4-carboxamide (10a). ^{1}H NMR (400 MHz, DMSO-d_6): δ 9.22 (s, 1H), 8.90 (s, 1H), 8.80 (br s, NH), 8.71 (s, 1H), 8.37 (d, J = 8.1, 2H), 8.07 (d, J = 8.1, 2H), 7.91 (d, J = 7.7, 1H), 7.86 (d, J = 8.6,1H), 7.47 (t, J = 8.1, 1H), 3.48–3.43 (m, 4H), 1.82–1.79 (m, 4H). ^{13}C NMR (100 MHz, DMSO-d_6): δ 167.20, 164.47, 150.96, 144.55, 143.21, 138.35, 138.20, 136.65, 135.39, 134.44, 129.64, 128.42, 126.31, 124.98, 124.76, 122.06, 117.21 49.18, 46.67, 26.19, 24.24. HRMS (ESI) calculated for $C_{24}H_{21}N_5O_2$ $(M+H)^+$: 412.1773, found 412.1765.

4.2.5.13. 6-Methyl-2-(4-(5-(pyrrolidine-1-carbonyl)pyridin-3-yl)phenyl)-1*H*-benzimidazole-4-carboxamide (10b). ^{1}H NMR (400 MHz, DMSO-d_6): δ 9.10 (br s, 1H), 9.04 (br s, NH), 8.76 (br s, 1H), 8.38 (s, 1H) 8.33 (d, J = 8.6, 2H), 8.03 (d, J = 8.6, 2H), 7.71 (s, 1H), 7.57 (s, 1H), 3.48–3.44 (m, 4H), 1.86–1.81 (m, 4H). ^{13}C NMR (100 MHz, DMSO-d_6): δ 166.89, 165.91, 151.09, 147.94, 146.50, 138.65, 135.85, 134.30, 134.18, 133.55, 130.42, 129.35, 128.62, 128.24, 126.62, 125.43, 122.07, 115.99, 49.29, 46.63, 26.43, 24.46, 21.69. HRMS (ESI) calculated for $C_{25}H_{23}N_5O_2$ $(M+H)^+$: 426.1929, found 426.1946.

4.2.5.14. 2-(4-(6-(Pyrrolidine-1-carbonyl)pyridin-3-yl)phenyl)-1*H*-benzimidazole-4-carboxamide (10c). ^{1}H NMR (400 MHz, DMSO-d_6): δ 9.03 (br s, NH), 8.66 (br s, 1H), 8.37 (d, J = 8.6, 2H), 8.33 (s, 1H), 8.07 (d, J = 8.6, 2H), 7.95 (d, J = 7.7, 1H), 7.90 (d, J = 8.1, 1H), 7.83 (br s, 1H), 7.53 (t, J = 8.1, 1H), 3.62 (m, 2H), 3.49 (m, 2H), 1.82 (m, 4H). ^{13}C NMR (100 MHz, DMSO-d_6): δ 166.90, 165.35, 153.71, 151.07, 146.51, 140.53, 136.24, 134.03, 133.79, 129.98, 128.10, 125.30, 124.89, 124.25, 122.28, 117.00, 49.02, 46.97, 26.53, 23.98. HRMS (ESI) calculated for $C_{24}H_{21}N_5O_2$ $(M+H)^+$: 412.1773, found 412.1761.

4.2.5.15. 6-Methyl-2-(4-(6-(pyrrolidine-1-carbonyl)pyridin-3-yl)phenyl)-1*H*-benzimidazole-4-carboxamide (10d). ^{1}H NMR

(400 MHz, DMSO-d_6): δ 9.10 (s, NH), 9.00 (s, 1H), 8.33 (d, J = 8.6, 2H), 8.30 (dd, J = 2.3, 8.2, 1H), 8.01 (d, J = 8.2, 2H), 7.82 (d, J = 8.2, 1H), 7.70 (s, 1H), 7.55 (s, 1H), 3.64 (t, J = 6.3, 2H), 3.49 (t, J = 6.8, 2H), 2.50 (t, J = 5.4, 3H), 1.85–1.83 (m, 4H). ^{13}C NMR (100 MHz, DMSO-d_6): δ 166.81, 165.75, 153.97, 151.21, 146.66, 138.91, 136.09, 135.80, 135.64, 133.22, 128.69, 128.44, 128.16, 125.26, 124.17, 122.18, 115.83, 49.09, 47.03, 26.65, 24.07, 21.75. HRMS (ESI) calculated for $C_{25}H_{23}N_5O_2$ (M+H)$^+$: 426.1929, found 426.1935.

4.2.5.16. 2-(4-(Pyridin-2-yl)phenyl)-1*H*-benzimidazole-4-carboxamide (10e). Compound reported by Tong et al.[27]

4.2.5.17. 2-(2′-Acetamido-[1,1′-biphenyl]-4-yl)-1*H*-benzimidazole-4-carboxamide (10f). ^{1}H NMR (270 MHz, CD_3OD): δ 8.19 (d, J = 8.3, 2H), 7.92 (d, J = 7.8, 1H), 7.68 (d, J = 7.8, 1H), 7.52 (d, J = 8.3, 2H), 7.48 (d, J = 8.1, 1H), 7.36–7.30 (m, 3H), 7.22 (t, J = 7.5, 1H), 1.98 (s, 3H). ^{13}C NMR (67 MHz, CD_3OD): δ 172.54, 153.64, 143.00, 138.24, 135.64, 131.40, 130.63, 129.55, 129.47, 128.45, 128.08, 127.97, 124.39, 123.50, 123.27, 122.56, 118.58, 22.90. HRMS (ESI) calculated for $C_{22}H_{18}N_4O_2$ (M+H)$^+$: 371.1507, found 371.1505.

4.2.5.18. 2-(3′-Acetamido-[1,1′-biphenyl]-4-yl)-1*H*-benzimidazole-4-carboxamide (10g). ^{1}H NMR (400 MHz, DMSO-d_6): δ 13.49 (s, $CONH_2$), 10.10 (s, NH), 9.38 (s, NH), 8.33 (d, J = 8.3, 2H), 7.99 (s, 1H), 7.88 (d, J = 7.7, 1H), 7.83 (d, J = 8.3, 2H), 7.74 (d, J = 7.8, 1H), 7.60 (s, 1H), 7.42 (d, J = 4.8, 2H), 7.34 (t, J = 7.8, 1H), 2.07 (s, CH_3). ^{13}C NMR (100 MHz, DMSO-d_6): δ 168.56, 166.22, 151.60, 142.07, 141.55, 140.02, 139.66, 135.41, 129.48, 128.17, 127.54, 127.26, 123.02, 122.42, 121.54, 118.35, 117.28, 115.05, 24.07. HRMS (ESI) calculated for $C_{22}H_{18}N_4O_2$ (M+H)$^+$: 371.1507, found 371.1509.

4.2.5.19. 2-(4′-Acetamido-[1,1′-biphenyl]-4-yl)-1*H*-benzimidazole-4-carboxamide (10h). ^{1}H NMR (270 MHz, DMSO-d_6): δ 8.32 (d, J = 8.4, 2H), 8.22 (d, J = 7.8, 1H), 8.14 (d, J = 8.1, 1H), 7.93 (d, J = 8.4, 2H), 7.75 (d, J = 8.6, 2H), 7.69 (d, J = 8.6, 2H), 7.54 (br s, 1H), 2.21 (s, 3H). ^{13}C NMR (100 MHz, CD_3OD): δ 168.98, 167.10, 153.10, 142.02, 139.85, 133.94, 129.92, 129.04, 128.67, 127.79, 127.48, 126.84, 126.31, 125.17, 122.55, 119.85, 116.65, 24.54. HRMS (ESI) calculated for $C_{22}H_{18}N_4O_2$ (M+H)$^+$: 371.1507, found 371.1508.

4.2.5.20. 2-(4′-(Pyrrolidine-1-carbonyl)-[1,1′-biphenyl]-4-yl)-1*H*-benzimidazole-4-carboxamide (10i). ^{1}H NMR (400 MHz, DMSO-d_6): δ 9.38 (br s, NH), 8.37 (d, J = 8.4, 2H), 7.96 (d, J = 8.4, 2H), 7.90 (d, J = 7.2, 1H), 7.84 (d, J = 8.4, 2H), 7.78 (d, J = 8.0, 1H), 7.65 (d, J = 8.0, 2H), 7.37 (t, J = 7.2, 1H), 3.51–3.48 (m, 4H), 1.90–1.83 (m, 4H). ^{13}C NMR (100 MHz, DMSO-d_6): δ 168.34, 166.79, 152.07, 141.63, 140.77, 137.14, 128.99, 128.75, 128.43, 128.36, 128.08, 127.94, 127.16, 127.05, 123.48, 122.92, 115.68, 49.10, 46.51, 26.53, 24.44. HRMS (ESI) calculated for $C_{25}H_{22}N_4O_2$ (M+H)$^+$: 411.1820, found 411.1817.

4.2.5.21. 6-Methyl-2-(4′-(pyrrolidine-1-carbonyl)-[1,1′-biphenyl]-4-yl)-1*H*-benzimidazole-4-carboxamide (11a). ^{1}H NMR (400 MHz, DMSO-d_6): δ 13.33 (s, $CONH_2$), 9.33 (s, NH), 8.31 (d, J = 8.5, 2H), 7.93 (d, J = 8.3, 2H), 7.83 (d, J = 8.3, 2H), 7.70 (s, 1H), 7.64 (d, J = 8.1, 2H), 7.53 (s, 1H), 3.48–3.26 (m, 4H, overlap), 1.87–1.82 (m, 4H). ^{13}C NMR (100 MHz, DMSO-d_6): δ 167.86, 166.20, 151.02, 140.95, 140.28, 139.77, 136.61, 135.72, 132.02, 128.59, 128.23, 127.90, 127.39, 126.51, 124.38, 121.90, 114.82, 48.95, 46.00, 25.99, 23.92, 21.29. HRMS (ESI) calculated for $C_{26}H_{24}N_4O_2$ (M+H)$^+$: 425.1977, found 425.1979.

4.2.5.22. 2-(4-(6-Acetamidopyridin-3-yl)phenyl)-1*H*-benzimidazole-4-carboxamide (11b). ^{1}H NMR (400 MHz, DMSO-d_6): δ 13.48 (s, $CONH_2$), 10.67 (s, NH), 9.38 (s, NH), 8.77 (s, 1H), 8.34 (d, J = 8.0, 2H), 8.21 (s, 2H), 7.97 (d, J = 8.0, 2H), 7.89 (d, J = 7.3, 1H), 7.81–7.75 (m, 1H), 7.36 (t, J = 8.0, 1H), 2.13 (s, 3H). ^{13}C NMR (100 MHz, DMSO-d_6): δ 169.96, 166.70, 152.32, 152, 03, 146.42, 142.03, 139.24, 136.72, 135.88, 130.42, 128.63, 128.06, 127.39, 123.54, 122.91, 115.54, 113.72, 24.46. HRMS (ESI) calculated for $C_{21}H_{17}N_5O_2$ (M+H)$^+$: 372.1460, found 372.1461.

4.2.5.23. 2-(4-(5-(Pyrrolidin-1-ylmethyl)pyridin-3-yl)phenyl)-1*H*-benzimidazole-4-carboxamide (11c). ^{1}H NMR (400 MHz, CD_3OD): δ 8.79 (s, 1H), 8.52 (s, 1H), 8.26 (d, J = 8.3, 2H), 8.15 (s, 1H), 7.92 (bd, 1H), 7.83 (d, J = 8.3, 2H), 7.71 (bd, J = 7.5, 1H), 3.84 (s, 2H), 2.69 (br s, 4H), 1.87 (br s, 4H). ^{13}C NMR (67 MHz, CD_3OD): δ 68.45, 57.61, 55.03, 24.10, 22.13. HRMS (ESI) calculated for $C_{24}H_{23}N_5O$ (M+H)$^+$: 398.1980, found 398.1989.

4.2.5.24. 2-(4′-(3-(Piperidin-1-yl)propoxy)-[1,1′-biphenyl]-4-yl)-1*H*-benzimidazole-4-carboxamide (11d). ^{1}H NMR (400 MHz, DMSO-d_6): δ 13.67 (s, $CONH_2$), 9.39 (br s, NH), 8.33 (d, J = 8.3, 1H), 7.96 (d, J = 8.0, 2H), 7.85 (br s, 1H), 7.72 (d, J = 8.0, 2H), 7.66 (d, J = 8.3, 2H), 7.33 (br s, 1H), 7.03 (d, J = 8.5, 2H), 4.09 (br s, 2H), 2.92 (br s, 2H), 2.11 (br s, 2H), 1.70 (br s, 4H), 1.48 (br s, 2H). ^{13}C NMR (100 MHz, DMSO-d_6): δ 167.35, 158.64, 143.68, 131.43, 129.95, 129.35, 128.12, 126.06, 115.05, 65.44, 53.83, 52.57, 24.12, 23.27, 22.21. HRMS (ESI) calculated for $C_{28}H_{30}N_4O_2$ (M+H)$^+$: 455.2446, found 455.2441.

4.2.5.25. 2-(4′-(2-(Piperidin-1-yl)ethoxy)-[1,1′-biphenyl]-4-yl)-1*H*-benzimidazole-4-carboxamide (11e). ^{1}H NMR (400 MHz, DMSO-d_6): δ 13.61 (br s, $CONH_2$), 9.42 (s, NH), 8.28 (d, J = 7.5, 2H), 7.87 (d, J = 6.8, 1H), 7.77 (d, J = 8.3, 2H), 7.73 (d, J = 7.5, 1H), 7.63 (d, J = 8.3, 2H), 7.31 (t, J = 7.5, 1H), 6.98 (d, J = 8.3, 2H), 4.06 (t, J = 5.3, 2H), 2.68 (t, J = 5.3, 2H), 1.46 (t, J = 5.3, 4H), 1.31 (br s, 2H). ^{13}C NMR (100 MHz, DMSO-d_6): δ 166.88, 159.01, 152.30, 142.30, 135.97, 131.92, 130.43, 129.52, 128.37, 128.01, 127.82, 127.38, 127.08, 126.86, 123.44, 122.78, 115.54, 65.75, 57.51, 54.67, 25.66, 24.08, 21.74. HRMS (ESI) calculated for $C_{27}H_{28}N_4O_2$ (M+H)$^+$: 441.2290, found 441.2291.

4.2.5.26. 2-(4′-(Cyclopropanecarboxamido)-2′,3-difluoro-[1,1′-biphenyl]-4-yl)-6-fluoro-1*H*-benzimidazole-4-carboxamide (11f). ^{1}H NMR (400 MHz, DMSO-d_6): δ 10.60 (s, NH), 9.26 (s, NH), 8.35 (t, J = 7.8, 1H), 7.99–7.60 (m, 5H), 7.43 (s, 1H), 7.41 (s, 1H), 1.80–1.75 (m, 1H), 0.84–0.81 (m, 4H). ^{13}C NMR (100 MHz, DMSO-d_6): δ 172.46, 165.10, 160.45, 160.42, 158.00, 157.97, 147.99, 141.44, 141.32, 138.44, 130.82, 130.50, 125.30, 124.05, 120.11, 116.39, 115.77, 115.27, 110.78, 106.43, 102.10, 14.84, 7.75. HRMS (ESI) calculated for $C_{24}H_{17}N_4F_3O_2$ (M+H)$^+$: 451.1381, found 451.1378.

4.2.5.27. 6-Fluoro-2-(4′-propionamido-[1,1′-biphenyl]-4-yl)-1*H*-benzimidazole-4-carboxamide (11g). ^{1}H NMR (400 MHz, DMSO-d_6): δ 10.03 (s, NH), 9.35 (s, NH), 8.27 (d, J = 8.0, 2H), 7.86 (d, J = 8.3, 2H), 7.24 (br s, 4H), 7.59 (s, 1H), 7.57 (s, 1H), 2.34 (q, J = 7.6, 2H), 1.08 (t, J = 7.6, 3H). ^{13}C NMR (100 MHz, DMSO-d_6): δ 172.38, 165.20, 158.47, 152.47, 141.81, 139.54, 133.45, 128.27, 127.58, 127.36, 127.16, 126.82, 125.98, 123.31, 119.53, 110.30, 101.68, 29.68, 9.75. HRMS (ESI) calculated for $C_{23}H_{19}N_4F_1O_2$ (M+H)$^+$: 403.1570, found 403.1575.

4.2.5.28. 2-(3′-(Cyclopropanecarboxamido)-3-fluoro-[1,1′-biphenyl]-4-yl)-6-fluoro-1*H*-benzimidazole-4-carboxamide (11h). ^{1}H NMR (270 MHz, DMSO-d_6): δ 10.38 (s, NH), 9.27 (s, NH), 8.36 (t, J = 8.1, 1H), 8.04 (s, 1H), 7.71–7.60 (m, 5H), 7.43 (s, 1H), 7.41 (s, 1H), 1.80 (m, 1H), 0.82 (m, 4H). ^{13}C NMR (67 MHz, DMSO-d_6): δ 174.42, 165.36, 160.90, 158.47, 148.31, 144.92, 140.54, 138.71, 137.95, 136.25, 131.24, 130.03, 124.00, 123.64, 122.00, 119.73, 117.77, 116.12, 114.85, 111.14, 102.37, 15.08, 7.74.

HRMS (ESI) calculated for $C_{24}H_{18}N_4F_2O_2$ $(M+H)^+$: 433.1475, found 433.1480.

4.2.5.29. 2-(4′-(Cyclopropanecarboxamido)-3-fluoro-3′-methoxy-[1,1′-biphenyl]-4-yl)-6-fluoro-1*H*-benzimidazole-4-carboxamide (11i). ^{1}H NMR (400 MHz, DMSO-d_6): δ 9.53 (s, NH), 9.27 (s, NH), 8.33 (t, J = 8.0, 1H), 8.10 (d, J = 8.3, 1H), 7.87 (d, J = 12.9, 1H), 7.78 (dd, J = 1.7, 8.3, 1H), 7.60 (bm, 2H), 7.44 (s, 1H), 7.37 (dd, J = 1.9, 8.5, 1H), 3.98 (s, 3H), 2.12 (m, 1H), 0.80–0.76 (m, 4H). ^{13}C NMR (100 MHz, DMSO-d_6): δ 172.08, 164.84, 160.48, 158.06, 149.56, 148.05, 144.20, 137.53, 135.84, 133.15, 130.55, 128.27, 123.45, 122.98, 121.81, 118.87, 115.17, 114.18, 110.60, 109.48, 101.92, 55.97, 14.26, 7.44. HRMS (ESI) calculated for $C_{25}H_{20}N_4F_2O_3$ $(M+H)^+$: 463.1581, found 463.1572.

4.2.5.30. 2-(4′-(Cyclopropanecarboxamido)-3′-methoxy-[1,1′-biphenyl]-4-yl)-6-fluoro-1*H*-benzimidazole-4-carboxamide (11j). ^{1}H NMR (400 MHz, DMSO-d_6): δ 9.51 (s, NH), 9.33 (s, NH), 8.30 (d, J = 8.3, 2H), 8.07 (d, J = 7.5, 1H), 7.92 (d, J = 7.5, 2H), 7.60 (s, 1H), 7.57 (s, 1H), 7.40 (s, 1H), 7.31 (d, J = 8.3, 2H), 3.98 (s, 3H), 2.12 (m, 1H), 0.81 (m, 4H). ^{13}C NMR (100 MHz, DMSO-d_6): δ 171.99, 164.97, 159.55, 152.79, 149.62, 141.92, 138.28, 135.81, 134.68, 131.53, 127.38, 127.06, 121.97, 118.66, 109.36, 101.31, 55.88, 14.22, 7.81. HRMS (ESI) calculated for $C_{25}H_{21}N_4F_1O_3$ $(M+H)^+$: 445.1675, found 445.1680.

Acknowledgments

We would like to thank Aurigene Discovery Technologies (India) for their help in the in silico studies and development of the project and Aurigene Discovery Technologies (Malaysia) for the PARP-1 and DHODH assay work. We would also like to thank Dr. Michael James Christopher Buckle for his review, proofreading and valuable discussion.

Supplementary data

Supplementary data associated with this article can be found, in the online version, at http://dx.doi.org/10.1016/j.bmc.2015.05.051.

References and notes

1. Ame, J. C.; Spenlehauer, C.; de Murcia, G. *Bioessays* **2004**, *26*, 882. http://dx.doi.org/10.1002/bies.20085.
2. Baldwin, J.; Michnoff, C. H.; Malmquist, N. A.; White, J.; Roth, M. G.; Rathod, P. K.; Phillips, M. A. *J. Biol. Chem.* **2005**, *280*, 21847. http://dx.doi.org/10.1074/jbc.M501100200.
3. Barkalow, J. H.; Breting, J.; Gaede, B. J.; Haight, A. R.; Henry, R.; Kotecki, B.; Viswanath, S. K. *Org. Process Res. Dev.* **2007**, *11*, 693. http://dx.doi.org/10.1021/op7000194.
4. Batt, D. G.; Copeland, R. A.; Dowling, R. L.; Gardner, T. L.; Jones, E. A.; Orwat, M. J.; Jaffee, B. D. *Bioorg. Med. Chem. Lett.* **1995**, *5*, 1549. http://dx.doi.org/10.1016/0960-894X(95)00252-O.
5. Batt, D. G.; Petraitis, J. J.; Sherk, S. R.; Copeland, R. A.; Dowling, R. L.; Taylor, T. L.; Jaffee, B. D. *Bioorg. Med. Chem. Lett.* **1998**, *8*, 1745. http://dx.doi.org/10.1016/S0960-894X(98)00308-4.
6. Bonn, D. *Lancet Oncol.* **2002**, *3*, 714. http://dx.doi.org/10.1016/s1470-2045(02)00950-6.
7. Caiafa, P.; Guastafierro, T.; Zampieri, M. *FASEB J.* **2009**, *23*, 672. http://dx.doi.org/10.1096/fj.08-123265.
8. Calabrese, C. R.; Almassy, R.; Barton, S.; Batey, M. A.; Calvert, A. H.; Canan-Koch, S.; Curtin, N. J. *J. Natl. Cancer Inst.* **2004**, *96*, 56. http://dx.doi.org/10.1093/jnci/djh005.
9. Chen, S.-F.; Ruben, R. L.; Dexter, D. L. *Cancer Res.* **1986**, *46*, 5014.
10. David, K. K.; Andrabi, S. A.; Dawson, T. M.; Dawson, V. L. *Front. Biosci. (Landmark Ed)* **2009**, *14*, 1116.
11. De Lorenzo, S.; Patel, A.; Hurley, R.; Kaufmann, S. H. *Front. Oncol.* **2013**, *3*. http://dx.doi.org/10.3389/fonc.2013.00228.
12. Dexter, D. L.; Hesson, D. P.; Ardecky, R. J.; Rao, G. V.; Tippett, D. L.; Dusak, B. A.; Forbes, M. *Cancer Res.* **1985**, *45*, 5563.
13. Evans, D. R.; Guy, H. I. *J. Biol. Chem.* **2004**, *279*, 33035. http://dx.doi.org/10.1074/jbc.R400007200.
14. Fatokun, A. A.; Dawson, V. L.; Dawson, T. M. *Br. J. Pharmacol.* **2014**, *171*, 2000. http://dx.doi.org/10.1111/bph.12416.
15. Griffin, R. J.; Srinivasan, S.; Bowman, K.; Calvert, A. H.; Curtin, N. J.; Newell, D. R.; Golding, B. T. *J. Med. Chem.* **1998**, *41*, 5247. http://dx.doi.org/10.1021/jm980273t.
16. Herrmann, M. L.; Schleyerbach, R.; Kirschbaum, B. J. *Immunopharmacology* **2000**, *47*, 273.
17. Kummar, S.; Chen, A.; Parchment, R.; Kinders, R.; Ji, J.; Tomaszewski, J.; Doroshow, J. *BMC Med.* **2012**, *10*, 25.
18. Messner, S.; Hottiger, M. O. *Trends Cell Biol.* **2011**, *21*, 534. http://dx.doi.org/10.1016/j.tcb.2011.06.001.
19. Munier-Lehmann, H.; Vidalain, P. O.; Tangy, F.; Janin, Y. L. *J. Med. Chem.* **2013**, *56*, 3148. http://dx.doi.org/10.1021/jm301848w.
20. Penning, T. D.; Zhu, G. D.; Gandhi, V. B.; Gong, J.; Liu, X.; Shi, Y.; Giranda, V. L. *J. Med. Chem.* **2009**, *52*, 514. http://dx.doi.org/10.1021/jm801171j.
21. Penning, T. D.; Zhu, G. D.; Gandhi, V. B.; Gong, J.; Thomas, S.; Lubisch, W.; Giranda, V. L. *Bioorg. Med. Chem.* **2008**, *16*, 6965. http://dx.doi.org/10.1016/j.bmc.2008.05.044.
22. Quénet, D.; El Ramy, R.; Schreiber, V.; Dantzer, F. *Int. J. Biochem. Cell Biol.* **2009**, *41*, 60. http://dx.doi.org/10.1016/j.biocel.2008.07.023.
23. Refaat, H. M. *Eur. J. Med. Chem.* **2010**, *45*, 2949. http://dx.doi.org/10.1016/j.ejmech.2010.03.022.
24. Sousa, F. G.; Matuo, R.; Soares, D. G.; Escargueil, A. E.; Henriques, J. A. P.; Larsen, A. K.; Saffi, J. *Carcinogenesis* **2012**, *33*, 1433. http://dx.doi.org/10.1093/carcin/bgs132.
25. Suto, M. J.; Turner, W. R.; Arundel-Suto, C. M.; Werbel, L. M.; Sebolt-Leopold, J. S. *Anticancer Drug Des.* **1991**, *6*, 107.
26. Thunuguntla, S. S. R.; Subramanya, H.; Kunnam, S. R.; Sanivaru, V. S. R.; Bingi, C.; Kusanur, R.; Arlt, M. Dihydroorotate Dehydrogenase Inhibitors: Google Patents, 2010.
27. Tong, Y.; Bouska, J. J.; Ellis, P. A.; Johnson, E. F.; Leverson, J.; Liu, X.; Penning, T. D. *J. Med. Chem.* **2009**, *52*, 6803. http://dx.doi.org/10.1021/jm900697r.
28. Underhill, C.; Toulmonde, M.; Bonnefoi, H. *Ann. Oncol.* **2010**. http://dx.doi.org/10.1093/annonc/mdq322.
29. White, A. W.; Almassy, R.; Calvert, A. H.; Curtin, N. J.; Griffin, R. J.; Hostomsky, Z.; Golding, B. T. *J. Med. Chem.* **2000**, *43*, 4084.
30. White, A. W.; Curtin, N. J.; Eastman, B. W.; Golding, B. T.; Hostomsky, Z.; Kyle, S.; Griffin, R. J. *Bioorg. Med. Chem. Lett.* **2004**, *14*, 2433. http://dx.doi.org/10.1016/j.bmcl.2004.03.017.
31. Zhu, G. D.; Gong, J.; Gandhi, V. B.; Liu, X.; Shi, Y.; Johnson, E. F.; Penning, T. D. *Bioorg. Med. Chem.* **2012**, *20*, 4635. http://dx.doi.org/10.1016/j.bmc.2012.06.021.